CHALMERS

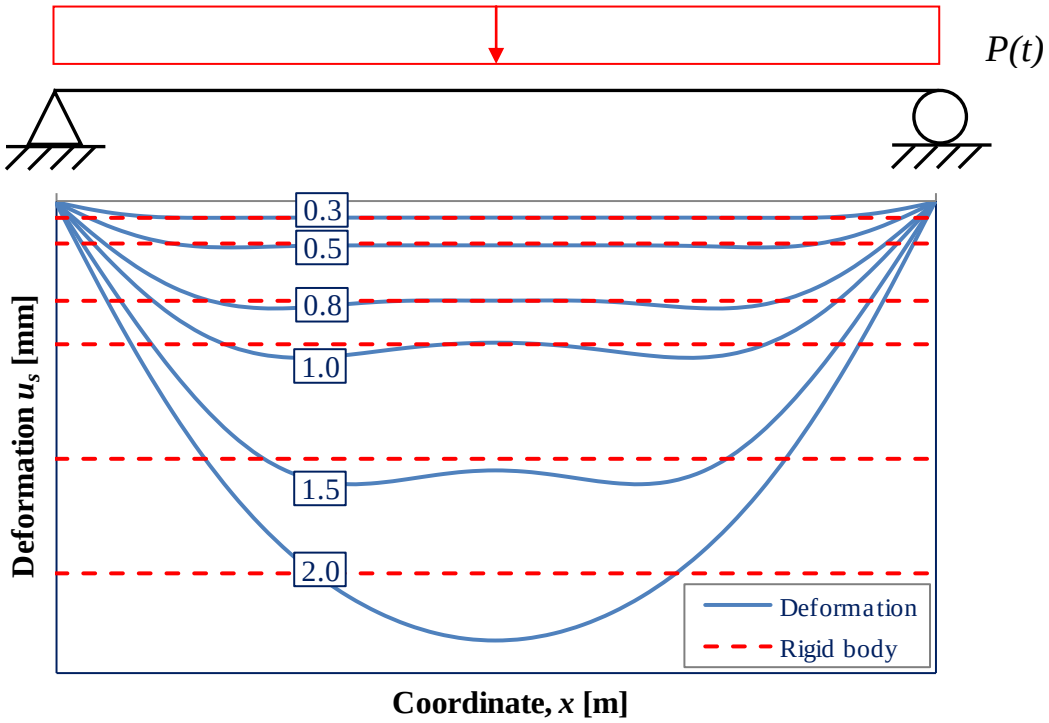

Structural Response of Reinforced Concrete Beams Subjected to Explosions

Time dependent transformation factors, support reactions and distribution of section forces

Master of Science Thesis in the Master's Programme Structural Engineering and Building Performance Design

SEBASTIAN ANDERSSON
HAMPUS KARLSSON

Department of Civil and Environmental Engineering
Division of Structural Engineering
Concrete Structures
CHALMERS UNIVERSITY OF TECHNOLOGY
Göteborg, Sweden 2012
Master's Thesis 2012:103

MASTER'S THESIS 2012:103

Structural Response of Reinforced Concrete Beams Subjected to Explosions

Time dependent transformation factors, support reactions and distribution of section forces

Master of Science Thesis in the Master's Programme Structural Engineering and Building Performance Design

SEBASTIAN ANDERSSON
HAMPUS KARLSSON

Department of Civil and Environmental Engineering
Division of Structural Engineering
Concrete Structures
CHALMERS UNIVERSITY OF TECHNOLOGY

Göteborg, Sweden 2012

Structural Response of Reinforced Concrete Beams Subjected to Explosions

Time dependent transformation factors, support reactions and distribution of section forces

Master of Science Thesis in the Master's Programme Structural Engineering and Building Performance Design

SEBASTIAN ANDERSSON

HAMPUS KARLSSON

Examensarbete / Institutionen för bygg- och miljöteknik,
Chalmers tekniska högskola 2012:103

Department of Civil and Environmental Engineering
Division of Structural Engineering
Concrete Structures
Chalmers University of Technology
SE-412 96 Göteborg
Sweden
Telephone: + 46 (0)31-772 1000

Cover: Initial displacement shape for an elasto-plastic simply supported beam subjected to an explosion compared to a rigid body motion.

Chalmers Reproservice
Göteborg, Sweden 2012

Structural Response of Reinforced Concrete Beams Subjected to Explosions

Time dependent transformation factors, support reactions and distribution of section forces

Master of Science Thesis in the Master's Programme Structural Engineering and Building Performance Design

SEBASTIAN ANDERSSON
HAMPUS KARLSSON
Department of Civil and Environmental Engineering
Division of Structural Engineering
Concrete Structures
Chalmers University of Technology

ABSTRACT

A shock wave in air resulting from an explosion is a highly impulsive load. A structural element subjected to an impulse load will behave differently than when subjected to a static load. This Master's thesis uses finite element analyses and simplified single degree of freedom systems to describe the structural response for a simply supported reinforced concrete beam subjected to an impulse load.

Theory about design of reinforced concrete members and how the member can be described with a single degree of freedom system, denoted SDOF system, are presented. Further, the magnitude and distribution of section forces are investigated for an impulse loaded reinforced concrete beam and how well these can be described different methods. Special attention is given to the phenomenon dynamic direct shear failure and how this is considered in Swedish and American design codes.

The transformation factors used to transform a structural member into an SDOF system come from an assumed deformation shape. The deformation shape is initially governed by wave propagation and the theoretical transformation factors do not describe the response fully adequate. Therefore, the concept of time dependent transformation factors is introduced. This concept, require an energy preservation method that is presented in this thesis, and makes the deformations in the SDOF approach and the finite element agree very well.

The use of an equivalent static load is shown to provide section forces on the unsafe side. It is also shown that their distribution cannot be adequately described with an equivalent static load.

The initial value of the support reaction may obtain a high magnitude when the structural member is subjected to a highly impulsive impulse load. This is treated in the literature in different ways. The current Swedish approach overestimates the support reaction considerably and the best approach is to use obtained time dependent transformation factors and a varying stiffness. Nevertheless, a more general approach on how to describe this is needed to describe the exact peak value and the time of its appearance. The SDOF model for design against direct shear is vague and further study is needed in order to treat this problem.

Key words: Explosion, impulse load, SDOF, direct shear, finite element analysis, concrete, dynamic response, time dependent transformation factors, support reaction

Strukturell respons för armerade betongbalkar utsatta för explosioner

Tidsberoende transformationsfaktorer, reaktionskrafter och fördelning av sektionskrafter

Examensarbete inom mastersprogrammet *Structural Engineering and Building Performance Design*

SEBASTIAN ANDERSSON
HAMPUS KARLSSON
Institutionen för bygg- och miljöteknik
Avdelning för konstruktionsteknik
Betongbyggnad
Chalmers tekniska högskola

SAMMANFATTNING

En stötvåg i luft från en explosion är en impulsiv last. En konstruktion som är utsatt för en impulsiv last kommer bete sig annorlunda jämfört med en statisk last. Det här examensarbetet behandlar fritt upplagda armerade betongbalkar som är utsatta för en impulsiv last. Detta görs genom FE analys och förenklade enfrihetsgradsmetoder.

Teori om hur armerade betongbalkar dimensioneras och hur de kan bli förenklade till enfrihetsgradssystem presenteras. Vidare undersöks storlek och fördelning på sektionskrafter och hur väl dessa kan bli förklarade med förenklade metoder. Speciellt fokus är lagt på fenomenet dynamic direct shear failure och hur detta dimensioneras för i svensk och amerikansk designkod.

Transformationsfaktorer som används för att göra om ett konstruktionselement till ett enfrihetsgradssystem kommer från en antagen utböjningsform. I ett tidigt skede beror utböjningsformen på vågutbredning vilket gör att de teoretiska värdena på transformationsfaktorerna inte är tillräckligt korrekta. Därför har tidsberoende transformationsfaktorer introducerats. Energin måste dock bevaras och ett tillvägagångssätt är presenterat i rapporten. Metoden som använts gör att deformationen i FE analysen och enfrihetsgradssystemet överensstämmer väldigt väl.

En statisk ekvivalent last undervärderar sektionskrafter nämnvärt. Även den tillhörande fördelningen kan inte beskrivas med en statisk ekvivalent last.

Stödreaktionen är väldigt hög initialt. Det beaktas av olika dimensioneringsregler på olika sätt. Dagens svenska metod övervärderar stödreaktionen och den bästa metoden är att använda tidsberoende transformationsfaktorer och en varierande styvhet. En mer exakt metod för att bestämma storleken och tidpunkten för den initiala toppen måste dock hittas.

Enfrihetsgradssystem för direct shear failure behöver utredas mer för att kunna tillämpas. De undersökta balkarna hade gått sönder i böjning om direct shear failure inträffar i ett tidigt skede.

Nyckelord: Explosion, impulsiv last, enfrihetsgradssystem, direct shear, finit element analys, armerad betong, dynamisk, tidsberoende transformationsfaktorer, stödreaktion

Contents

Preface

This Master's thesis investigates the response of reinforced concrete beams subjected to impulse loading. It has been carried out in cooperation with the Division of Structural Engineering at Chalmers University of Technology and Reinertsen Sverige AB. The studies were carried out at Reinertsen's office in Göteborg between January and June 2012.

Thanks go out to Reinertsen for providing necessary literature, stationery and computer programs as well as a place to perform the studies. The supervision and guidance given by Morgan Johansson, PhD Reinertsen, is highly appreciated. We would also want to thank Kent Gylltoft who has been our examiner.

Finally, we want to thank each other for having worked hard throughout the project.

Göteborg

Sebastian Andersson and Hampus Karlsson

Notations

Roman upper case letters

A	Area
A_I	Equivalent area state I
A_{II}	Equivalent area state II
A_s	Area of reinforcement
C	Damping
E	Young's modulus
E_c	Young's modulus for concrete
E_{eq}	Equivalent Young's modulus for cracked reinforced concrete
E_s	Young's modulus for steel
F	External force
F_c	Force in concrete
F_s	Force in steel
G	Shear modulus
I	Moment of inertia
I	Impulse
I_c	Moment of inertia for concrete
I_I	Moment of inertia state I
I_{II}	Moment of inertia state II
I_k	Characteristic impulse
K	Stiffness
L	Length
M	Moment
M_{cr}	Cracking moment
M_{Ed}	Designing moment
M_f	Bending moment in midpoint
M_{Rd}	Ultimate moment capacity
M_{yd}	Moment capacity when yielding starts
N	Normal force
P	Pressure
P_{peak}	Peak pressure load
R	Internal resisting force
R_m	*Maximum* internal resisting force
R_s	Direct shear resistance

T Natural period

V Shear force

V_{Ed} Designing shear force

V_{el} Elastic support reaction

V_{pl} Plastic support reaction

V_s Support reaction

W_e External energy

W_i Internal energy

W_k Kinetic energy

W_{tot} Total energy

Q_{eq} Total equivalent load

Q_{el} Elastic equivalent load

Q_{pl} Plastic equivalent load

Roman lower case letters

a Acceleration

a Length of slab

a_τ Shear span

b Width of cross-section

b Width of slab

c Concrete cover

c Damping

c_p Pressure wave velocity

c_s Shear wave velocity

d Effective depth of cross-section

f_{cc} Concrete compressive strength

f_{cd} Design value of concrete compressive strength

f_k Characteristic value of material property

f_d Design value of material property

f_y Yield stress

f_{yd} Design value of yield stress

h Height of cross-section

i	Impulse intensity
i_k	Characteristic impulse intensity
k	Stiffness
k_e	Equivalent stiffness
k_I	Stiffness state I
k_{II}	Stiffness state II
l	Length
m	Mass
m_e	Equivalent mass
m_{el}	Equivalent elastic mass
m_f	Dynamic bending moment
m_{pl}	Equivalent plastic mass
p	Momentum
q	Distributed load
q_{cr}	Distributed crack load
q_{eq}	Equivalent distributed load
q_u	Ultimate distributed load
r	Radius of curvature
s	Reinforcement bar spacing
t	Time
t_a	Arrival time
t_Δ	Load duration
u	Displacement
$\dot{u}$	First derivative of u with respect to time t, velocity
$\ddot{u}$	Second derivative of u with respect to time t, acceleration
u_{el}	Elastic displacement
u_{ep}	Elasto-plastic displacement
$u_{ep,el}$	Elastic par of elasto-plastic displacement
$u_{ep,pl}$	Plastic par of elasto-plastic displacement
u_{pl}	Plastic displacement

u_s Displacement of system point

u_{tot} Total displacement

u_x Displacement of wave in vertical direction

u_y Displacement of wave in horizontal direction

v Velocity

v_s Velocity in system point

x Coordinate

x Depth of compression zone

x_I Depth of compression zone state I

x_{II} Depth of compression zone state II

y Coordinate

z Coordinate

z Coordinate from neutral axis

z Internal lever arm for reinforcement

Greek upper case letters

Δ Direct shear slip

$\dot{\Delta}$ First derivative of Δ with respect to time t, velocity

$\ddot{\Delta}$ Second derivative of Δ with respect to time t, acceleration

Φ Deformation shape

Greek lower case letters

α Damping constant Rayleigh damping

α_R Stress block factor

α_s Ratio between Young's modulus for steel and concrete

β Damping constant Rayleigh damping

β_R Stress block factor

δ_{el} Displacement error

ε Strain

$\dot{\varepsilon}$ Strain rate

ε_{cc} Concrete compression strain

ε_{ct} Concrete tensile strain

ε_{cu} Ultimate concrete strain

ε_s Steel strain

ε_y Yield strain

ε_{el} Elastic strain

ε_{pl} Plastic strain

ϕ Bar diameter

γ Damping ratio

γ_F Ratio between actual peak force and characteristic peak force

γ_I Ratio between actual impulse and characteristic impulse

κ_k Transformation factor for the internal force

κ_F Transformation factor for the external load

κ_m Transformation factor for the mass

κ_{mF} Transformation factor for the mass and the external load

λ Wave length

λ_s Shear span

θ Support rotation

θ_{pl} Plastic rotation

$\theta_{pl,d}$ Maximum plastic rotation

ρ Density

ρ Amount of reinforcement

σ Stress

σ_{cc} Concrete compressive stress

σ_{ct} Concrete tensile stress

$\sigma_y^{'}$ Fictitious yield stress

τ Shear stress

υ Poisson's ratio

ω Angular frequency

1 Introduction

1.1 Background

An explosion occurs when there is a sudden expansion of matter. This rapid expansion creates a shock wave that in turn results in an impulse load acting on the surroundings. Explosions can either be intentional or accidental; an act of war or terror versus an industrial or traffic accident for example. The consequences of such an event can be devastating to nearby structures and people. As they are spontaneous events and difficult to predict it is important to build defence structures and to adapt the design of potentially targeted buildings so that they can withstand this type of extreme loading. Explosions have recently struck Nordic capital cities, Oslo in July 2011 and Stockholm in December 2010.

Explosion shock waves are highly impulsive and dynamic loads. They are intense and occur over a very short period of time, typically a few milliseconds. The response of a structure to a dynamic load varies considerably to that of a static load. The dynamic response is more difficult to explain and therefore simplified approaches are often used in order to explain the behaviour of the structure. A well established method is to transform the structural element into an equivalent single degree of freedom system, often referred to as an SDOF system, by choosing a system point in the structure. Transformation factors are used to relate the element's mass, resistance, damping and external force to the corresponding equivalent parameters in the simplified SDOF system. Subsequently, the maximum moments and shear forces acting on the structure can be found.

The material behaviour will significantly influence the resistance of a structure. Reinforced concrete has been proven to perform well when subjected to explosions due to its high mass and ductile behaviour, which dissipates a large amount of energy. However, it has a complex stress-strain relationship since the concrete cracks and the steel reinforcement yields. Therefore, the relationship is often idealised to linear elastic, ideal plastic and elasto-plastic relationships. The same idealisations can be used for other materials but this thesis will largely focus on reinforced concrete members.

This work is a continuation of three previous Master's theses. Nyström (2006), Ek and Mattsson (2009), and Augustsson and Härenstam (2010) dealt with the response of reinforced concrete beams and slabs to an explosion by using simplified approaches, where the main focus was bending response. The results from the simplified design approach were compared to more detailed finite element methods where it was concluded that the equivalent SDOF approach using transformation factors could be somewhat misleading. This was especially the case for plastic and elasto-plastic analyses. More investigations will therefore be carried out in order to explain the influence of transformation factors and how the member can be designed for moment and shear force.

Moment and shear force distributions in an impulse loaded structure differ significantly compared to the expected static distributions. A phenomenon that has been observed in some reinforced concrete structures subjected to impulse loads is called direct shear. Short after detonation, often within the first millisecond, large shear forces will occur close to the supports, which will cause an almost vertical crack propagating through the member. This does not occur when the same structure is subjected to a static load. Knowledge about dynamic direct shear failure is limited.

The Swedish Fortifications Agency (in Swedish; Fortifikationsverket) has recently given out a handbook, which treats direct shear failure briefly and MSB, (Myndigheten för samhällsskydd och beredskap), Swedish Civil Contingencies Agency, requests to know more about it in order to take it into account in design if needed.

1.2 Aim

The aim of this Master's thesis is to complement the analyses carried out in previous Master's theses and provide a more comprehensive understanding about design considerations for structures subjected to explosions. The report considers two main areas:

1) The moment and shear force caused by an impulse load was studied in detail for reinforced concrete beams. The thesis also investigates and presents how the shear force can be determined and designed for. Additional attention was given to the phenomenon of direct shear failure and how it can be taken into account in design with regard to explosions.

2) Transformation factors have been proven to be somewhat misleading according to Ek and Mattsson (2009) and Augustsson and Härenstam (2010). This thesis presents how these differ from more detailed finite element analyses and how can it be taken into account in a simplified design approach.

1.3 Method

A literature review of previous work in the area of interest was carried out in order to understand and generally describe explosions, impulse loading and design methodology. The literature review was extended to include how shear force and the direct shear phenomenon behave and how they are taken into account today in Swedish and American design code. The American design approach against explosions is chosen as a reference since it is one of the most comprehensive methods.

Investigations were carried out by performing detailed analyses in the commercial finite element software ADINA, which is suitable for dynamic analyses. These analyses are the reference for simplified methods and are assumed to represent the real behaviour of a structure subjected to an explosion. It is important to realise the software's limitations and restrictions. The result of the finite element analyses was therefore critically been evaluated by questioning the procedure and the modelling assumptions made in the analyses. Several analyses with different input data were performed in order to obtain a reliable result, which is more general to any explosion situation.

The simplified approaches were used with three material idealisations including, linear elastic, ideal plastic and elasto-plastic. The first two are used in order to describe the more complicated elasto-plastic material description, which is the most realistic material response despite overlooking strain hardening.

In this study an SDOF approach with different material responses was compared with their assumed real behaviour. It was also updated in order to correlate better by investigating the transformation factors. The design moment and shear force on the structure according to design codes are compared to the real loads and the rightness is evaluated. The issues of time dependent transformation factors were also addressed to consider possible effects of the loads on the structure.

1.4 Limitations

The analyses only treat reinforced concrete beams. It is most common to use concrete when designing structures against explosions due to the great mass and the possibility of ductile behaviour that consume a lot of energy. However, much of the basic equations are applicable to other materials as well. The reinforced concrete stress-strain relationship will be simplified to a linear elastic response, plastic response and elasto-plastic response to reduce the calculation efforts when investigating the shear force. This is a relatively good approximation.

The studies are limited to a simply supported beam. However, some variation of cross-section, length and loading will be done to validate the behaviour. No analyses will be carried out on slabs but some theory about their behaviour is presented.

A more detailed analysis of reinforced concrete beams was intended to be used to compare with the simplified method by taking both concrete cracking and reinforcement yielding into account. However, the detailed model was not completed and is therefore only documented in Appendix I in order to not take focus from other investigations.

This thesis will investigate the primary effects of impulse loads induced by shock waves in air from an explosion. It will focus on the early behaviour of the structure by investigating moment, shear force and displacement. The influence of ground shock waves and bomb fragments will be neglected, as will secondary effects such as the load from collapsing structures.

The thesis will not consider the material effect of high strain rates, which act to enhance the performance of the structure. By neglecting the positive effects of an increasing strain rate the worst case scenario will be studied. It is discussed in the American design code and is therefore further described in the Section 2.4.1.5.

1.5 Outline of the report

Chapter 2 is a theory chapter that covers basic explosion theory, reinforced concrete behaviour and design approaches. In addition, dynamic systems are described and the transformation from a real structure into an equivalent single degree of freedom system is presented.

Chapter 3 will describe a cross section and some load cases that will be used for further studies. Hand calculations will be shown for the example and parameters that will be used in further studies are calculated. It will also cover some consideration that needs to be taken into account when using finite element modelling of the problem.

Chapter 4 is the first result part in this thesis. Here deformation of the structure is discussed and this leads to an introduction of time dependent transformation factors for the equivalent SDOF system.

Chapter 5 compares the section forces obtained by the equivalent static load and compares these with finite element solutions. The magnitude and distribution are discussed.

Chapter 6 investigates the support reaction, which must be found if direct shear failure can be described adequately. Several methods are compared in order to see which is the most preferable in design.

Chapter 7 evaluates the simplified single degree of freedom system for direct shear. This is done by constructing iso-damage curves to be able to see whether a bending failure or a direct shear failure will occur.

The different results are discussed individually in every chapter and then followed by a more general discussion and conclusion. The Appendix will give a more comprehensive picture of the investigations performed in here. In Appendix I, a detailed analysis where a solid 2D model taking concrete cracking and reinforcement yielding into account is presented. This model had convergence problems when subjected to an impulse load and is presented in Appendix I in order to not take focus from other investigations.

2 Theory

2.1 Explosions

An explosion occurs when there is a need of energy release. Energy is released when an amount of matter with a certain volume suddenly expands. This sudden release of energy manifests in the form of light, sound, temperature and pressure, all of which we recognise as an explosion. The pressure will create a shock wave, which will spread outwards spherically from the point of energy release, see Figure 2.1. As the shock wave advances away from its origin the pressure will decrease rapidly and return to the standard atmospheric pressure. The speed of this process is supersonic, ending after a few milliseconds.

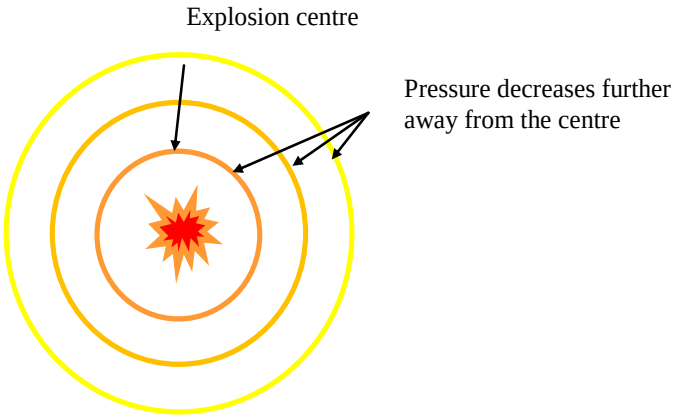

Figure 2.1. An illustration of how the energy propagates outwards from the source of the explosion.

A shock wave can be described through a pressure curve in relation to time. After some time, the arrival time, the shock wave front will reach the area of interest and subject it to a positive pressure. Because the shockwave forces the air to move as it spreads outward from the explosion centre it will create a lack of air behind, causing a partial vacuum or negative pressure phase. A principal pressure-time curve of an idealised shock wave is illustrated in Figure 2.2. The positive pressure phase is of a higher magnitude and has a shorter duration than the negative phase. However, a shock wave is according to Johansson and Laine (2007), often simplified by assuming a linear decrease of pressure and by neglecting the negative phase due to its relatively low amplitude, see Figure 2.3. In order to avoid convergence problems when modelling, a very steep inclination is given to the pressure line between arrival time and peak pressure.

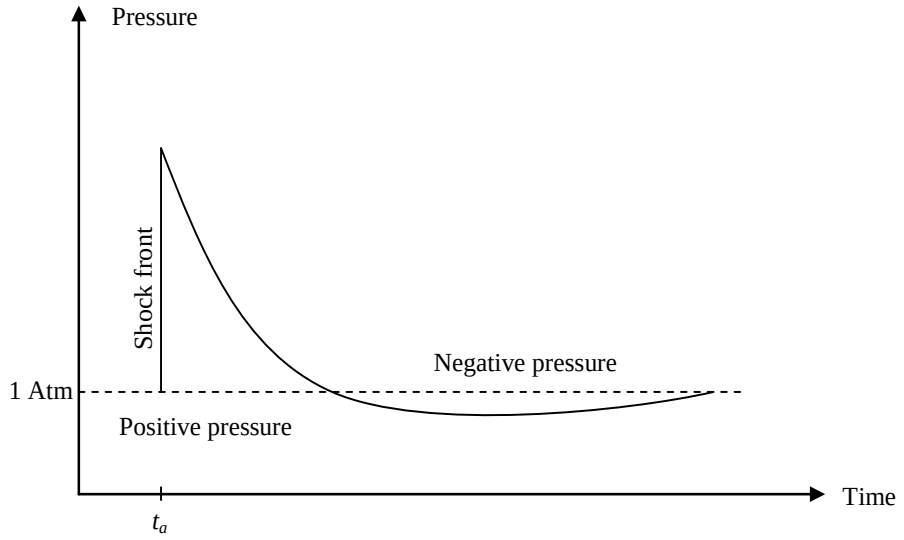

Figure 2.2. An idealised shock wave from an explosion. The high amplitude positive phase is followed by a longer negative phase with lower amplitude.

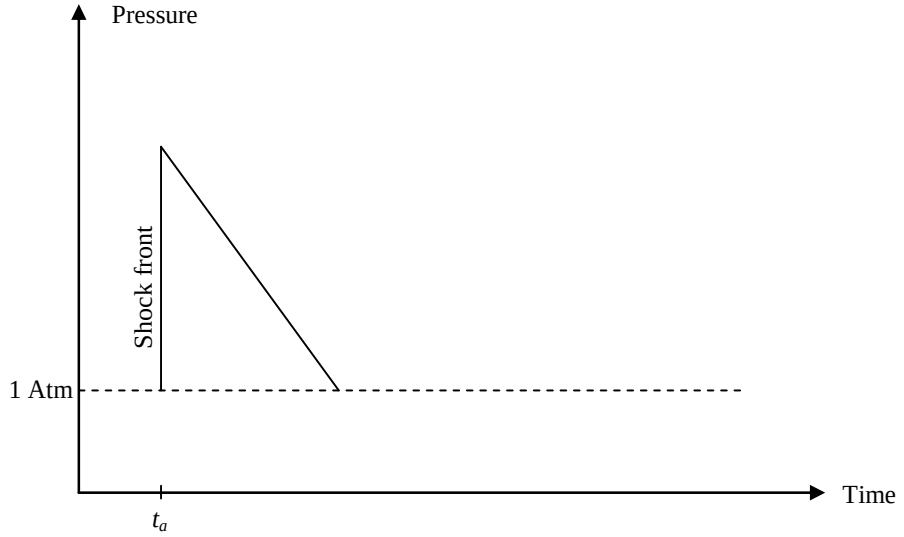

Figure 2.3. A simplified shockwave assumes linearly decreasing pressure and neglects the negative phase.

An idealised shock wave progresses through air without being disturbed. However, in a real environment the magnitude and spreading of the shock wave will be affected by many phenomena. When a shock wave reaches a stiffer object the wave is reflected against its surface. This reflection causes some major changes in the properties of the shock wave and can result in an increase of pressure up to twenty times larger than that of the original wave, see Johansson and Laine (2007).

There are two main types of reflection: regular reflection and mach reflection. Regular reflection is further divided into normal reflection and skewed reflection. Normal reflection happens when the incoming wave approaches the surface perpendicularly as shown in Figure 2.4. Mach reflection is a special case of skewed reflection and happens when the angle between the incoming wave and the reflecting surface is

around 40^{o}, see Figure 2.4. It is characterised by a part of the shock wave reflecting regularly with another part just sliding along the surface.

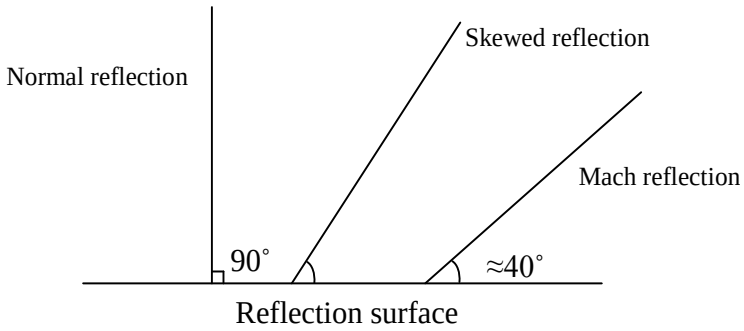

Figure 2.4. A shock wave is reflected at a surface. Two special cases of reflection are normal reflection and Mach reflection.

Diffraction is another phenomenon that affects the waves' magnitude and duration, describing how the shock wave spreads behind and past a building or an object. This is a very complex proceeding and depends on the geometry of the structure. Nevertheless, effects of reflections and diffractions are taken into account by applying a larger load. Specific consideration of how a wave is reflected will not be taken. For more detailed information regarding reflections and diffractions, the reader is referred to Johansson and Laine (2007).

There are empirical expressions for the values of peak pressure and duration from a certain explosion at scaled distances, Johansson and Laine (2007). The Swedish Civil Contingencies Agency, MSB (2011), has defined a load that a protective facility should be able to resist. This is in Johansson and Laine (2007) referred to as an archive bomb. The archive bomb consists of 125 kg of high explosive TNT exploding in air at a distance of 5 metres from the structure.

2.2 Structural response of reinforced concrete subjected to static load

2.2.1 Beams

2.2.1.1 Introduction

Engström (2011a) defines a beam as a linear structural member predominantly loaded in flexure. According to Eurocode 2, CEN (2004), the structural member is a beam if the span to depth ratio is greater than 3 and the width is less than 5 times the depth of the member. The load is transferred to the supports in one direction. There are two main design issues that need to be addressed: moment and shear. These are described in the following sections.

2.2.1.2 Moment

There are three models to explain the behaviour of concrete beams in Eurocode 2, CEN (2004). They are called state I, state II and state III and can be seen in Figure 2.5.

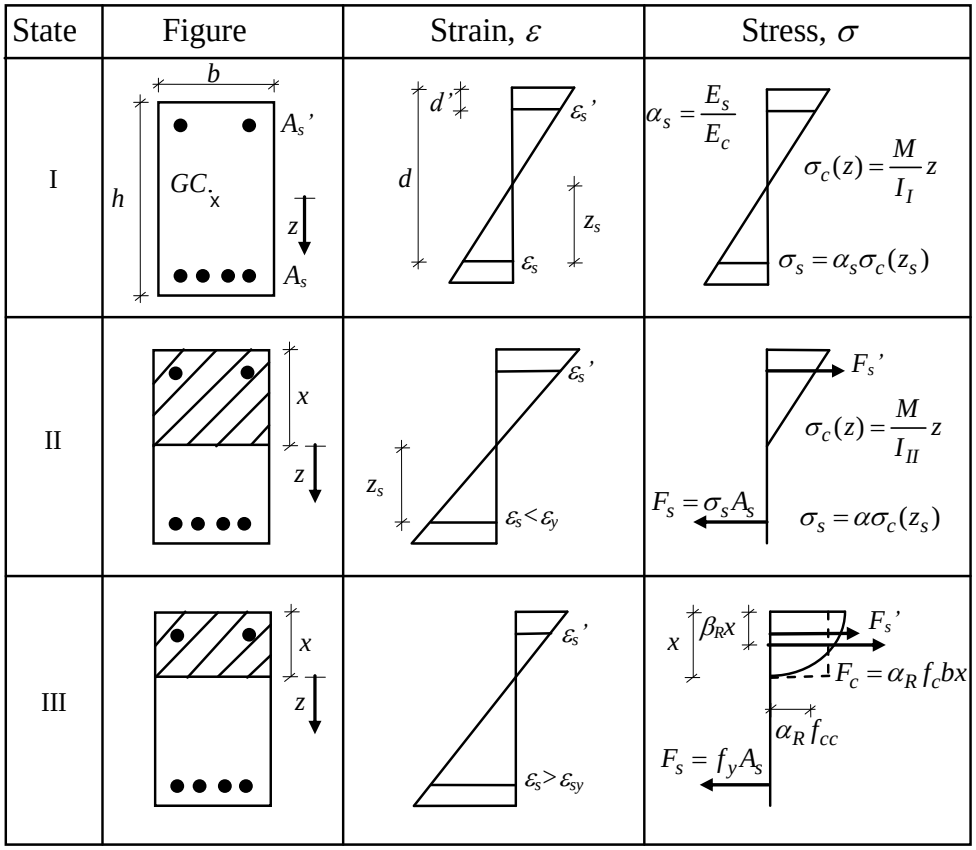

Figure 2.5. The different states of a concrete section and internal forces.

State I is when the concrete is not cracked and the behaviour is assumed to be linear elastic. It is often reasonable to neglect the influence of reinforcement in this state. Thus, the crack resisting moment of the cross-section can be easily determined with help of the moment of inertia *I*, the location of the neutral axis and concrete tensile strength.

Concrete is weak in tension and will crack early. A state II model is often used when a cracked concrete beam is studied for low loads. This model assumes linear elastic behaviour both for concrete and reinforcement but neglects the influence of cracked zones. It is an adequate assumption for the reinforcing steel and for concrete at stresses below the steel yield stress. The reinforcement can be converted into an equivalent concrete area. Thereafter a moment of inertia for state II can be calculated and consequently the moment capacity.

When the steel begins to yield and the concrete has a non-linear compression strength a state III model is used. It takes both concrete cracking and steel reinforcement yielding into account. The moment capacity is determined by using moment equilibrium. The ultimate capacity can be calculated by assuming reinforcement

yielding and ultimate compressive strain in concrete in most outer fibre. Concrete stress block factors α_R and β_R are used to approximate the non-linear distribution in the concrete with a stress block with a lever arm to the neutral axis. If the steel in a state III model has not begun to yield, the concrete will suddenly fail in compression. This is brittle failure mode and should be avoided if possible.

These three different states can be demonstrated in a moment-curvature relationship for a continuous concrete beam. A moment curvature relationship can also be described with a force displacement relationship where the force is the external force. A typical moment-curvature relationship for a small reinforced concrete region can be seen in Figure 2.6a. This moment-curvature relationship can be modified due to time dependent deformation and creep but will not be considered in this thesis. An additional axial force will change this relationship and a specific case for each axial force must be obtained.

The moment-curvature relationship can be simplified from a multi-linear to a bi-linear relationship where the slope of the curve is an approximation of the flexural stiffness at the different stages. This bi-linear relationship is illustrated in Figure 2.6b. It is sufficient to use this simplification if the purpose is to calculate the need for plastic rotation according to Engström (2011a). In order to determine the yield bending moment and its corresponding curvature at the breakpoint, a state II section analysis should be carried out assuming tension reinforcement strain has just reached the yield strain. For more detailed description how to do such an analysis the reader is referred to Engström (2011a).

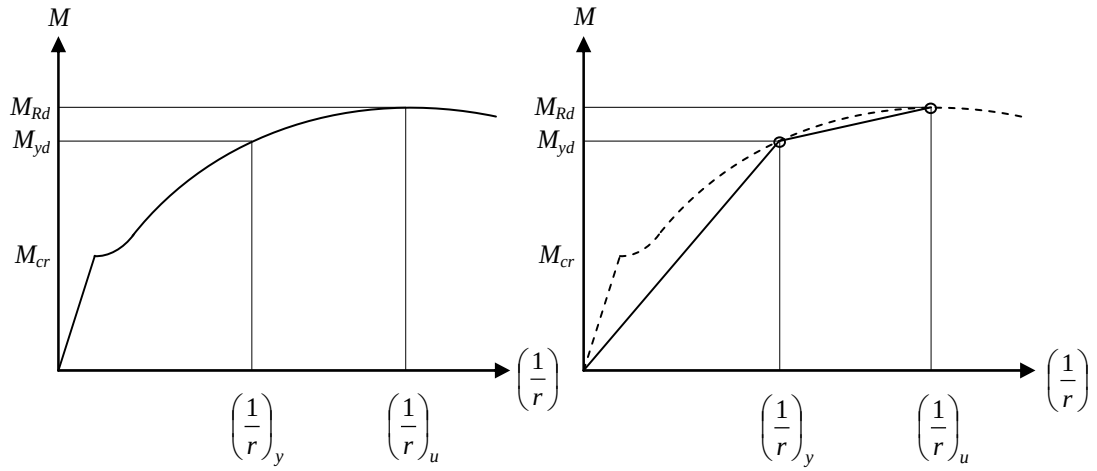

Figure 2.6. A moment curvature diagram (a) and the corresponding simplified moment curvature diagram (b).

When a section in a reinforced concrete beam cracks, it will suddenly lose stiffness and the remaining stiffness will depend on the provided reinforcement. The parts that are uncracked will be stiffer and moment redistribution will take place as they attract more moment. When the concrete cracks it is often assumed that the cracked part of the section cannot take any stress. However, the uncracked concrete between flexural cracks will carry some stress with help of the bond between the reinforcement and the concrete. This contribution is large just when the concrete cracks but declines as more

sections crack. This is referred to as the tension stiffening effect and can be seen in Figure 2.7. In further investigations, this thesis does not consider tension stiffening.

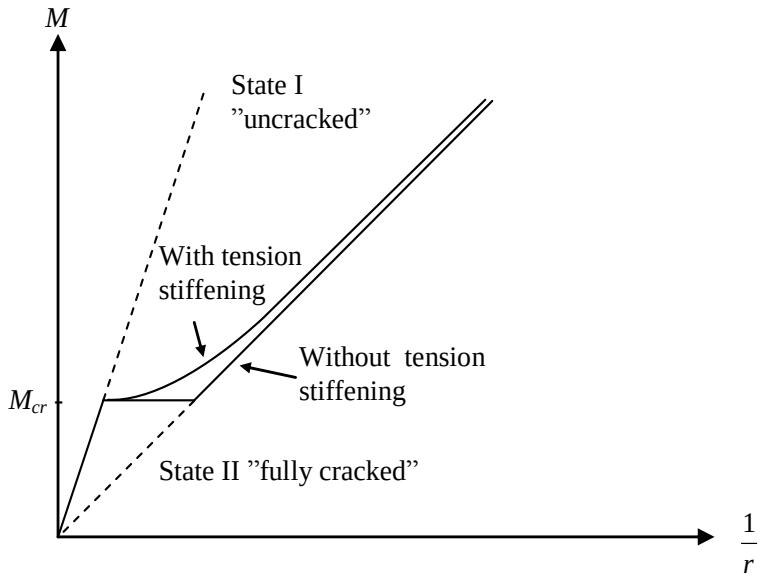

Figure 2.7. Response of a region with regard to ‘tension stiffening’ in a concrete member subjected to pure bending. Based on linear stress-strain relationship for both concrete and steel.

After a while cracking will exist all along the length of the concrete beam and the stiffness of each section is merely dependent on the amount of reinforcement. The stiffness distribution in the cracked state may be different from that in the uncracked state due to uneven reinforcement arrangement within the beam. Loading the beam even further will result in reinforcement yielding. The yielding will start in the highest stressed section and in this section the steel deforms more than in adjacent sections where the steel still have an elastic response. This will create a region with concentrated plastic rotation, a so called plastic hinge.

2.2.1.3 Shear

A load on a concrete structure will in addition to moment give rise to shear stresses over the span. The flexural stress and the shear stress can be combined by using principal stresses. The concrete will crack if the principal stress exceeds the concrete’s tensile strength at any point in the beam. Failure due to shear forces is often brittle and happens suddenly.

For a beam loaded in pure shear this means that the principal stresses will be 45^{o} to the longitudinal axis, see Figure 2.8. Eventually, the tension principal stresses exceed the tensile strength and a crack will occur. The crack will propagate in the direction of the maximum principal stress, i.e. 45^{o} to the longitudinal axis. The crack can either start as a flexural crack in the outermost fibre and then develop as a shear crack through the depth of concrete, Figure 2.9a, or proceed as a web shear crack in the centre of the depth Figure 2.9b.

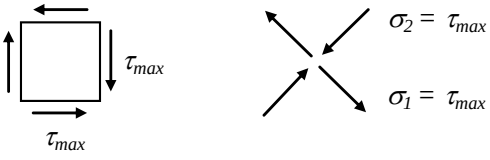

Figure 2.8. Principal stresses due to pure shear.

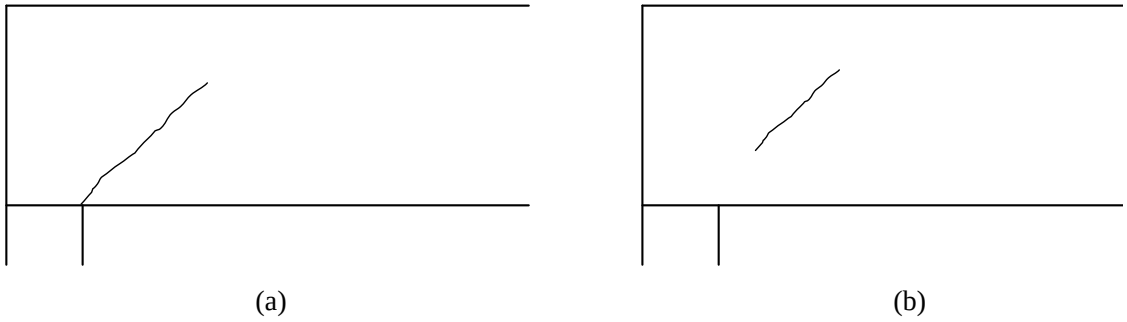

Figure 2.9. Different shear cracks: (a) Flexural shear crack and (b) Web shear crack.

A strut-and-tie model can be used to explain the behaviour in shear and is illustrated in Figure 2.10. The remaining uncracked concrete compression zone can be interpreted as a compression chord, the concrete between the cracks as a compression strut and the tensile reinforcement as a tension tie. A shear failure is characterised by either slip along the crack or crushing of the compression strut. The resistance against compression of a concrete compression strut can be obtained by equilibrium equations.

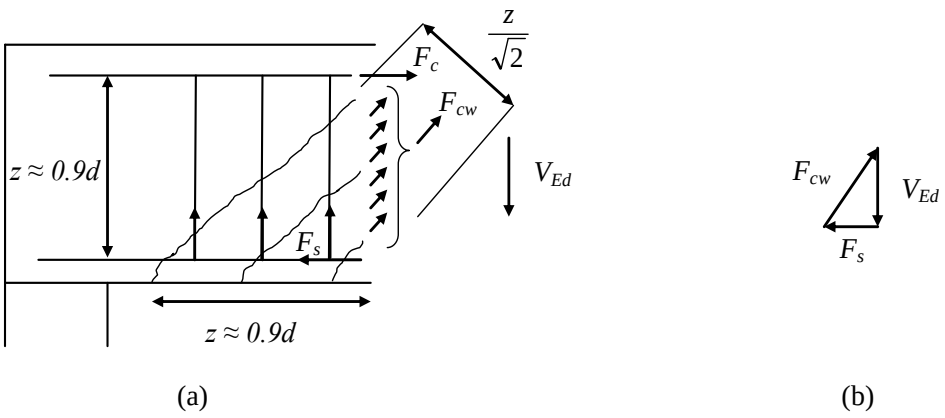

Figure 2.10. Strut-and-tie model for shear cracks.

There are four main mechanisms that resist shear failure along a cracked section in a flexure reinforced concrete beam, see Figure 2.11.

1. The crack is not smooth and will therefore have some friction during slip.
2. Ballast can be trapped in the crack and create mechanical interlocking.
3. The remaining uncracked concrete compression zone will resist slip along the crack.

4. Dowel action of the tension reinforcement acts as a significant resistance mechanism for large deformations.

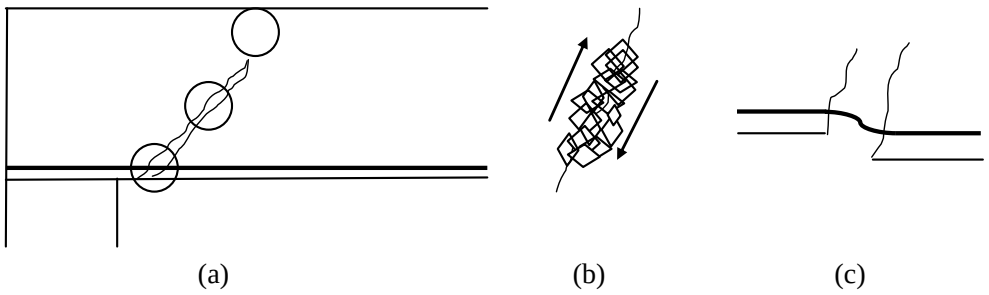

Figure 2.11. Mechanisms for crack resistance (a): friction in crack (b), mechanical interlocking (b), uncracked compression zone and dowel action of tensile reinforcement (c) .

However, these mechanisms are often not sufficient to rely on when designing against shear failure. Firstly, the capacity against concrete crushing and slippage along the crack needs to be considered. Shear reinforcement should be introduced if the capacity is too low to take tension forces across the cracks. The shear reinforcement also ties the main reinforcement bars together and confines the concrete. The designer can, within some limitations, decide in which angle the final shear crack will form at by designing the shear reinforcement in static load cases.

Shear reinforcement are commonly made up of stirrups or links perpendicular to the axis of the beam, shown in Figure 2.12a, but can also be at an angle. By using inclined reinforcement as shown in Figure 2.12b, more shear reinforcement may cross the crack, which means that a higher resistance will be obtained. However, the installation is more complex and can be more expensive than using more reinforcement. The direction of shear forces will alternate in a dynamically loaded system meaning that shear reinforcement must be provided in both directions. Lacing, shown in Figure 2.12c, can be used for this purpose and provides large rotational capacity according to DoD (2008).

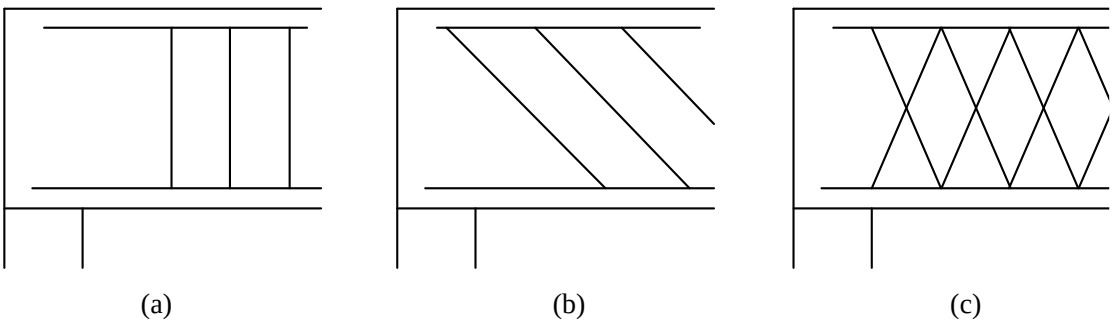

Figure 2.12. Different shear reinforcement: (a) stirrups, (b) inclined reinforcement and (c) lacing.

2.2.2 Slabs

2.2.2.1 Introduction

It was initially intended to extend the analyses in this thesis to include slabs. Due to this projects time limitation though, it was not possible to analyse slabs further. Although the theory presented below will not be further used it shows how a slab can be designed and can therefore be of interest.

A slab is a structural element, often concrete material, which has significantly greater width than height, Engström (2011b). The main difference compared to a beam element is that transverse action will also have to be considered due to the great width.

A slab can carry the load in one or two directions, often supported by continuous walls or beams. A one-way slab can be seen as a wide beam and designed accordingly per unit width. However, a two way slab carries the load in two directions and will therefore require 3-D analysis in order to obtain proper reaction forces and deformations. In this report, slab will refer to a two way slab.

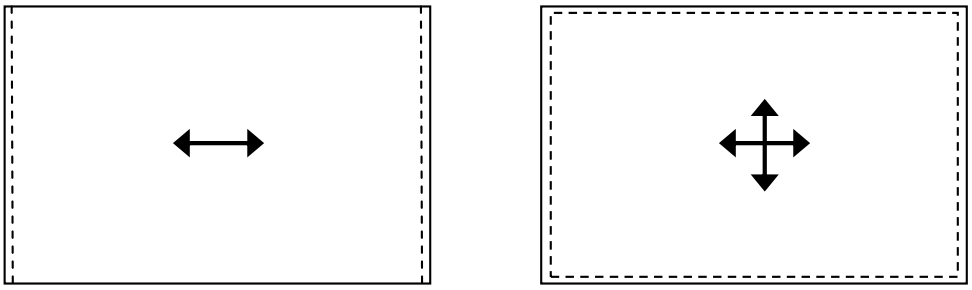

Figure 2.13. One-way and two-way slabs. The dotted lines show that the edges are simply supported.

A slab is normally statically indeterminate, which means that the choice of material model will influence the result. The material behaviour is the same as for the described beam behaviour in Section 2.2.1.2 but stresses will exist in 3 directions. The reinforced concrete slab will go from uncracked to cracked, to reinforcement yielding and further up to failure as the load is increased. The non-linear behaviour allows the designer to decide the behaviour of reinforced concrete by arranging the reinforcement accordingly. The reinforcement configuration will change the stiffness and the corresponding reactions throughout the sections.

Since reinforced concrete slabs are rather complex to analyse, models are often simplified. There are three methods for designing reinforced concrete in the ultimate limit state. The most detailed is a non-linear finite element method with the real behaviour. It requires a finite element solution that explicitly models the reinforcement yielding and the concrete cracking. The other alternatives are strip and yield line method. These assume ideal plastic behaviour and since there is no relationship between moment and curvature in the plastic state, the collapse load cannot be solved directly. It has to be approached from either upper bound or lower bound solutions.

2.2.2.2 Strip method

The strip method is a static method providing lower bound results when analysing plastic reinforced concrete slabs (Engström, 2011b). The general idea is to assume a moment distribution in the slab in the ultimate limit state and then calculate a corresponding maximum load.

The moment distribution must be in equilibrium in the ultimate limit state. The slab is divided into strips in both main directions. The load should be carried by the strips together. Any load distribution is allowed as long as the load that is carried by the strips together is the same as the actual load on a considered element lying on both strips. The slab can be divided into different strip patterns and load distributions, see Figure 2.14, which will give different accuracy of the predicted failure load. The more the division of the slab looks like the final mechanism, the better the lower bound solution will converge with the actual load and the better the behaviour up to failure can be estimated. The obtained failure load is however, always underestimated. Moments in the main directions are easily obtained on the safe side.

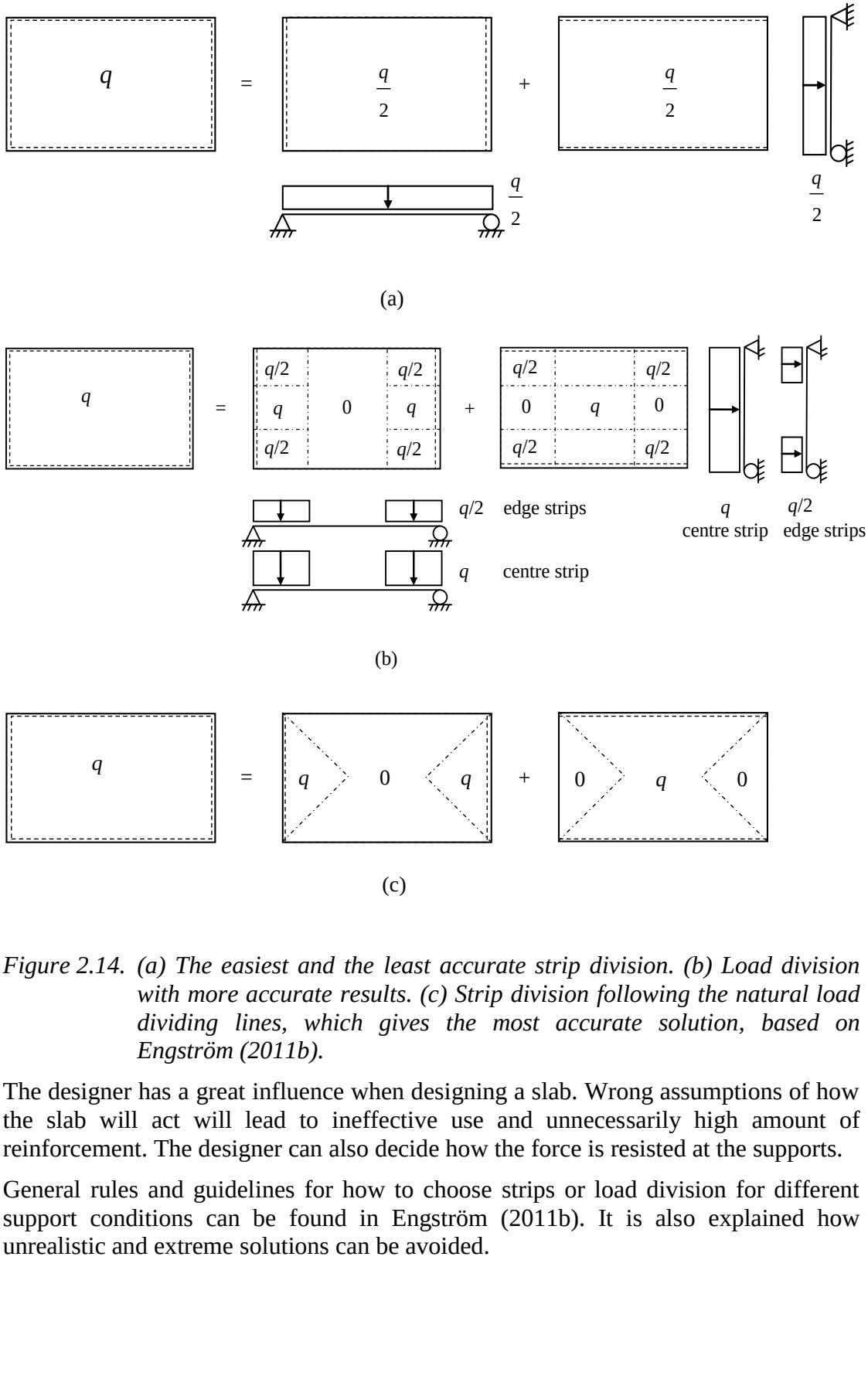

Figure 2.14. (a) The easiest and the least accurate strip division. (b) Load division with more accurate results. (c) Strip division following the natural load dividing lines, which gives the most accurate solution, based on Engström (2011b).

The designer has a great influence when designing a slab. Wrong assumptions of how the slab will act will lead to ineffective use and unnecessarily high amount of reinforcement. The designer can also decide how the force is resisted at the supports.

General rules and guidelines for how to choose strips or load division for different support conditions can be found in Engström (2011b). It is also explained how unrealistic and extreme solutions can be avoided.

2.2.2.3 Yield line method

A yield line is a line with plastic hinges where the deformation has reached the yield strain and the moment capacity cannot be further increased. It starts at the most stressed point and will, as in theory of plastic hinges, eventually form a mechanism and the slab will fail. The yield line method is an upper bound approach and will therefore always provide an answer on the unsafe side since the slab will fail in the failure mechanism that requires least energy. As a result, it might be a lengthy process to find the worst failure mechanism. The development of a potential failure mechanism is shown in Figure 2.15 for a slab simply supported on four edges. This might not be the most dangerous collapse mechanism. However, the yield line method is a very effective approach when analysing existing slabs, where a simple crack pattern can be used and a collapse load higher than the actual collapse load will be obtained.

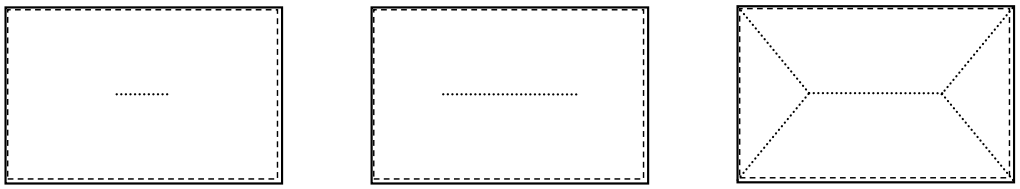

Figure 2.15. Yield line development. The most stressed point starts to yield and the yield line will develop until a mechanism is formed

When the slab deflects, the parts defined by a yield line must fit together. This is a kinematic requirement which needs to be fulfilled for all collapse mechanisms. The kinematic requirement can be ensured if a yield line or its extension passes through the intersection of the adjacent part's rotational axes. From Figure 2.16 it is clear that the yield line between parts 1 and 2 passes through the intersection of rotation axes AB and AC. However, the yield line between part 2 and 3 does not intersect the intersection between rotation axes AC and BD because the axis never intersect. To overcome this, the rotational axes AC and BD are extended to infinity which creates and illusion that they intersect. The centre yield line between parts 2 and 3 will approach the imaginary intersection and therefore the kinematic requirement can be seen as fulfilled.

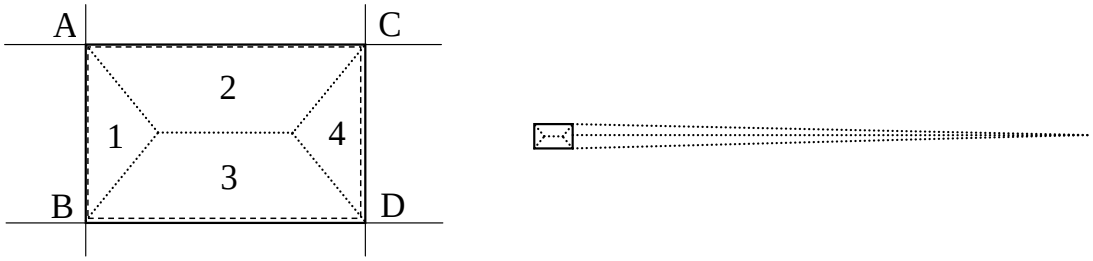

Figure 2.16. The kinematic requirement must be fulfilled for the mechanism to form.

2.2.2.4 Shear

Shear forces in slabs can be resisted in the same manner as for beams in B-zones, which are zones where plane sections remain plane under loading, Al-Emrani *et al*. (2008). A strip model can be used to calculate the shear resistance and placement of shear reinforcement. Shear failure of a slab supported on continuous walls subjected to uniform loading is generally not the governing failure mode since the shear force per unit length is relatively small. However, close to concentrated forces or supports, i.e. discontinuity regions, great shear forces can occur. A flat slab supported on columns for instance. Flat slabs or point load action will not be considered in this thesis. Since the shear force occurs in two directions for slabs it is rather complex and will not be treated further in this thesis.

2.2.3 Plastic rotation capacity

Reinforced concrete members have a limited plastic rotation capacity. Therefore, the predicted failure mechanism may not occur if sufficient rotation at a plastic hinge cannot develop and the member may consequently fail before the full mechanism is developed. Experiments of plastic rotation capacity may show low accuracy with theoretical models (Johansson and Laine, 2009). Several methods exist for calculating the rotational capacity, giving varying results. One potential source of the difference in results is that steel properties have changed significantly over the last decades, Johansson (1997). The method used in Eurocode 2 can be used to estimate a conservative value of the maximum allowed rotation. The method uses a diagram taking concrete strength, reinforcement class and the ratio between the compressed zone and the effective depth into account, see Figure 2.17.

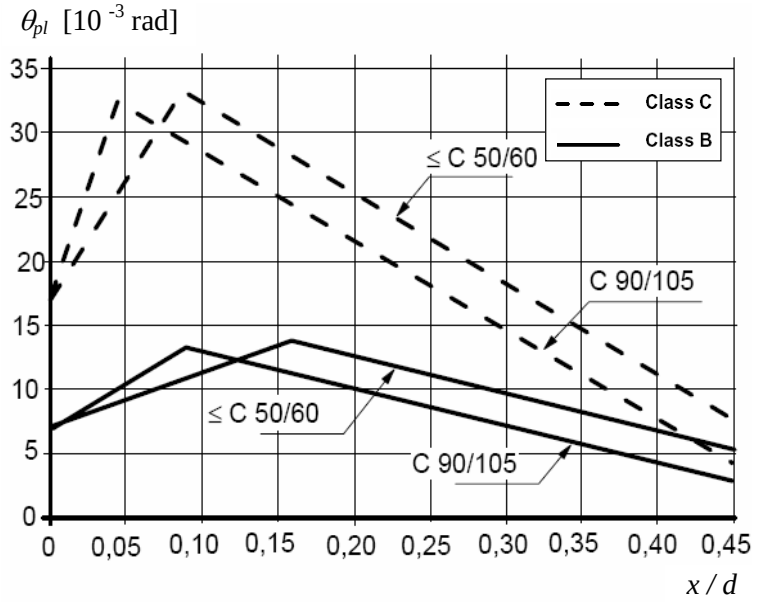

Figure 2.17. Diagram for evaluating the plastic rotation capacity according to Eurocode 2, CEN (2004).

For low values of the ratio between compressed zone height and the effective depth the limitation will be governed by the ultimate steel strain. Concrete crushing strain will govern the limitation for higher ratios. For higher values of the ratio than shown in the diagram, a sudden abrupt failure will occur.

2.3 Simplified material behaviour

2.3.1 Introduction

As realised in Section 2.2, reinforced concrete is a complex material. Therefore it can be preferable to simplify the behaviour. Three simplified models are used in this thesis to describe the behaviour of reinforced concrete: linear elastic, plastic and elasto-plastic. The response of these models often gives a reasonably accurate result but is seen as potential sources of error in previous Master's theses, Augustsson and Härenstam (2010), Nyström (2006) and Ek and Mattsson (2009). This thesis intended to in addition to analyses with simplified material behaviour also model the material's non-linear behaviour, explicitly taking reinforcement yielding and cracking of concrete into account. This model was never completed but is documented in Appendix I.

2.3.2 Linear elastic

The simplest way to model the material behaviour is to model it as a linear elastic material. By doing so, no permanent deformations will remain after unloading and the stress strain relationship will be linear as shown in Figure 2.18. From Hooke's law, a force-displacement relationship can be determined as

$$R = k \cdot u \tag{2-1}$$

where the internal resistance force is denoted *R*, the stiffness k and the displacement *u*. The stiffness can be found for any structure by relating the deformation to the load instead of moment to curvature.

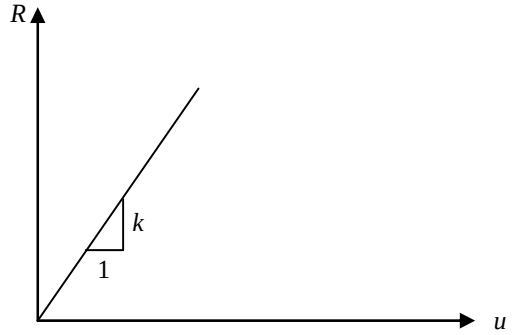

Figure 2.18. Linear elastic force-displacement relationship.

2.3.3 Ideal plastic

When modelling the material with ideal plastic behaviour, the deformations are zero if the stress in the material is kept below the yield stress. It also means that the material cannot take higher stresses than the yield stress. As soon as the yield stress is reached it will start to deform, where the limit of this deformation is in theory infinitely large. However, the deformation is in practice limited by the plastic rotation capacity. The ideal plastic force-displacement relationship is illustrated in Figure 2.19. R_m is the internal resistance force corresponding to the yield stress.

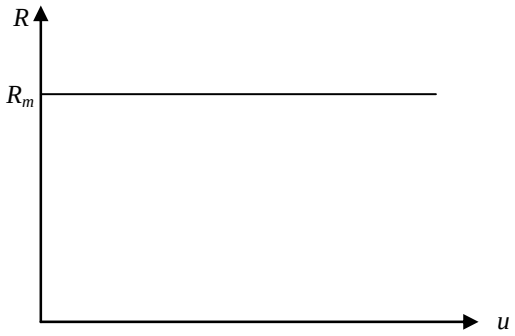

Figure 2.19. Ideal plastic force-displacement relationship.

The relationship can be described with equation (2-2) where F denotes the external force and u the displacement.

$$R = \begin{cases} F & \text{for } F < R_m \text{ and } u = 0 \\ R_m & \text{for } F \geq R_m \text{ or } u \neq 0 \end{cases} \tag{2-2}$$

2.3.4 Elasto-plastic

The simplified elasto-plastic material behaviour is constructed by combining the simplified elastic and ideal plastic material responses described in Section 2.3.2 and Section 2.3.3 respectively. Thus, a force-displacement relationship can be obtained, see Figure 2.20a. Initially, as the load increases the material response has elastic behaviour until the material reaches the yield limit. The elastic deformation is completely reversible. When the limit is reached, the material cannot take more stress and permanently deforms. Therefore, it can be modelled with the ideal plastic behaviour. If the structure is unloaded when permanent deformations has developed, the unloading curve will be parallel to the elastic curve and when it is loaded again the plastic deformations will take place where it last ended, see Figure 2.20b.

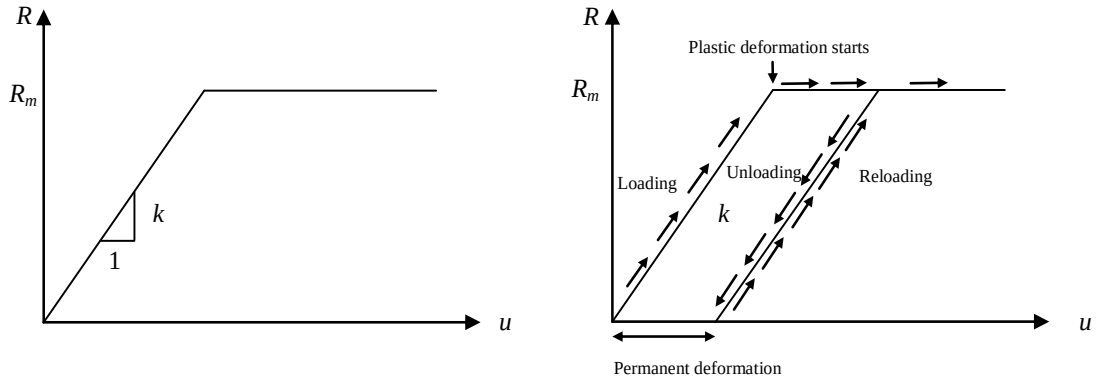

Figure 2.20. Elasto-plastic (a) force-displacement relationship (b) response while loading, unloading and reloading.

The elasto-plastic relationship can be written as

$$R = \begin{cases} k \cdot u_{el} & \text{for } F < R_m \\ R_m & \text{for } F \geq R_m \end{cases} \tag{2-3}$$

2.4 Impulse loaded systems

2.4.1 Definitions of dynamic parameters

2.4.1.1 Force

According to Newton's second law, force F is defined as the product of mass m and acceleration a.

$$F = ma \tag{2-4}$$

The force is defined as positive in the direction the acceleration is taking place. It can also be recognised that if the mass is increased, the acceleration response due to a force F will decrease.

2.4.1.2 Pressure

Pressure P is defined as a force F acting on an area A.

$$P = \frac{F}{A} \tag{2-5}$$

2.4.1.3 Momentum and Impulse

A body with mass m and velocity v has, per definition, a momentum p.

$$p = mv \tag{2-6}$$

When an external force acts on a body, the body will gain or lose momentum Δp. This change in momentum is defined as the impulse. If a body is subjected to a positive force F from time t_0 to t_1, the velocity will increase and the momentum will increase to p_1. The new momentum can be calculated by using Newton's second law

$$p_1 = mv + \int_{t_0}^{t_1} F(t)\, dt \tag{2-7}$$

where the right expression is the generated impulse I from a force.

$$I = \int_{t_0}^{t_1} F(t)\, dt \tag{2-8}$$

This represents the area under the force-time graph. The shock wave from an explosion is measured in pressure, which is a measurement of force acting on an area. Therefore, the impulse can also be written as

$$I = A \cdot \int_{t_0}^{t_1} P(t)\, dt \tag{2-9}$$

The area under the pressure-time graph is sometimes referred to as the impulse intensity *i*, transferred to the body indicated in Figure 2.21.

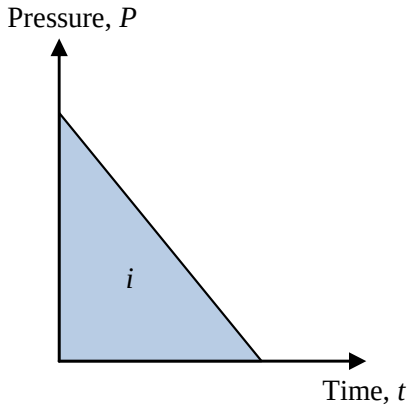

Figure 2.21. Simplified pressure-time curve.

There are two extreme values of an impulse: infinitely high pressure for an infinitesimally short time and lower pressure for an infinitely long time, see Figure 2.22. The latter is more similar to a static load. A real impulse load will be somewhere in between. The infinitely high pressure during a very short time is called the characteristic impulse.

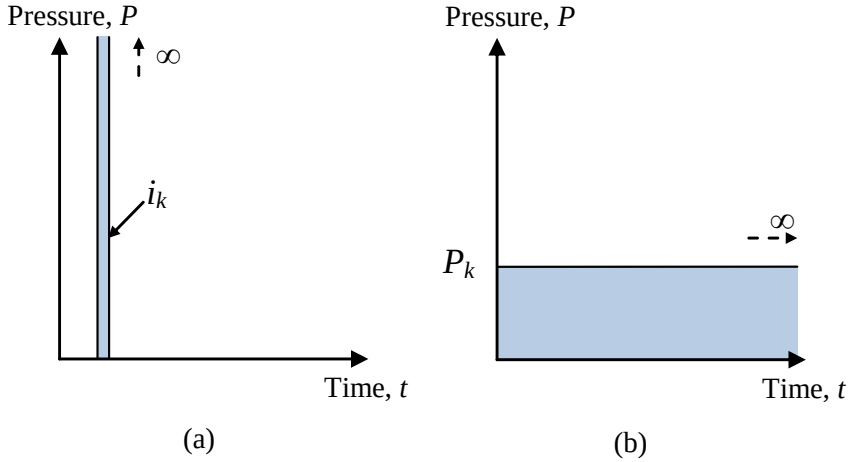

Figure 2.22. Two extreme cases of the pressure impulse: a) Characteristic impulse and b) pressure load.

The response to a more general impulse can be explained by using damage curves. Those are curves that show the same damage for different combinations of forces and impulses. The concept of damage curves are further discussed and presented in Section 2.4.2.7. The characteristic impulse will be used in this thesis to estimate a response on the safe side when estimating the external work done.

2.4.1.4 Work

Work equilibrium is a well-established method for analysing the response of a structure subjected to an external force. It relies on the law of energy conservation, which says that no energy can disappear, just transform. If a force acts on a structure the resulting work must be converted into kinetic or potential energy within the structure. Therefore, the method puts the external work W_e, caused by the external load, equal to the internal work W_i made by the structure; i.e.

$$W_e = W_i \tag{2-10}$$

The external work is force times distance, for example a force that moves an object. It can also be an impact where kinetic energy is transferred into potential energy. This is more similar to an explosion, where an impulse load strikes a structure and causes it to absorb energy by deforming. A characteristic impulse has a very short duration and the external energy can therefore be assumed to be the kinetic energy of the structure. This means that no energy is resisted as internal work. As soon as the impulse acts for a longer time, the structure will absorb some of the energy and the external work done will be smaller than for the characteristic impulse. The kinetic energy for a body with mass m is

$$E_k = \frac{mv^2}{2} \tag{2-11}$$

where v is the velocity of the body. By using equation (2-6) and assuming a characteristic impulse load, the external work can be described by the kinetic energy of the impulse as

$$W_e = E_k = \frac{I_k^2}{2m} \tag{2-12}$$

Energy is absorbed in the structure by deformation. Consequently, the stiffness of the structure and its ability to deform is important for the final response. As described in Section 2.3, three idealisations of materials are used. They will behave slightly different, and the internal work will be:

Elastic $$W_i = \frac{ku_{el}^2}{2} \tag{2-13}$$

Plastic $$W_i = Ru_{pl} \tag{2-14}$$

Elasto – plastic $$W_i = \frac{ku_{ep,el}^2}{2} + R_m u_{ep,pl} \tag{2-15}$$

The internal work can be interpreted as the area under the force-displacement curves shown in Figure 2.23.

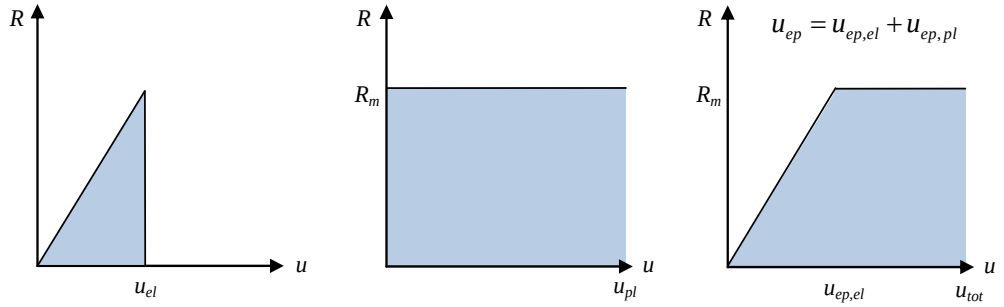

(a) (b) (c)

Figure 2.23. Three different idealised material relations; linear elastic, ideal plastic and elasto-plastic.

The maximum deformation can later be found from the work equilibrium equation (2-10). The deformation in the elasto-plastic model will follow the equation (2-13) until the reaction force reaches the yield reaction when the total deformation needs to be considered.

$$u_{el} = \frac{I_c}{m\omega} \qquad \text{where} \quad \omega = \sqrt{\frac{k}{m}} \tag{2-16}$$

$$u_{pl} = \frac{I_c^2}{2mR_m} \tag{2-17}$$

$$u_{ep} = u_{ep,pl} + u_{ep,el} = \left(u_{pl} - \frac{u_{ep,el}}{2} \right) + u_{ep,el} = \frac{I_c^2}{2mR_m} + \frac{R_m}{2k} \quad \text{if} \quad u_{tot} > u_{ep,el} \tag{2-18}$$

It is most often preferable to use a ductile material in extreme load situations, as long as the obtained displacement can be allowed. The ductile material will deform and dissipate more energy. The structure will be damaged through plastic deformation and will require reparation. However, this can be overlooked as long as safety is guaranteed for involved functions and people. To avoid total collapse and ensure safety, the deformation of columns for example must be limited so that they do not fail through second order effects.

2.4.1.5 Strain rate

The closer a structure is to an explosion, the higher the amplitude and the shorter the duration of the load. Consequently, structures close to an explosion may be subjected to a very intense, impulsive load. In this case the structural response differs considerably to a static load response; the design approach must therefore also differ. The loading from an explosion can be up to 100 million times faster than a static load. The high velocity of an explosion load results in a very high strain rate compared to a case with static loading. For static loading the value of strain rate is around 10^{-5} s^{-1} and for blast loading somewhere between 10^{2} s^{-1} and 10^{3} s^{-1} as illustrated in Figure 2.24.

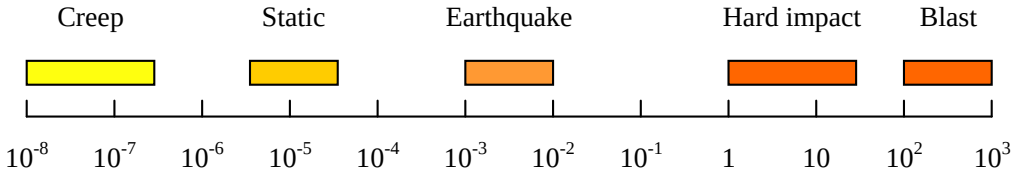

Figure 2.24. Approximate strain rates for different loadings, based on Johansson (2000).

A change of strain rate can also result in a change of properties for the material. It is known that the mechanical properties of concrete are affected by the rate of loading. Much research has been done on this subject in order to establish a relationship for the Dynamic Increase Factor (DIF), which is the ratio between static strength and dynamic strength. These studies show that the increased strain rate also results in an increased material strength, as shown in Figure 2.25. The value of the DIF differs a lot between tensile and compressive strength and it is also hard to evaluate the different test results that cause a large scatter.

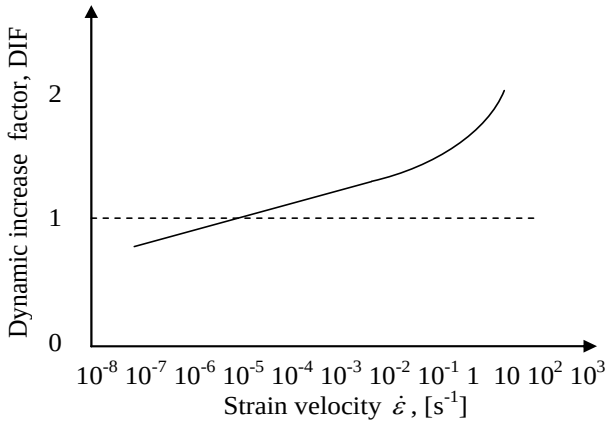

Figure 2.25. An approximated relationship between the dynamic magnification factor and the strain velocity for compressed concrete, based on Johansson (2000).

The effects due to the change in strain rate are divided into two main effects: viscous effects for lower strain rates and structural effects for higher strain rates. These effects are not discussed in here and for more information the reader is referred to Johansson (2000). The change of strain rate is also shown to affect the reinforcement steel, which results in some increase of yield and ultimate stress for higher strain rates. Strain rate is for example considered in the American design code, DoD (2008) but is neglected in this thesis.

2.4.1.6 Wave propagation

Explosions are rapid processes in which the whole structure may not be active. For instance, after an explosion the maximum moment in the front wall of a box structure can occur before any of the impacts are realised by the back wall. The information travels through a material as both a longitudinal and a transverse wave, see Figure 2.26. These are commonly referred to as pressure wave and shear waves. Shear waves cannot occur in liquids or gases and are weak in comparison to the pressure wave, Laine (2012).

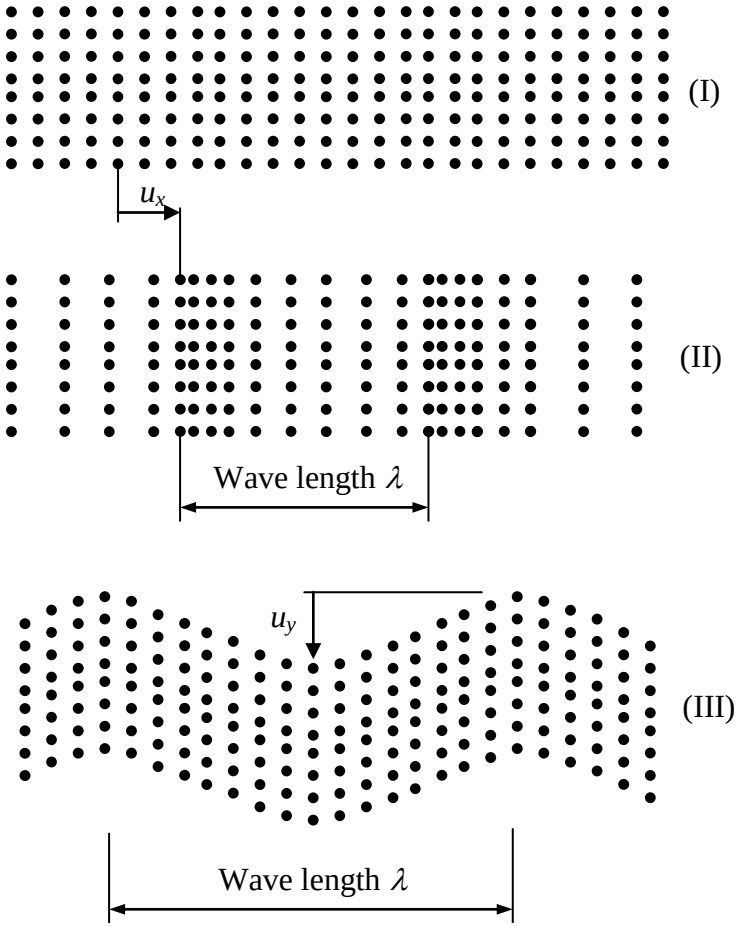

Figure 2.26. Waves through a specimen: (I) material at rest (II) pressure wave, (III) shear wave, Laine (2012).

According to Laine (2012) a pressure wave has the velocity

$$c_p = \sqrt{\frac{E}{\rho \cdot (1-\nu^2)}} \tag{2-19}$$

where E is the elastic modulus and ρ is the density of the material. This should be the case if an axial force acted on the beam. However, the information in a beam loaded perpendicularly to its longitudinal axis is more likely to be transferred by transverse waves to the support. The speed of a shear wave through a material depends on the material's shear modulus G, Laine (2012).

$$c_s = \sqrt{\frac{G}{\rho}} \tag{2-20}$$

where, the shear modulus can be written as

$$G = \frac{E}{2(1+\nu)} \tag{2-21}$$

2.4.2 Equivalent SDOF system

2.4.2.1 Introduction

A single degree of freedom system, abbreviated SDOF, is a convenient model to use when analysing dynamically loaded systems. It consists of a body with the mass *m* and a spring with stiffness *k*, see Figure 2.27. The body is only free to move in one direction and the position can be described with one coordinate, Biggs (1964). This body is also considered completely rigid with no internal movement within. In reality vibrations of a system will always have some damping from internal friction forces for example. Therefore, the mass-spring system is often complemented with a damper *c*, which will decrease the amplitude for every oscillation.

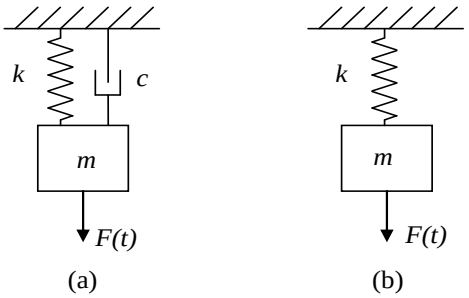

Figure 2.27. Forced SDOF-systems: a) damped b) undamped.

The SDOF system can either vibrate freely or be forced by a time-dependent force. If the system is subjected to explosion loading, it is initially forced to deform for a very short time. After a short time the external force will disappear and the behaviour is better represented by a freely vibrating system. Although the shock wave forces the system to deform during the first milliseconds, the maximum displacement and section forces can often occur much later. This depends on the load and the properties of the structure.

The maximum displacement is of interest and they occur very soon after the load arrival. The effect of damping will be low on the first oscillation, where the maximum displacement normally occurs but affects the later oscillations more. Therefore, it is not necessary to include dampers when considering maximum displacement as a result of explosion loads, Johansson and Laine (2009). However, it is important to realise that dampers should be included if the continuing state of vibration is to be considered. In a real structure it is not likely that the maximum values occur after the first oscillation. With that in mind, damping effect is mainly neglected in this thesis apart from in the theory section for comprehensiveness.

2.4.2.2 Equation of motion

If a forced damped SDOF system is considered, it is recognised that the displacement and velocity will create resisting forces from the damper and the spring. If the body is accelerating it will have an inertia force in the accelerating direction according to Newton's second law.

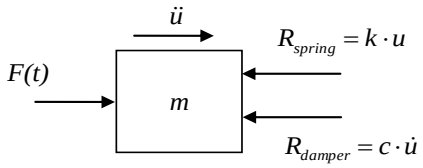

Figure 2.28. Free body diagram of a SDOF-system.

As velocity and acceleration are the derivative and second derivative, respectively, of the displacement with respect to time, the equation of motion can be found as,

$$m\ddot{u} + c\dot{u} + ku = F(t) \tag{2-22}$$

from established force equilibrium.

2.4.2.3 Transformation into an equivalent SDOF-model

A structure has multiple degrees of freedom (MDOF) but it can be turned into an SDOF system by choosing a "system point" and applying an equivalent mass, a damper and a resisting force Biggs (1964). The system point is often chosen as the centre point or the point where the displacement is largest, Johansson and Laine (2009). The relation between the parameters in the equivalent SDOF system and in the MDOF system can be described with transformation factors.

Transformation factors are derived from an assumed deformation shape *u(x)*, Johansson and Laine (2009). They must be chosen with regard to support conditions, stiffness distribution, load profile and material model. Therefore, advanced analytical solutions may be necessary for complex loading cases and when the stiffness distribution varies. Since the factors are directly influenced by the assumed deformation shape, they must be individually derived for every structural element and load condition.

Since the damping effect is neglected, see Section 2.4.2.1, three transformation factors are of interest when converting a structural element into an equivalent SDOF system for impulse loading. They are denoted with a κ with index to the parameter they affect

$$m_e = \kappa_m m \tag{2-23}$$

$$k_e = \kappa_k k \tag{2-24}$$

$$F_e = \kappa_F F \tag{2-25}$$

Where letters without index are the structural elements real mass, stiffness and force respectively and index *e* stands for equivalent parameters in the SDOF-system. By considering energy conservation for the structural element and the corresponding equivalent SDOF the factors can be derived. κ_m comes from the conservation of

kinetic energy, κ_k comes from conservation of internal energy and κ_F from conservation of external energy. According to Biggs (1964) the transformation factors for internal and external energy are equal, i.e.

$$\kappa_k = \kappa_F \tag{2-26}$$

The transformation factors can be found from,

$$\kappa_m = \frac{1}{L}\int_{x=0}^{x=L} \frac{u(x)^2}{u_s^2}\,dx \tag{2-27}$$

$$\kappa_F = \frac{1}{L}\int_{x=0}^{x=L} \frac{u(x)}{u_s}\,dx \tag{2-28}$$

the derivation is shown in e.g. Johansson and Laine (2009). By implementing (2-26) in equation (2-22), the equation of motion for a structural element can be written as

$$\kappa_{mF} m\ddot{u} + c\dot{u} + ku = F(t) \tag{2-29}$$

where

$$\kappa_{mF} = \frac{\kappa_m}{\kappa_F} \tag{2-30}$$

Values of these transformation factors for some different load cases and material models for beams and slabs can be seen in Table 2.1, Table 2.2 and Table 2.3.

Table 2.1. Transformation factors for a beam subjected to a point load. From Johansson and Laine (2009).

	Point load on beam element			
	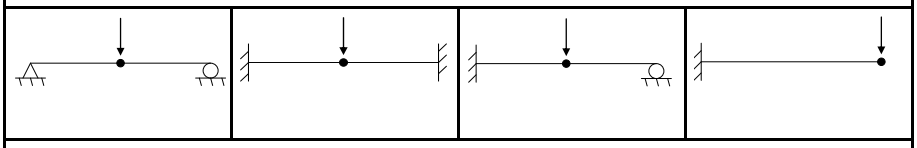			
	Elastic deformation curve			
κ_M	0.486	0.371	0.445	0.236
κ_F	1.000	1.000	1.000	1.000
κ_{MF}	0.486	0.371	0.446	0.236
	Plastic deformation curve			
κ_M	0.333	0.333	0.333	0.333
κ_F	1.000	1.000	1.000	1.000
κ_{MF}	0.333	0.333	0.333	0.333

Table 2.2. Transformation factors for a beam subjected to uniform load. From Johansson and Laine (2009).

	Uniformly distributed load on beam element			
	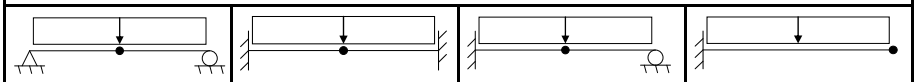			
	Elastic deformation curve			
κ_M	0.504	0.406	0.483	0.257
κ_F	0.640	0.533	0.600	0.400
κ_{MF}	0.788	0.762	0.805	0.642
	Plastic deformation curve			
κ_M	0.333	0.333	0.333	0.333
κ_F	0.500	0.500	0.500	0.500
κ_{MF}	0.667	0.667	0.667	0.667

Table 2.3. Transformation factors for a plate subjected to a uniformly distributed load, Based on Augustsson and Härenstam (2010).

	Uniformly distributed load on slab element	
	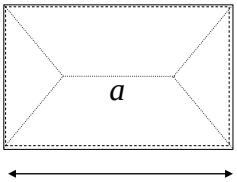	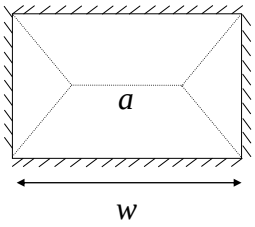
	Elastic deformation curve	
κ_M	0.250	
κ_F	$4/\pi^2$	
κ_{MF}	0.617	
	Plastic deformation curve	
κ_M	(1+a/w)/6	(1+a/w)/6
κ_F	(1+a/2w)/3	(1+a/2w)/3
κ_{MF}	(1+a/w)/(2+a/w)	(1+a/w)/(2+a/w)

The transformation factors have a good agreement with reality when an elastic response of the structure is assumed, see Augustsson and Härenstam (2010). In the aforementioned thesis, significant divergence between hand calculations and FE-analyses is found for beams assuming ideal plastic behaviour and for plates assuming both plastic and elasto-plastic behaviour. This is believed to be influenced by the assumption about constant deformation shape and the influence of multi-linear response in beams. Moreover, it recommends that more studies on these phenomena must be carried out. The problems with transformation factors are also addressed by further studies in Chapter 4.

2.4.2.4 Work

A system in motion is affected by external, internal and kinetic energy, which must always be in equilibrium. The transformation factors described in Section 2.4.2.3, relate the real energy in the system with the energy in an equivalent SDOF system.

$$W_k = \frac{\kappa_m m v_s^2}{2} \tag{2-31}$$

$$W_i = \kappa_F R u_s \tag{2-32}$$

$$W_e = \kappa_F F u_s \tag{2-33}$$

As shown in section 2.4.1.4, the external energy of a SDOF-system for an impulse load can be expressed as:

$$W_e^{SDOF} = W_k = \frac{I_k^2}{2m_e} \tag{2-34}$$

This assumes no energy is lost from deformation and that the work done by the external force is equal to the external all energy will become kinetic energy. The problematic part is deciding which mass should be used in equation (2-34). Johansson and Laine (2009) have used $m_e = \kappa_{mF} \cdot m$. This results in an equivalent SDOF energy, which will only be adequate if external and internal energy levels are compared in the SDOF system. However, if the SDOF energy is going to be compared with another analysis, it is necessary to consider equation of motion for the equivalent SDOF-system in its basic form when investigating and comparing energy levels with a FE-solution, i.e.

$$\kappa_m m\ddot{u} + \kappa_F k u = \kappa_F F \tag{2-35}$$

instead of using the simplified expression in equation (2-29). In order to derive the real work for an SDOF model, it is necessary to go back to the definition of impulse in Section 0.

$$I = \int_{t_0}^{t_1} F(t)dt = mv \tag{2-36}$$

For an equivalent SDOF-system this should be multiplied with the transformation factors, i.e.

$$I^{SDOF} = \kappa_F \int_{t_0}^{t_1} F(t)dt = \kappa_m m v_s \tag{2-37}$$

A characteristic impulse means that

$$I_k = \int_{t_0}^{t_1} F(t)dt = i \cdot b \cdot l \tag{2-38}$$

and hence, the momentum for the equivalent mass in the SDOF-system can be expressed as

$$\kappa_m m v_s = \kappa_F I_k \tag{2-39}$$

and the square of the midpoint velocity can be obtained as

$$v_s^2 = \left(\frac{\kappa_F I_k}{\kappa_m m} \right)^2 \tag{2-40}$$

If this is inserted into equation (2-31) the kinetic energy becomes

$$E_k = \frac{I_k^2}{2\kappa_m m} \kappa_F^2 = \frac{I_k^2}{2\kappa_{mF} m} \kappa_F \tag{2-41}$$

If this is compared with the expression used by Johansson and Laine (2009), it can be seen that the additional term κ_F is not considered and that it would result in a too high energy since $\kappa_F < 1.0$. Moreover, the internal work is also overestimated since a transformation factor is only used on the kinetic energy.

Calculating the energy incorrectly will not affect the energy balance nor the resulting displacement since the transformation factor for the load cancels out when considering the individual parts of the equation of motion, i.e.

$$E_k = \frac{I_k^2}{2\kappa_{mF} m} \kappa_F = \kappa_F \frac{ku^2}{2} = W_i \tag{2-42}$$

Nevertheless, if the absolute energy in a FE-analysis and an equivalent SDOF-system is compared it is necessary to calculate the external and internal energy as shown in equation (2-41) and (2-42).

2.4.2.5 Dynamic reaction

In order to determine the maximum shear forces in the system it is of interest to determine the dynamic reaction force at the supports. The equivalent SDOF-system is modelled to have the same displacement as the system point in the real system, but the internal reaction force in the SDOF-system is not necessarily the same as the real reaction force. In order to obtain this reaction, it is necessary to set up a dynamic equilibrium where the inertia force *I(t)* is considered in the calculations. The inertia force has the same shape as the assumed deflection shape of the structure. The magnitude and the position of the resultant of the inertia force can be determined, as shown in Appendix B.2. Moment equilibrium can be established around the resultant and an expression for the dynamic reaction can be obtained. In Biggs (1964) this dynamic reaction is solved for beams and two-way slabs with different kinds of boundary conditions and load cases for both elastic and plastic analysis. The data is then presented in tables.

For clarification, an example of a simply supported beam with evenly distributed load can be studied, see Figure 2.29a. To establish dynamic equilibrium, half of the beam is considered as shown in Figure 2.29b. It is known that in the middle of the beam the shear force *S* is equal to zero and the dynamic bending moment can be expressed in terms of the resistance *R* as:

$$m_f = \frac{RL}{8} \tag{2-43}$$

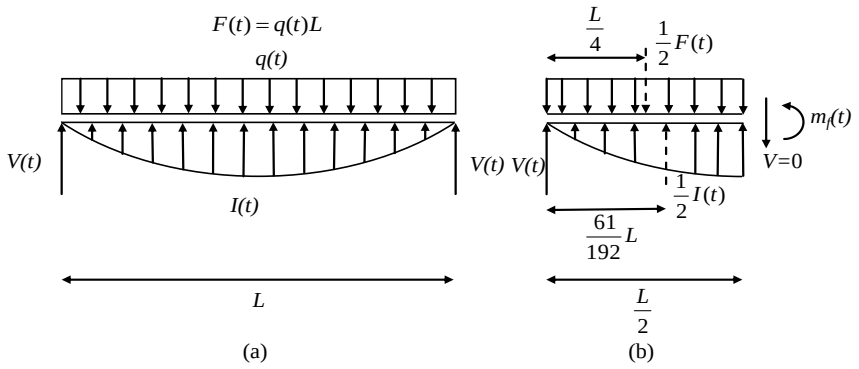

Figure 2.29. Determination of dynamic reactions. Based on Biggs (1964).

As mentioned above, the distribution of the inertia force corresponds to the assumed deflection shape which is used to determine the position of the resultant. For a simply supported beam with an evenly distributed load, this shape can be expressed as:

$$\Phi(x) = \frac{16}{5L^2}\left(L^3 x - 2Lx^3 + x^4\right) \tag{2-44}$$

When the position of the resultant is known, see Appendix B.2, moment equilibrium is established around the resultant of the inertia force and the following expression is obtained:

$$V \cdot \frac{61}{192}L - m_c - \frac{1}{2}\left(\frac{61}{192}L - \frac{1}{4}L\right) = 0 \tag{2-45}$$

Equation (2-45) is then solved for V with help of the expression for the dynamic bending moment and an expression for the dynamic reaction in terms of load and resistance is obtained, see Equation (2-46).

$$V = 0.39R + 0.11F \tag{2-46}$$

Both R and F in this case are functions of time but this equation must also be valid for a static case where the shear force V should be equal to $0.5F$. If equation (2-46) is studied and the fact that $R=F$ in case of static loading, it can be seen that this equation also holds for this case.

The same procedure can be performed for various support conditions for plastic and elastic cases. These are tabulated in Biggs (1964). The dynamic reaction for a simply supported beam with ideal plastic behaviour can be written as

$$V = 0.38R + 0.12F \tag{2-47}$$

Fortifikationsverket (2011) has derived an expression, shown in Appendix B.1, for the reaction force at the support for a simply supported beam as

$$V = \frac{1}{2}\left[\left(1 - \frac{\kappa_F^2}{\kappa_m}\right)F + \frac{\kappa_F^2}{\kappa_m}R\right] \tag{2-48}$$

where κ_F and κ_m are the transformation factors for force and mass respectively. This method is very similar to that of Biggs (1964)

$$\kappa_F = 0.640 \qquad \kappa_m = 0.504$$

$$V = \frac{1}{2}\left[\left(1-\frac{\kappa_F^2}{\kappa_m}\right)F + \frac{\kappa_F^2}{\kappa_m}R\right] = 0.094F + 0.406R \tag{2-49}$$

and for the plastic case

$$\kappa_F = 0.500 \qquad \kappa_m = 0.333$$

$$V = \frac{1}{2}\left[\left(1-\frac{\kappa_F^2}{\kappa_m}\right)F + \frac{\kappa_F^2}{\kappa_m}R\right] = 0.125F + 0.375R \tag{2-50}$$

However, an advantage of Fortifikationsverket's approach is that it lets the designer use a varying deformation shape by assuming the transformation factors over time and hence the position of the resultant may not have to be calculated for all displacement shapes that might occur. It is also clearer what actually affects the support reaction and will therefore also be used in this thesis.

2.4.2.6 Equivalent static load

A dynamic load can be translated into an equivalent static load in order to make it more convenient to calculate section forces. Moreover, designers are generally more familiar with static loads. The corresponding static load is obtained by deciding the load that generates the same external work as the impulse load. In line with definitions of internal work, Section 2.4.1.4, different expressions will be obtained depending on which material response is assumed. The equivalent static load corresponds to the response that is obtained when the maximal deformation is obtained and consequently does not follow the behaviour up to that point. The equivalent static load can be written as

$$Q_{el} = I_k\omega \qquad \text{where} \qquad \omega = \sqrt{\frac{k}{m}} \tag{2-51}$$

$$Q_{pl} = \frac{I_k^2}{2mu_{pl}} \tag{2-52}$$

for elastic and plastic response respectively, Johansson and Laine (2009). I_k is the characteristic impulse, m is the mass, k is the stiffness and u_{pl} is the plastic displacement. This corresponds to the ultimate resistance in the structure i.e.

$$Q_{el} = ku_{el} \tag{2-53}$$

$$Q_{pl} = R_m \tag{2-54}$$

When the equivalent static load is established it can be applied on the structure and the moment and shear force distributions can be found. The static equilibrium calculations mean that the reaction forces on the system are not governed by the same parameters as the normal static approach. This gives the reaction force in the support as

$$V_{el} = \frac{Q_{el}}{2} = \frac{ku_{el}}{2} \tag{2-55}$$

$$V_{pl} = \frac{Q_{pl}}{2} = \frac{R_m}{2} \tag{2-56}$$

And bending moment in the centre as

$$M_{f,el} = \frac{Q_{el}L}{8} = \frac{ku_{el}L}{8} \tag{2-57}$$

$$M_{f,pl} = \frac{Q_{pl}L}{8} = \frac{R_mL}{8} \tag{2-58}$$

The dynamic bending moment is the same as derived in Biggs (1964). However, the support reaction is higher according to this method once the positive phase of the pressure wave has passed i.e. $F = 0$. Moreover, the equivalent static load does not take the early shear force resulting from the inertia forces into account as Biggs' and Fortifikationsverket's approaches do, Section 2.4.2.5. Johansson and Laine (2009) explain that high shear forces can initially occur close to the supports and that these must be further investigated. This statement refers to this phenomenon of initial high shear forces.

Since the plastic equivalent load is governed by the plastic deformation, an upper limit to the displacement must be introduced and will consequently be the failure criterion. The possibility of large rotational deformations will decrease the needed equivalent static load and hence the reaction forces, Johansson and Laine (2009). The elastic approach is rather straight forward as the moment and shear capacities are compared with the maximum load effect. However, the maximum section forces in a linear elastic analysis do not depend on the parameters taken into account in a static analysis. The maximum field moment in a simply supported structure with elastic response can be calculated as

$$M_{f,el} = \frac{Q_{el}L}{8} = \frac{I_k\omega L}{8} = \frac{i \cdot L^2}{8}\sqrt{\frac{k}{m}} \tag{2-59}$$

For a rectangular section the stiffness for an equivalent SDOF system can be written

$$k = \kappa_F \frac{384EI}{5L^3} = \kappa_F \frac{384Ebh^3}{60L^3} \tag{2-60}$$

And the mass for the equivalent SDOF model is

$$m = \kappa_m \rho \cdot b \cdot h \cdot L \tag{2-61}$$

The maximum field moment can therefore be calculated to

$$M_{f,el} = \frac{i \cdot L^2}{8} \sqrt{\frac{384Ebh^3}{60\kappa_{mF}\rho bhL^4}} = \frac{i \cdot h}{\sqrt{10}} \sqrt{\frac{E}{\kappa_{mF}\rho}} \tag{2-62}$$

This shows that the maximum field moment in a structure with elastic response is independent of the length.

2.4.2.7 Iso-damage curves

The worst case scenarios are defined by extreme cases and these are often used for design. The two extreme cases for an impulse load are described in Section 0, which are infinitely high pressure with infinitesimally short duration or a low pressure for an infinitely long duration. The response to a more general load, as seen in Figure 2.30, can be obtained by using iso-damage curves. These are curves that show the structural response to different combinations of pressure and impulse. The curve defines the combination of pressure and impulse that will cause a certain deformation, which can later be used to investigate if the structure will fail. As long as the actual pressure and impulse is lower than the limiting line, no failure is expected.

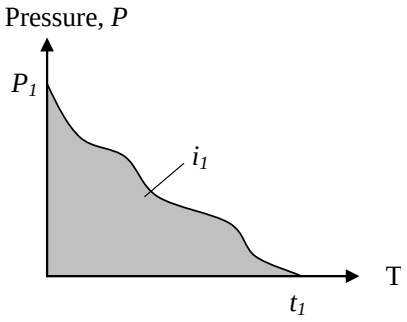

Figure 2.30. A general pressure-time curve.

An iso-damage curve can be found by solving the equation of motion for different load cases and thereby obtain a failure line for any combination of pressure and impulse. As a consequence, the shape of the curve is dependent on the material resistance and the load shape. Iso-damage curves are constructed by e.g. Nyström (2006) and Johansson and Laine (2009), the reader is referred to those for more information. The general appearance of iso-damage curves for different load shapes are shown in Figure 2.31. It is often convenient to express pressure and impulse with ratios between the actual peak pressure and impulse intensity and their characteristic values.

$$\gamma_I = \frac{i_1}{i_k} \tag{2-63}$$

$$\gamma_F = \frac{P_1}{P_k} \tag{2-64}$$

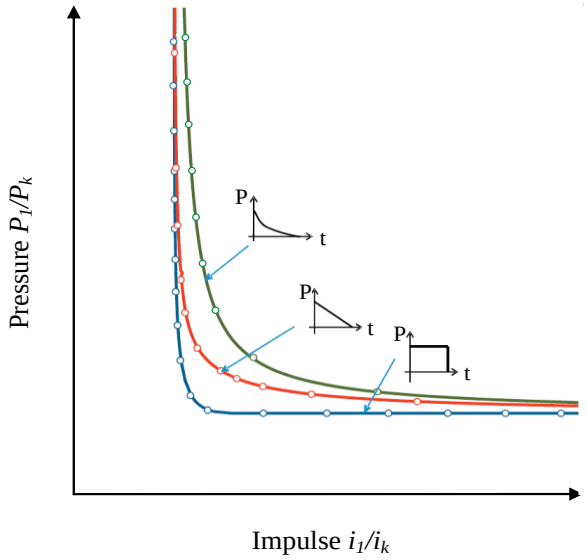

Figure 2.31. Iso-damage curves for 3 load shapes. Based on Krauthammer et. al. (2008)

In many cases it is adequate to use the characteristic impulse. Johansson and Laine (2009) give an estimation of how large the error will be when using the characteristic impulse compared to the real load. This is in an elastic case a function of the structural period T and the load duration t_1, see Table 2.4. The type of load curve is defined by n, which denotes the power of the load curve. γ_I is the ratio between the actual impulse and the characteristic impulse and γ_F is the ratio between peak force and the characteristic peak force as shown in equation (2-63) and (2-64). It means that if the ratio between the structural period and the load duration is higher than the number in the table, the percentage of difference in displacement shown in the left column can be expected. For plastic response, no structural period can be determined and the difference in displacement is only a function of γ_I and γ_F and is shown in Table 2.5.

Table 2.4. Displacement error for elastic response when using the characteristic impulse compared to the real load curve. From Johansson and Laine (2009).

δ_{el} [%]	γ_I [-]	$\frac{T}{t_1} = \frac{\gamma_F}{\gamma_I}$ $n = 0$	$\frac{T}{t_1} = \frac{1}{2}\frac{\gamma_F}{\gamma_I}$ $n = 1$	$\frac{T}{t_1} = \frac{1}{3}\frac{\gamma_F}{\gamma_I}$ $n = 2$
1	1.01	12.89	10.60	8.84
2	1.02	9.22	7.45	6.13
3	1.03	7.51	6.10	5.00
4	1.04	6.52	5.33	4.35
5	1.05	5.86	4.75	3.90
10	1.10	4.20	3.41	2.78
15	1.15	3.48	2.82	2.29
20	1.20	3.06	2.47	1.98
25	1.25	2.78	2.23	1.77
50	1.50	2.10	1.56	1.18
75	1.75	1.80	1.23	0.91
100	2.00	1.57	1.02	0.74

Table 2.5. Displacement error for plastic response when using the characteristic impulse compared to the real load curve. From Johansson and Laine (2009).

δ_{pl} [%]	γ_I [-]	γ_F [-] $n = 0$	γ_F [-] $n = 1$	γ_F [-] $n = 2$
1	1.005	100	-	-
2	1.010	52	70	77
3	1.015	35	46	52
4	1.020	27	35	39
5	1.025	21	29	32
10	1.049	11	15	17
15	1.072	7.7	10	12
20	1.095	6.0	8.0	9.0
25	1.118	5.0	6.7	7.5
50	1.225	3.0	4.0	4.5
75	1.323	2.3	3.1	3.5
100	1.414	2.0	2.7	3.0

In general, it is likely that the structure has more than one failure mode with another governing equation of motion, Krauthammer *et al*. (2008). This can be incorporated in the diagram easily. The structure's damage curve will then be a threshold curve of the lower values as seen in Figure 2.32. Failure will occur in both failure modes if the combination of pressure and impulse is in the upper right quadrant. In the example given, failure in only mode 1 will occur for low impulses with high pressure while low pressure with long duration will cause the structure to fail in mode 2.

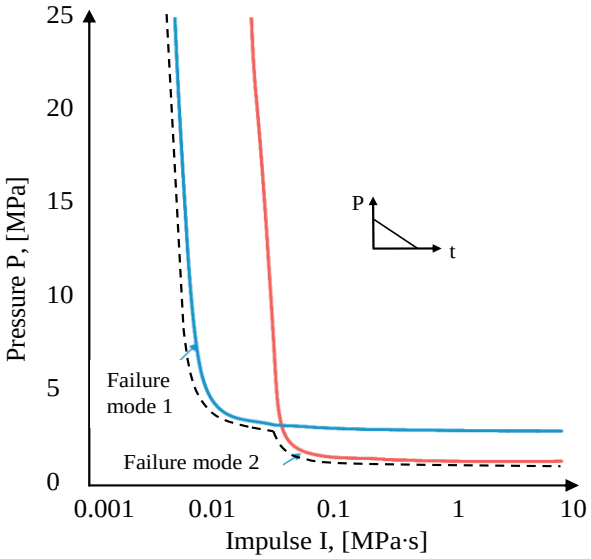

Figure 2.32. Iso-damage curves for two potential failure modes. The lower values of these will create a threshold curve indicated with a dotted line. Based on Krauthammer et al. (2008).

2.5 Direct shear

2.5.1 Static response

The direct shear phenomenon has been observed in static loadings with small shear span to effective depth, i.e. in deep members, Kriz and Raths (1965) as cited by Ross (1983). Direct shear can occur in areas with geometrical or load discontinuity, Crawford *et al.* (1999), tending to be brittle and to cause a sudden failure. It is a localised shear response of a structural concrete element characterised by cracking and slippage almost perpendicular to the longitudinal axis. Mattock and Hawkins (1972) gave a hypothesis of the phenomenon from experimental testing. Firstly, small inclined cracks develop along a shear plane, see Figure 2.33a. These cracks will define compression struts analogous to normal shear cracks but much smaller, both in length and width. The compression struts will carry the applied shear force by compression and transverse action since they are surrounded by uncracked concrete on both sides. Force equilibrium of such a strut can be established, as shown in Figure 2.33c, where V is the applied shear force, C is the compression component of the resistance, V' is the transverse resistance of the strut, T is the tension reinforcement force and N is a potential tensile normal force. As the load increases the struts will rotate and compress, creating a "slip" along the shear plane. Flexural reinforcement will be strained and work in dowel action when slip takes place. A consequence of the rotation is that the ends of the cracks will propagate vertically. A

failure plane can therefore either form in the shear plane or a plane parallel to the shear plane. Eventually, the concrete compression struts will fail in combined compression and shear action, and the reinforcement steel will yield, causing the whole section to shear off with a more or less vertical failure surface.

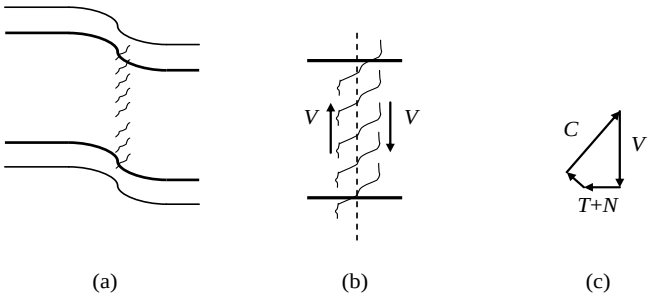

Figure 2.33. (a) Small diagonal cracks form along a shear plane. As they rotate, the cracks will propagate slightly vertically (b). Hence, the actual failure can occur in a parallel plane to the original shear plane. The resistance can be described with a strut and tie analogy (c), based on Mattock and Hawkins (1972).

Consequently, vertical stirrups will not contribute to the shear resistance except by confining the concrete and providing support for the flexural reinforcement which acts in dowel action.

Concrete shrinkage or accidental damage can cause a pre-existing crack through the depth of the member. The direct shear resistance will always be lower for a shear plane with an existing crack since the resistance is only governed by shear transfer along the cracks, aggregate interlocking and dowel action of the reinforcement, Mattock and Hawkins (1972). However, if the section is heavily reinforced, it will have a similar response to an initially uncracked section. In this thesis shrinkage of concrete will not be considered and the elements are assumed to be intact when loaded.

2.5.2 Dynamic response

Dynamic direct shear failures have been reported in experiments by Kieger *et al.* (1980-1984) and Slawson (1984), see Figure 2.34. These are observed close to the supports short after the arrival of the shock wave for highly impulsive loads. According to Low and Hao (2002) a high stiffness with a short span increases the risk for direct shear failure. It has also been shown that a load with high amplitude for a short duration increases the risk for direct shear failure. If the structure survives the direct shear mode, it will go into flexible mode. The early behaviour of a beam subjected to an impulse load must therefore be studied in order to explain what causes these types of failures.

Figure 2.34. Slab that has developed direct shear behaviour, Slawson (1984)

It has been shown in previous research (Slawson 1984; Kieger and Getchell 1980-1984; Johansson and Laine; 2009, Nyström, 2006; Augustsson and Härenstam; 2010) that the initial deformation shape for a structure subjected to blast loading is not the same as that predicted at maximum deformation. Within the first few milliseconds after load arrival the deformation shape is characterised by a nearly rigid body motion of the centre part of the element as shown in Figure 2.35. The un-deformed parts of the element close to the supports have not deformed as much, which creates a large difference in deformation over a small length. No flexible behaviour is observed in the early time span, which suggests that the direct shear failure mode and the flexible failure mode can be considered independent of one another.

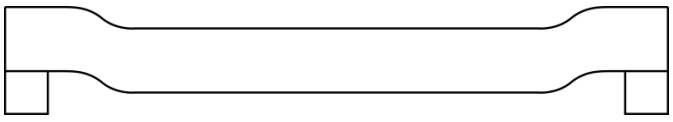

Figure 2.35. Research has indicated that a structural element subjected to an impulse load will initially deform as a rigid body motion.

The theory behind dynamic direct shear failure mode is not well understood. One possible reason of the early behaviour is explained by Ross (1983). He uses simple elastic wave propagation theory to explain reflections of the shock wave approaching the element, see Figure 2.36. After the wave has progressed through the depth of the member, it encounters a boundary between the edge and the air or supports. The wave is transmitted into the supports while it completely reflects at the edge of the beam in between the supports since the impedance of air is close to zero. As a result, the relative difference between the velocities will be twice the previous velocity, which will cause a velocity discontinuity close to the support, and therefore a high shear force.

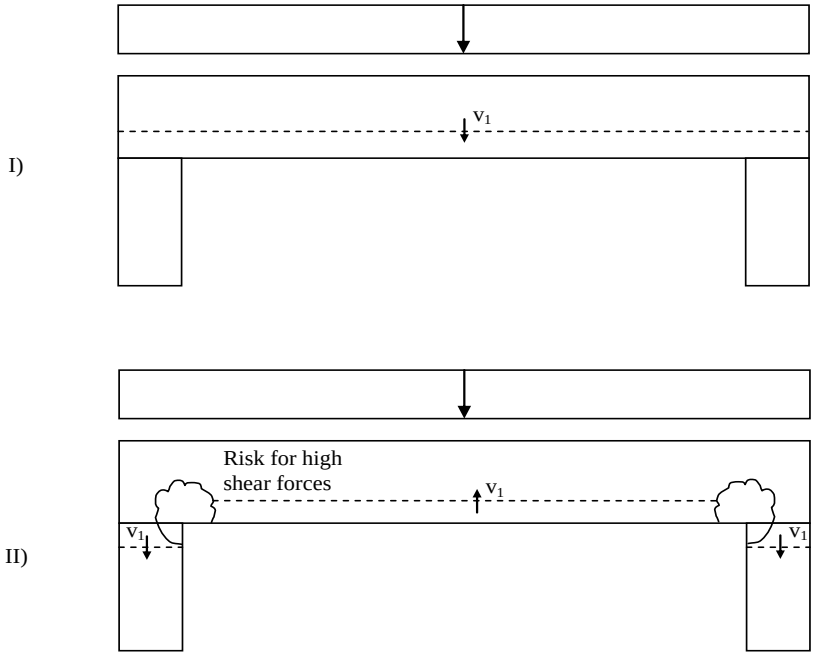

Figure 2.36. Ross (1983) explains the dynamic direct shear phenomenon with elastic wave theory in which the wave is transmitted at the supports and totally reflected in the centre. This generates a relative difference of double velocity in the centre part compared to the velocity at the supports.

Another way of explaining the early behaviour is made by Johansson and Laine (2009) and previous Master's theses; Nyström, (2006), Augustsson and Härenstam, (2010). They realise that the information of a load travels with an approximate velocity of 3500 m/s in concrete. As a result, the centre part will not be aware of the support conditions before information about this has reached them. The boundary conditions can therefore be seen as time dependent, where they are initially not active and later moves with the information speed in the structure. The governing speed should probably be the velocity of a shear wave.

Since the centre part moves much more and faster than the supports, a discontinuity region will occur close to the supports with very high shear inertia forces. These can be calculated with for example, Biggs (1964) or the equivalent static load concept described in Section 2.4.2.6. However, it is important to remember that these methods are only valid when the assumed deformation shape takes place.

Ardila-Geraldo (2010) stated that a structure will fail in shear if the shear demand is larger than the capacity. He investigated the actual shear demand at the supports by comparing with experiments and found that the support reaction can be found by varying the deformation shape and stiffness in an SDOF model. He derived an expression for the initial stiffness by taking the rigid body motion into account. This expression was later calibrated by FE analysis and experimental testing. He proposed that the stiffness should be taken as

$$k_e(t) = \begin{cases} 10 \cdot k_s \left(1 - 9\frac{t}{T}\right) & \text{if} \quad t < 0.1T \\ k_s & \text{if} \quad t \geq 0.1T \end{cases} \tag{2-65}$$

where T is the structural period and k_s is the theoretical bending stiffness assuming the elastic flexural displacement shape. The relationship is illustrated in Figure 2.37.

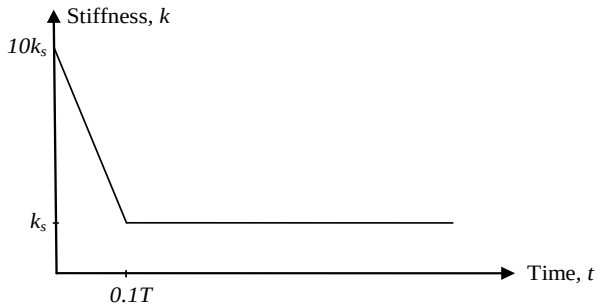

Figure 2.37. Stiffness variation derived by Ardila-Geraldo (2010), assuming a near rigid body motion.

The support reaction is then calculated with a modified Biggs equation

$$V(t) = \alpha F(t) + \beta R \tag{2-66}$$

where α and β have been calibrated from FE-analyses and

$$0.02 \leq \beta \leq 0.12 \qquad \text{when} \quad t \leq 0.1T \tag{2-67}$$

$$\alpha = 0.5 - \beta \tag{2-68}$$

It is important to find the correct initial reaction force at the supports in order to investigate the direct shear behaviour. Therefore a study on the shear force at early stages will be carried out in Chapter 6.

2.5.3 Simplified model for dynamic direct shear

An SDOF model can be used to explain the behaviour of direct shear analogously to the flexible case. The system point should be taken in a point very close to the supports. The shear force at the support should be evaluated and used in this model. This is done by using the flexible equation of motion, equation (2-29), and calculating the dynamic reaction force with Biggs', Fortifikationsverket's or the equivalent static load method, described in Sections 2.4.2.5 and 2.4.2.6. Since the direct shear happens very early, before any significant flexible behaviour, the flexible SDOF equation of motion and the direct shear equation of motion, equation (2-29) and (2-69) can be considered uncoupled.

The initial response when a structure is subjected to an explosion is a rigid body motion, which means that the transformation factors used to transform the structure to the single degree of freedom system is close to κ_{mF} = 1. The shear slip, Δ, at the

supports can then be calculated with the simplified equation of motion for the direct shear case, see Figure 2.38. As for the flexible case, damping is neglected.

$$M_s \cdot \ddot{\Delta} + R_s = V(t) \tag{2-69}$$

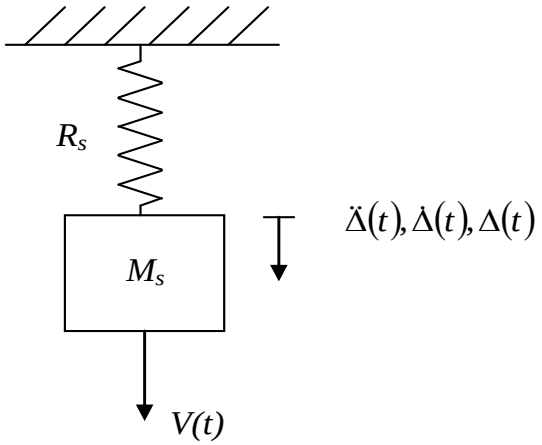

Figure 2.38. Equivalent SDOF-model for direct shear, based on Crawford et al., 1999). The stiffness R_s can be taken from the direct shear resistance function in Figure 2.39. Damping effects are neglected.

The resistance R_s is taken from the direct shear resistance function developed by Hawkins (1974). He used static tests to find a relationship between the shear slip and the shear stress. The relationship was later modified by Krauthammer (1986) in order to take rate effects and normal forces into account by applying a factor 1.4 to the relationship found by Hawkins. The relationship is shown in Figure 2.39 and is explained below. In this thesis, rate effects have been ignored to give results on the safe side.

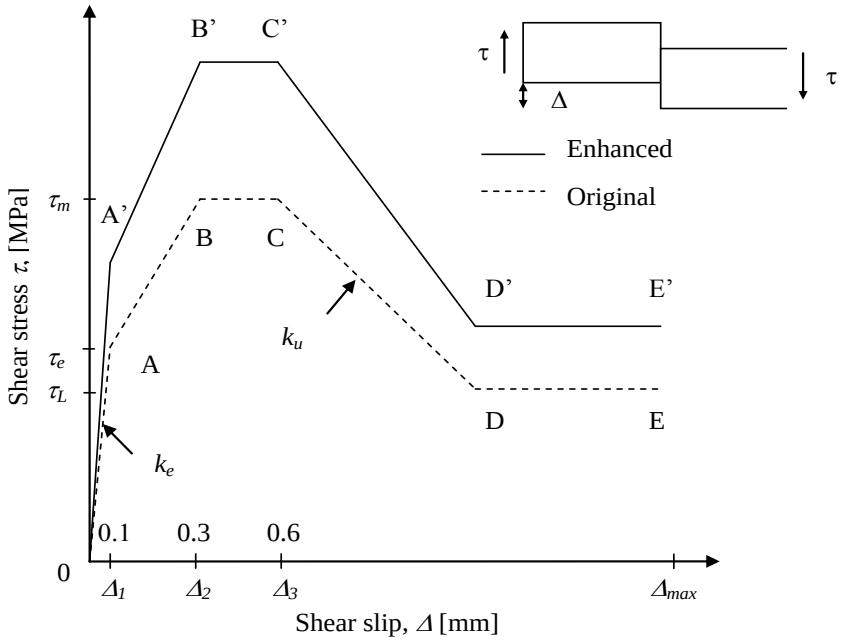

Figure 2.39. Shear resistance versus the slip along a shear plane. The enhanced curve takes strain rate and normal forces into account. Based on Mattock and Hawkins (1972) and later modified by Krauthammer (1986).

The resistance function is an empirical model based on static tests. The first segment from 0-A has an elastic response until a slip of 0.1 mm has been reached. For shear slip in this range, the influence of reinforcement dowel action can be neglected. Thus, the elastic part is independent of the amount of reinforcement crossing the shear plane. For very low slips, the slip can be approximated with the crack width. This leads to the formulation of the shear resistance in segment 0-A, see Table 2.6. The first equation can be used for both pre-cracked and uncracked sections. For larger shear slips, $\Delta > \Delta_1$, dowel action becomes significant and should be considered. Between A and B the shear resistance will increase until a shear slip of 0.3 mm is reached. The resistance will remain constant until a slip of 0.6 mm is reached. For large specimens, the plateau can be somewhat longer. The stiffness is negative between C and D, independent of the amount of reinforcement and only slightly dependent on the concrete strength. The resistance will later remain constant until a failure shear slip Δ_{max} is reached. This segment is merely dependent on reinforcement dowel action. The resistance function equations are shown in Table 2.6.

Table 2.6. Definition of Direct Shear Resistance Function converted into SI-units see Figure 2.39. Based on Crawford et al. (1999).

Region	Definition
0-A	The response is elastic, and the slope, k_e of the curve defined by the shear resistance, τ_e, for a slip of $\Delta_1 = 0.1$ mm. That resistance is given by the expression $\tau_e = 1.138 + 0.157\, f_c$ Where both τ_e and f_c are in MPa. The initial part should be taken as elastic to not more than $\tau_e \le \frac{\tau_m}{2}$.
A-B	The slope of the curve decreases continuously with increasing displacements until a maximum shear strength, τ_m, is reached at a slip of $\Delta_2 = 0.3$ mm. The maximum strength is given by the expression $\tau_m = 0.664\sqrt{f_c} + 0.8\rho_{vt} f_y \le 0.35 f_c$ where τ_m, f_c and f_y are in MPa and ρ_{vt} is the ratio between the total area of reinforcement crossing the shear plane divided by the area of the plane. f_y is the yield strength of the reinforcement crossing the plane. The direction of the reinforcement is not discussed but should have an impact on the resistance.
B-C	The shear capacity remains constant with increasing slips. C corresponds to a slip of $\Delta_3 = 0.6$ mm.
C-D	The slope of the curve is negative, constant and independent of the amount of reinforcement crossing the shear plane. The slope is given as $k_u = 0.543 + 0.0295\, f_c \quad \left[\text{N/mm}^3\right]$
D-E	The shear capacity remains constant. The deformation at E varies with the level of damage, with a failure at a slip of $\Delta_{\max} = 0.423\left(e^x - 1\right)$ Where $x = \frac{5.18}{\sqrt{f_c / d_b}}$ And d_b is the bar diameter in mm. The limiting shear stress is defined as $\tau_L = 0.85\left(\frac{A_{sb}}{A_c}\right) f_{su}$ where is A_{sb} the area of the bottom reinforcement, A_c is the area of the concrete section and f_{su} is the ultimate strength of the bottom reinforcement.

Chee (2008), evaluated previous carried out experiments by Kieger and Getchell (1982), with the two SDOF models. These experiments were performed on slabs and the resistance function was obtained by combining the direct shear resistance in each direction. Chee (2008), found good agreement and could use the SDOF models to predict which failure mode that would occur. The resistance function was taken as:

$$R = R_x + R_y \tag{2-70}$$

Where R_x and R_y are the resistance function for the slab in each direction. Reliability analyses have also been performed with this resistance function by Low and How (2002) with good accuracy.

2.5.4 Design approaches

2.5.4.1 Swedish design approach

The concepts of direct shear, described by Swedish fortification Agency, Fortfikationsverket, (2010), are presented in this section. First it is shown how the shear force effect is calculated and then how the resistance is calculated. The shear force should be checked for the initial elastic response and in the elasto-plastic oscillating phase.

A shear span is calculated by taking the early rigid body motion into account and is used to give a lower limit for when normal shear resistance can be used. If the shear span to effective depth is less than 1.5 a strut and tie model should be used according to Boverket (2004). This could be seen as the direct shear resistance. The limit is defined as

$$\frac{a_\tau}{d} \leq 1.5 \tag{2-71}$$

The procedure will not be explained in detail, but worth mentioning that the strut and tie method does not take into account that the crack is almost vertical. For more information the reader is referred to Chapter 6 in Boverket (2004).

The normal approach for shear design is described below. The maximum total reaction can be calculated as:

$$V_{tot} = \left(1 - \frac{\kappa_F^2}{\kappa_m}\right) p \cdot a \cdot b + \frac{\kappa_F^2}{\kappa_m} q_{eq} \cdot a \cdot b \tag{2-72}$$

where a and b are the length and width of a slab and for a beam a is the length and b is the loaded width of the beam. κ_F and κ_m are the transformation factors for the element, see section 2.4.2.6 for values, q_{eq} is the equivalent static load and p is the peak pressure. Plastic response is assumed if

$$\frac{p}{q_{eq}} > 2 \tag{2-73}$$

and the plastic transformation factors should then be used. From this, the support reaction can be calculated as

$$V_{Sd} = k_v V_{tot} \tag{2-74}$$

where k_v depends on the deformation shape of the structure. For a simply supported beam k_v will be 0.5.

The shear capacity shall be examined in the shear span, i.e. half the distance between the support and zero shear force. It can be shown that the shear effect at this point is half the support reaction, see Appendix C for derivation.

$$V_d = 0.5 k_v V_{TOT} \tag{2-75}$$

The shear span a_τ can be calculated as

$$\frac{a_\tau}{L} = 0.025 + 0.25\sqrt{\frac{q_{eq}}{p}} \qquad \text{for simply supports} \tag{2-76}$$

$$\frac{a_\tau}{L} = 0.01 + 0.35\sqrt{\frac{q_{eq}}{p}} \qquad \text{for fixed supports} \tag{2-77}$$

where L is the length of the span, q_{eq} is the equivalent static load and p is the peak pressure. For slabs, L should be replaced by the shorter width b since it gives a smaller shear span and a higher shear effect. From this expression it can be identified that the shear span is increasing for lower pressures. Moreover, it is clear that using equation (2-71) the limit for using normal shear force resistance for a simply supported beam is defined as

$$\frac{a_\tau}{d} = \left(0.025 + 0.25\sqrt{\frac{q_d}{p}}\right)\frac{L}{d} \le 1.5 \tag{2-78}$$

The capacity of a concrete section without influence of shear reinforcement is a limit for a form of crushing of compression strut and is defined as

$$V_c = k_c b d \tag{2-79}$$

where d is the effective depth and k_c is depending on the shear span, the protection level and reinforcement amount.

$$k_c = k_\tau \frac{f_\rho}{s} \tag{2-80}$$

Here s is a factor for the protection level used by the Swedish military and depends on how much damage the exposed structure can be allowed:

$s = 1.2$ for protection level B1, B2 and B3

$s = 1.0$ for protection level C

and f_ρ is a factor that depends on the amount of reinforcement (ρ)

$$f_\rho = 0.7 + \frac{\rho - 0.1}{3} \tag{2-81}$$

where $\rho = \frac{A_s}{b \cdot d}$ (2-82)

and k_τ depends on the shear span and the concrete strength.

$$k_\tau = k_{\tau,0} = 0.25 f_c \quad \text{if} \quad \frac{a_\tau}{d} < 0.45 \tag{2-83}$$

$$k_\tau = 0.45 \frac{k_{\tau,0}}{\frac{a_\tau}{d}} \quad \text{if} \quad \frac{a_\tau}{d} \geq 0.45 \tag{2-84}$$

If the shear force capacity is not sufficient, i.e. $V_d > V_c$ according to equations (2-75) and (2-79), shear reinforcement must be introduced. The required shear reinforcement can be calculated as

$$V_s = V_{tot}\left(1 - \sqrt{\frac{V_c}{V_d}}\right) \quad \text{For the initial elastic response} \tag{2-85}$$

$$V_s = V_{tot,\min}\left(1 - \sqrt{\frac{V_c}{2V_{d,\min}} \cdot \frac{8a_\tau}{L}}\right) \quad \text{For the oscillating elasto-plastic response} \tag{2-86}$$

where minimum values $V_{d,min}$ and $V_{tot,min}$ are obtained by setting p/q=1 and L as the shorter span b for slabs. The shear reinforcement can then be calculated as

$$V_t = \frac{A_s}{\sin(\theta) \cdot f_{yk}} \tag{2-87}$$

where θ is the angle of shear reinforcement to the flexural reinforcement in tension. Consequently, no consideration is taken that the shear crack can be vertical.

In case of elastic response the shear reinforcement should be evenly distributed over the length

$$x = a_\tau \cdot \left(1 + \sqrt{1 - \frac{V_c}{V_d}}\right) \tag{2-88}$$

In case of elasto-plastic response the shear reinforcement should be evenly distributed over the length

$$x = 0.25 \cdot L \cdot \left(1 + \sqrt{1 - \frac{V_c}{V_{d,\min}} \cdot \frac{8 \cdot a_\tau}{L}}\right) \tag{2-89}$$

where the distance between the shear reinforcement should not be greater than $0.75 \cdot (1+\cot\theta) \cdot d$. L should be set as the shorter span b for slabs.

2.5.4.2 American design approach

DoD (2008) defines direct shear as the rapid growth of a vertical crack through the depth of a concrete member. Diagonal steel reinforcement anchored in the support can prevent this and is required if the

- design support rotations are greater than 2°
- concrete direct shear capacity is insufficient
- section is in tension.

The direct shear capacity of concrete is considered to be zero if the rotation is greater than 2° or if the section is in tension, which can be the case with an indoor explosion. Diagonal reinforcement is not recommended to be designed in beams. Instead, rotations should be limited and the concrete direct shear capacity sufficient. The direct shear capacity is not zero for simply supported members even if the support rotation is greater than 2°. Consequently there is no need for diagonal reinforcement if the direct shear capacity is adequate. The direct shear capacity for concrete can be written as for a slab and beam respectively.

$$V_d = 0.16 f'_{dc} bd \quad \text{for slabs} \tag{2-90}$$

$$V_d = 0.18 f'_{dc} bd \quad \text{for beams} \tag{2-91}$$

where V_d is the direct shear capacity of an element with width b and effective depth d. f'_{dc} is the ultimate dynamic compression strength of the concrete, which is 10% greater than the ultimate compression strength.

$$f'_{dc} = 1.1 \cdot f_c \tag{2-92}$$

If diagonal bars are required, the required area can be expressed as

$$A_s = \frac{(V_s b - V_d)}{f'_{ds} \cdot \sin(\alpha)} \tag{2-93}$$

Where A_s is the required shear reinforcement bar area, V_s is the ultimate shear force at the face of the support per unit width, α is the angle of the bars and f'_{ds} is the dynamic design stress for the reinforcement, which depends on the maximum support rotation. How to determine the dynamic design stress for different support rotations is presented in DoD (2008), with a lower value corresponding to the yield stress f_{yd} for small values of the maximum support rotations.

For an unreinforced concrete member loaded in bending the maximum allowable shear stress, V_c, can be calculated with equation (2-94) or (2-95).

$$V_c = 2 \cdot (f_{dc})^{1/2} \tag{2-94}$$

$$V_c = \left[1.9 \cdot \left(f_{dc}\right)^{1/2} + 2500 \cdot \rho\right] \quad \leq \quad 3.5\left(f_{dc}\right)^{1/2} \tag{2-95}$$

Where ρ is the reinforcement ratio of tensile reinforcement at the support.

According to DoD (2008), the ultimate shear force at the face of a support is reasonably estimated for a short duration blast load as a function of the maximum internal resistance only. If the ultimate resistance is not reached, the actual elastic resistance value should be used to obtain the shear forces at the supports. This corresponds to using the equivalent static load introduced in Section 2.4.2.6. The values for different support and load conditions are shown in Table 2.7.

An interesting observation is that this corresponds to using the equation as in the Swedish approach, see equation (2-72), with transformation factors assuming a rigid body motion, i.e. $\kappa_m = \kappa_F = 1$. Consequently, the contribution from the load is not taken into account as it is for the Swedish approach. This should be on the unsafe side initially but conservative during the plastic oscillation.

Table 2.7. The maximum support reaction according to DoD (2008). R_u and r_u are the ultimate internal resistance force and force per unit length.

Edge Conditions and Loading diagrams	Support Reactions, V_s	
	Left support	Right support
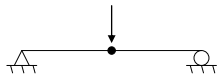	$\frac{R_u}{2}$	$\frac{R_u}{2}$
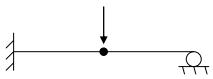	$\frac{11R_u}{16}$	$\frac{5R_u}{16}$
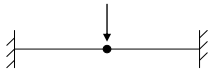	$\frac{R_u}{2}$	$\frac{R_u}{2}$
	R_u	–
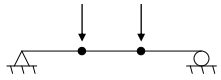	$\frac{R_u}{2}$	$\frac{R_u}{2}$
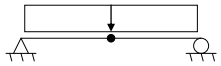	$\frac{r_u L}{2}$	$\frac{r_u L}{2}$
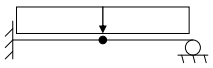	$\frac{5r_u L}{8}$	$\frac{3r_u L}{8}$
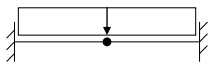	$\frac{r_u L}{2}$	$\frac{r_u L}{2}$
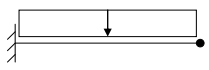	$r_u L$	–

The shear force at the supports of a slab is harder to determine but expressions can be found in DoD (2008). It is derived by using the yield line procedure and depends on which yield line figure that is chosen. The reader is referred to DoD (2008) for more information.

3 Reinforced concrete beam subjected to impulse load

3.1 Introduction

In order to give a better understanding of the behaviour of a reinforced concrete beam subjected to an explosion, an example is carried out. The beam is modelled in the finite element program ADINA which is considered to best represent the real behaviour. The result will be compared to the result that can be obtained by simplified hand calculations and with an equivalent SDOF approach described in Section 2.4.2. The problem will be simplified by only considering four material responses, namely; linear elastic state I, linear elastic state II, ideal plastic and elasto-plastic. The beam is modelled in ADINA with beam elements with the different simplified material behaviours. The example will later be extended by modelling the real non-linear behaviour in Appendix I.

3.2 Definition of geometry and loading

A 3 metre high and 400 mm deep reinforced concrete wall in a protective facility or a building without windows will be analysed. The wall is reinforced with steel reinforcement B500B ϕ20 s200 which is placed 40mm from the edge. Since a dynamically loaded system will be strained in both directions it is important to reinforce both sides of the member equally. The concrete strength is C30/37. The wall is subjected to a uniform pressure that decreases with time. For this case the so called archive bomb, introduce in Section 2.1, has been used as a reference load; i.e. 125 kg of TNT detonated 5 metres away from the wall and assuming spherical spreading, Johansson and Laine (2007). This will give a peak pressure of 5000 kPa and an impulse intensity of 2800 Ns/m^2, which corresponds to load duration of 1.12 ms when assuming a triangular load impulse as mentioned in Section 2.1. The archive bomb is referred to as load case 1, also denoted LC1. The wall will be subjected to other load cases with the same impulse intensity. All load cases and their corresponding values are presented in Figure 3.1. Further, when no specific load case is mentioned load case 1 is used.

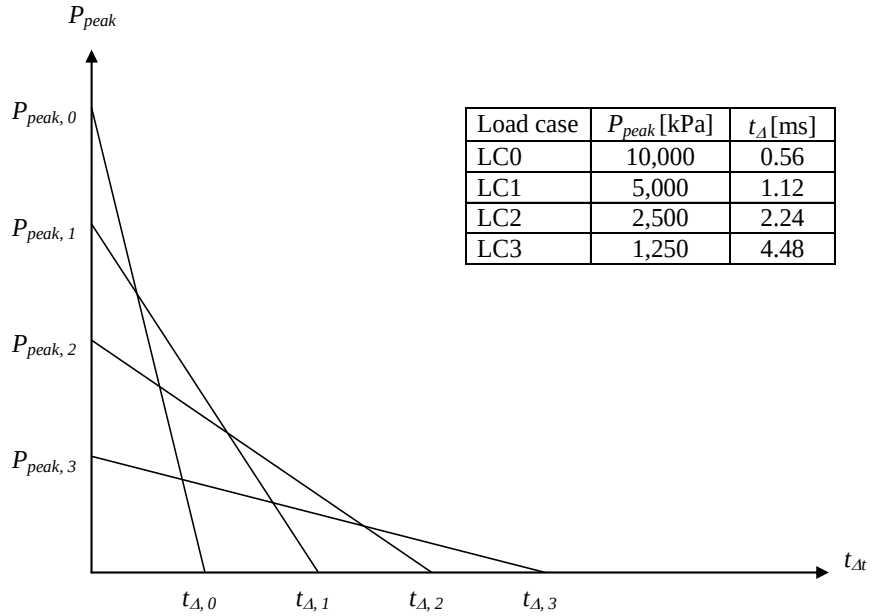

Load case	P_{peak} [kPa]	t_{Δ} [ms]
LC0	10,000	0.56
LC1	5,000	1.12
LC2	2,500	2.24
LC3	1,250	4.48

Figure 3.1. An illustration of the different load cases and their corresponding values of peak pressure P_{peak} and load duration t_{Δ}. All loads have the same impulse intensity i.

The wall is not hindered to rotate at the rigid supports, which only support the wall in one direction. Thus, the wall can be simplified as a simply supported beam element with a width of 1 metre, see Figure 3.2. The data is summarised in Table 3.1.

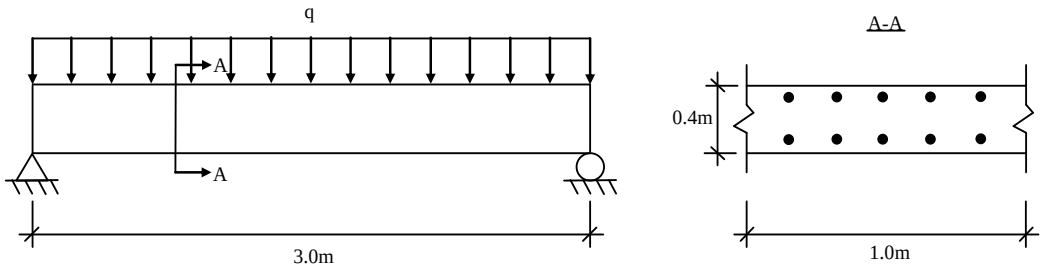

Figure 3.2. The dimensions of the beam used in the example.

Table 3.1. Summarised data for the example beam.

Data for the example			
Length, *L*	3.0 m	Impulse intensity, *i*	2800 Ns/m^2
Depth, *h*	0.4 m	Peak pressure, P_c	5000 kPa
Width, *b*	1.0 m	Active time, t_{Δ}	1.12 ms
Reinforcement	ϕ20s200 B500B		
Concrete	C30/37		
Concrete cover, *c*	50 mm		

The beam can be simplified into a single-degree of freedom system by choosing a system point and then applying an equivalent mass, stiffness and force to it. The centre point of the beam has been chosen as the system point in this example. The transformation of a beam into a SDOF-system is done by using transformation factors. The transformation factors depend on the shape of the beam deflection, which means that different transformation factors will be used for the different material behaviour. They are tabulated in Section 2.4.2.3. The equation of motion can then be solved analytically or numerically. The central difference method will be implemented in MATLAB for this example, and is presented further in Appendix A.

3.3 Equivalent SDOF system

3.3.1 Mass

The hand calculation uses the work equilibrium method described in Section 2.4.2.4. In order to calculate the maximum deflection and the work equilibrium, the stiffness, equivalent mass and the maximum resistance force must be calculated. The mass can be calculated to

$$m = \rho \cdot h \cdot w \cdot L = 2400 \cdot 0.4 \cdot 1.0 \cdot 3.0 = 2880\,\text{kg} \tag{3-1}$$

As shown in Section 2.4.2.3, the only parameter needed to be transformed into an equivalent parameter is the mass. It will depend on the deflection shape and hence we obtain different equivalent masses for the elastic and plastic cases, respectively. The κ_{mF} values are presented in Section 2.4.2.3. The equivalent mass for the elastic and the plastic materials respectively is

$$m_{el} = \kappa_{mF} m = 0.788 \cdot 2880 = 2270\ \text{kg} \tag{3-2}$$

$$m_{pl} = \kappa_{mF} m = 0.667 \cdot 2880 = 1921\ \text{kg} \tag{3-3}$$

3.3.2 Stiffness

The stiffness for a simply supported beam can be calculated as

$$k = \frac{384EI}{5L^3} \tag{3-4}$$

Hence, the moment of inertia for state I and II is to be found. The influence of the reinforcement in the compression zone in state I and II can be neglected. The tension reinforcement is considered by transforming the steel area into a corresponding equivalent concrete area.

$$A_{s,eq} = \frac{E_s}{E_c} A_s = \alpha A_s \tag{3-5}$$

where

$$A_s = \frac{A_{\phi 20}}{s} = \frac{314}{0.2} = 1571\ \text{mm}^2 \tag{3-6}$$

$$\alpha = \frac{E_s}{E_c} = \frac{200}{33} = 6.36 \tag{3-8}$$ (3-7)

The effective depth is

$$d = h - c = 400 - 50 = 350\ \text{mm} \tag{3-9}$$

Then the moment of inertia for state I can be calculated as

$$I_I = \frac{bh^3}{12} + A_s(\alpha - 1)\cdot\left[\left(d - \frac{h}{2}\right)^2 + \left(\frac{h}{2} - d'\right)^2\right] = \\ = \frac{1000\cdot 400^3}{12} + 1571\cdot(6.36-1)\cdot\left[\left(350 - \frac{400}{2}\right)^2 + \left(\frac{400}{2} - 50\right)^2\right] = 5.71\cdot 10^9\ \text{mm}^4 \tag{3-10}$$

In state II, the moment of inertia must be calculated from the cracked cross-section. By assuming negligible normal forces, the height of the compressed zone *x* can be calculated by area equilibrium

$$x = \frac{b\frac{x^2}{2} + \alpha A_s d}{bx + \alpha A_s} \tag{3-11}$$

The height of the compressed zone is then obtained

$$x = 74\ \text{mm} \tag{3-12}$$

The moment of inertia in state II can then be calculated as

$$I_{II} = \frac{bx^3}{3} + \alpha A_s(d-x)^2 = \frac{1000\cdot 74^3}{3} + 6.36\cdot 1571\cdot(350-74)^2 = 8.97\cdot 10^8\ \text{mm} \tag{3-13}$$

The stiffness for the cracked and uncracked state can be calculated using equation (3-4).

$$k_I = \frac{384\cdot 33\cdot 10^9\cdot 5.33\cdot 10^{-3}}{5\cdot 3^3} = 5.00\cdot 10^8\ \frac{\text{N}}{\text{m}} \tag{3-14}$$

$$k_{II} = \frac{384\cdot 33\cdot 10^9\cdot 8.97\cdot 10^{-4}}{5\cdot 3^3} = 8.42\cdot 10^7\ \frac{\text{N}}{\text{m}} \tag{3-15}$$

3.3.3 Maximum internal resistance

When the plastic case is considered, there is no stiffness and instead the internal resistance is explained by the maximum capacity. As a simplification, the plastic material behaviour is modelled as a straight line, which starts to yield at the maximum capacity. A comparison is made and the difference is only 2% between the ultimate moment capacity and moment capacity when the steel just yields, see equation (3-20).

The ultimate moment capacity must therefore be calculated. An explanation is given in Figure 2.5. The compressed zone, *x*, can be calculated from equation (3-16), if is assumed that the steel yields and that the section reaches its ultimate capacity when the concrete reaches the ultimate compressive strain in the outermost fibre. Factors α_R and β_R are stress block factors that are 0.81 and 0.416 respectively when the section has reached its ultimate capacity according to Eurocode 2, CEN (2004).

$$x = \frac{f_{yd} A_s}{\alpha_R f_{cd} w} = \frac{\frac{500}{1.15} \cdot 1571}{0.81 \cdot \frac{30}{1.5} \cdot 1000} = 42 \text{ mm} \tag{3-16}$$

The partial coefficients used for steel and concrete are equal to 1.15 and 1.5 respectively. An explosion is categorised as an accidental load and therefore these partial coefficients should be set to 1.0 for steel and 1.2 for concrete. Nevertheless, the values used in this thesis will not affect the comparison. However, it should be noticed that in design the correct partial coefficients corresponding to an accidental load should be used. The moment capacity can then be established by moment equilibrium around the steel reinforcement.

$$\begin{aligned} M_{Rd} &= \alpha_R f_{cd} \cdot x \cdot b \cdot (d - \beta \cdot x) = \\ &= 0.81 \cdot \frac{30}{1.5} \cdot 0.042 \cdot 1 \cdot (0.35 - 0.416 \cdot 0.042) = 227 \text{ kNm} \end{aligned} \tag{3-17}$$

According to Biggs (1964) the maximum internal resistance is defined as

$$R_m = \frac{8 M_{Rd}}{L} = \frac{8 \cdot 227 \cdot 10^3}{3} = 606 \text{ kN} \tag{3-18}$$

The moment capacity when the reinforcement steel start to yield is calculated by assuming the strain in the tension reinforcement is equal to the yield strain. The moment at this point can be calculated as

$$M_{yd} = \frac{E_C \varepsilon_{sy}}{2} \cdot \frac{x_{II}^{\ 2}}{d - x_{II}} \cdot b \cdot \left(d - \frac{x_{II}}{3} \right) = 223 \text{ kNm} \tag{3-19}$$

The ratio between the two moment capacities are stated as

$$\frac{M_{yd}}{M_{Rd}} = 0.98 \tag{3-20}$$

The state II stiffness has been used in the elasto-plastic model. This will give a slightly larger elastic deformation than in the real case. This is because a bi-linear relationship is assumed which will give a longer elastic branch, see Figure 3.3.

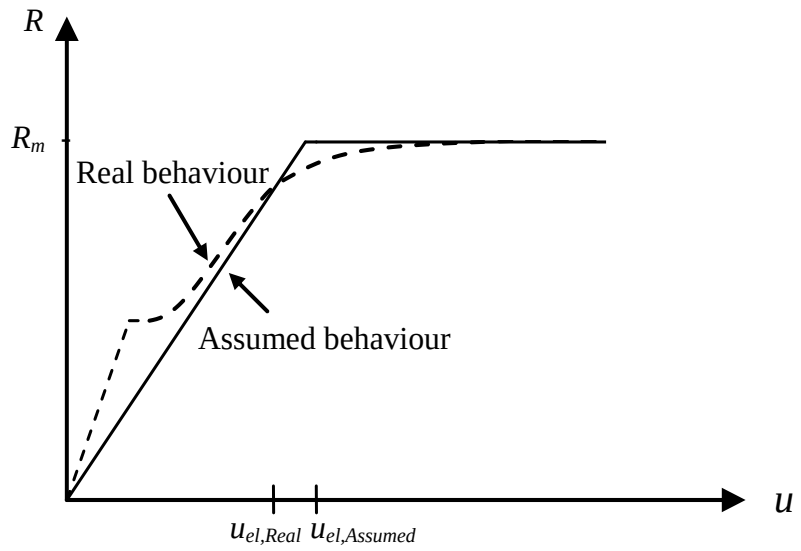

Figure 3.3. The difference between the real behaviour and the assumed bi-linear elasto-plastic behaviour used in the SDOF model.

3.4 Hand calculations

3.4.1 Maximum required deformation

The required deformation for having energy equilibrium assuming linear elastic behaviour can be calculated as

$$u_{el} = \frac{I_c}{m\omega} \tag{3-21}$$

The deformations in state I and state II can be obtained as

$$u_{el,I} = \frac{2800 \cdot 1 \cdot 3}{\sqrt{2270 \cdot 5.00 \cdot 10^8}} = 7.9\,\text{mm} \tag{3-22}$$

$$u_{el,II} = \frac{2800 \cdot 1 \cdot 3}{\sqrt{2270 \cdot 8.42 \cdot 10^7}} = 19.2\,\text{mm} \tag{3-23}$$

According to equation (2-17) the plastic deformation can be expressed as

$$u_{pl} = \frac{I_c^2}{2mR} \tag{3-24}$$

This will give the required plastic deformation

$$u_{pl} = \frac{(2800 \cdot 3 \cdot 1)^2}{2 \cdot 1921 \cdot 605.5 \cdot 10^3} = 30.3\,\text{mm} \tag{3-25}$$

The total deformation for the elasto-plastic case can be calculated according to equation (2-18) as

$$u_{ep} = \frac{I_c^2}{2mR} + \frac{R}{2k} \tag{3-26}$$

The total elasto-plastic deformation will therefore be

$$u_{ep} = 30.3 \cdot 10^{-3} + \frac{605 \cdot 10^3}{2 \cdot 8.42 \cdot 10^7} = 33.9 \,\text{mm} \tag{3-27}$$

Of which the elastic deformation is

$$u_{ep,el} = \frac{R}{k} = \frac{605 \cdot 10^3}{8.42 \cdot 10^7} = 7.1 \,\text{mm} \tag{3-28}$$

Then the plastic part of the deformation can be calculated as

$$u_{ep,pl} = u_{ep} - u_{ep,el} = 26.8 \,\text{mm} \tag{3-29}$$

In the ideal plastic and the elasto-plastic cases, the maximum capacity is assumed and the energy is dissipated with plastic deformation. The failure criterion will therefore not be the moment capacity. It is rather the rotational capacity of the section that is important.

3.4.2 Dynamic reactions

The dynamic reactions can be calculated for the instant when maximum deformation takes place by using an equivalent static load, described in Section 2.4.2.6. For the elastic case it is

$$Q_{el} = I_c \omega \tag{3-30}$$

This gives a value for the uncracked case

$$Q_{el,I} = 2800 \cdot 3 \cdot 1 \cdot \sqrt{\frac{5.00 \cdot 10^8}{2270}} = 3942 \text{ kN} \tag{3-31}$$

And for the cracked case

$$Q_{el,II} = 2800 \cdot 3 \cdot 1 \cdot \sqrt{\frac{8.42 \cdot 10^7}{2270}} = 1618 \text{ kN} \tag{3-32}$$

The plastic equivalent load is calculated from

$$Q_{pl} = R_m = 606 \text{ kN} \tag{3-33}$$

R_m is calculated according to equation *(3-18)*. The moment effect on the beam at mid span can then be calculated as

$$M_{Ed} = \frac{QL}{8} \tag{3-34}$$

According to Johansson and Laine (2009) the support reaction can be found as

$$V_{Ed} = \frac{Q}{2} \tag{3-35}$$

This gives the dynamic reaction presented in Table 3.2. Johansson and Laine (2009) also mention that higher support reactions can occur at an early stage when the beam is subjected to an impulse load.

Table 3.2. Dynamic reactions at maximum deflection

	u [mm]	M_{Ed} [kNm]	V_{Ed} [kN]
Elastic state I	7.9	1478	1971
Elastic state II	19.2	607	809
Plastic	30.3	227	303

An interesting observation is that less stiff elements will deform more but will not require as much capacity. However, there is an upper limit for how much an element can deform. For the elastic cases a simple capacity check can be carried out. For the plastic case the plastic rotation capacity must be limited.

The Eurocode 2 approach to perform this check is described in section 2.2.3. Firstly, the shear slenderness should be checked. This is done by dividing the shear span with the effective depth of the member. The shear span for a simply supported beam is half the length.

$$\lambda_s = \frac{x_0}{d} = \frac{L}{2d} = \frac{3}{2 \cdot 0.35} = 4.29 \tag{3-36}$$

The diagram in Figure 3.4 is used for finding the plastic rotation capacity. It is only valid for λ_s=3. For other values it should be corrected with

$$k_\lambda = \sqrt{\frac{\lambda_s}{3}} = 1.20 \tag{3-37}$$

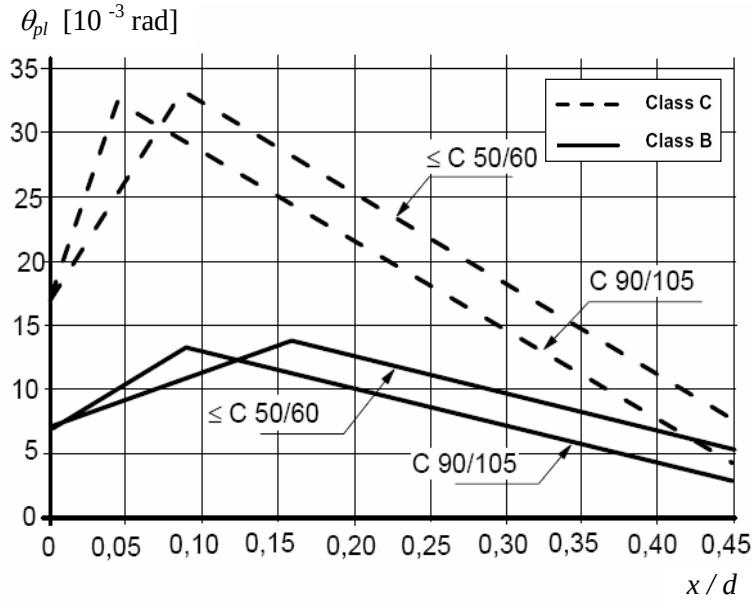

Figure 3.4. Diagram for evaluating the plastic rotation capacity according to Eurocode 2, CEN (2004).

In this example, the ratio between the compressed zone and the effective depth of the beam is

$$\frac{x_u}{d} = \frac{42}{350} = 0.12 \tag{3-38}$$

Class B reinforcement is used, then the plastic rotation capacity can be found as $\theta_{pl} = 12.5 \cdot 10^{-3}$ rad from Figure 3.4. It can be observed that the capacity is limited by the ultimate steel strain. However, it is a good design since the plastic rotation capacity is high.

The maximum plastic rotation capacity can then be calculated as

$$\theta_{pl,d} = k_\lambda \theta_{pl} = 1.20 \cdot 12.5 \cdot 10^{-3} = 15 \cdot 10^{-3} \text{ rad} \tag{3-39}$$

The plastic rotation capacity can be related to the plastic displacement for a simply supported beam as

$$u_{pl,d} = \frac{L\theta_{pl,d}}{2} = \frac{3 \cdot 15 \cdot 10^{-3}}{2} = 22.5 \text{ mm} \tag{3-40}$$

which is smaller than the deformation in the elasto-plastic model. However, in equation (3-32) it is shown that the plastic deformation needed is 26.8 mm, i.e. larger than the capacity, which means that the beam will not be able to resist the blast load and will fail when the deformation reaches 22.5 mm.

3.5 FE-analysis ADINA – considerations and restrictions

3.5.1 Introduction

For detailed analyses the finite element program ADINA will be used. It is a good choice when analysing a structure's dynamic response. However, some important considerations and modelling simplifications must be introduced such as: usage of equivalent Young's modulus, FE elements, wave propagation, integration schemes, output and damping.

3.5.2 Equivalent Young's Modulus

The choice of modelling a simplified material in ADINA is by using a linear or bi-linear material response. Hence, this will cause some modelling issues concerning the correct Young's Modulus and thereby the correct speed of the waves in the material.

When the calculation in state II is performed, ADINA will not recognise that the section is cracked and will use the moment of inertia of the full uncracked concrete section. In order to model a cracked section and obtain the state II stiffness, the Young's modulus will be multiplied with the ratio between the moment of inertia in state II and state I from equation (3-10) and (3-13).

$$E_{II} = \frac{I_{II}}{I_I} E_I = \frac{8.97 \cdot 10^{-4}}{5.71 \cdot 10^{-3}} \cdot 33 = 5.18 \,\text{GPa} \tag{3-41}$$

ADINA cannot model ideal plastic material behaviour. Instead, a bi-linear relation with a Young's modulus multiplied with 100 to approximate a fully plastic behaviour is used.

$$E_{pl} = 100 E_I = 3300 \text{ GPa} \tag{3-42}$$

It could be argued that the wave speed in the material should be maintained by changing the moment of inertia instead of Young's modulus. This will affect the fictional yield stress and the geometry of the beam and will consequently be a more complex way of modelling. The modelling can be performed in three ways, shown in Figure 3.5. The first scheme is used above in order to calculate an effective Young's modulus. This method does not maintain the wave speed in the beam, see equation (2-19), which will change with the square root of the factor used for the Young's modulus. Scheme 2 maintains the wave speed by only changing the moment of inertia I. As a result, the geometry and the fictional yield stress must be changed. If the height of the beam is increased to more than three times the span length it becomes a deep beam and ADINA cannot guarantee accurate solutions when using beam elements with the Euler-Bernoulli beam theory formulation. Therefore, a third scheme is introduced, which maintains the wave speed by increasing the density. Since the mass must be constant this unfortunately also affects the geometry and fictional yield stress. This is the most complicated scheme and is not preferable since it does not provide a solution to the deep beam problem.

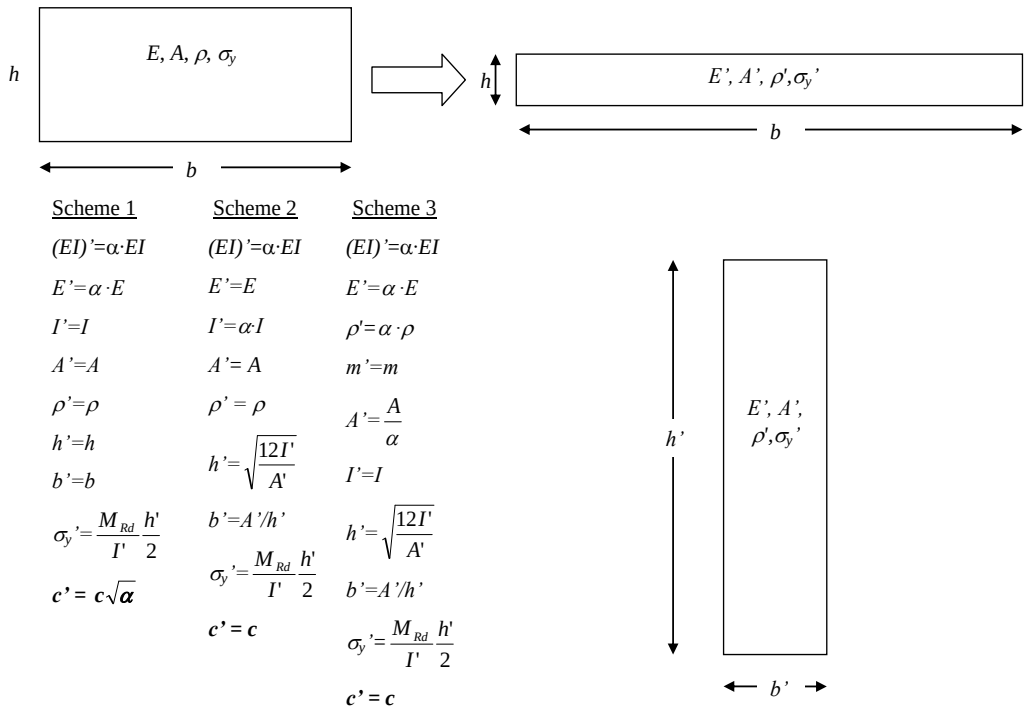

Figure 3.5. The methods for changing stiffness when a cracked section or an ideal plastic section is considered.

If the bending stiffness *EI* decreases and schemes 2 or 3 are used, the equivalent section will become wider and lower. Consequently, the deep beam formulation will never occur and these schemes are applicable at all times provided that the original section is not a deep beam. The ideal plastic case is modelled with larger bending stiffness *EI*. This will mean that the depth of the beam increases and problems in the modelling can occur.

Scheme 1 is preferable to use since it only changes the Young's modulus. Therefore, the influence of the wave speed must be investigated. This is carried out by keeping *EI* constant, i.e. changing Young's modulus and the moment of inertia with the same factor, i.e.

$$I' = \frac{I}{\alpha} \qquad \text{and} \qquad (EI)' = EI \tag{3-43}$$

It is carried out in an elasto-plastic case but gives the same results in the elastic and ideal plastic cases. As can be seen in Figure 3.6, the deformation changes when the wave speed is decreased. The solution with 9 times less elasticity modulus diverges slightly after having reached the turn point. This corresponds to 3 times lower wave speed. Considerable change is not noticed until the velocity is wrong with a factor of five, i.e. E / 25. If the moment of inertia is increased 100 times, the beam becomes a deep beam and the deformation diverges a lot; i.e. such a combination cannot be used. The solution using an equivalent elasticity modulus, though, agrees well with the real behaviour. It can therefore be justified to use scheme 1 when modelling the state II behaviour.

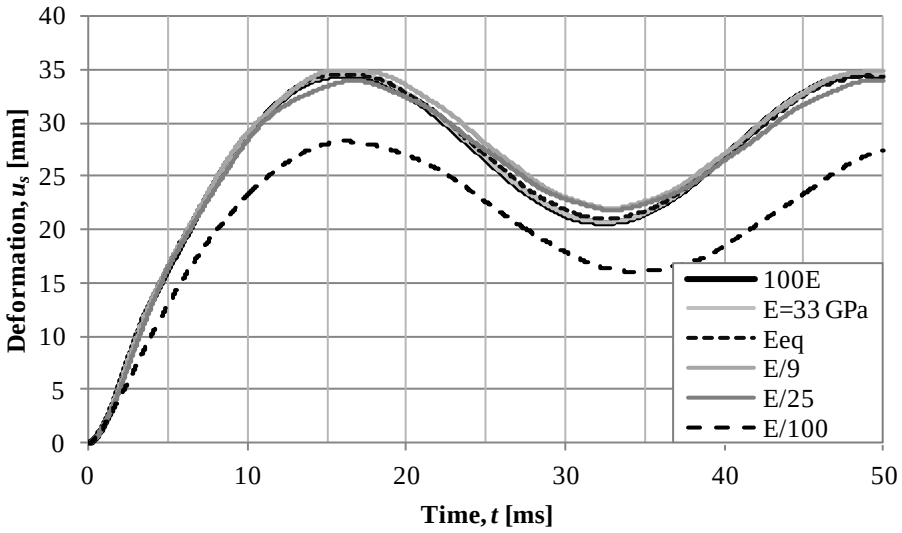

Figure 3.6. The displacement in midpoint for different wave speeds in the beam.

The deformation in the midpoint is very similar if the wave speed is the "real" wave speed or higher. Therefore, the model with ideal plastic behaviour is believed to be reasonably correct. It is not possible to investigate how the wave speed influences an ideal plastic 3 metres beam since the moment of inertia cannot be increased considerably before deep beam is obtained. Therefore, Studies of a 15 metres long beam have also been carried out. The α-value was 100. The deformation is higher for the model with higher wave speed while scheme 2 and 3 provide the same result.

The wave speed in the beam is complicated and is researched by ADINA at the moment. As will be seen in Section 3.5.4, the time-step also influences the wave propagation and the existing problems with wave propagation should be known. However, the currently used modelling techniques are sufficiently accurate for this case and small changes in the wave speed can be neglected.

3.5.3 FE-elements

Beam elements will mainly be used for this thesis. A detailed analysis will be performed using 2D-solid plane stress elements will also be performed.

All elements in the beam will be modelled as elastic, plastic or elasto-plastic. Ek and Mattsson (2009) modelled the beam with one plastic element in the midpoint. They obtained a large divergence in their result since the elastic elements oscillated around the plastic element.

ADINA chooses 7 integration points over the height of the cross-section, regardless of the user's choice, when performing 3D beam analyses. It has been shown in previous master theses (Ek and Mattsson, 2009; Augustsson and Härenstam, 2010) that ADINA will not have the assumed capacity of a 3D beam cross-section. The stress are correct at the integration points but the stress distribution in between is described with a polynomial which gives another capacity compared to what would be expected. This is illustrated in Figure 3.7.

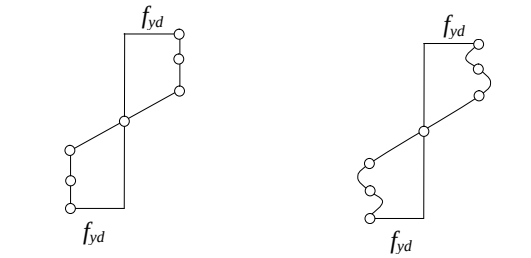

Expected stress distributon

Stress distribution using 7 integration points

Figure 3.7. The stress distribution over the height using 7 integration points.

However, when 2D beam elements are used it is possible to use 3 integration points over the height in ADINA, which will make the stress vary linearly through the cross section, see Figure 3.8. In this example only 2D action is used, which means that 2D-beam elements with 3 integration points over the height are used. A fictional yield stress can therefore be introduced. The input fictional yield stress is dependent on the stress distribution and indirectly dependent of the integration points. The input fictional yield stress can therefore be calculated to

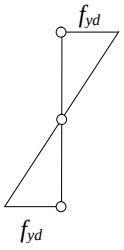

Stress distribution

$$f_{yd} = \frac{M_{Rd}}{W_{el}} \quad \text{with} \quad W_{el} = \frac{bh^2}{6}$$
$$f_{yd} = \frac{6 \cdot 227 \cdot 10^3}{1 \cdot 0.4^2} = 8.51\,\text{MPa} \tag{3-44}$$

Figure 3.8. Stress distribution when using 3 integration points over the height. A fictional yield stress, f_{yd} can be introduced.

3.5.4 Wave propagation

3.5.4.1 Introduction

Wave speed is of importance when investigating the initial behaviour of an impulse loaded structural element. Therefore, the modelling of wave propagation in ADINA needs to be investigated. This is done for both beam elements and solid 2D-elements. It should be mentioned that ADINA always uses the elastic wave regardless of the structures response, ADINA (2010). The investigation has been made with an impulse with constant amplitude for 1 ms, see Figure 3.9.

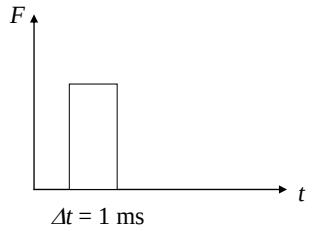

Figure 3.9. Impulse load used for wave propagation studies.

3.5.4.2 Beam elements

The two cases shown in Figure 3.10 were investigated. The support reaction was investigated and the wave was assumed to arrive when the magnitude reached 0.5% of the maximum value. As presented in Section 2.4.1.6, the time until a pressure wave in one dimension would arrive at the support should be:

$$t = \frac{L}{c} = \frac{1.5}{\sqrt{\frac{33 \cdot 10^9}{2400}}} = 0.404 \cdot 10^{-3}\,\text{s} \tag{3-45}$$

The time until a shear wave would arrive should be:

$$t = \frac{L}{c} = \frac{1.5}{\sqrt{\frac{33 \cdot 10^9}{2 \cdot (1+0.2) \cdot 2400}}} = 0.627 \cdot 10^{-3}\,\text{s} \tag{3-46}$$

Large divergence between the theoretical wave speed and the analysis were found. The first case should correspond very well to a pressure wave and the second case to a transverse wave. Both cases have approximately the same arrival time. It is 0.21 and 0.22 ms respectively. For case one a major shock front seems to arrive approximately at the theoretical arrival time but some disturbance has arrived before. This could be due to some numerical errors in the calculation.

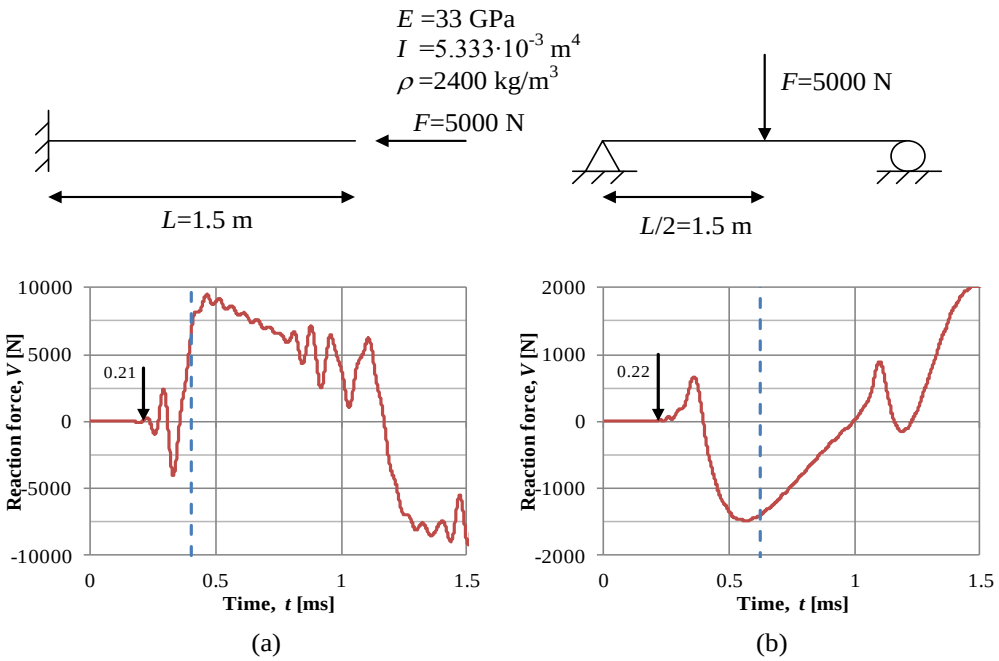

Figure 3.10. Support reaction over time for the two experiments. The blue dotted line represent the theoretical arrival time for the waves.

The wave speed in the beam model seems to be independent of Poisson's ratio. The same result is obtained if no transverse deformation is allowed, i.e. $\nu = 0$. This suggests that the wave speed is calculated as the speed of a pressure wave when using beam elements regardless of the actual speed. This should not be true for a shear wave and therefore it may not be appropriate to model the wave propagation with beam elements.

The wave speed depends on Young's modulus, E, of the material as seen in Section 2.4.1.6. The elastic modulus was therefore varied while the area and bending stiffness was kept constant, according to scheme 1 in Section 3.5.2, in order to see how the arrival time to the support changed. The elastic modulus was increased 25 times, which gives the following input variables.

$$E' = 25E \qquad I' = \frac{I}{25} \qquad c' = 5c \tag{3-47}$$

The result is visualised in Figure 3.11. According to equations (3-45) and (3-46) with parameters from equation (3-47) the arrival time should be approximately 0.08 ms for a pressure wave and 0.125 ms for a shear wave. The theoretical values are represented with a blue dotted line. Again, it can be seen that the support reaction has some disturbance before the major front arrives. The shear wave does not seem to be modelled appropriately using beam elements.

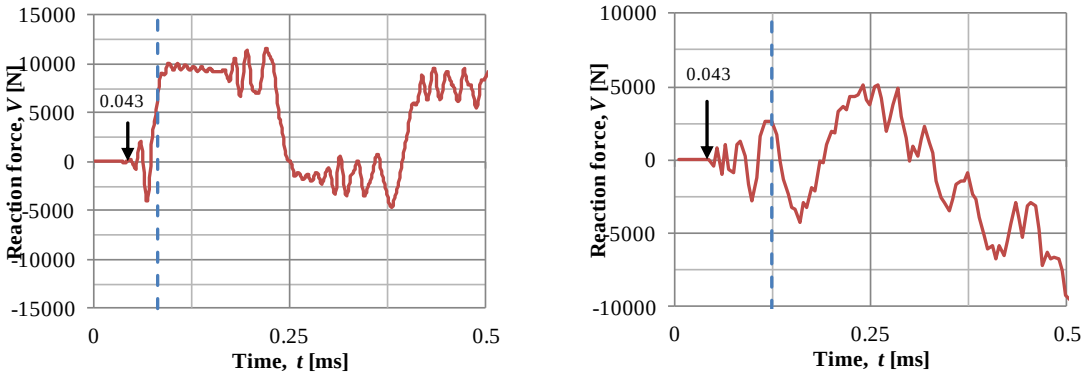

Figure 3.11. The reaction force over time for a beam with a higher Young's modulus, E' = 25E.

It was not possible to model a much lower elastic modulus since the program interprets the high moment of inertia as a deep beam section, which does not give adequate values using Euler-Bernoulli beam theory, compare reasoning in Section 3.5.2. This is a modelling limitation but will not influence the results in further analyses since Young's modulus is always higher and the moment of inertia is always lower.

3.5.4.3 2D-solid elements

The wave speed may not be modelled correctly with linear beam elements and in order to get a better understanding, the wave speed was also studied using 2D solid plain stress elements. It is also interesting to study whether the model distinguishes a shear wave from a pressure wave. The influence of Poisson's ratio is also studied to see how much it influences the wave speed for the two cases.

To study the wave speed the simple cantilever beam of length 1.5m was used, see Figure 3.12a. A load in the form of a pressure load is applied to the tip of the beam. This load is applied in the axial direction to the beam, see Figure 3.12a. To measure the wave speed the reaction in the horizontal direction of the beam is studied at the support. For this case the influence of Poisson's ratio is very small, this can be seen in Figure 3.12b. The wave speed is higher when studied in the FE-analysis compared to the expected theoretical value. The theoretical wave speed for the pressure wave is

$$c = \sqrt{\frac{E}{\rho\left(1-\nu^2\right)}} = \sqrt{\frac{33\cdot 10^9}{2400\cdot\left(1-0.2^2\right)}} = 3785 \text{ m/s} \tag{3-48}$$

and the corresponding arrival time is

$$t_a = \frac{L}{c} = \frac{1.5}{3785} = 0.40\,\text{ms} \tag{3-49}$$

It can also be observed that the influence of Poisson's ratio is very small leading to that this is presumably a pressure wave.

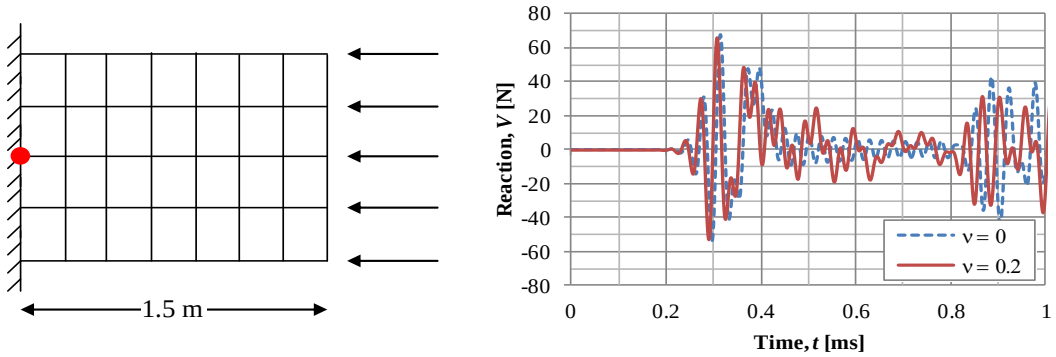

(a) (b)

Figure 3.12. The wave speed when using 2D-solid elements. The dot in (a) indicates in which point the reaction is measured.

When studying the shear wave the same cantilever beam model is used. The load is applied as a shear load at the tip of the beam and is distributed along the whole height of the beam, see Figure 3.13a. The reaction in the vertical direction is then studied at the support.

This study shows that that the influence of Poisson's ratio is higher for the shear wave than a pressure wave, see Figure 3.13b. This is expected due to the influence of Poisson's ratio when calculating the shear modulus. The fact that the wave speed obtained in the second analysis is lower strengthens the assumption that it is a shear wave not a pressure wave. As for the first case the wave speed obtained in the FE-analysis is higher compared with the theoretical value. The theoretical shear wave speed is

$$c = \sqrt{\frac{G}{\rho}} = \sqrt{\frac{33 \cdot 10^9}{2400 \cdot 2(1+0.2)}} = 2394 \text{ m/s} \tag{3-50}$$

and the corresponding arrival time is

$$t_a = \frac{L}{c} = \frac{1.5}{2394} = 0.629 \text{ ms} \tag{3-51}$$

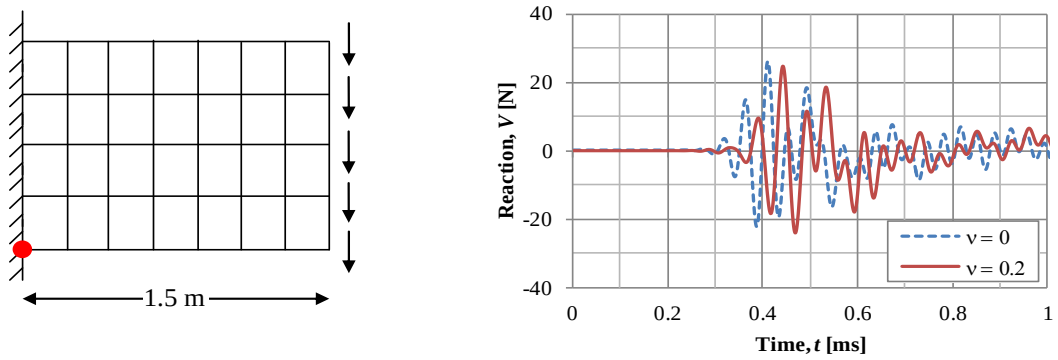

(a) (b)

Figure 3.13. The modelling of a shear wave. Larger difference between the model with ν = 0.2 or ν = 0 implies that shear action is of more importance.

3.5.4.4 Influence by choice of time step

The wave propagation problem was investigated in contact with ADINA support, ADINA (2012). ADINA suggested that the initial disturbed region before the wave front occurs because the critical time has not been used and therefore numerical errors occur. According to ADINA, using a time-step close to the critical time step is vital in order to capture the wave properly. It is also suggested that the implicit method should be carried out with the Bathe Composite Method, which provides better results. The shear wave propagation is currently a researched subject ADINA (2012), and a straightforward recommendation for the critical time step for a shear wave does not exist. Reasonably, it would be the element length over the shear wave speed but this relationship could not be found. The critical time step is the time the wave propagates one element, ADINA (2010) and defined as

$$\Delta t_c = \frac{L_e}{c} \tag{3-52}$$

Where L_e is the element length and

$$c_{Beam} = \sqrt{\frac{E}{\rho}} \quad \text{or} \quad c_{Beam} = \sqrt{\frac{G}{\rho}} \tag{3-53}$$

$$c_{2Dsolid} = \sqrt{\frac{E}{\rho(1-\nu^2)}} \quad \text{or} \quad c_{2Dsolid} = \sqrt{\frac{G}{\rho}} \tag{3-54}$$

for beam and 2D-solid elements, respectively, according to ADINA (2010).

The chosen time step affects the wave propagation considerably. Figure 3.14 shows the support reaction when the critical time step is used. As seen, the agreement between the theoretical wave front (blue dotted line) and the wave front in ADINA is good. The previous found numerical errors before the wave front are decreased considerably. However, it does not seem like the shear wave can be well explained by beam elements and this is further supported by the fact that Poisson's ratio does not affect the answer.

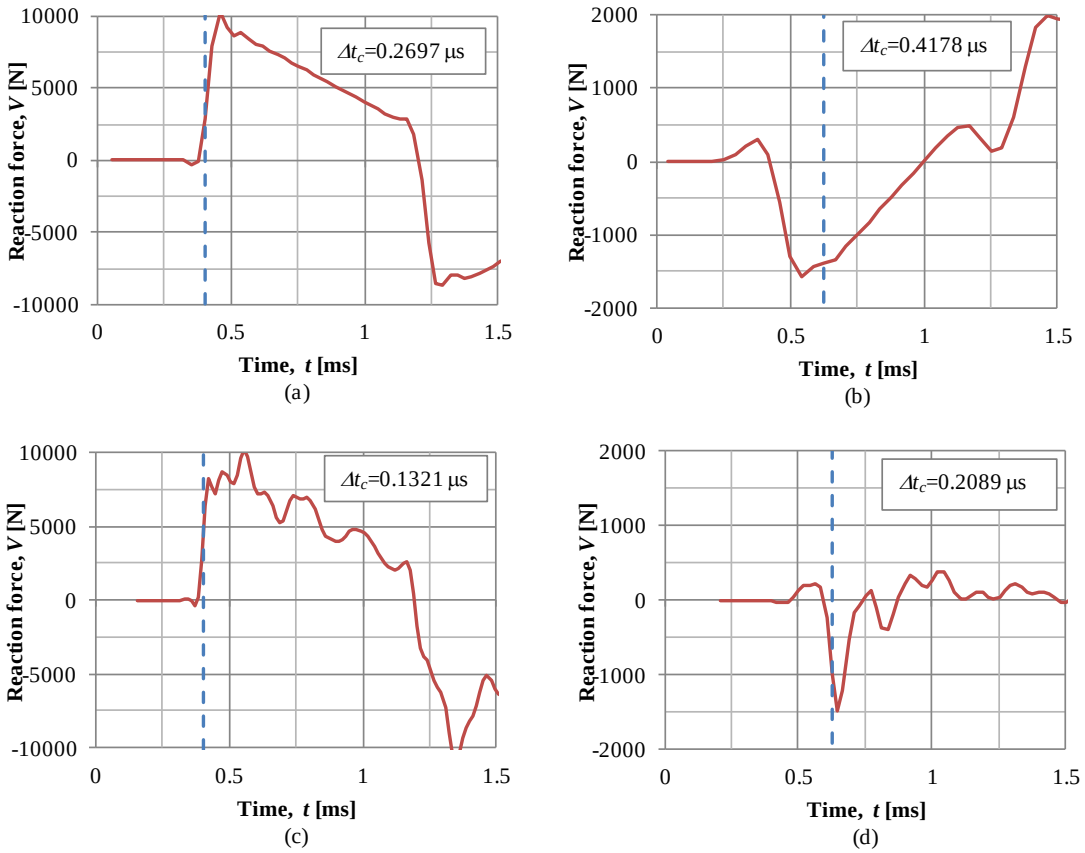

Figure 3.14. Support reaction when using the critical time step for a) beam elements with axial force, b) beam elements with transverse force, c) solid 2D-elements with axial force and d) solid 2D-elements with transverse force.

Since wave propagation affects the result it is necessary to model the wave correctly. However, other simplifications may induce problems when modelling the wave speed but it is important to know the real solution.

3.5.5 Integration schemes

ADINA can use two integration schemes; the implicit method and the explicit method. For the implicit time integrations the trapezoidal rule is used. This method is also referred to as the constant-average acceleration method of Newmark, which is obtained if the Newmark method is used and the parameters δ and α are set to 0.5 and 0.25, respectively. For explicit time integration the Central Difference Method is used. This is described in Appendix A and is the Newmark method with $\delta = 0.5$ and $\alpha = 0$. The explicit method is a faster method but has a small critical time step that has to be fulfilled in order to get stable results. Since analyses of explosions require small time steps anyways, though, it can be beneficial to use the explicit method in more complex analyses. Augustsson and Härenstam (2010) showed that there is not a significant difference when using a 2D beam element, but the trapezoidal rule integration scheme is preferable when 3D beam elements are considered.

When using the explicit method for a linear elastic beam modelled with beam elements, the deformations did not correspond well to the expected one using hand calculations or the implicit method, see Figure 3.15. The latter two, though, agree

very well as also seen in for example previous Master's theses. According to ADINA, this is due to the fact that the explicit method always uses a lumped mass matrix while the trapezoidal rule uses a consistent mass matrix. However, using the implicit method with a lumped mass matrix does not correspond to the explicit solution. An interesting observation is that there is a very good agreement between the simplified SDOF method using the transformation factor κ_{mF} =1 and the explicit solution.

This problem is identified but will not be treated further in this thesis and the implicit method will be used in further analyses. A recommendation for further work is that care should be taken when the explicit integration scheme is used.

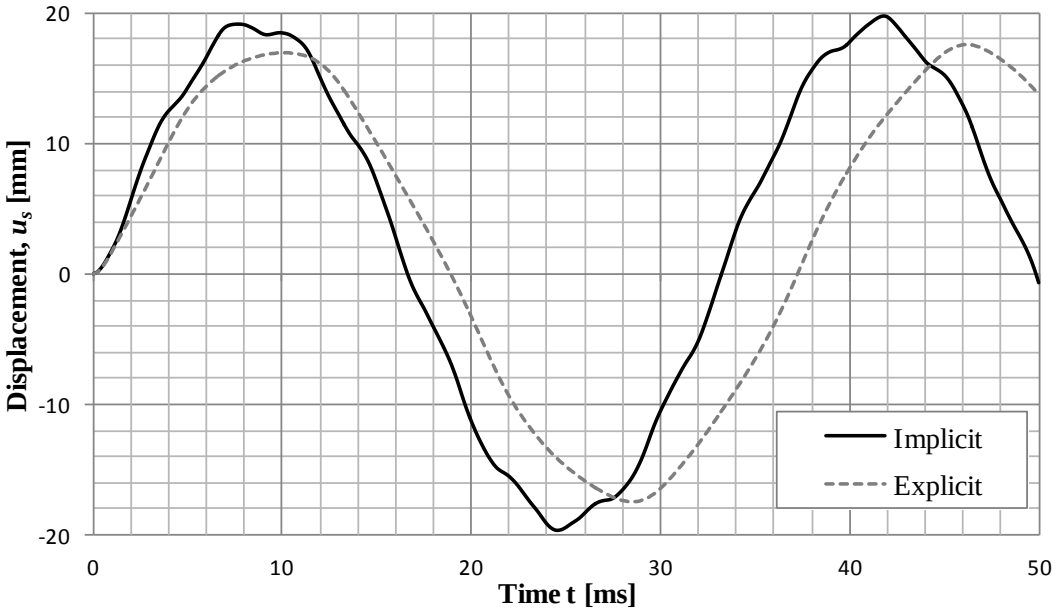

Figure 3.15. ADINA's two integration schemes give different results. The explicit method always uses a lumped mass which gives incorrect values.

3.5.6 Output

Section forces can be extracted in two ways; either by using section forces in the integration points or as nodal forces. Section forces can only be used when the response is linear elastic. Otherwise, nodal forces must be obtained in every element node. Therefore, nodal forces have been used and further treated in other programs.

3.5.6.1 Shear force

The shear force is constant within an element as shown in Figure 3.16. The constant shear force corresponds to the shear force in the centre of the element. This means that the nodal force is the same in both element nodes but with opposite sign because of ADINA's sign convention. The shear force has been taken as the nodal force in the first node of every element and positioned in the centre of the element.

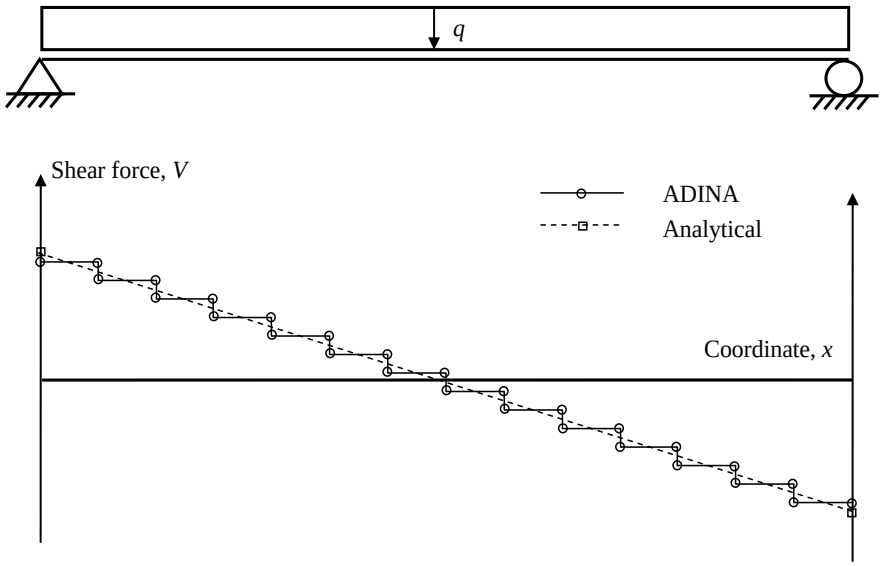

Figure 3.16. ADINA gives output in the nodes. The analytical support reaction can be obtained by interpolation in static cases. This is impossible for dynamic cases where the shear force does not vary linearly.

The nodal force in the first node of the element closest to the support is not the same as the support reaction. For a static case, the nodal forces in two nodes can be used to linearly interpolate the support reaction. However, if the shear force distribution is non-linear, as it is for a dynamic case, this cannot be done. Instead, the actual value of the support reaction can be found in ADINA and used for the support reaction.

The support reaction is slightly higher than the nodal force in the first element at the beginning of an impulse loading and then decreases to obtain a lower value. The results should reasonably agree better if more elements are used. 30 elements seem to have adequate accuracy compared to 100 elements as shown in Figure 3.17. The support reaction is exactly the same for both choices of number of elements.

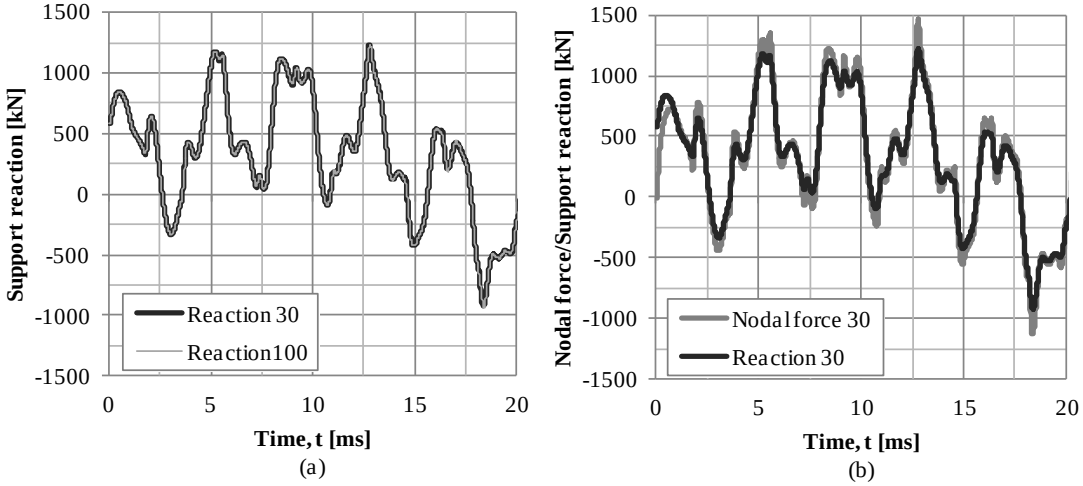

Figure 3.17. Comparison between support reaction and shear force in node closest to the supports for different number of elements

3.5.6.2 Moment

The moment varies linearly over an element and has been taken as the moment in the first node of every element and positioned in the node. The moment in a structure with plastic response can never exceed the maximum moment capacity. However, as will be seen in Chapter 5, the nodal moment can be higher for some time steps. The reason for this is unknown but is believed to depend on numerical errors in ADINA. The stresses in an analysis with the same input data never exceed the input fictional yield stress calculated in Section 3.5.3.

Nodal moments are only a post-process of the results and the analyses use stresses when calculating the result. Consequently, the actual result remains accurate. Figure 3.18 shows the moment in midpoint when using nodal moments or by calculating a moment from corresponding stress. The curves follow each other, but the nodal moment exceeds the maximum at two points. The moment calculated with the stress distribution is never greater than the maximum moment. This raises the question that the moment distributions should possibly be examined with stresses instead of nodal moments.

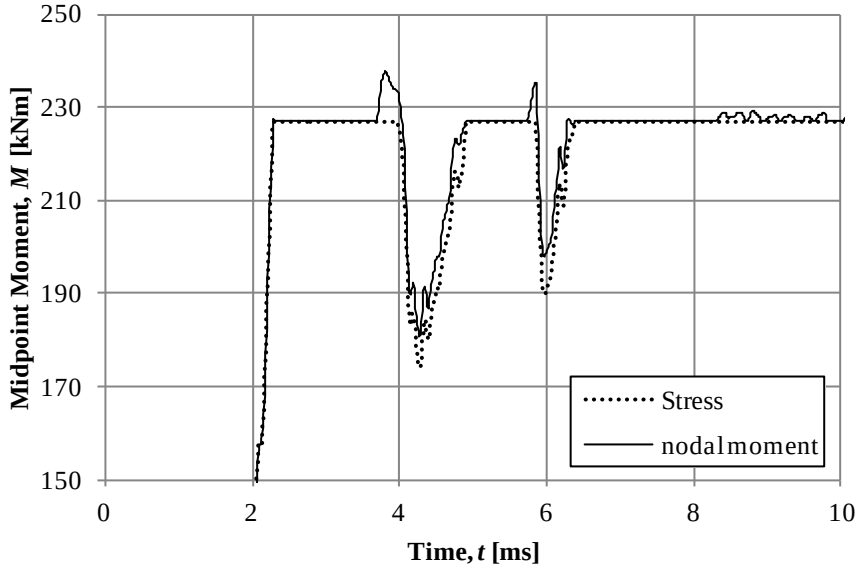

Figure 3.18. Comparison between nodal moment results and moment calculated from the stress distribution.

4 Displacement

4.1 Midpoint displacement

4.1.1 Elastic analysis

The SDOF-model represents the deformation obtained by the FE-analysis well when a linear elastic material behaviour is considered. The only pronounced difference is that the SDOF method gives a smooth curve while the oscillations from the FE-analysis are uneven. The result for the linear elastic material behaviour in state I and II are shown in Figure 4.1. It can be seen that the state II section, which is less stiff, gives a higher deformation but oscillates with a lower frequency. The simplified hand calculation method generally gives a slightly larger maximum deformation than what can be obtained in the more accurate methods due to the simplification of a characteristic impulse load. Very good agreement is also found for less impulsive loads but they, as expected, diverge more from the hand calculation since the load is less like a characteristic impulse load.

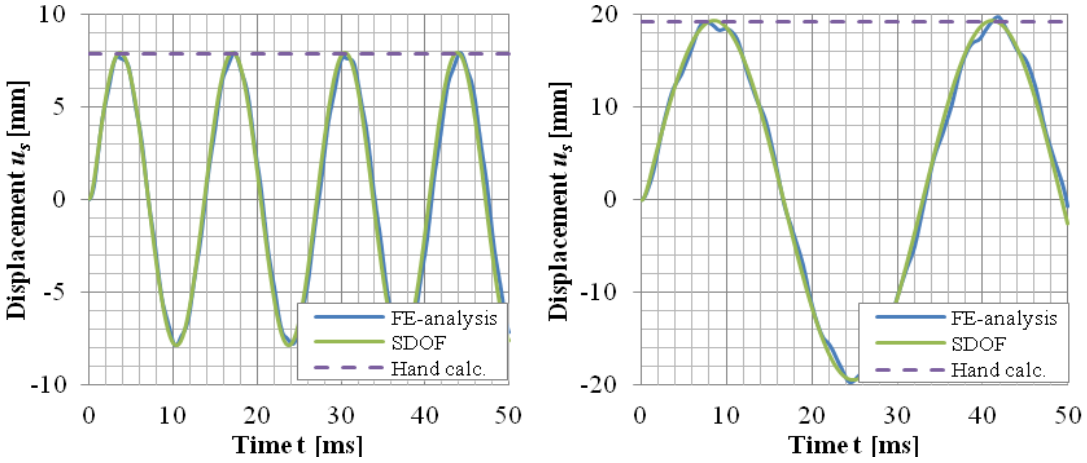

Figure 4.1. Displacement versus time for different analyses for a concrete beam with linear elastic response modelled in a) state I and b) state II subjected to a load with peak pressure 5000 kPa and load duration of 1.12 ms.

The small oscillations in the midpoint deformation in the FE-analysis occur because the FE-analysis takes higher modes of vibration into account, see Figure 4.2. The SDOF-model does only consider the fundamental mode of vibration, which makes it smooth.

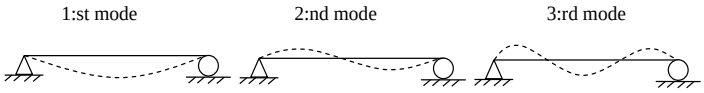

Figure 4.2. Modes of vibration for a simply supported beam.

4.1.2 Ideal plastic analysis

There is a significant divergence between the FE-analysis, equivalent SDOF-model and hand calculations for the ideal plastic material model. These convergence problems have also been encountered in e.g. Augustsson and Härenstam (2010). The difference between the SDOF analysis and the hand calculation method is dependent on the assumption of a characteristic impulse load. According to Section 2.4.2.7, the error in displacement for an ideal plastic structure, can be evaluated from

$$\gamma_F = \frac{F_{peak}}{R_m} = \frac{5000 \cdot 3}{605} = 24.8 \tag{4-1}$$

For a triangular load this corresponds to an error in displacement of approximately 5-10 %. For decreasing γ_F, the error increases. This means that for a less impulsive load, load case 3, the difference should increase. This is also the case in Figure 4.3 and Figure 4.4, which show the response for load case 1 and 3, respectively.

The difference between the SDOF calculations and the FE analysis may arise due to an incorrect assumption of the deformation shape. Consequently, the transformation factor used in the SDOF-model will be underestimated and the maximum deflection overestimated. The midpoint deformation for an ideal plastic beam using the three approaches can be seen in Figure 4.3. The SDOF and FE-solutions agree better if load case 3, with lower peak pressure and longer duration is used, see Figure 4.4. However, there is still a significant divergence that must be investigated.

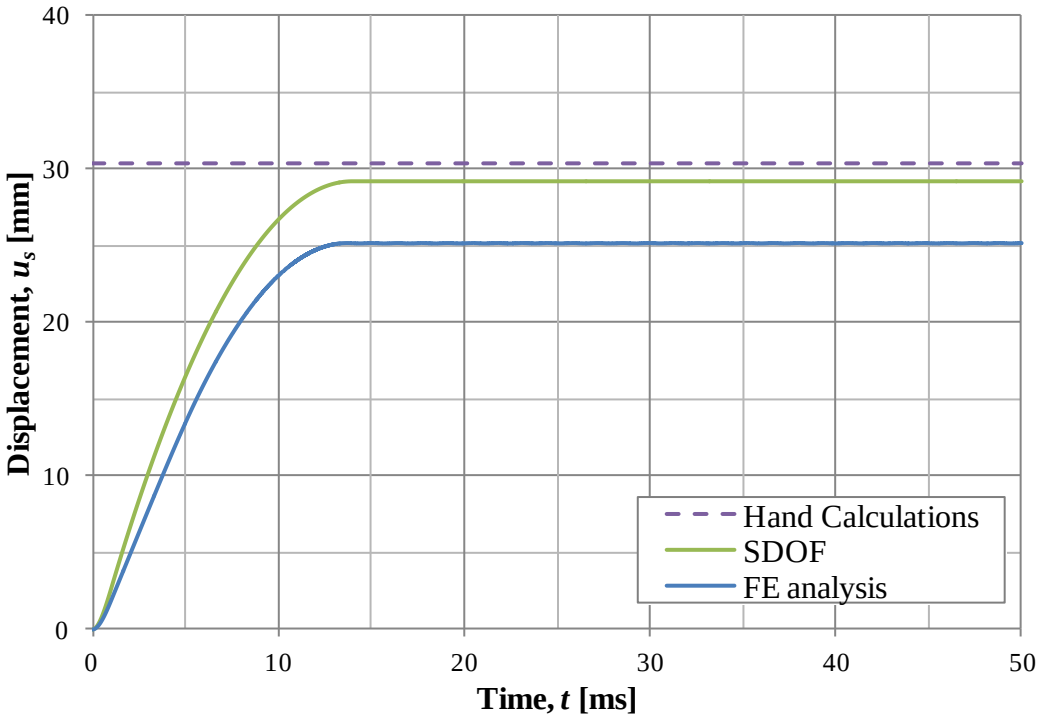

Figure 4.3. Displacement versus time for different analyses for a reinforced concrete beam with ideal plastic response subjected to load case 1.

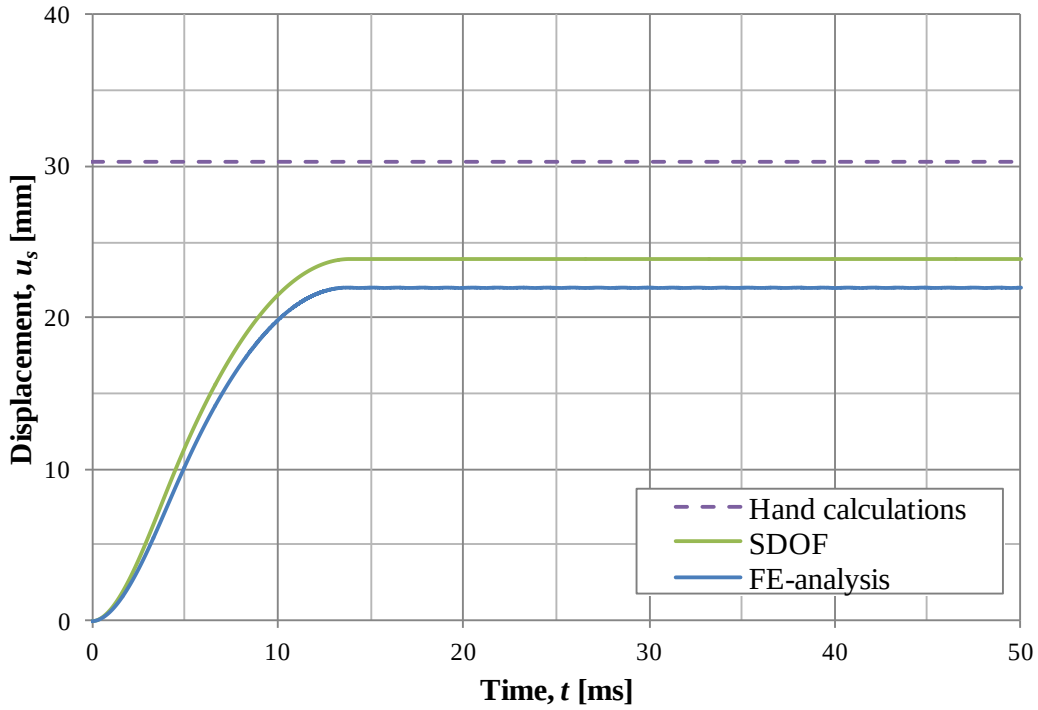

Figure 4.4. Displacement versus time for different analyses for a concrete beam with ideal plastic response subjected to load case 3.

4.1.3 Elasto-plastic analysis

The elasto-plastic model is the most realistic model and consequently the most interesting. The deflection in an elasto-plastic SDOF-model can be found by combining the linear elastic and the ideal plastic material models. The main problem in the elasto-plastic simplification is which transformation factors should be used. Three alternatives are studied here:

Elastic response:

$$\kappa_{mF} = 0.788 \tag{4-2}$$

Plastic response

$$\kappa_{mF} = 0.667 \tag{4-3}$$

Elasto-plastic response

$$\kappa_{mF} = \begin{cases} 0.788 & \text{when } R < R_m \\ 0.667 & \text{when } R = R_m \end{cases} \tag{4-4}$$

The midpoint deformation for the different alternatives is shown in Figure 4.5 for load case 1 and in Figure 4.6 for load case 3.

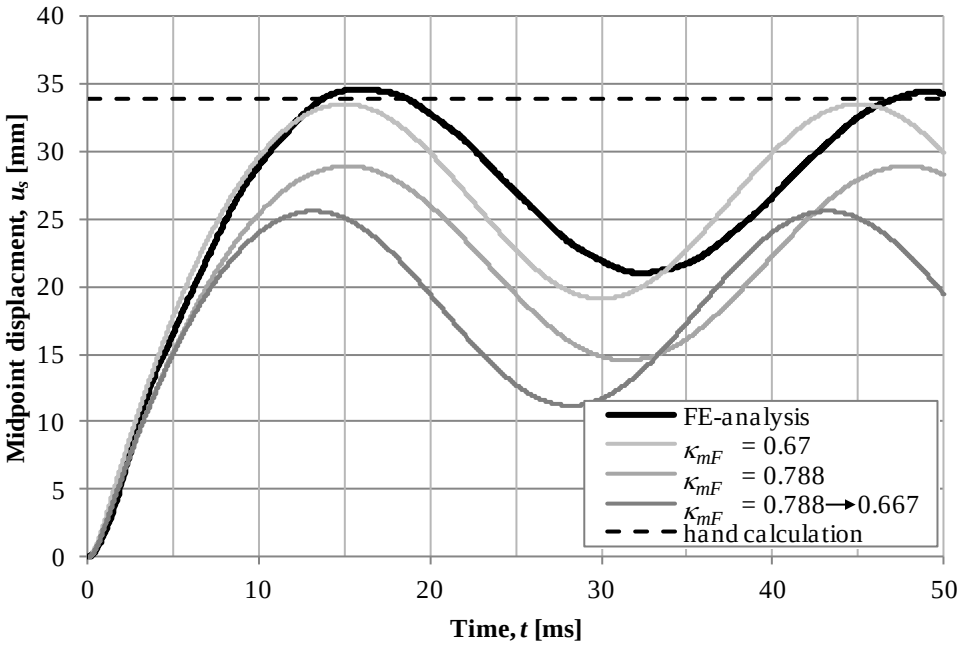

Figure 4.5. Displacement versus time for different analyses for a concrete beam with elasto-plastic response subjected to load case 1.

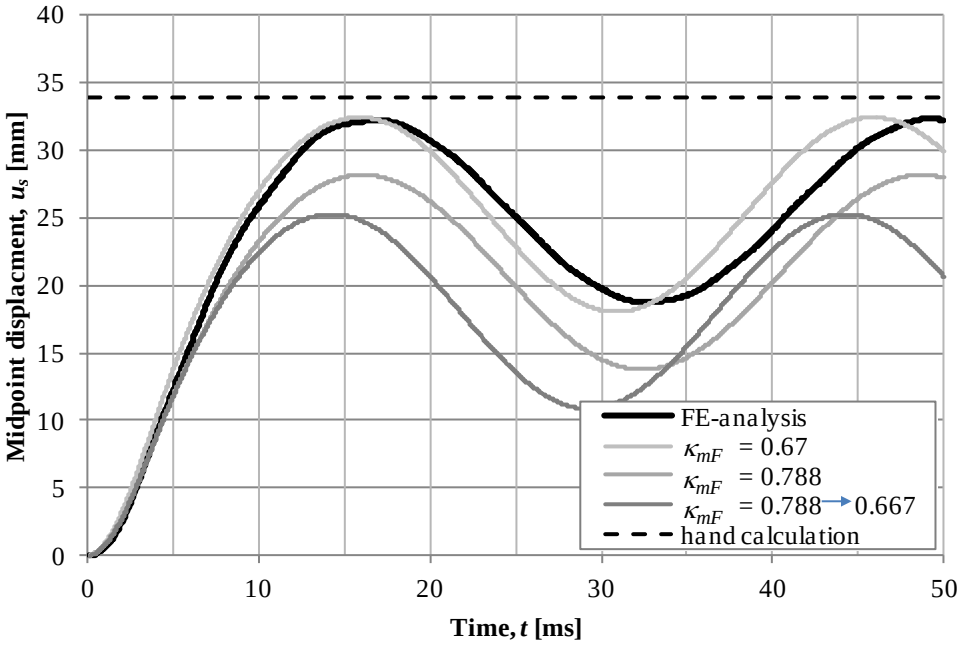

Figure 4.6. Displacement versus time for different analyses for a concrete beam with elasto-plastic response subjected to load case 3.

Presumably, the best modelling should be to have an elastic transformation factor in the elastic region and a plastic transformation factor when the structure has started to yield in the midpoint. However, this approach underestimates the deformation significantly. If the transformation factor for linear elastic response is used, the deformation is slightly better estimated. The best convergence is obtained when the plastic transformation factor is used during the whole deformation process.

This has been seen as a coincidence resulting from combining incorrect assumptions, Johansson (2012). Knowing that this is not correct it can be used as a crude simplification. It is better for less impulsive loads, load case 3. Nevertheless, this is not sufficient accuracy and more precise transformation factors can be found from a detailed FE-analysis similar to the simpler material models. This is done in Section 4.4.4.

4.2 Deformation shape

4.2.1 Introduction

The transformation factors come from an assumed displacement shape. Therefore, it is of interest to investigate the real deformation shape and compare it to the assumed theoretical deformation shape. This has been seen as a potential reason why the SDOF solutions have not agreed perfectly with the more detailed FE analyses. The deformation shapes that vary with the peak load and time duration have been taken out from FE analyses for every time step and are then compared to get better understanding of the beam's behaviour when it is subjected to an impulse load. The deformation shape for many time steps are shown in Appendix G.

4.2.2 Elastic analysis

The initial response for a linear elastic beam is not the same as that assumed. This is seen for all load cases although the difference is greater for a more impulsive load, load case 1 than for load case 3, see Figure 4.7 and Figure 4.8. Notice the different scales. The early deformation is characterised with a near rigid body motion.

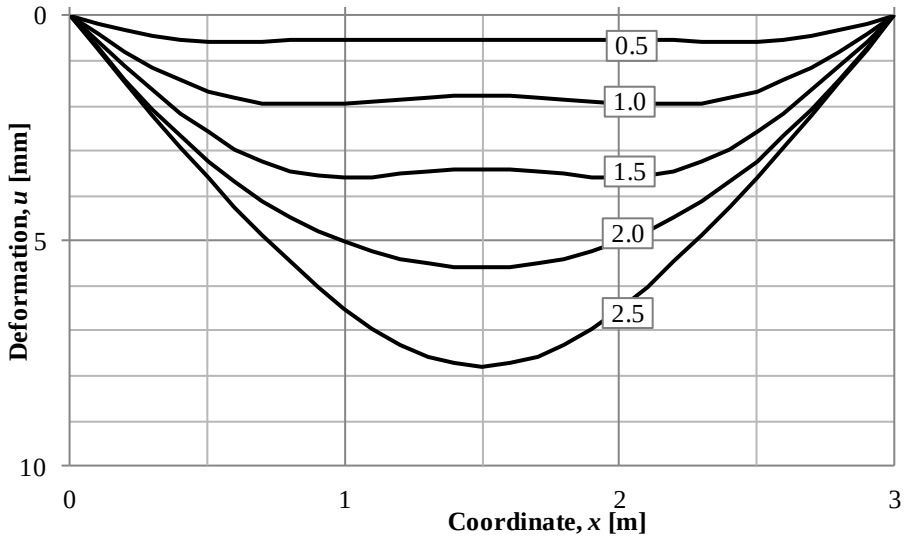

Figure 4.7. The early deformation shape for a linearly elastic beam subjected to load case 1, P_{peak} = 5000 kPa and t_{Δ} = 1.12 ms.

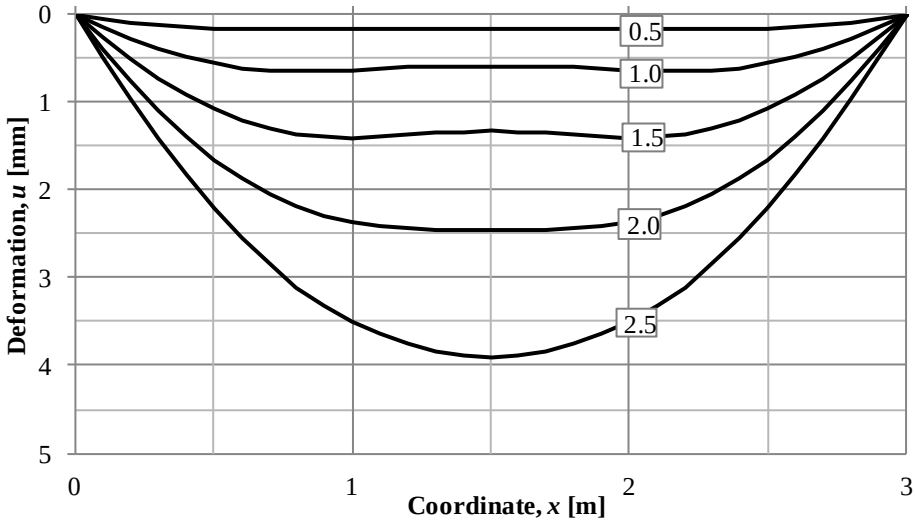

Figure 4.8. The early deformation shape for a linearly elastic beam subjected to load case 3, P_{peak} = 1250 kPa and t_{Δ} = 4.48 ms.

In order to investigate if the beam follows a rigid body motion this was compared by modelling the rigid body motion in the FE analysis for the same load but without supports, see Figure 4.9. In this is can be observed that some parts of the beam will eventually start to move faster than a rigid body motion after 0.5 milliseconds. Two arcs start to form close to the supports and progress towards the centre where they come together and the assumed elastic deflection shape will emerge at around 2 milliseconds. The centre part has now deformed more than a rigid body motion. The reason for why some parts move faster than a rigid body motion is unknown but is believed to depend on the force propagating through the beam in a wave motion. The duration of this behaviour is approximately the same as for the wave propagating 3 metres, i.e. the length of the beam.

$$L = c \cdot t = \sqrt{\frac{E}{\rho}} \cdot t = \sqrt{\frac{5.18 \cdot 10^9}{2400}} \cdot 0.002 = 2.95 \text{ m} \tag{4-5}$$

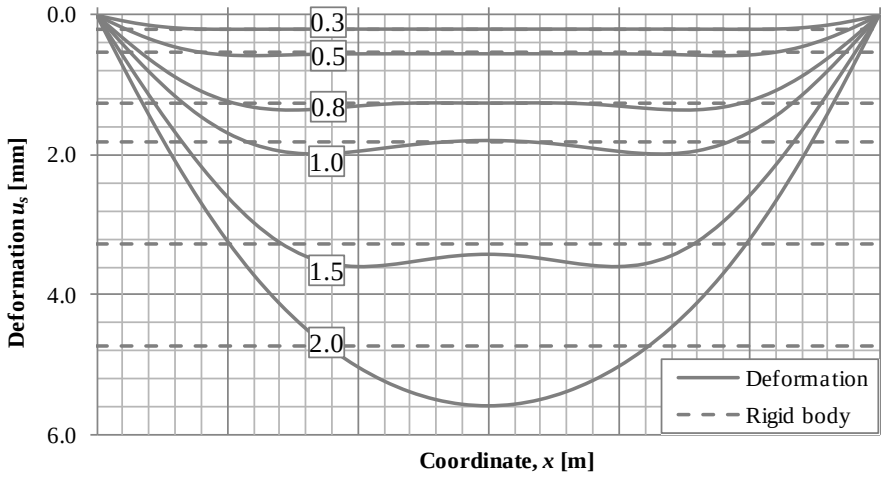

Figure 4.9. Comparison between a rigid body motion and the elastic deformation. The numbers denote which time, in milliseconds, the deformation occurs.

A parameter study was performed according to scheme 1 in Section 3.5.2. The bending stiffness, *EI*, was kept constant by varying Young's modulus, *E* and the moment of inertia *I*. These models generate the same response in static analyses, while the dynamic analyses differ. The wave speed depends on Young's modulus and the influence of wave propagation can therefore be investigated by implementing this scheme. A higher Young's modulus will make this wave form occur earlier. Problems were encountered when decreasing Young's modulus; this is discussed in Section 3.5.2. This means that the initial deformation shape depends on the wave speed. When increasing Young's modulus, the wave speed increases and the wave propagates faster through the structural element.

4.2.3 Ideal plastic

The initial deformation shapes have been investigated for the ideal plastic material model. It can be seen that there is a very pronounced rigid body motion in the centre when subjected to load case 1, see Figure 4.10. The length of this zone decreases and the deformation will eventually be concentreated in the midpoint. It takes more than 5 ms until a concentrated plastic hinge has formed in the centre and the deformation shape is somewhat like that assumed for plastic response. The significance of the rigid body motion is decreased for a less impulsive load, load case 3, as seen in Figure 4.11.

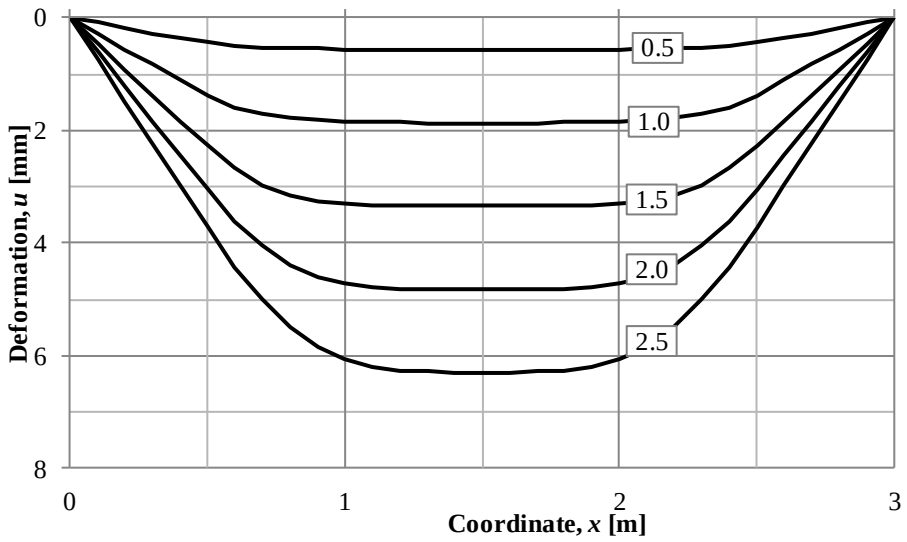

Figure 4.10. Deformation shape versus time for a concrete beam with ideal plastic response subjected to a load with peak pressure 5000 kPa and a load duration of 1.12 ms.

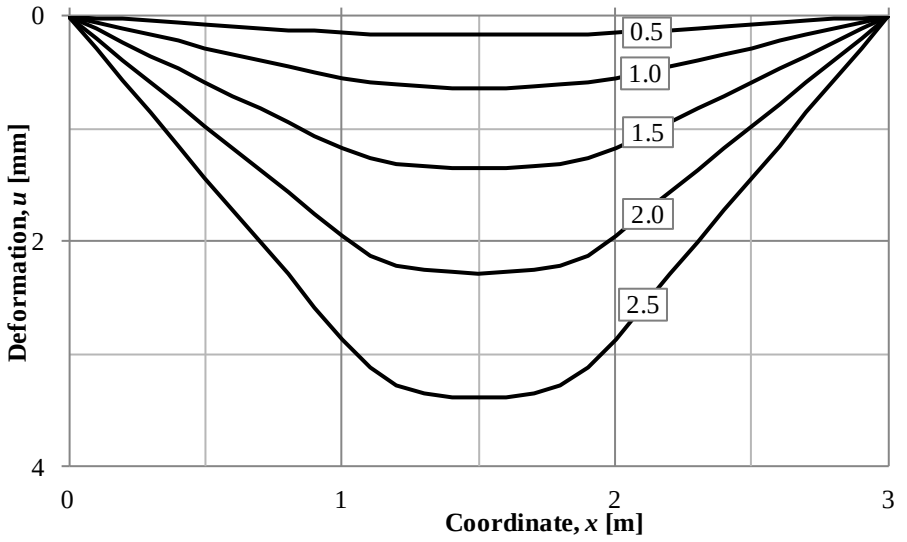

Figure 4.11. Deformation shape versus time for a concrete beam with ideal plastic response subjected to a load with peak pressure 1250 kPa and a load duration of 4.48 ms.

The ideal plastic model assumes a very high Young's modulus and since ADINA (2010) always uses the elastic wave propagation this may induce incorrectness with the wave propagation. If the displacement shape is investigated at a very early phase, i.e. 0.05 ms, the wave form that occurs in an elastic structure takes place.

4.2.4 Elasto-plastic analysis

The elasto-plastic deformation picture is the most realistic one and can be explained with the two simplified material models in Section 4.2.2 and 4.2.3. The initial deformation shape is similar to the one obtained in the linear elastic case until the structure starts to yield. Close to the edges the beam will be displaced more than in the centre. Yield will not start in the centre as expected in a static case. It will start closer to the edges and move towards the centre. This is further shown when the moment and shear distribution is investigated in Chapter 5.

The deformation shape for load case 1 is exactly the same as for the linearly elastic case for the first 2.5 ms, see Figure 4.7 for load case 1 and Figure 4.8 for load case 3. The deformation shape is then affected by plasticity somewhere in the beam.

After the initial elastic deformation the response will be more similar to the plastic response. A concentrated plastic hinge will eventually form in the midpoint of the beam as seen in Figure 4.12.

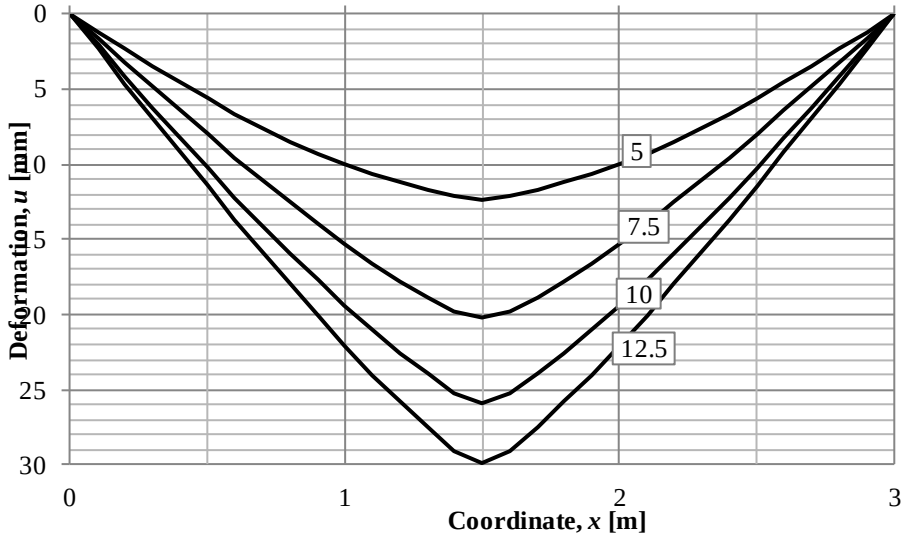

Figure 4.12. Later deformation shape for the elasto-plastic material model subjected to load case 1.

4.3 Energy balance

4.3.1 Introduction

The energy balance in the FE and SDOF analyses was compared. In line with the definition of work, the system has kinetic energy, W_k, internal energy, W_i, and external energy, W_e. The sum of the internal and kinetic energy should be equal to the external energy to have balance in the system.

$$W_e = W_i + W_k \tag{4-6}$$

The external energy is simply the force times the displacement. This is done in the FE-analysis by integrating the force acting on every node times the corresponding displacement for that node at every time according to equation (4-7). The same calculation is performed for the SDOF-approach but using the system point

displacement. The kinetic energy is also found easily by multiplying the square of the velocity in every node with the mass for that node, see equation (4-8). In the SDOF method this is done by multiplying the equivalent mass with the square of the system point velocity. The last energy is the internal energy. This can be calculated as the integral of the moment times the change in curvature over an element if no consideration is taken to shear or normal deformations, see equation (4-9). In the SDOF model it is simply the integral of the resistance times the deformation. The formulas are summarised in Table 4.1.

Table 4.1. Definition of work for the FE analysis and the SDOF model respectively.

	FE analysis	SDOF model	
Kinetic energy	$W_k = \int_{x=0}^{x=L} \frac{m(x)v(x)^2}{2} dx$	$W_k = \frac{\kappa_m m v_s^2}{2}$	(4-7)
Internal energy	$W_i = \frac{1}{2} \int_{x=0}^{x=L} M(x)u''(x)dx$	$W_i = \kappa_F R u_s$	(4-8)
External energy	$W_e = \int_{x=0}^{x=L} q(x)u(x)dx$	$W_e = \kappa_F F u_s$	(4-9)

It is important to realise that the energy in the system is proportional to

$$W \propto \frac{\kappa_F^2}{\kappa_m} \tag{4-10}$$

and that the deformation is proportional to

$$u \propto \frac{\kappa_F}{\kappa_m} \tag{4-11}$$

This can give a higher energy level although the deformation is lower. For instance, if the transformation factors are increased with the same factor, say ξ,

$$\left(\frac{\kappa_F}{\kappa_m}\right)_{new} = \frac{\xi\kappa_F}{\xi\kappa_m} = \frac{\kappa_F}{\kappa_m} \tag{4-12}$$

$$\left(\frac{\kappa_F^2}{\kappa_m}\right)_{new} = \frac{\left(\xi\kappa_F\right)^2}{\xi\kappa_m} = \xi \cdot \frac{\kappa_F^2}{\kappa_m} \tag{4-13}$$

This will make the energy increase while the deformation of the midpoint remains unaffected.

4.3.2 Elastic analysis

The theoretical external work for the state II linearly elastic model can be determined

$$W_e = W_k = \frac{8400^2}{2 \cdot 0.788 \cdot 2880} \cdot 0.64 = 9949 \text{ J} \tag{4-14}$$

The energy in the two systems can be seen in Figure 4.13 and Figure 4.14. The first observation is that the energy in the FE-analysis is higher than that expected using hand calculations. The kinetic energy is very similar but the system gets some internal energy which makes the total work somewhat larger than the theoretical work obtained using hand calculations. It is shown in Appendix E, in which several load cases are examined, that for a load more similar to a characteristic impulsive load, load case 0 in Figure 3.1, the total work is even higher while a load more similar to a static load has a better agreement with hand calculations. The external energy is in equilibrium with the internal energy. This is believed to depend on that the transformation factors are higher for a very impulsive load, while they are more similar to the theoretical transformation factors for a less impulsive load, load case 3.

The total work in the FE-analysis is reasonably well described by the equivalent SDOF model as seen in Figure 4.13 and Figure 4.14. The total work is slightly lower and much smoother in the SDOF model than in the FE-analysis. This is again since the SDOF model only considers the first mode of vibration. The first peaks of the kinetic energy in the two systems are almost identical. The energy in the SDOF model is the same as the theoretical energy.

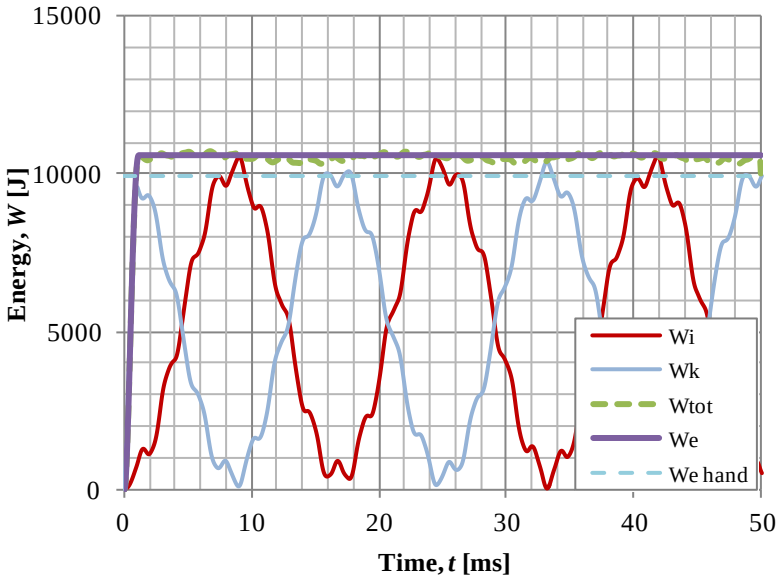

Figure 4.13. The energy balance in the FE analysis for load case 1.

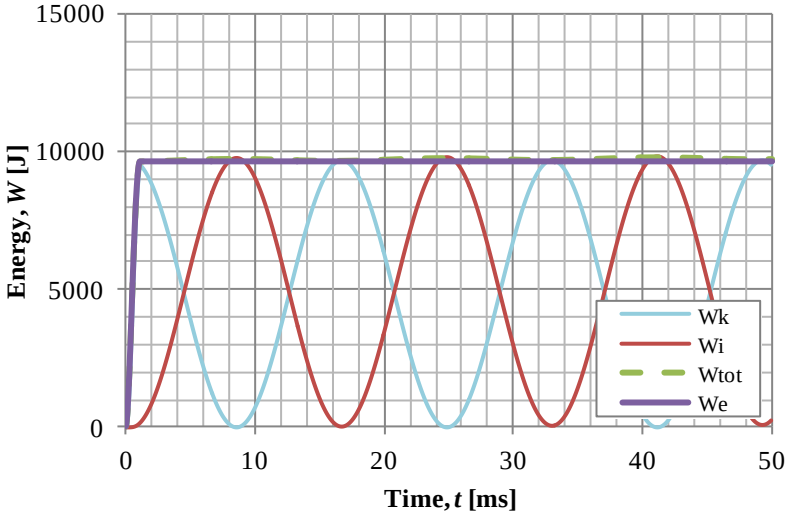

Figure 4.14. Energy balance in the SDOF model for load case 1.

4.3.3 Ideal plastic analysis

Similarly to the elastic case, the work has been investigated for the plastic case. The theoretical external work can be estimated to

$$W_e = W_k = \frac{I_k^2}{2\kappa_{mF} m}\kappa_F = \frac{8400^2}{2 \cdot 0.667 \cdot 2880} 0.5 = 9183 \text{ J} \tag{4-15}$$

As for the elastic case, the total work is slightly underestimated with hand calculations but acceptable agreement is obtained. The kinetic energy, W_k, is much lower than what the theoretical solution predicts, which means that the structure absorbs more energy as internal energy in the beginning; i.e. the load intensity is lower than that corresponding to a characteristic load. The structure decreases its velocity and eventually the external energy is balanced with internal energy.

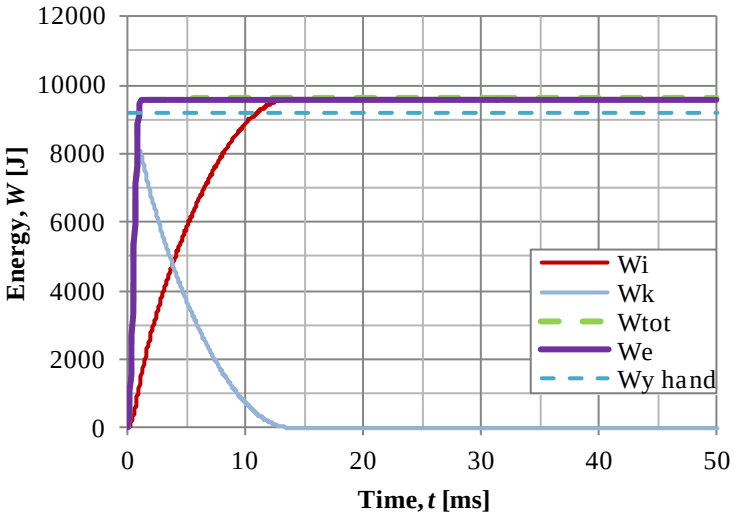

Figure 4.15. Energy balance for the FE-analysis with ideal plastic response.

The energy in the SDOF model is lower than in the FE analysis. This is because the actual transformation factors are higher than what the theoretical value suggests, compare with reasoning in Section 4.3.2. As a result all the energies will be lower. The SDOF energy is also lower than the theoretical energy. This is probably a consequence of that the internal energy increases very fast and that it cannot be said that all energy is transformed to the structure as kinetic energy.

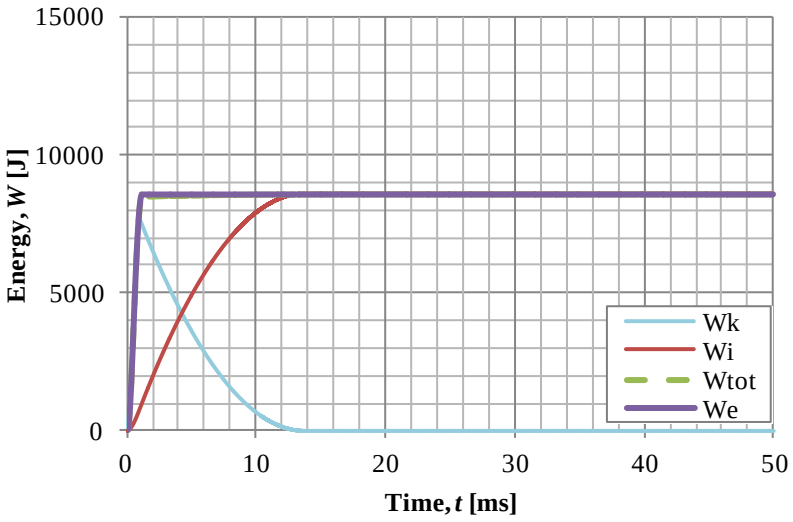

Figure 4.16. The energy balance in the SDOF-model.

Although the energy is lower in the SDOF model, the displacement is larger as seen in Section 4.1.2. This is due to that the displacement depends on the factor

$$u_{pl} = \frac{I_k^2}{2\kappa_{mF} \cdot m \cdot R} \tag{4-16}$$

where the theoretical κ_{mF} is initially underestimated, which makes the deformation become larger. The work depends on

$$W_e = \frac{I_k^2}{\kappa_{mF} \cdot m} \kappa_F \tag{4-17}$$

and this transformation factor ratio is underestimated with the theoretical values, compare reasoning in equations (4-12) and (4-13).

4.3.4 Elasto-plastic analysis

In the elasto-plastic case two hand calculations were made, using either the elastic transformation factors or the plastic transformation factors. As seen in both the linear elastic and ideal plastic case, the total energy is higher in the FE model than in the hand calculations, for load case 1 shown in Figure 4.17. The same reasoning is made here. The theoretical transformation factors are underestimated and will decrease the external energy.

At around 1 ms, when the load has just disappeared, a sudden change in energy happens. This can also be seen in the elastic case and is believed to depend on elastic oscillations. It can also be seen that the internal energy initially is larger than in the

SDOF analyses, see Figure 4.18, Figure 4.19 and Figure 4.20, and that the external energy is not the same as the kinetic energy.

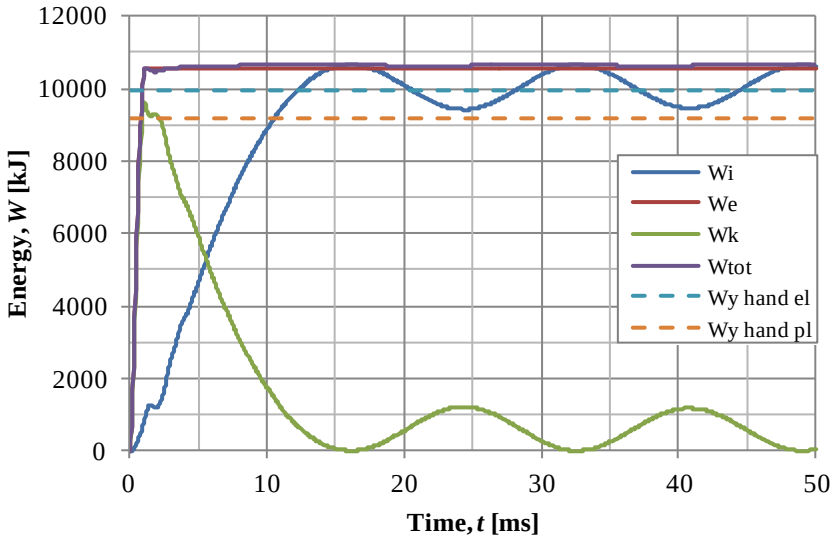

Figure 4.17. The energy balance for an elasto-plastic beam subjected to load case 1 analysed with FE.

The energy balance is calculated for the SDOF-model with different transformation factors, see Figure 4.18, Figure 4.19 and Figure 4.20. Common for all cases is that the energies are lower than the energy in the FE-model. It is lowest for the plastic transformation factor. This is due to that the transformation factors for this assumption are most incorrect.

The methods that use the elastic transformation factor have the same external and internal work until it changes to the plastic transformation factor in the latter method. There is a sudden drop in the kinetic energy at this time. This results in an unbalanced energy while the other two methods keep the balance between total work and external work.

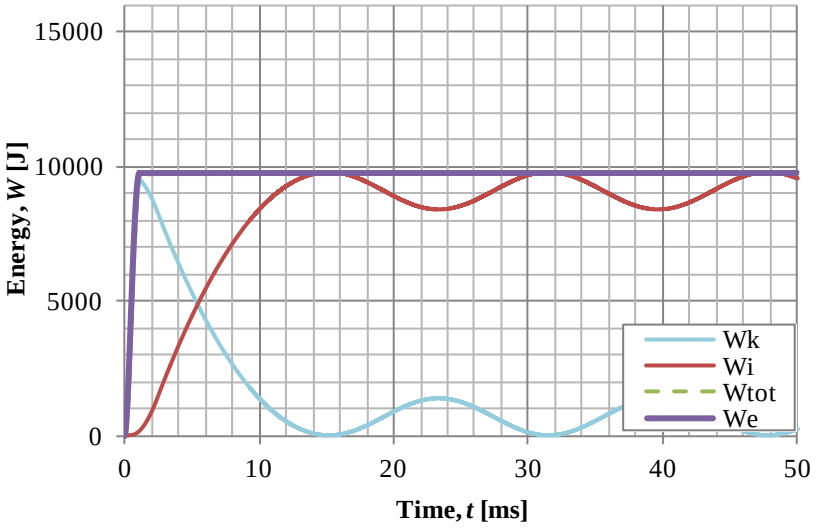

Figure 4.18. Energy balance for an SDOF solution with transformation factors elastic theoretical transformation factors.

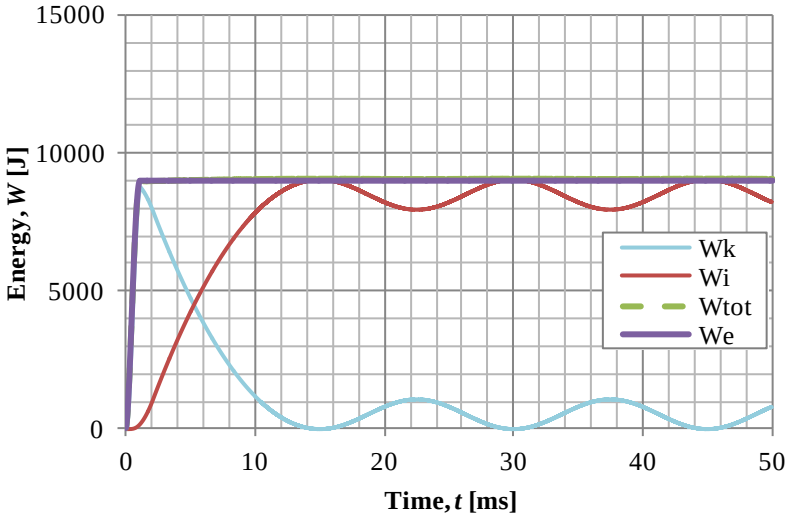

Figure 4.19. Energy balance for an SDOF solution with ideal plastic transformation factors.

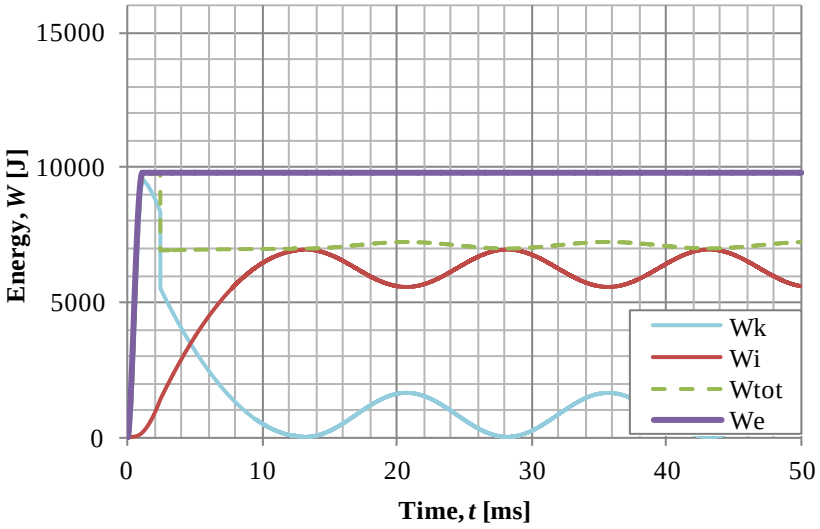

Figure 4.20. Energy balance for an SDOF solution using theoretical elastic transformation factors until the maximum resistance is reached and then by using theoretical plastic transformation factors.

4.4 Transformation factors

4.4.1 Calculation of factors

The disagreement between the displacement of the midpoint in the FE-analysis and the SDOF-model is believed to be affected by assuming the wrong deformation shape at early phases of the deformation. As shown in Section 4.2, a beam subjected to an impulse load will initially not have the assumed deformation shape.

The transformation factors for the actual deflection shape for every time step can be found from the FE-analysis. The transformation factors are found with the formulas

$$\kappa_m(t) = \frac{1}{L}\int_0^L \frac{u(x,t)^2}{u_s(t)^2}dx = \frac{1}{L}\cdot\frac{\sum_i^n u_i(t)^2 L_i}{u_s(t)^2} = \frac{1}{n}\frac{\sum_i^n u_i(t)^2}{u_s(t)} \tag{4-18}$$

$$\kappa_F(t) = \frac{1}{L}\int_0^L \frac{u(x,t)}{u_s(t)}dx = \frac{1}{L}\cdot\frac{\sum_i^n u_i(t) L_i}{u_s(t)} = \frac{1}{n}\frac{\sum_i^n u_i(t)}{u_s(t)} \tag{4-19}$$

where n is the number of free nodes, i.e. all nodes except the support nodes. L_i is the length of an element and is constant for every element which means that it can be expressed as the total length divided with number of elements. u_i is the displacement in the i:th node and u_s is the deformation of the system point, in this case the centre. These transformation factors are only of interest when the energy is considered as shown in Section 2.4.2.4.

The load-mass transformation factor can then be found as

$$\kappa_{mF}(t) = \frac{\kappa_m(t)}{\kappa_F(t)} \tag{4-20}$$

The time dependent transformation factors are also shown in Appendix F. The individual transformation factors for the load and mass respectively are also shown here.

4.4.2 Elastic analysis

The midpoint deflection for assuming linear elastic response can be very well approximated with an equivalent SDOF-model; the solutions agree very well as seen in Section 4.1.1. As a result, the currently used transformation factor should be a good approximation of the elastic behaviour. The theoretical value of the load-mass transformation factor for elastic deformation is

$$\kappa_{mF} = 0.788 \tag{4-21}$$

If the transformation factor is calculated from the resulting deformation at every time step, seen in Figure 4.21, the theoretical value of the transformation factor agrees very well after a few milliseconds for all load cases. In addition, the agreement is improved if the load has a lower peak pressure and longer duration, i.e. load case 3.

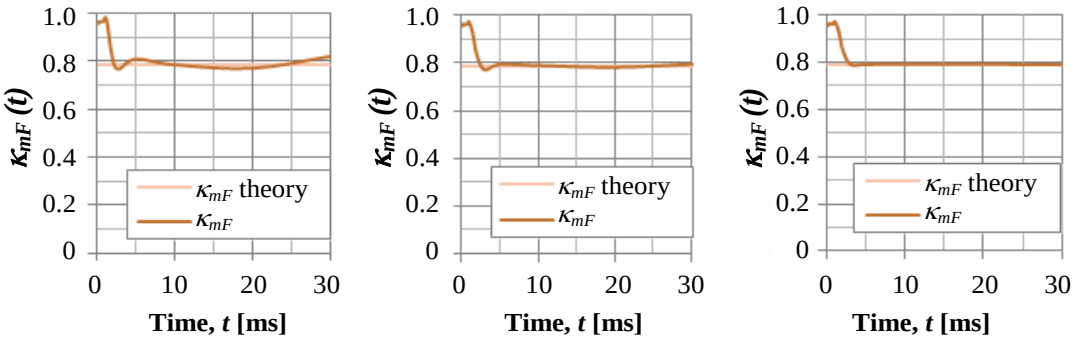

Figure 4.21. Transformation factor for elastic material model obtained from FE-analysis as a function of time for a) Load case 1, b) Load case 2 and c) Load case 3.

As shown in the Figure 4.21, there is a peak in the first few milliseconds. This occurs for all load cases and is of approximately the same magnitude and duration. The displacement shape at this time span is different to the shape assumed for an elastic deflection and is more similar to a rigid body motion, see Figure 4.9.

However, this first peak in the transformation factor does not seem to have a significant influence on the midpoint deformation since the agreement is very good for the elastic case even when using a constant value of κ_{mF}. It can also be noted that the transformation factor goes quickly towards the theoretical value.

4.4.3 Ideal plastic analysis

The midpoint deformations in an SDOF model and an FE-analysis diverge significantly for the ideal plastic case. If the deformation shape is obtained from ADINA, a transformation factor can be calculated for every time step. In Figure 4.22, the transformation factor κ_{mF} is shown for different load cases.

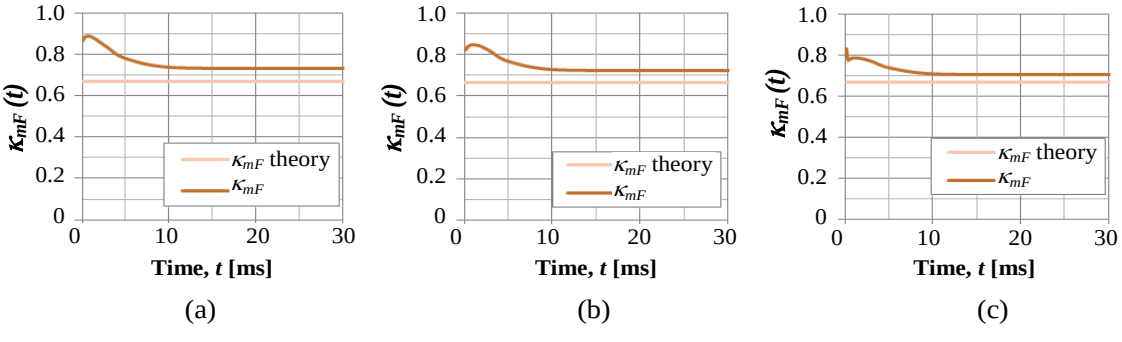

Figure 4.22. The transformation factor κ_{mF} versus time compared with the plastic theoretical values for a concrete beam with ideal plastic response subjected to a) load case 1, b) load case 2 and c) load case 3.

It appears like the first few milliseconds have a higher value of the transformation factor for all load cases. The transformation factor is initially higher for a more load case 1 but is not as high as for the linear elastic case, in Section 4.4.2. The duration of the higher value of the transformation factor is longer and the actual value approaches

the theoretical but does not fully reach it in the first 30 milliseconds. Again, a more intense load, load case 1, has a higher value and diverge more from the ideal plastic theoretical solution, which is 0.667. The final value is 0.731 and the decrease has ceased for load case 1. For the longer load duration, load case 3, a value of 0.707 is the final value. Therefore, it can be stated that the deformation shape is dependent on how intense the load is. If the load would be completely static, the theoretical transformation factor would be in perfect agreement with the obtained result.

Augustsson and Härenstam (2010) investigated this problem briefly, and found that a modified value of the transformation factor κ_{mF} should be taken as 0.771 for a 2.7 metre long and 0.35 metre high beam subjected to load case 1. Their beam had a lower internal resistance value and it is of interest to investigate if the transformation factor is affected by the maximum capacity.

If the transformation factor was changed so that it fitted the ideal plastic deformation curve, the best agreement was found when κ_{mF} = 0.771, i.e. the same as Augustsson and Härenstam (2010). Hence, this implies that the ultimate resistance has no significant influence on the transformation factors. The transformation factor decreases with the load magnitude. For load case 2 it is 0.752 and load case 3 it is 0.724. Therefore, the transformation factor seems to be dependent on the load and not the ultimate resistance. The reason for why these two values agree is further studied in Section 4.5 where a time dependent transformation factor is implemented.

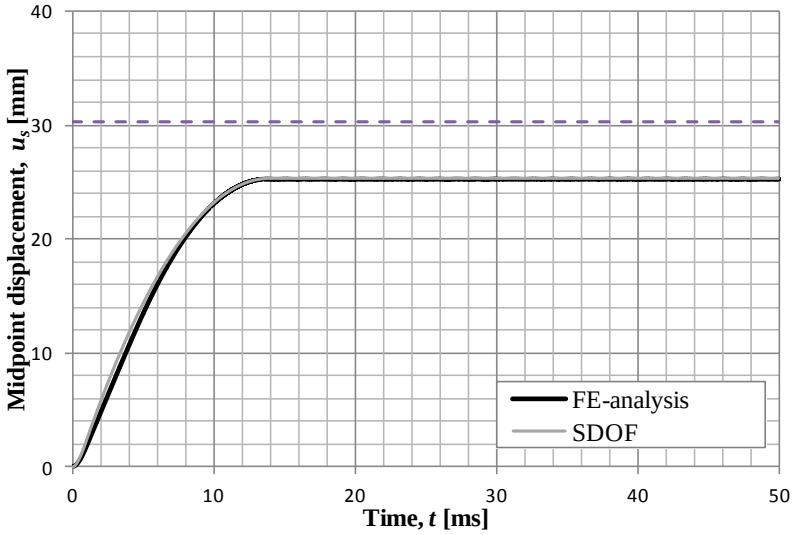

Figure 4.23. Midpoint deformation for an ideal plastic beam subjected to load case 1, assuming a constant transformation factor of 0.771.

4.4.4 Elasto-plastic analysis

The different transformation factors obtained from the FE-analyses for the elasto-plastic material behaviour are compared both with the plastic and elastic theoretical values. This indicates that using the theoretical plastic value will generate a result on the safe side and give a larger deflection. As expected, though, the real values of the transformation factors are somewhere in between the theoretical values. For very high peak pressures and short load duration κ_{mF} will converge towards a mean value between these theoretical values, see Figure 4.24a. In contrast, for a beam subjected to

a lower load with longer duration, κ_{mF} converges towards a lower value which corresponds more to the plastic theoretical value, see Figure 4.24b and Figure 4.24c.

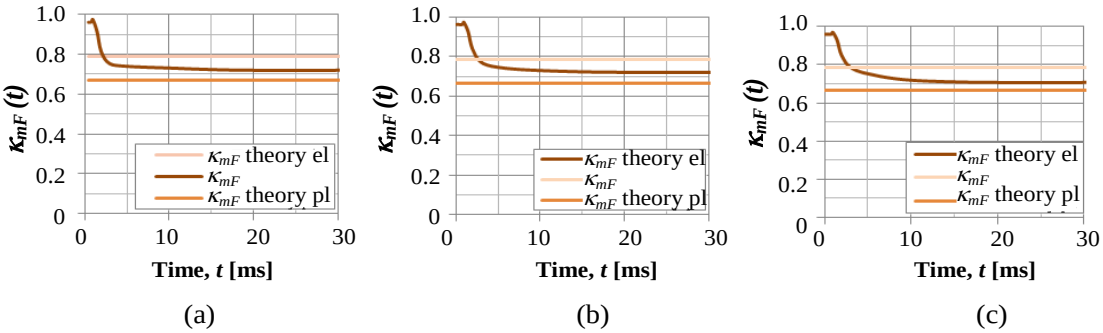

Figure 4.24. The transformation factor κ_{mF} versus time compared with the elastic and plastic theoretical values for a concrete beam with elasto-plastic response subjected to a) load case 1, b) load case 2 and c) load case 3.

The early peak can be recognised as the near rigid body motion that takes place soon after load arrival, also seen in the linear elastic case. Subsequently, the beam starts to plasticise and the value of the transformation factor approaches a value between the theoretical plastic and elastic values respectively.

4.5 Implementation of varying transformation factors into the equivalent SDOF model

4.5.1 Introduction

The time dependent transformation factors have been implemented in the SDOF model in order to see if they would generate a better agreement with the FE analysis. The time dependent transformation factors are taken from the transformation factor figures for every material model and load case in Section 4.4. The equation of motion can be written as

$$\kappa_{mF}(t)m\ddot{u} + ku = F(t) \tag{4-22}$$

4.5.2 Preservation of energy

Initial investigations of this subject showed that the deformations became smaller when using the time dependent transformation factors. This is on the unsafe side. This is believed to depend on two reasons. Firstly, the mass is increased when the impulse load is working on the structure. This means that the acceleration will be lower according to Newton's second law, see equation (2-4). Secondly, the kinetic energy is changed every time the mass is changed since it is proportional to the mass.

It is clear when investigating the energy balance that something happens when time dependent transformation factors are used, see Figure 4.25. The energy level is initially higher when the transformation factors are high but decreases suddenly when they decrease as seen in Section 4.4. This creates unbalanced energy levels and must

be compensated with energy preservation. This is unrealistic since energy cannot disappear in the structure and gives a completely wrong deformation.

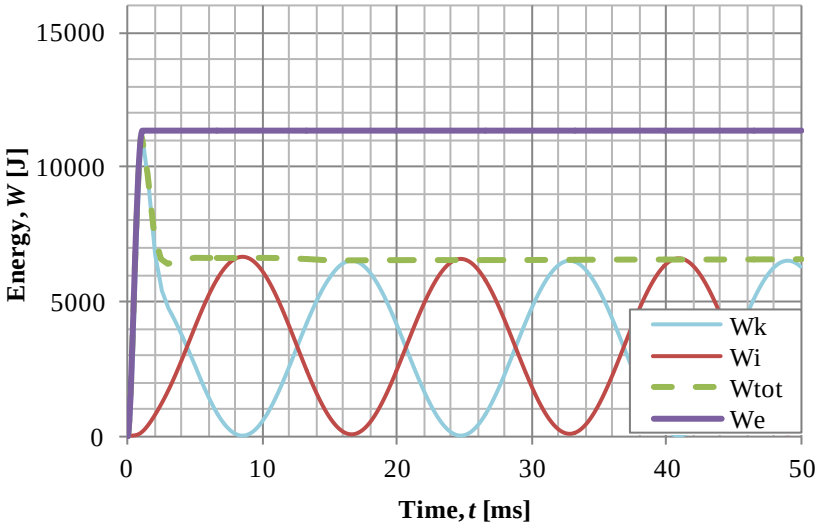

Figure 4.25. Energy balance in an SDOF model with varying transformation factors. A sudden drop occurs when the transformation factors decreases.

The sudden drop in energy can be compensated by preserving the kinetic energy, see Figure 4.26. This is done by calculating the deformation and corresponding velocity with the transformation factor for the previous time step and correct these by increasing the velocity with the square root of the change in transformation factor of the load. This is further explained in Appendix D. The energy balance will be shown for all material models in Sections 4.5.3, 4.5.4 and 4.5.5.

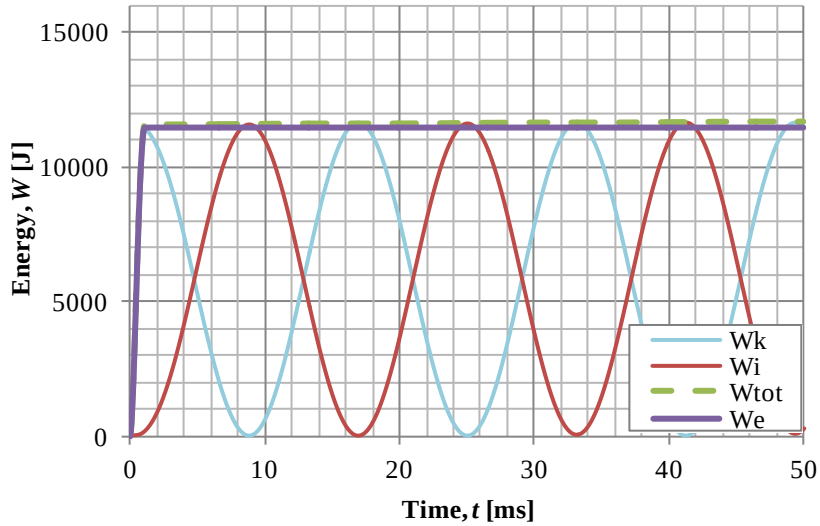

Figure 4.26. Energy balance when preserving the kinetic energy according to Appendix D.

4.5.3 Elastic analysis

The theoretical linear elastic analyses have a good agreement but for comprehensiveness and understanding of the more realistic material models it is desirable to vary the transformation factors also in the elastic case.

If the varying transformation factors are used without preserving energy, the deformation of the midpoint is lower than in the simplified method and the FE-analysis as shown in Figure 4.27. If the kinetic energy is preserved, it can be seen that a very good agreement between the FE analysis and the SDOF model is obtained.

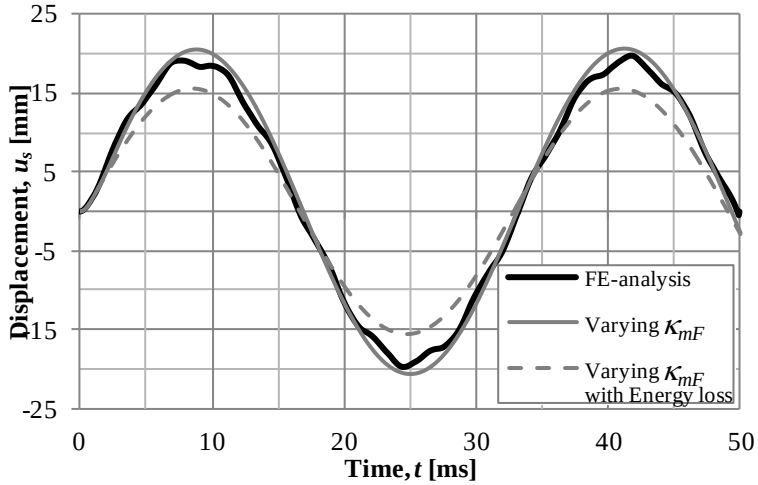

Figure 4.27. Displacement in midpoint when varying the transformation factors.

Since the transformation factors are changed to a higher value initially, the external energy becomes higher. The energy in the theoretical SDOF model is lower than the FE analysis and the change of transformation factors should make the energy levels agree better. However, the energy is slightly higher in the SDOF system than in the FE analysis, see Figure 4.29 and Figure 4.30. As a result, a small difference in the displacement can occur and, as seen in Figure 4.27, it is somewhat higher than in the FE-analysis. This could be a consequence of not capturing every displacement shape perfectly and the corresponding transformation factor.

The energy preservation is shown in Figure 4.28 and Figure 4.29. As seen the maximum level is not affected, which supports the hypothesis that it is the estimation of transformation factors that causes the slight overestimation of the maximum energy in the system.

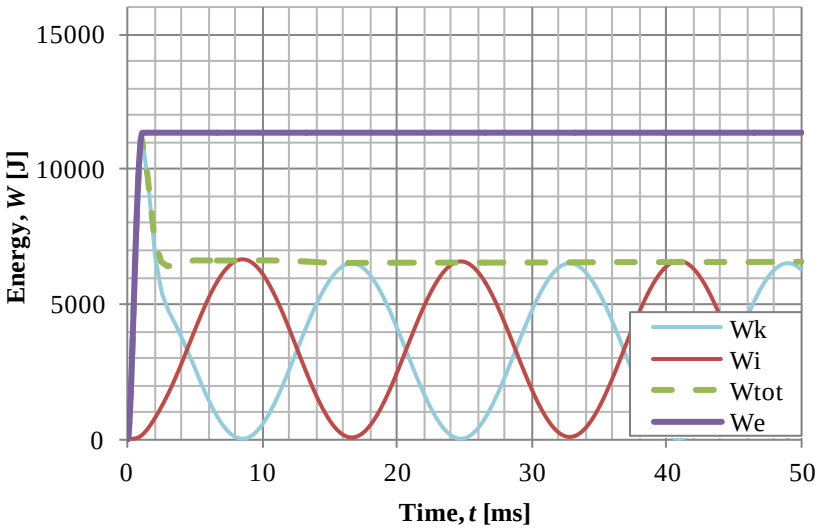

Figure 4.28. Time dependent transformation factors cause a sudden drop in energy.

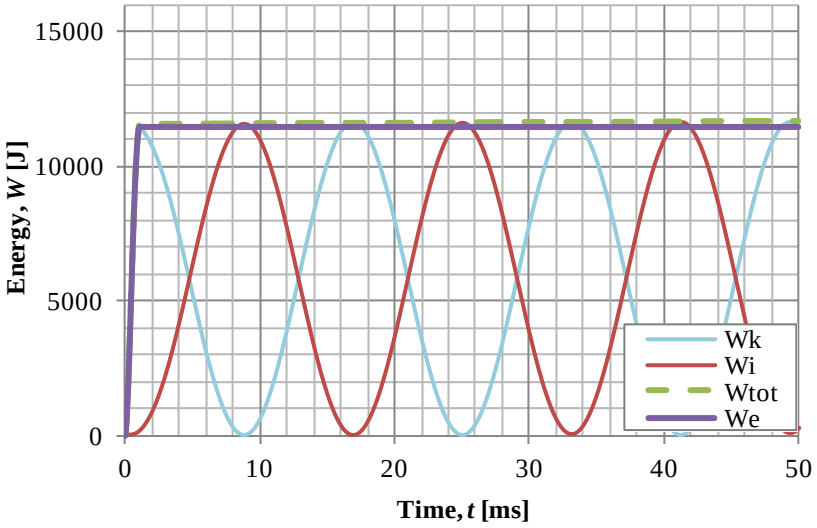

Figure 4.29. Preserved energy in the SDOF model with time dependent transformation factors.

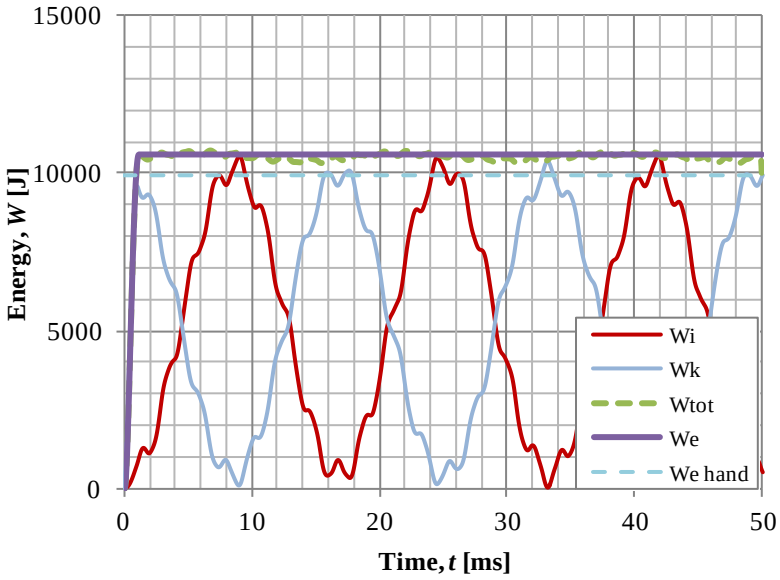

Figure 4.30. The energy balance in the FE-analysis. The maximum level is slightly lower than what is obtained with SDOF model.

4.5.4 Ideal plastic analysis

Similar to the elastic case transformation factors are found from the FE analysis and used in the SDOF approach. As a result, the displacement decreases since kinetic energy "disappears" when the transformation decreases, see Figure 4.31. The energy decrease is not as sudden as for the linear elastic case since the transformation factors decrease gradually. If the energy is preserved, Figure 4.32, as for the elastic case, a very good agreement between the displacement in the SDOF model and the FE analysis is found, see Figure 4.33. The total energy is also here overestimated, compare reasoning in Section 4.5.3. For comprehensiveness, more load cases can be seen in Appendix E.

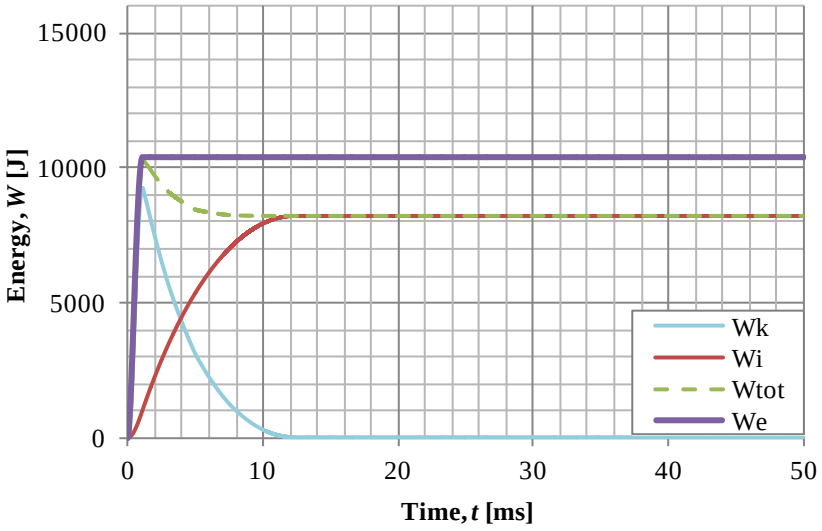

Figure 4.31. Energy balance when time dependent transformation factors are used without preserving energy levels.

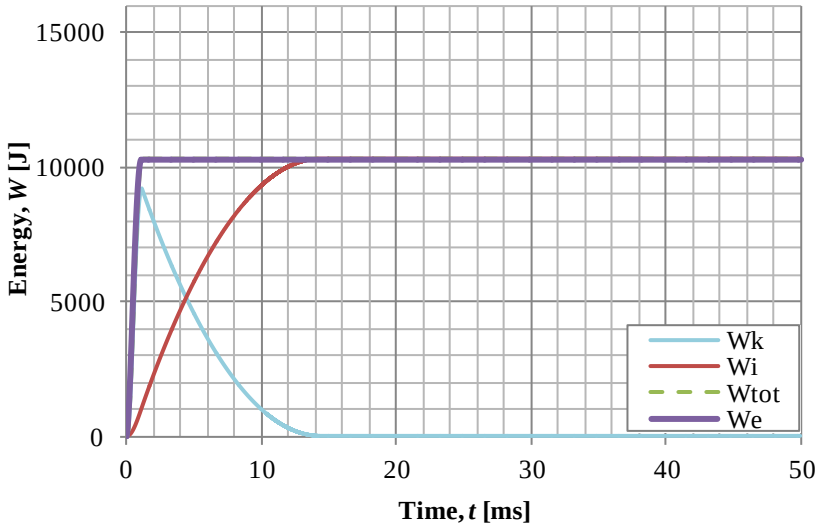

Figure 4.32. Preserved energy when using time dependent transformation factors.

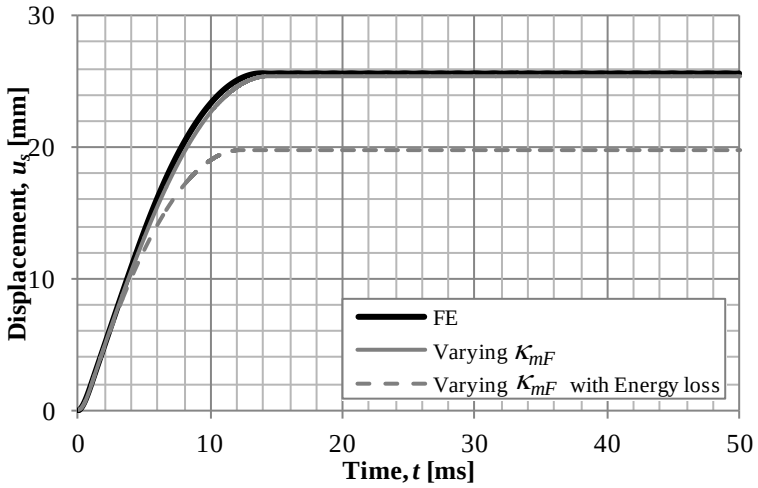

Figure 4.33. Displacement when the transformation factors are varied.

4.5.5 Elasto-plastic analysis

Since very good agreement has been found when varying the transformation factors for the simplified material models, this is also done in the elasto-plastic case. Actually, this has already been done when the transformation factors were varied from the theoretical elastic to the theoretical plastic ones. This gave lower midpoint deformation and this is also the case when using the transformation factors from the FE analysis, see Figure 4.34. When using time dependent transformation factors from the FE analysis and preserving the energy, a very good agreement for the midpoint displacement is obtained, see Figure 4.34.

If the energy balance is investigated, there is a clear drop where the transformation factors are varied, see Figure 4.35. This is preserved and the energy is in balance see Figure 4.36.

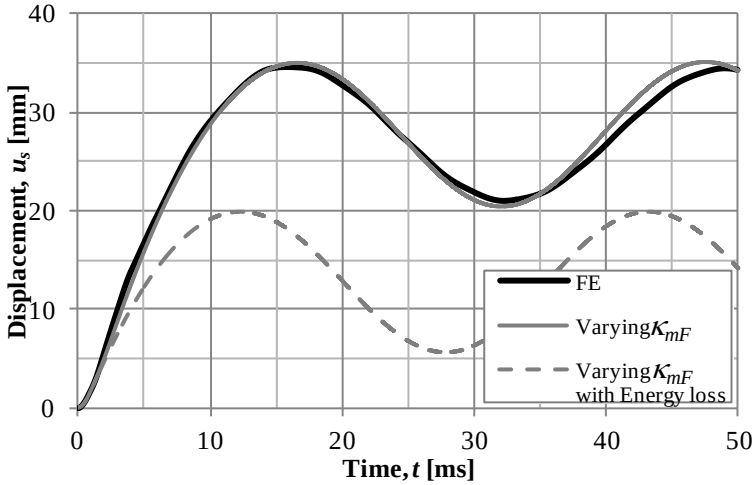

Figure 4.34. Midpoint displacement vs. time when varying the transformation factors.

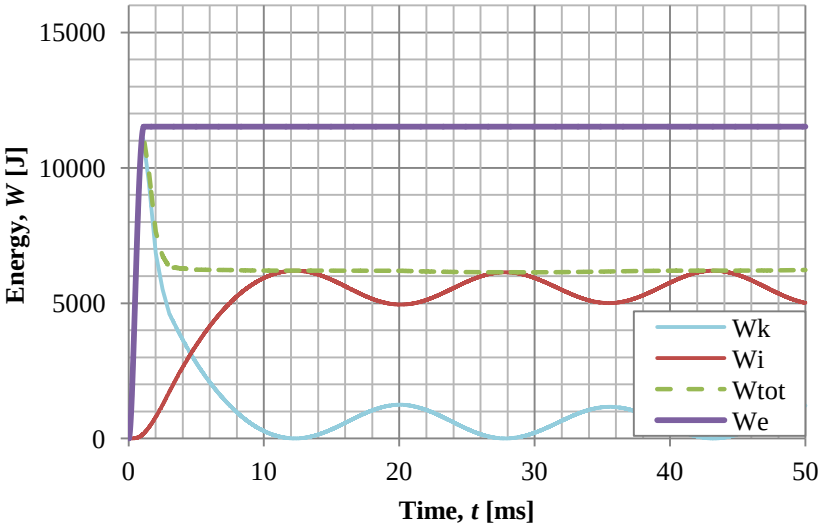

Figure 4.35. Energy balance before preserving energy.

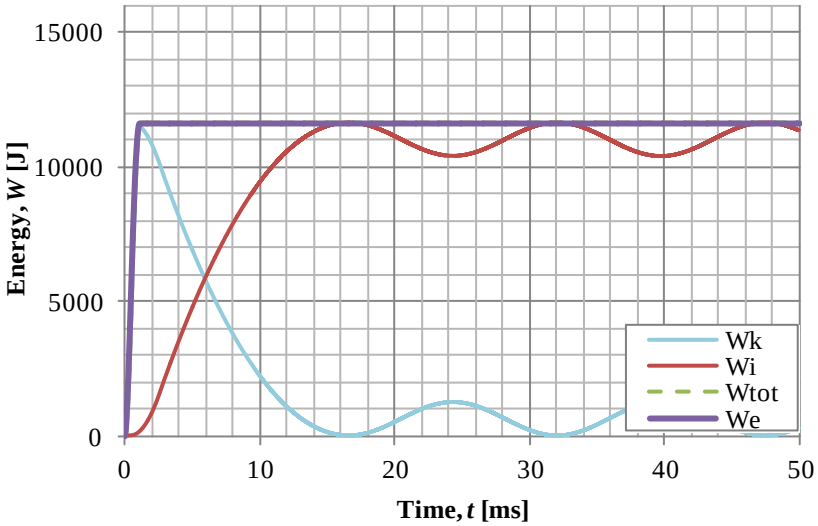

Figure 4.36. Energy balance when preserving energy.

The same procedure is carried out for the case when the transformation factor changes from the theoretical elastic value to ideal plastic when the internal resistance has reached its maximum value in the SDOF model. This also gives very good agreement, which is better than using the transformation factors from the FE analysis. This shows that this simple modification is sufficient to increase the accuracy in the elasto-plastic analysis.

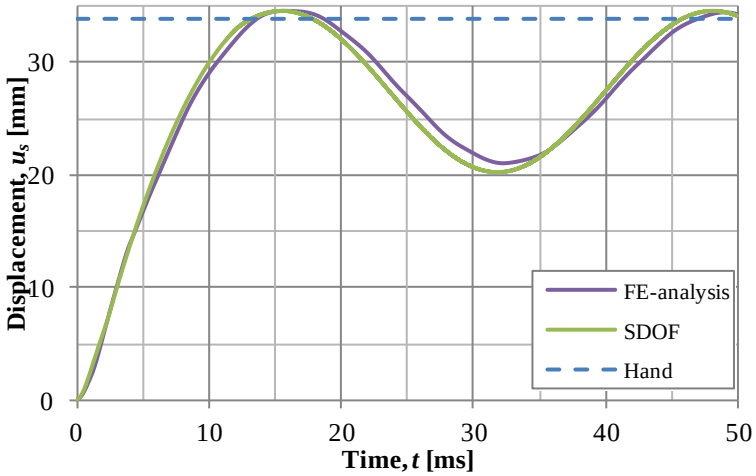

Figure 4.37. Midpoint displacement when preserving energy and using time dependent transformation factors with theoretical elastic values when the SDOF model has elastic response and plastic theoretical values when it has plastic response.

4.6 Discussion of results

The deformation when using theoretical transformation is not well described for a beam with ideal plastic or elasto-plastic response. This is because the deformation shape differs from that assumed. For the elasto-plastic case, it was found that it is possible to use the plastic transformation factors with good results. However, the reason for this is unknown and is believed to be due to a combination of two errors.

The resulting deformation shape in FE-analysis carried out has been investigated and it is shown that implementation of time dependent transformation factors makes the deformation from an SDOF model agree better with finite element solutions. However, this requires that an energy preservation scheme is used.

The time dependent transformation factors have been taken from an FE analysis. It would not be practical to calculate transformation factors from an FE analysis in order to implement in a simplified method. However, if a relationship for time dependent transformation factors can be found in the future, this method can be used directly in a simplified SDOF method. This relationship should take load, material parameters and corresponding deformation shape into account. It is further interesting to see how accurate these transformation factors must be in order to describe the response adequately.

The investigation in this Chapter shows that even a simplified relationship for the transformation factors can be used for the elasto-plastic model. This uses the elastic theoretical and the plastic theoretical transformation factors when the response is elastic or plastic respectively. The ideal plastic case has a longer duration of error

when using theoretical transformation factors and does never reach the theoretical value. Therefore, the influence of the transformation factors become larger and could be described with a linear decreasing function. The elastic transformation factors can be seen as a good approximation already.

It is interesting to discuss how the wave actually propagates through the beam. The proposed method makes the solution agree well with the FE-analyses. The question is whether the FE-analyses describe reality well enough. It is shown in Section 3.5.4 that the wave propagation in a model made with beam elements and solid 2D elements differs. This is especially the case with shear waves that is not described well at all with beam elements. A critical time step, where the wave only propagates one element per time step, must be used in order to capture the wave properly. There is however no recommendation from ADINA which critical time step that should be used for a shear wave. The developed method for implementing transformation factors can however be used for other displacement shapes. Consequently, the above method can be used, although the deformation shapes are not correctly described.

The above discussion only concerns the deformations. It is also indispensable to describe the section forces and the support reaction. They are influenced by the deformation shape and consequently the transformation factors. The influence of time dependent transformation factors on section forces and support reaction will be investigated and discussed in Chapters 5 and 6.

5 Moment and shear force

5.1 Introduction

Ultimately, the maximum shear force and moment effect are of interest in the structure. Therefore, a study on how the moment and shear force are distributed in the beam has been carried out. As will be seen in this chapter, they can differ markedly to the expected distributions for static loadings.

When the structure has a plastic or elasto-plastic response, the moment is limited to the maximum moment and the structure dissipates energy by plastic deformation. Therefore, in these cases, the failure criterion is displacement rather than moment resistance. Nevertheless, the moment distributions are still of interest since they are used for reinforcement arrangement. However, if the structure is assumed to have an elastic response it is necessary to check the moment capacity.

The shear force must be checked for all material models. The maximum shear force is not necessarily found at the supports, and the distribution may differ significantly to that predicted in an equivalent static case.

Johansson and Laine (2009) suggest that a static equivalent load can be used in order to design the structure for moment and shear forces. This is applied to the structure as a uniformly distributed load and section forces can be found. This method is here used in order to compare with results from FE analyses.

The shear and moment distribution is shown together with the deformation shape for many time steps within the first oscillations in appendix G.

5.2 Elastic analysis

The shear and moment distributions have been found for the linear elastic beam. This is done by finding the nodal forces and moments for many time steps. The distributions are initially not at all similar to that obtained in a static case.

The moment in midpoint is shown in Figure 5.1. The moment in the midpoint is very small the first millisecond and then it increases to the maximum value around the same time that the maximum deformation is the largest. It can be seen that the moment is approximately the same during the second oscillation. This is not realistic since the beam has some damping and the value at the second oscillation will be smaller. Also the negative moment is as large as the positive

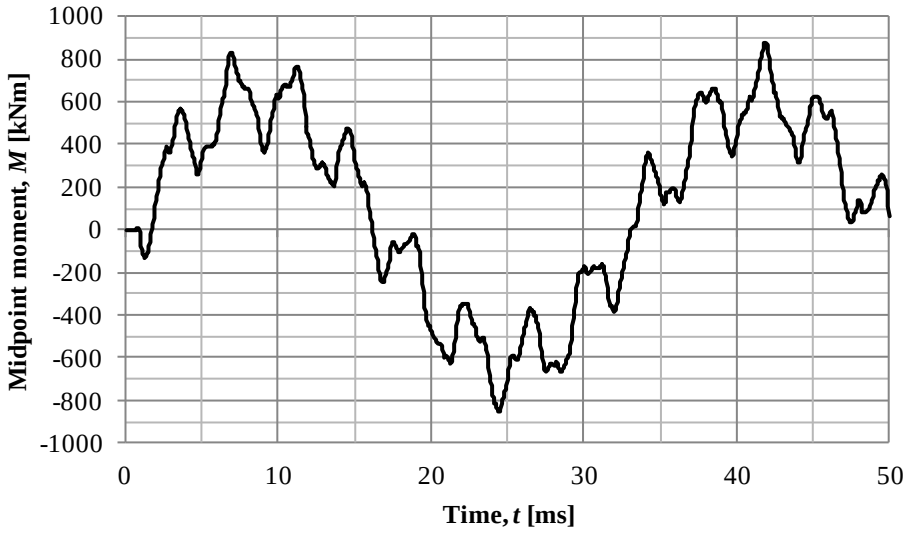

Figure 5.1. Midpoint moment for a linear elastic beam.

In Section 4.2.2, it is shown that the initial deformation shape is different to what would be expected in a static load case. The largest deformations start closer to the supports and it is not until after about 2 ms that the largest displacement can be found in midpoint. The moment is directly influenced by curvature and will consequently develop from supports and progress to the centre. This is shown in Figure 5.2. Initially, the moment is slightly negative in the midpoint until. After about 1.5 ms the moment starts to decrease in the sections closest to the supports and the moment in the centre increases. This continues after about 2.5 ms and a somewhat expected moment distribution is obtained.

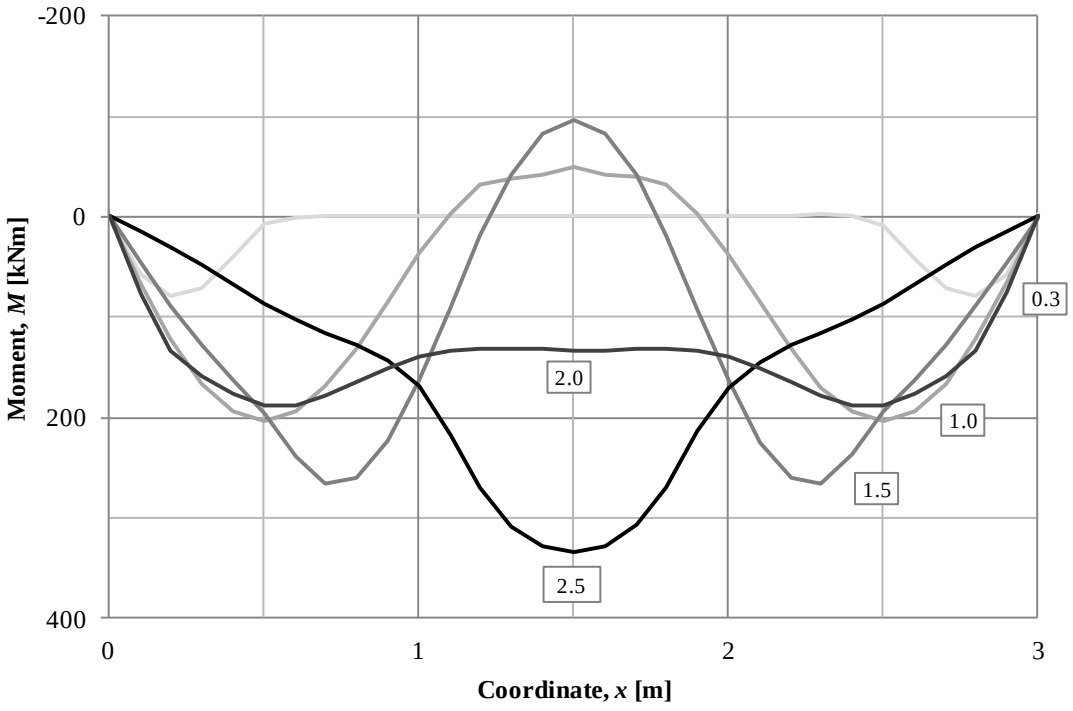

Figure 5.2. The moment distribution early after load arrival. The numbers denotes the time for the adjacent or, in the centre, the above line. The moment develops from the edges towards the centre.

Between 2.5 ms and the time for maximum displacement, as seen in Figure 4.1 at about 8 ms, the moment distribution is relatively similar to the expected, see Figure 5.3. At maximum deformation, the same peculiar distribution as the initial response occurs, where the centre part oscillates between the adjacent parts.

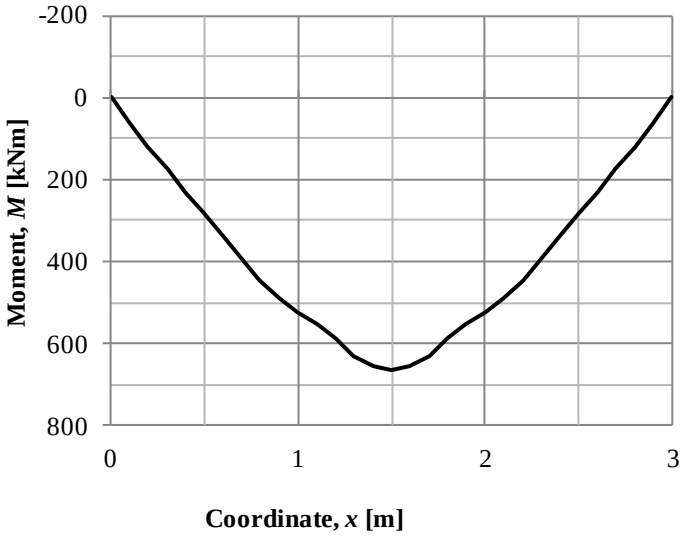

Figure 5.3. Moment distribution at the time t=8 ms.

The support reaction is shown in Figure 5.4. Initially, a peak occurs within the first milliseconds but the maximum value is not obtained until the maximum deformation is reached. It can also be seen that the reaction force is the same in both direction since it is an elastic oscillation. The support reaction is further investigated in Chapter 6.

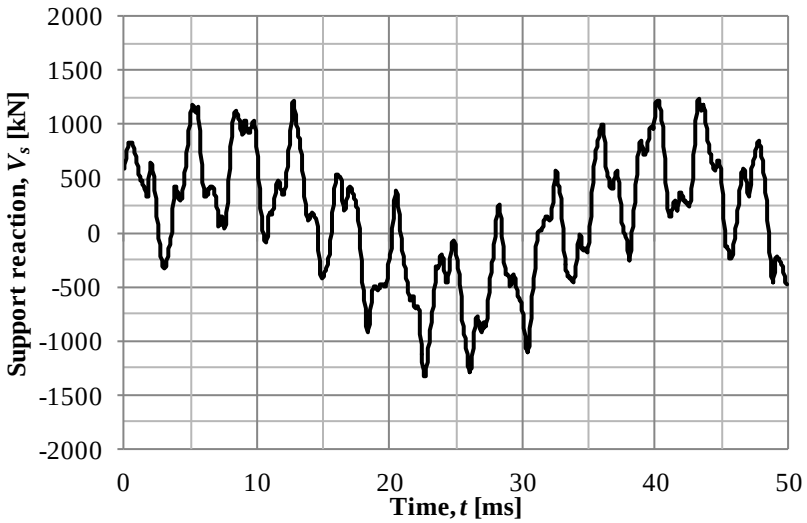

Figure 5.4. Support reaction for a linear elastic beam.

The shear force distribution is the derivative of the moment and will consequently also have a peculiar shape. High shear stresses occur soon after load arrival close to the supports. This is where the moment is changing quickly due to large rotations. The shear force is always zero in the midpoint. The area close to the midpoint has no shear force shortly after load arrival because a near rigid body movement takes place. However, the shear force builds up and becomes very high near the midpoint after some time. The early shear force distribution is shown in Figure 5.5.

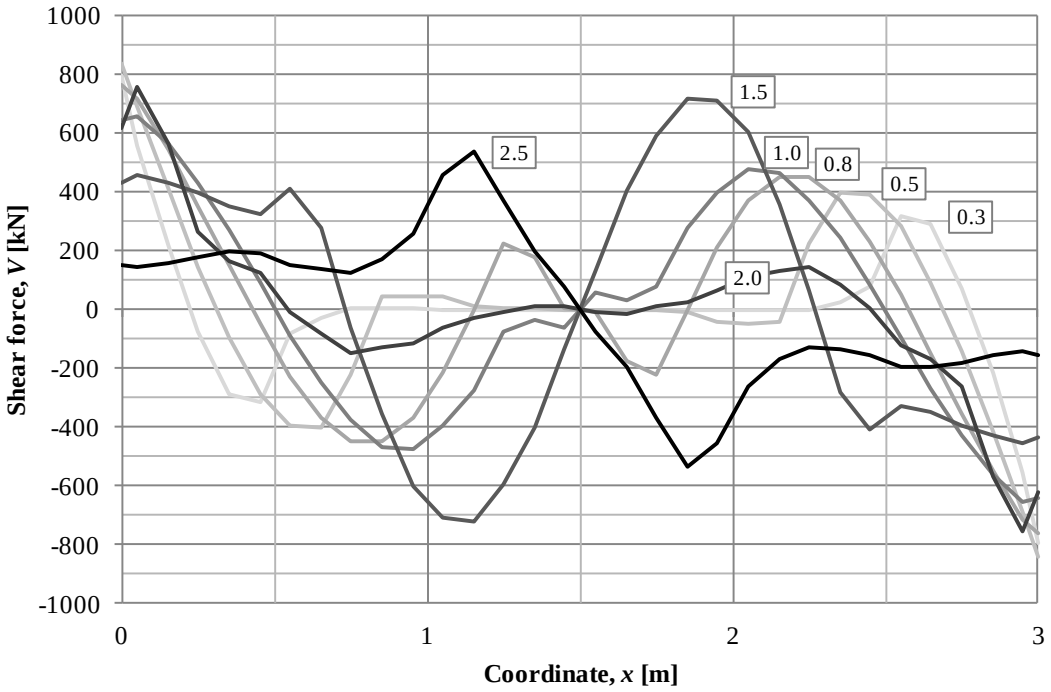

Figure 5.5. Shear force distribution soon after load arrival. High shear stresses occur close to the supports.

For some time increments the reaction at the support is lower than the adjacent value in the centre of an element. This is believed to depend on accelerations of the nodes closest to the support. The support node does not accelerate at all. This is also discussed in 3.5.6.

5.2.1 Comparison with equivalent static load

The equivalent static load is used in order to compare the magnitude and distribution of moment and shear force in Figure 5.6 and Figure 5.7. It is calculated for state II in section 3.4.2 and is

$$Q_{el,II} = 1618 \text{ kN} \tag{5-1}$$

The corresponding uniformly distributed load is then

$$q_{el,II} = \frac{q_{el,II}}{L} = \frac{1618}{3} = 809 \text{ kN} \tag{5-2}$$

The moment and shear force varies over the length as

$$M(x) = \frac{q_{el,II}}{2}\left(Lx - x^2\right) \tag{5-3}$$

$$V(x) = \frac{q_{el,II}}{2}\left(L - 2x\right) \tag{5-4}$$

The moment envelop has been found for a linearly elastic beam and is shown in Figure 5.6. The envelop covers two oscillations, i.e. 50 ms. The envelop was the same if only the first oscillation was considered. The moment envelop is shown together with the corresponding moment distribution from the equivalent static load. The equivalent static load underestimates the moment obtained from the FE-analysis especially in the midpoint of the beam.

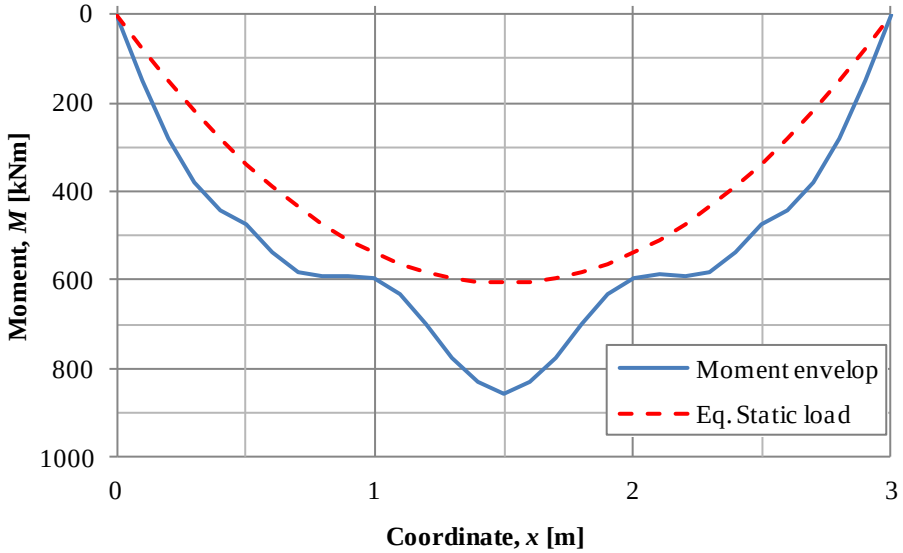

Figure 5.6. Moment envelop compared to the moment from the static equivalent load. The static equivalent load underestimates the moment distribution from a more sophisticated Fe-analysis.

The shear envelop is shown in Figure 5.7 together with the corresponding shear force from the equivalent static load. The shear force is also considerably underestimated if the equivalent static load is used. Moreover, the distributions are very different. The shear force envelop from the FE-analysis looks like the distribution from a point load; i.e. constant level until the midpoint where it changes direction.

The shear force and moment are very similar in both directions since the oscillation is elastic as can be seen in for the moment in midpoint Figure 5.1 and the reaction force at the supports Figure 5.4.

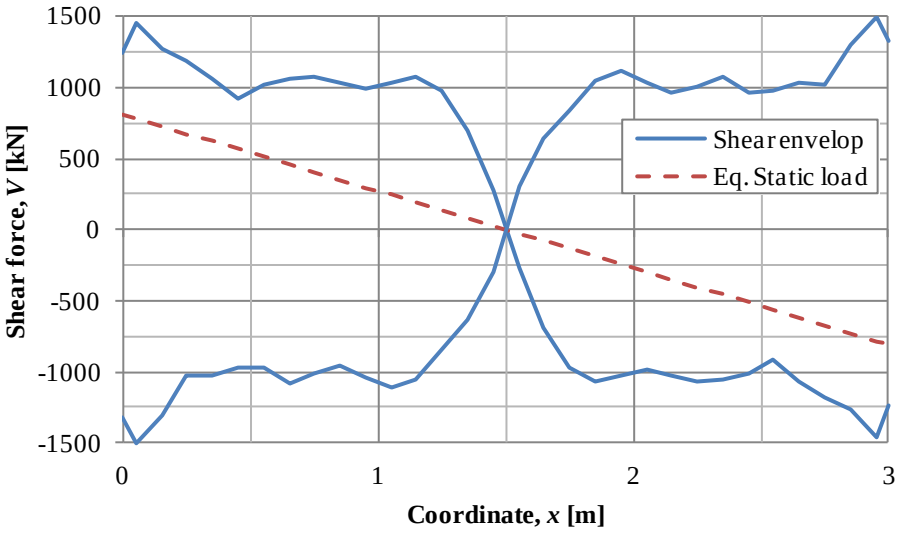

Figure 5.7. Shear force envelop from the FE-analysis compared to the equivalent static load. The shear force underestimated by using the equivalent static load.

If the peak pressure is decreased to 1250 kPa and the duration is increased to 4.48 ms i.e. load case 3, the solutions agree much better as seen in Figure 5.8. Nevertheless, the equivalent static load still provides values somewhat on the unsafe side.

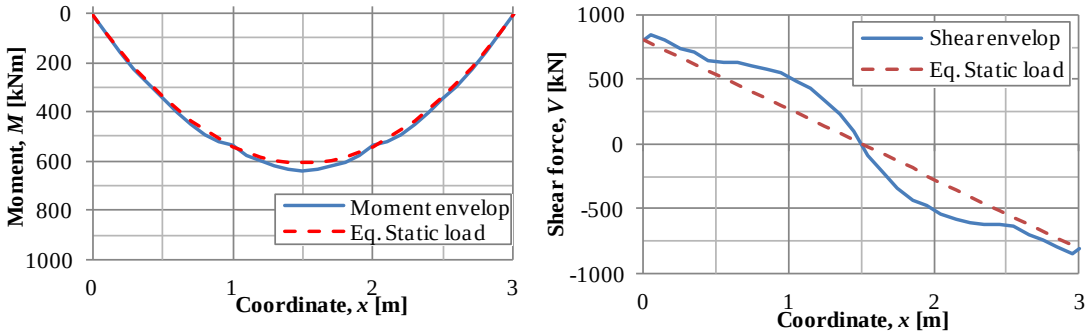

Figure 5.8. The moment and shear envelops for a less impulsive load with peak pressure 1250 kPa and duration 4.48 ms.

For comprehensiveness a table has been compiled where the relative error, ξ, compared to the ratio between peak pressure and equivalent static load is shown. The envelops are shown in Appendix H and the results are summarised in Figure 5.9, which shows the relative error compared to the ratio between peak pressure and equivalent static load for midpoint moment and support reaction. The relative error is defined as

$$\xi = \frac{V_{dyn} - V_{sta}}{V_{sta}} \quad \text{or} \quad \xi = \frac{M_{dyn} - M_{sta}}{M_{sta}} \tag{5-5}$$

The shear force is taken as the support reaction and the moment is taken as the midpoint moment.

The result shows that a large error is found for very high ratios of P_c/q_{eq} and even for relatively small ratios it gives a significant error. The error is larger for shear forces, which can be underestimated with up to 150 %. This is very dangerous to use in design. The absence of damping in the model may influence the result considerably. This is further investigated in Section 5.2.2.

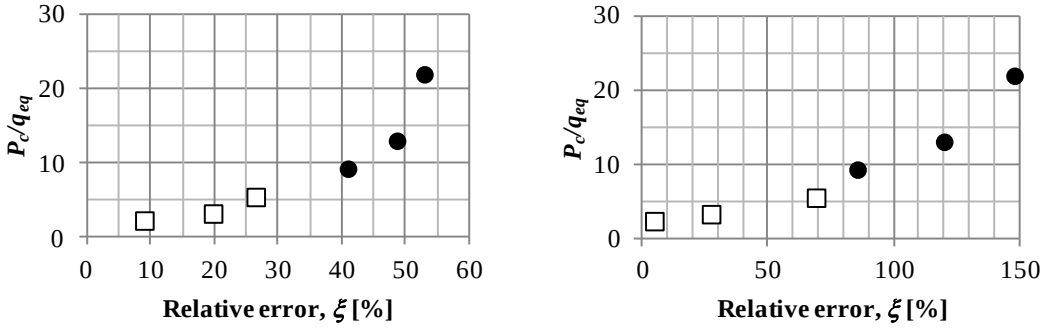

Figure 5.9. Relative error vs. ratio between peak pressure and equivalent static load for a) moment and b) shear force, where load case 1 is marked with circles and load case 3 with squares.

The equivalent static load takes no consideration to contribution from the load on the support reaction. This is done by for example FortV (2011). The support reaction is then overestimated according to Figure 5.10. It seems like the best agreement is found for a ratio between peak pressure and equivalent static load of around 5.

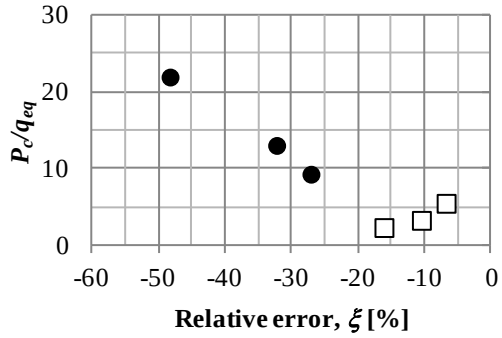

Figure 5.10. The relative error for different ratios using FortV's approach for the support reaction, where load case 1 is marked with circles and load case 3 with squares.

5.2.2 Influence of damping

If Rayleigh damping with 5% as described in Section 4.4, is assumed for the normal beam subjected to a high intense load the error is decreased considerably but a relatively large divergence still exists, Figure 5.11. Load case 1 is used and the P_c/q_{eq} value is 5.4. This is reasonably a better explanation of a real elastic concrete structure. The shear force and moment is still very high close to the centre of the beam. This must be considered in design of an elastic structure. The errors, though, are now lower:

$$e = \frac{678 - 607}{607} = 11\,\% \text{ for moment}$$
$$\mathrm{e} = \frac{951 - 808}{808} = 18\,\% \text{ for shear force at support} \qquad (5\text{-}6)$$

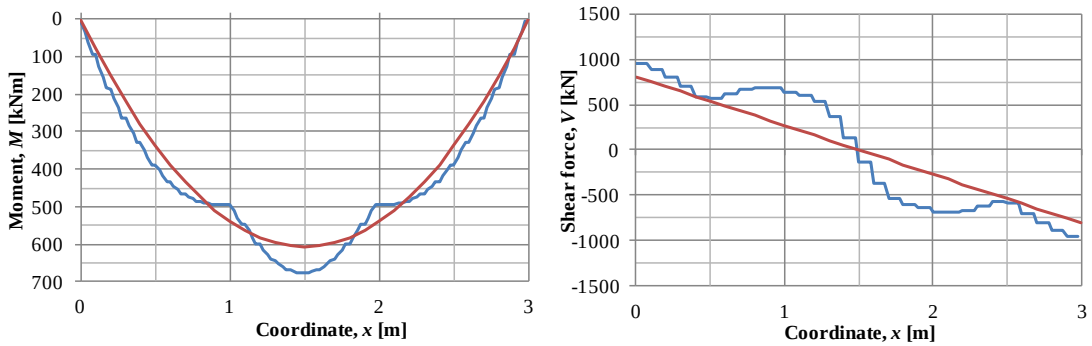

Figure 5.11. Envelops when 5% Rayleigh damping has been used.

The damping does not affect the maximum deformation in the midpoint considerably, but the peaks in the support reaction and moment are reduced rather much, see Figure 5.12. The early peak in the support reaction is not reduced, hence, it can be considered to be correct in the undamped analysis.

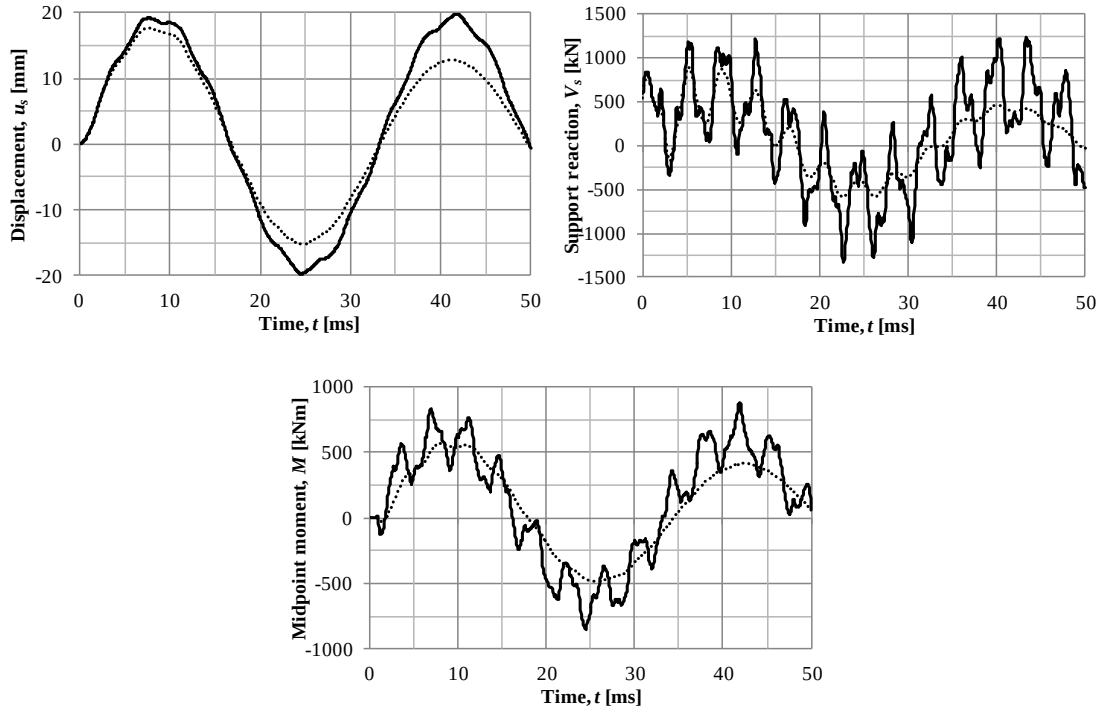

Figure 5.12. The undamped and damped support reaction and displacement and moment in midpoint.

The influence of damping and comparisons for different cross sections with and without damping are shown in Appendix H.

The relative error is decreased considerably if damping is introduced as can be seen in Figure 5.13. The equivalent static load actually overestimates the moment and support reaction for very low ratios P_c/q_{eq}.

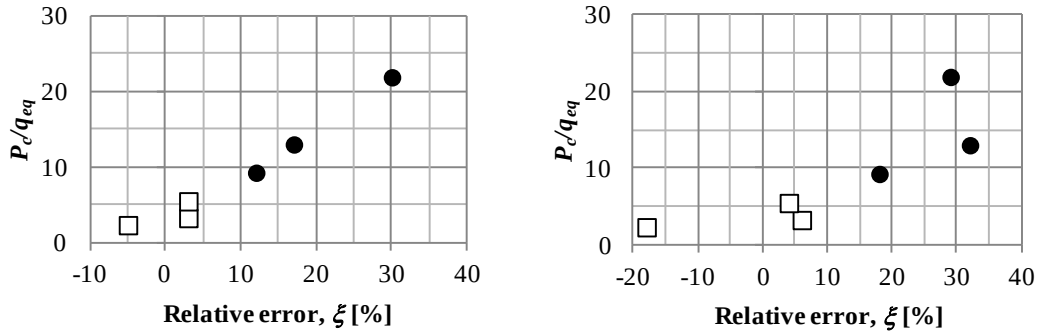

Figure 5.13. The relative error for damped elastic case. Load case 1 is marked with circles and load case 3 with squares.

Fortifikationsverket's approach will overestimate the support reaction even more since the support reaction is even lower for a damped case.

5.3 Ideal plastic analysis

The moment and shear distribution in the ideal plastic case has been studied. The ideal plastic beam has a maximum moment capacity of 227 kNm and this value is reached soon after load arrival in most sections of the beam since almost no elastic deformations take place, see Figure 5.14. The moment will then decrease from the edges until a concentrated plastic hinge is formed in the midpoint. This can be shown by the plastic strain in the beam Figure 5.15. The plastic strain starts closer to the edges and increases and becomes concentrated in the centre.

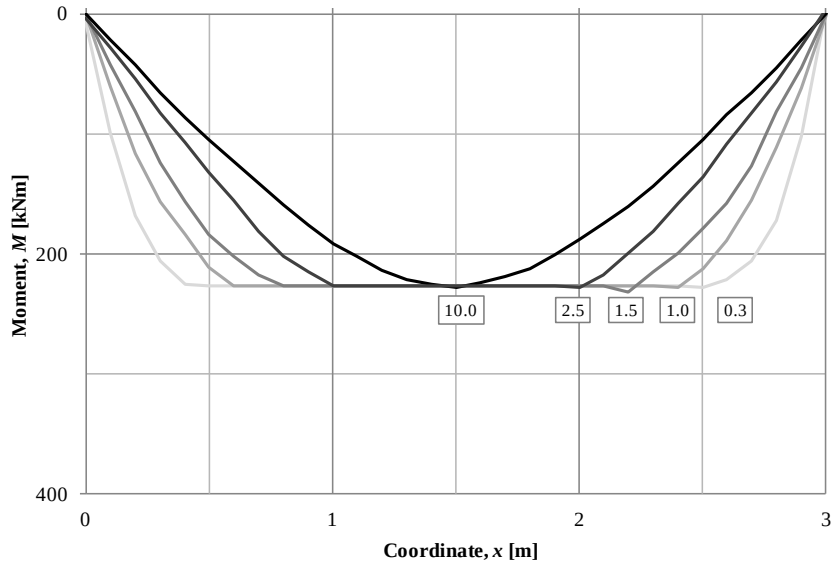

Figure 5.14. The moment distribution for different times in the ideal plastic case. The adjacent number denotes the time when the specific distribution occurs.

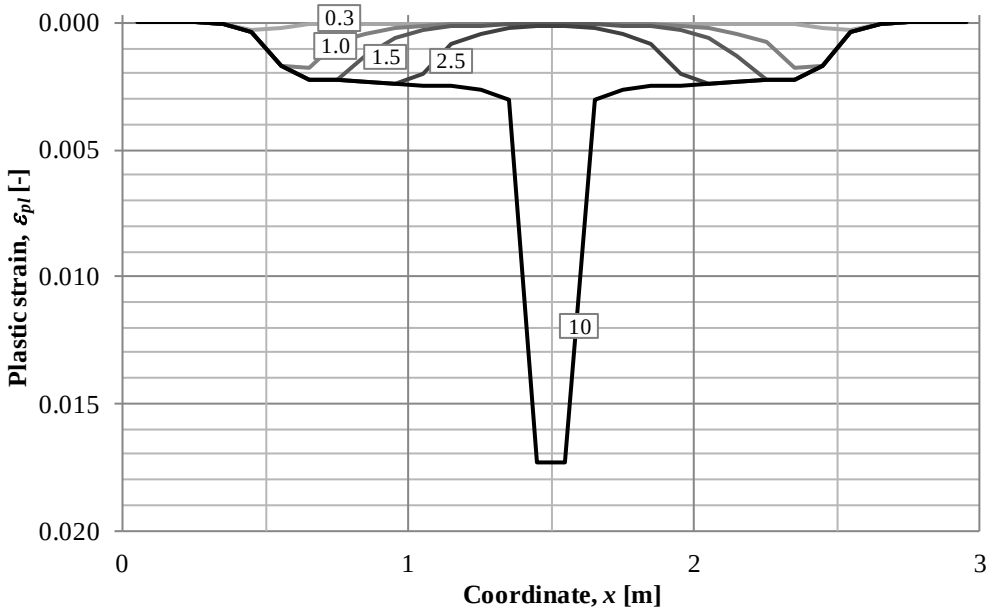

Figure 5.15. Plastic strain in the ideal plastic beam.

Once the maximum deformation is reached, the moment will alternate between positive and negative yield moment, see Figure 5.16. This is due to elastic oscillations with a very high stiffness, which should not happen in an ideal plastic material. Actually, the deformation oscillates with a high frequency and low amplitude when the maximum deformation is reached in the ideal plastic case. It is easier to understand in an elasto-plastic case where it is clear that the midpoint oscillates. The worst case will occur soon after load arrival and therefore the beam should be designed for the first response in both directions.

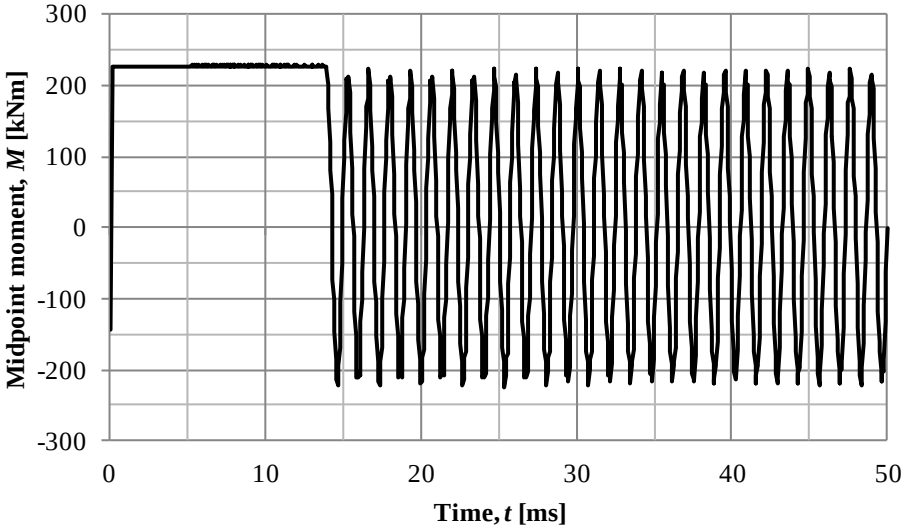

Figure 5.16. Moment in midpoint in an ideal plastic beam over time.

The shear force has the same behaviour to that in the linear elastic case, i.e. not similar to the static distribution. It starts as high values close to the supports which later decreases and stabilises on a level until the maximum displacement is reached.

The shear force is zero close to the midpoint in the beginning. Thereafter, it increases and has eventually a linear distribution between the two plateaus.

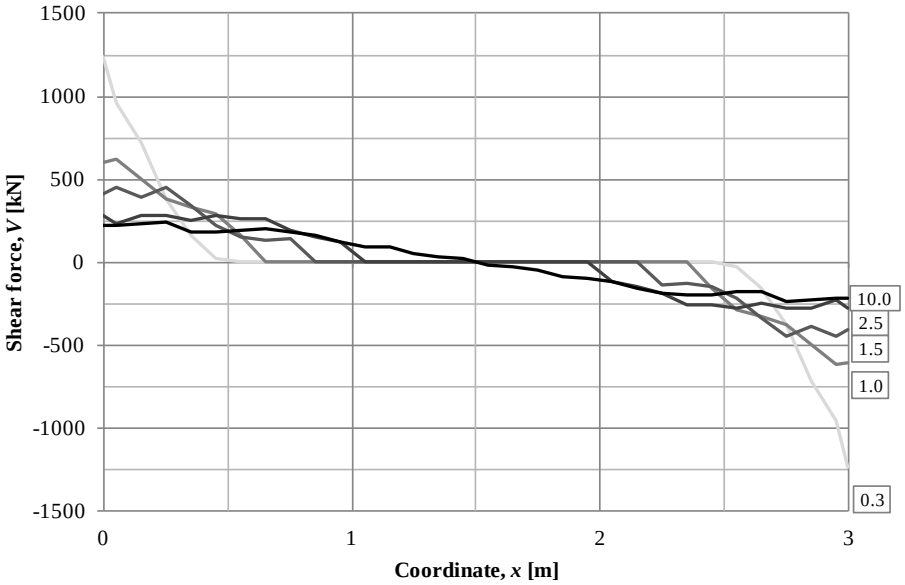

Figure 5.17. Shear distribution for different times. The shear force is high close to the supports in the early phase of the response.

5.3.1 Comparison with equivalent static load

The equivalent static load in the plastic load case is calculated in equation *(3-33)* and is

$$Q_{pl} = 606 \text{ kN} \tag{5-7}$$

The corresponding uniformly distributed line load can be written as

$$q_{pl} = \frac{Q_{pl}}{L} = \frac{606}{3} = 202 \text{ kN} \tag{5-8}$$

The section forces can then be obtained by

$$M(x) = \frac{q_{pl}}{2}\left(Lx - x^2\right) \tag{5-9}$$

$$V(x) = \frac{q_{pl}}{2}\left(L - 2x\right) \tag{5-10}$$

The maximum moment in midpoint is well described by the equivalent static load. However, it does not take into account that almost the whole beam will have this moment at some time. The large moment close to the beam edges only occur in the initial phase as shown in Section 5.3. This will provide an adequate reinforcement amount but an unwanted reinforcement arrangement would be obtained if curtailment and anchorage lengths would be designed by considering the moment distribution from the equivalent static load.

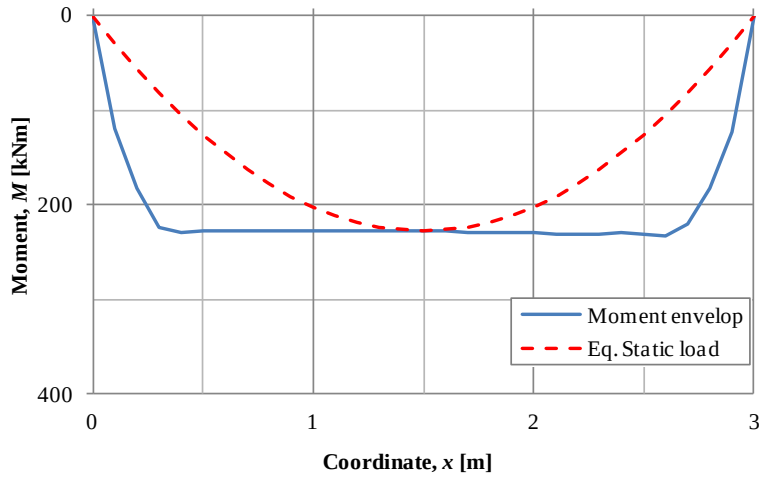

Figure 5.18. The moment envelop compared to the eq. static load. The equivalent static load does not describe the high moments close to the supports.

Similarly, the shear force is relatively well described by the equivalent static load. However, the shear force close to the support is considerably higher in the beginning close to the support. This is a direct consequence of the sudden moment changes that occur over a short beam length in the initial phase.

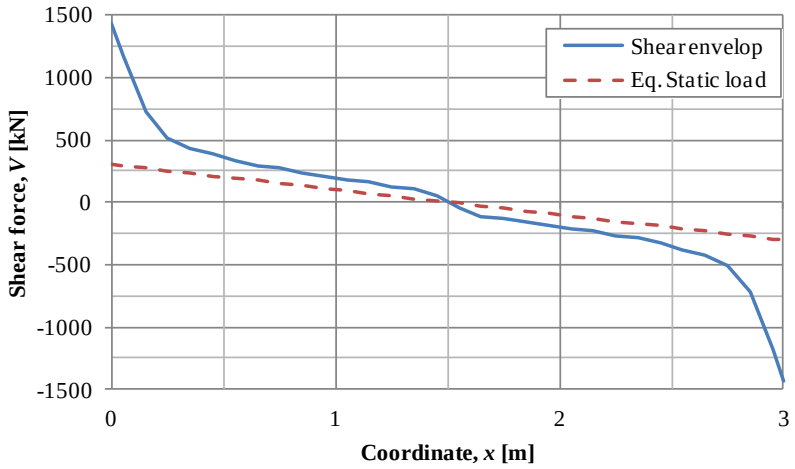

Figure 5.19. Shear force envelop compared to the shear force from the equivalent static load. The shear force close to the supports is underestimated when it is based on the equivalent static load.

The same relation can be found for a less intense load, load case 3. The divergence is smaller as can be seen in Figure 5.20 but is still not accurate.

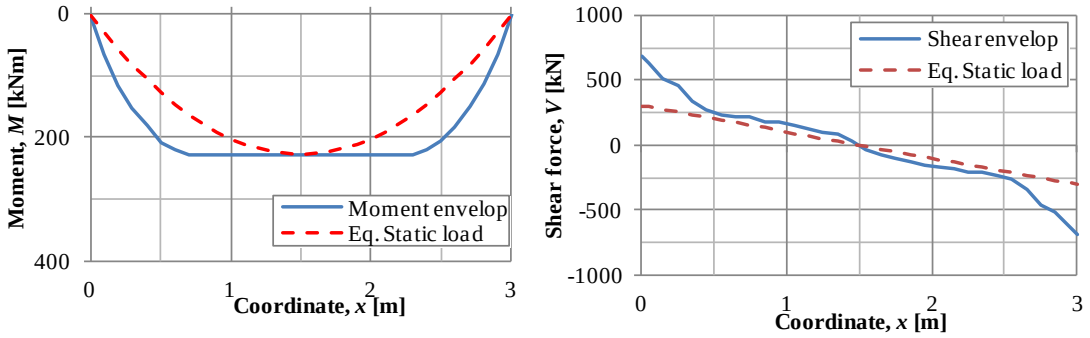

Figure 5.20. The envelops compared to the internal forces generated from the equivalent static load for a less intense load, load case 3.

5.4 Elasto-plastic analysis

The shear and moment distribution in linear elastic and ideal plastic models may not be possible in reality. They are just simplifications in order to understand the more realistic elasto-plastic model. Ultimately, it is important to find the reaction forces in an elasto-plastic model. Since the moment can increase to infinity in an elastic model and peculiar moment distributions can be obtained from several modes, it cannot be seen as a good representation of a concrete structure. In a similar way the ideal plastic model does not deflect if it has not begun to yield. Therefore, the moment, and consequently the shear force, will be overestimated in the initial phase close to the supports since the gradient of the moment is larger than expected.

Initially, the behaviour for is identical to the linear elastic case, see Figure 5.21 and Figure 5.22. The moment builds up from the edges and the moment in the midpoint is not increasing until after around 2 ms. Compared to the linear elastic case there is no difference until 2.5 ms when the moment has reached the maximum moment capacity. The shear force also follows the linear elastic model until yielding occurs in the structure. The shear force peak close to the centre in the linear elastic model is evened out because the moment does not increase beyond the yield moment. Therefore, the increase in moment is less drastic and the shear is lower.

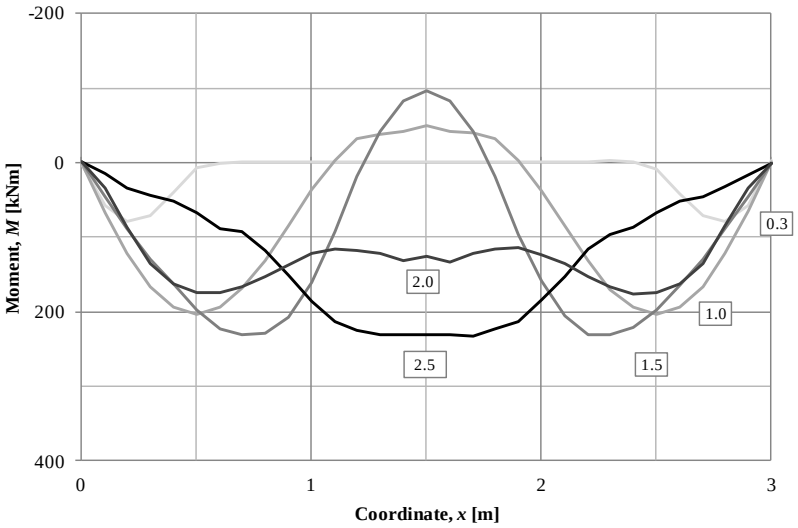

Figure 5.21. Moment distribution in the elasto-plastic model.

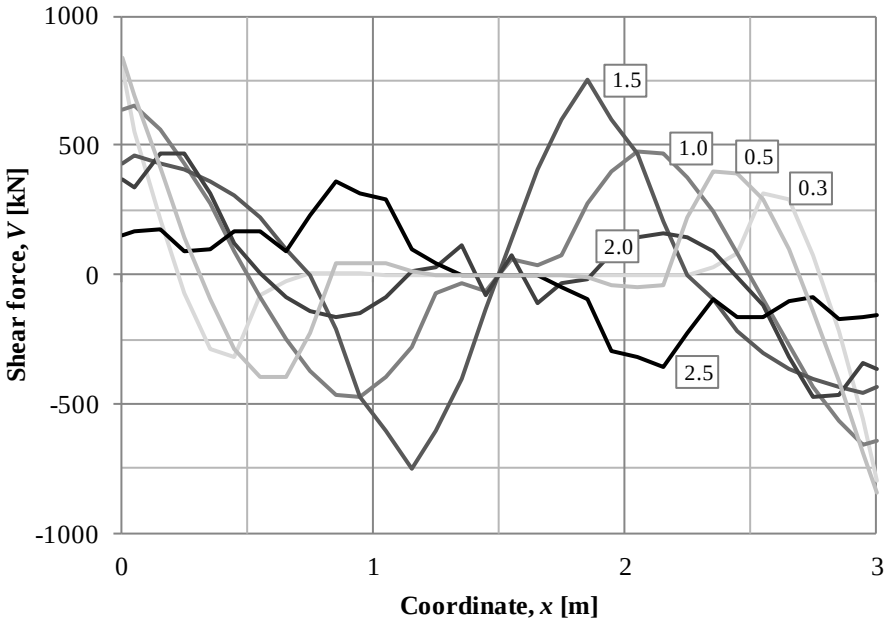

Figure 5.22. Shear force distribution in the elasto-plastic model.

Yielding occurs away from centre after 1.5 ms as can be realised by the plastic strain in the beam, shown in Figure 5.23. There is no plastic strain before this time. The plastic strain becomes more concentrated in the centre and forms a plastic hinge.

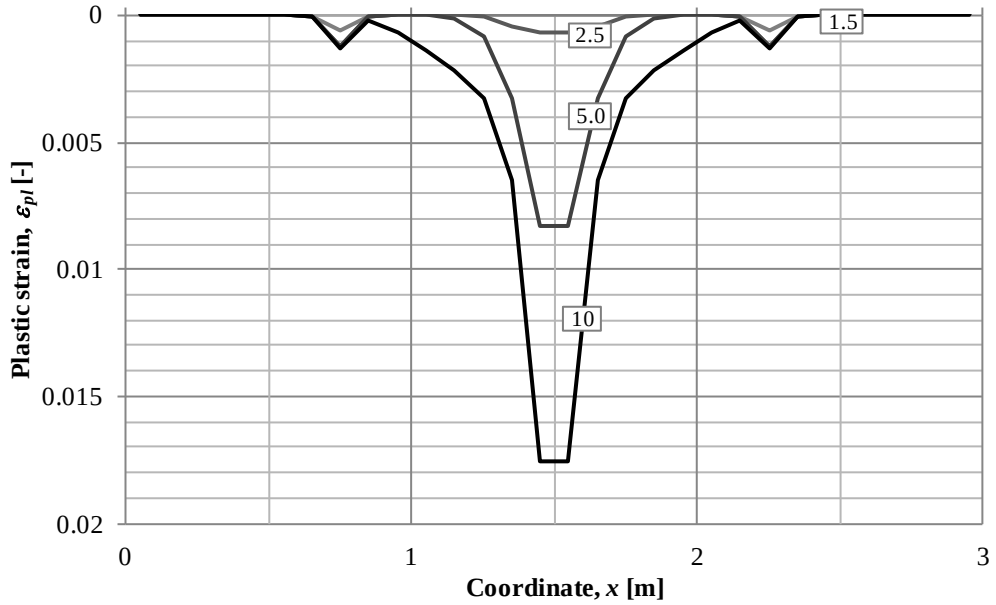

Figure 5.23. Plastic strain in the beam for different times.

The maximum shear in the linear elastic model does not occur initially. It occurs at the maximum deformation; this will never occur in the elasto-plastic model since the structure starts to yield, which affects the change in moment considerably and consequently the shear force. Therefore, the shear force will be smaller than obtained using the linear elastic model.

5.4.1 Comparison with the equivalent static load

In the maximum moment and shear force are compared to the distribution when using the equivalent static load. The moment is limited to 227 kNm as for the ideal plastic case. The shear force can initially be governed by the elastic behaviour and is therefore compared to the shear force resulting from both the elastic and plastic equivalent static load, see Sections 5.2.1 and 5.3.1 for values.

The maximum moment along the beam is shown Figure 5.24. It is similar to the plastic distribution but will not be as high close to the supports. As a result, the moment can be better explained by the equivalent static load although it does not take into account that a large part of the beam reaches the yield stress at some point. As mentioned for the ideal plastic case, care has to be taken when anchorage and curtailment of reinforcement are designed.

It can also be seen that the moment is higher than the maximum moment in some parts of the beam. This is impossible and depends on that the moment has been extracted from nodal moments. This is discussed in Section 3.5.6.2.

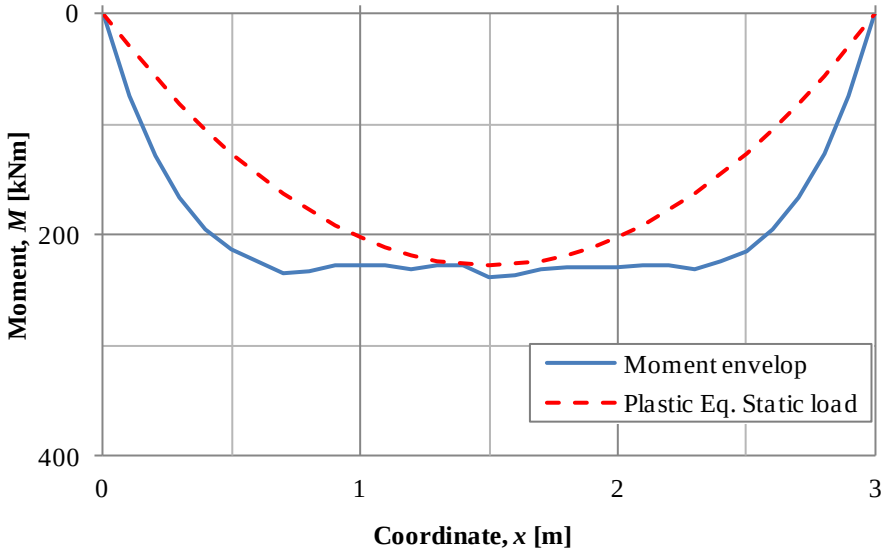

Figure 5.24. Moment envelop compared to the equivalent static load for load case 1.

The maximum positive shear force from the elastic static equivalent load, which is based on elastic state II stiffness, agrees much better with the shear force in the structure from the FE analysis than what the plastic equivalent static load does, see Figure 5.25. Nevertheless, it overlooks that the shear force can be higher closer to the centre. Further, the shear force is not the same in both directions. Early after load arrival large negative shear forces will occur close to the centre in the elastic phase, see Figure 5.22, when the moment is much less in the centre than close to the edges. The negative peak disappears and negative shear force does not occur until the beam starts to oscillate back. It is then better explained with the plastic equivalent static load.

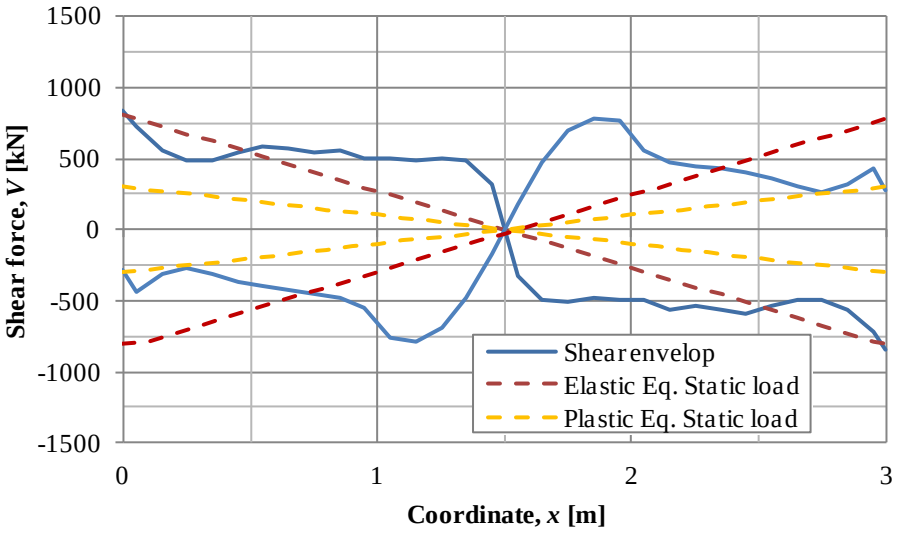

Figure 5.25. Shear envelop and the two static loads for load case 1.

The result is similar for a less intense load, load case 3. The difference is that the moment will be smaller close to the edges and is better predicted with the plastic equivalent static load, see Figure 5.26a. The shear force is close to the elastic equivalent static load in the centre and close to the plastic equivalent static load at the edges, Figure 5.26b.

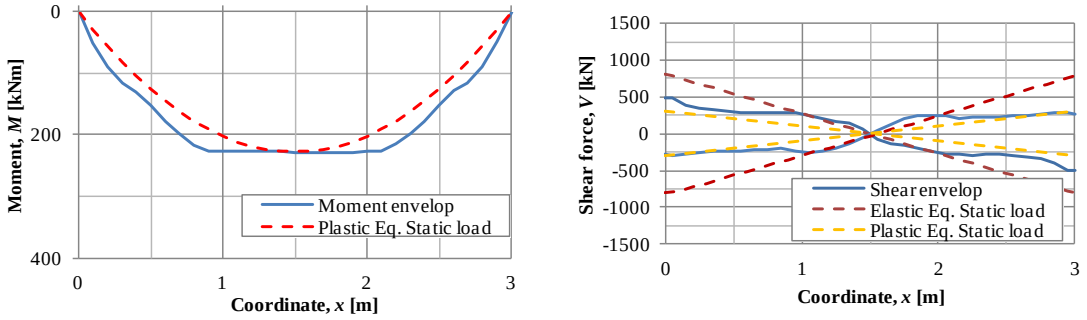

Figure 5.26. The moment and shear envelop for a less intense load, load case 3.

5.5 Discussion of results

The moment demand on an impulse loaded elastic beam is higher than what is predicted using the static equivalent load. The more intense the load is, the larger deviation is obtained. This may not be of any importance in a concrete structure, which will yield and redistribute moments. However, for timber and high class steel cross sections that do not possess any plastic behaviour, such an underestimation of the moment may cause failure.

More studies need to be carried out using the steel and timber properties in order to investigate the actual response for those materials. For instance, timber is not a preferable material for very intense loads. It will break anyways since it has insufficient resistance. Therefore, only a load corresponding to load case 3 or an even less intense load will in reality be of interest for acting on the timber structure. The deviation is also much smaller for such cases.

If an elastic material is to be used in design, an up scaling factor could be introduced for moments and shear forces. More investigations should be carried out in this subject and since this thesis mainly investigates concrete structures this elastic effect will not be considered further.

The shear force is not adequately described using the equivalent static load. Both the support reaction and the shear force close to the centre are underestimated. The support reaction is the largest shear force and is further investigated in Chapter 6.

Damping effects have been neglected when performing the elastic analysis. Damping does not affect the displacement of the midpoint significantly. However, the moment and shear force demand is affected considerably. Damping exists in all real structures and even a 5 % damping ratio will decrease the deviation considerably. For timber structures it is possible to have a very large damping up to 20 %, Johansson (2012).

The plastic and elasto-plastic analyses show that the distribution of shear forces and moments are not the same as that predicted by a static equivalent load. Fortifikationsverket (2011) and MSB (2011) demand that no curtailment of the steel reinforcement is done. Having seen the moment distribution in Sections 5.2.1, 5.3.1 and 5.4.1, this is a very reasonable requirement. Moreover, anchorage of reinforcement bars should be performed with care. Alternatively, existing structures with varying reinforcement arrangement could be analysed with a varying stiffness in order to see the effect of the moment redistributions. The observation that high shear forces occur close to the centre for all material models implies that the distance where shear force reinforcement is arranged should be extended towards the centre.

The shear force demand is governed by the elastic behaviour soon after load arrival. However, the shear force in the ideal plastic material model is not reliable since it depends on the initial stiffness, which has been overestimated by the modelling. The elasto-plastic model assumes an equivalent state II young's modulus. Initially, though, the concrete is uncracked and a state I model should possibly be used instead. This is difficult to take into account in a simplified model. A brief discussion of this problem is given in Section 6.2.

A shear crack in a statically loaded structure starts at an angle close to 45 degrees to the flexural reinforcement. As load redistribution occurs, the angle of the shear crack can be flatter. This flatter angle is used for static shear design. However, the small duration of the shear force that occurs in an impulsively loaded beam may mean that load redistribution may not be possible and consequently that shear cracks cannot have a small angle as used in static design. Moreover, the time for a crack to form should be investigated since the small duration mean that a whole crack may not have time to form. A more detailed analysis taking concrete cracking and reinforcement yielding into account could therefore be used to determine more accurate behaviour.

6 Support reaction

6.1 Definition of used methods

The support reaction is of interest when analysing a structure with respect to direct shear and shear force design. As seen in Chapter 5, the support reaction is very high initially. It is therefore necessary to find the reaction at the support. The obtained support reactions from the FE analysis were compared to the to the method used by Biggs (1964), Fortifikationsverket (2011) and the equivalent load approach described in Sections 2.4.2.5 and 2.4.2.6 in order to see whether they can be used to estimate the actual shear force adequately.

The three alternative, simplified methods are intended to be used in order to estimate the maximum value of the support reaction, V_d. However, it is possible to use all methods with a varying external load and internal resistance from the SDOF-model. Since Biggs' (1964) and Fortifikationsverket's (2011) methods are very similar for theoretical values of the transformation factors, see Section 2.4.2.5, they are here described with Fortifikationsverket's approach. Fortifikationsverket's (2011) approach is beneficial since it can use varying transformation factors studied in Chapter 5. The methods used in further analyses are

$$V_{MAX}(t) = \left(1 - \frac{\kappa_F^2}{\kappa_m}\right) F_{peak} + \frac{\kappa_F^2}{\kappa_m} R_m \quad \text{with } \kappa_m \text{ and } \kappa_F \text{ constant} \tag{6-1}$$

$$V_d^{\kappa}(t) = \left(1 - \frac{\kappa_F^2}{\kappa_m}\right) F(t) + \frac{\kappa_F^2}{\kappa_m} R(t) \quad \text{with } \kappa_m \text{ and } \kappa_F \text{ constant} \tag{6-2}$$

$$V_d^{\kappa(t)}(t) = \left(1 - \frac{\kappa_F(t)^2}{\kappa_m(t)}\right) F(t) + \frac{\kappa_F(t)^2}{\kappa_m(t)} R(t) \quad \text{with } \kappa_m(t) \text{ and } \kappa_F(t) \tag{6-3}$$

$$V_d^{eq}(t) = \frac{R(t)}{2} \tag{6-4}$$

In later diagrams these are referred to as Max V, theoretical κ_{mf}, time dependent κ_{mf} and equivalent static load respectively.

The internal resistance obtained from the SDOF-model where the energy is preserved will be used when the time dependent transformation factors are used, see Section 4.5.

The constant transformation factors used are

$$\kappa_F = 0.64 \text{ and } \kappa_m = 0.504 \qquad \text{for elastic case} \tag{6-5}$$

$$\kappa_F = 0.50 \text{ and } \kappa_m = 0.333 \qquad \text{for plastic case} \tag{6-6}$$

Ardila-Geraldo (2010) uses varying transformation factors and varying internal resistance within a tenth of the structure's period in order to describe the support reaction. It is only a mathematical trick in order to describe the support reaction and the varying stiffness is not implemented into the SDOF model, see Figure 6.1. In other words, this means that the SDOF internal resistance is calculated and then initially

increased when the support reaction is considered. This method uses equation (6-3) with the internal resistance:

$$R(t) = \begin{cases} 10 \cdot R(t)\left(1 - 9\frac{t}{T}\right) & \text{if} \quad t < 0.1T \\ R(t) & \text{if} \quad t \geq 0.1T \end{cases} \tag{6-7}$$

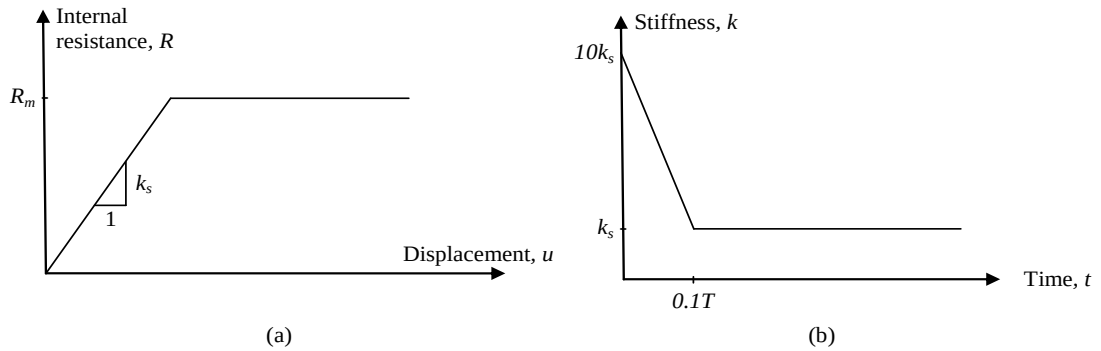

Figure 6.1. Definition of the internal resistance and initial increased stiffness according to Ardila-Geraldo (2010).

In further analyses, this approach will be referred to as varying κ_{mf} and stiffness. This will only be used for the elastic and the elasto-plastic material models since Ardila-Geraldo (2010) only considered the elastic phase. Consequently, five different approaches are compared to the result from the FE-analysis.

6.2 Elastic analysis

The support reaction forces for a linear elastic reinforced concrete beam subjected to an impulse load were found using several approaches. The initial peak reaction can occur when the concrete is uncracked and has state I behaviour. However, it is here assumed that it is cracked and an equivalent young's modulus corresponding to state II is used.

The FE-analysis provides a rough curve, which oscillates up and down. The reason for this is likely because several modes and that no damping were considered. As seen in Section 5.2.2 damping has considerable influence on the peaks. The highly varying reaction curve can be smoothed out by plotting a mean value for 1000 points, i.e. 500 points after the actual value and 500 before, see Figure 6.2. The time-step is 0.01 ms so this corresponds to an average over 10 ms.

$$V_{mean}^{FE}(t) = \frac{\sum_{i=0}^{n=1000} V(t_{i-500})}{n} \tag{6-8}$$

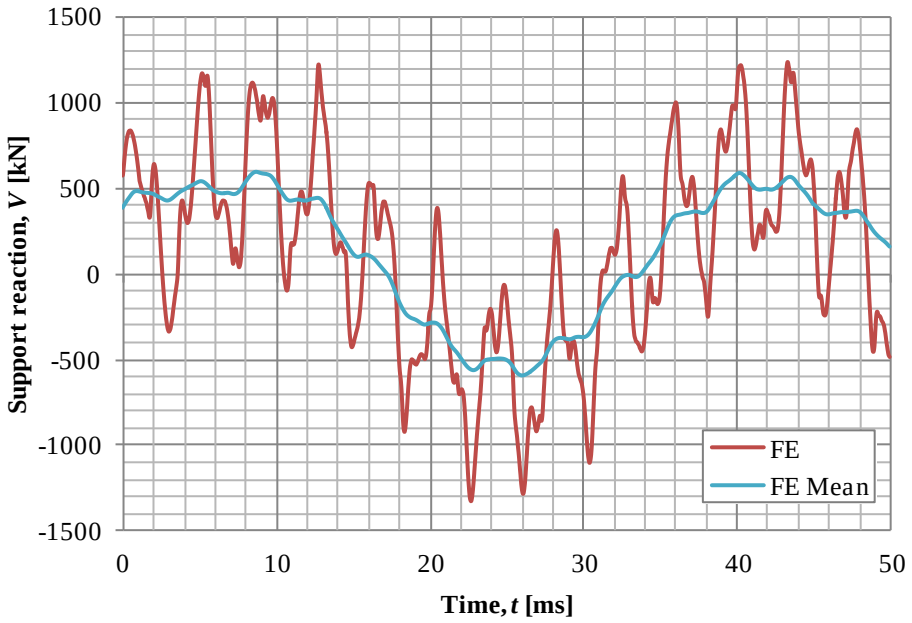

Figure 6.2. The roughness of the Fe-curve can be relieved by using a mean value for every 10^{th} millisecond.

In Figure 6.3 it can be seen that Fortifikationsverket's maximum support reaction with theoretical transformation factors is greatly overestimated compared to the FE-analysis. The reason for this deviation is that it combines the maximum values of the internal resistance and peak load, which in reality never overlap. Initially, when the load is active, the internal resistance is insignificant. At a later phase the support reaction is merely affected by the internal resistance.

The equivalent load concept will give a maximum support reaction force that does not capture the peaks of the FE-analysis, see Figure 6.3. Also, the early peaks of the two simplified methods are overlooked by using the equivalent load. However, it lies above the mean value of the FE-analysis and Fortifikationsverket's solution for later times. This means that it is slightly conservative when estimating the mean value of the support reaction.

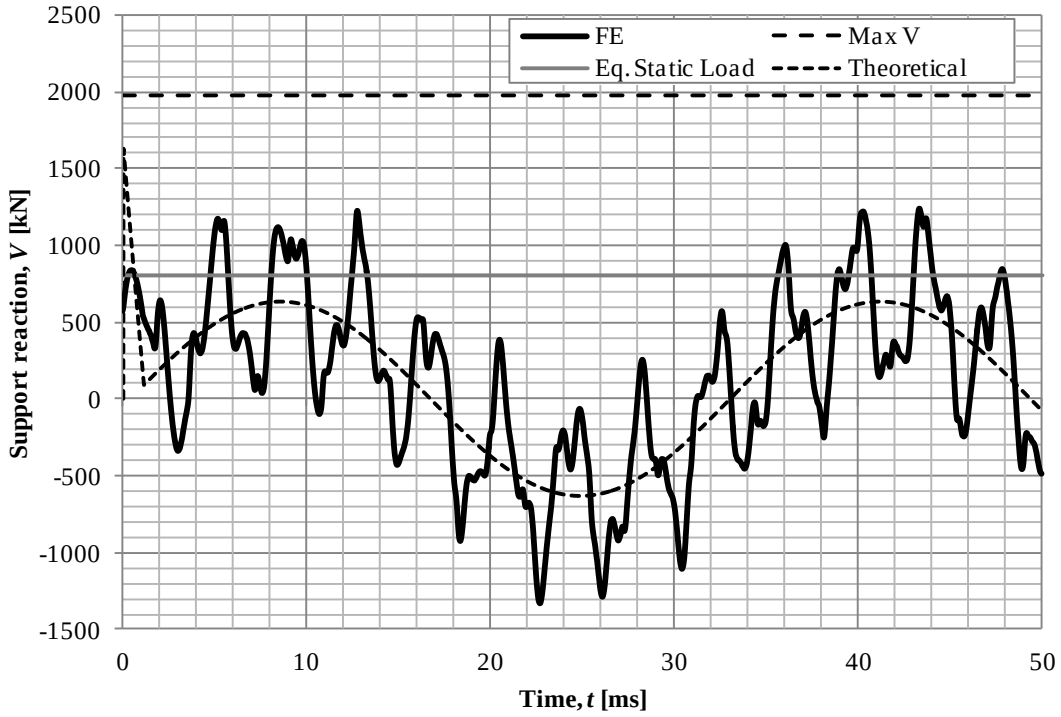

Figure 6.3. Reactions for the linear elastic model calculated with the different methods for load case 1.

Fortifikationsverket's approach combined with time dependent internal resistance, from an SDOF solution, and external force seems to correspond to a mean value of the FE analysis. It can be seen in Figure 6.4 that the reaction force is approximately a mean value of the reaction force obtained in the FE-analysis. The initial difference can be due to that the methods initially assume an elastic deformation shape while the actual deformation is close to a rigid body motion.

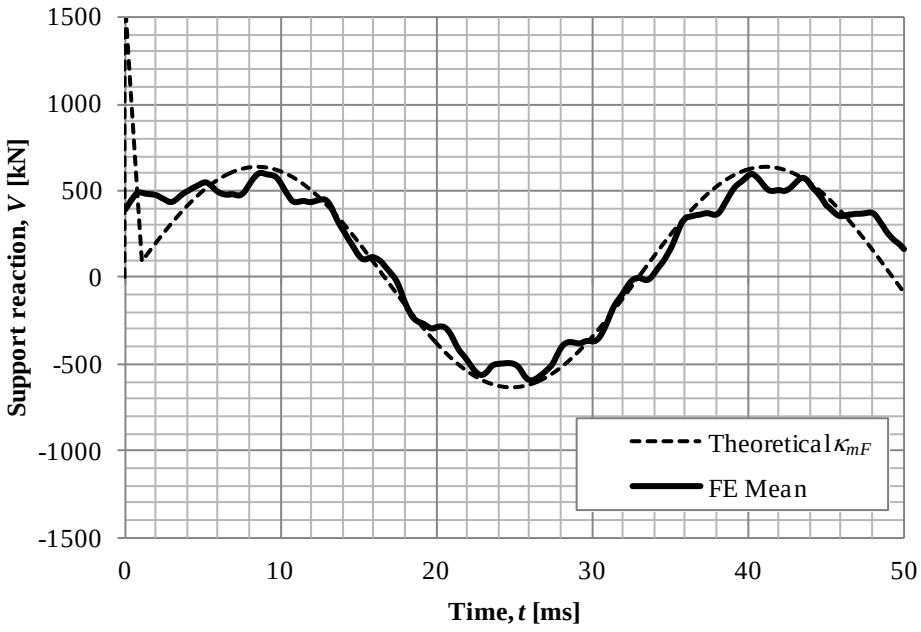

Figure 6.4. The reaction force using theoretical transformation factor method compared to the mean value of the support reaction from FE-analysis for every 5^{th} ms.

Figure 6.5 shows a magnification of the first five milliseconds for the different methods in Figure 6.3. Varying values of the transformation factor and internal resistance have been implemented in Fortifikationsverket's approach. It underrates the actual value significantly although it has a similar shape to the FE analysis.

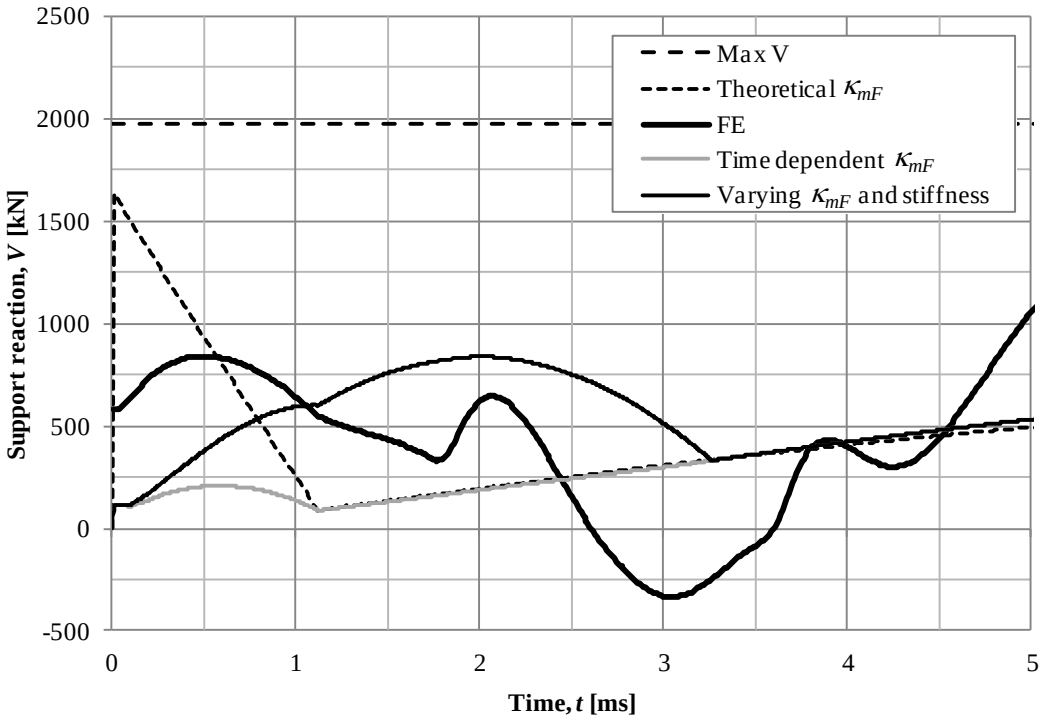

Figure 6.5. The early support reaction with the different methods for a load with peak pressure 5000 kPa and 1.12 ms duration.

Here, the stiffness is also varied according to equation (6-7) together with the transformation factors. This results in a good estimation of the maximum value. However, the maximum value does not occur at the same time. The maximum value in the FE analysis is obtained at half the load duration, while the proposed method's maximum value occurs at half the structure's period. After some time, the reaction force from these methods is the same as for the one with constant transformation factors.

In order to investigate if this is just a coincidence, the same studies were performed for load case 3. It can be seen in Figure 6.6 that the support reaction is lower and that the peaks are reduced. The solution with theoretical transformation factors agree well with the mean value of the support reaction. The static equivalent load overestimated the support reaction and the maximum support reaction is greatly overestimated.

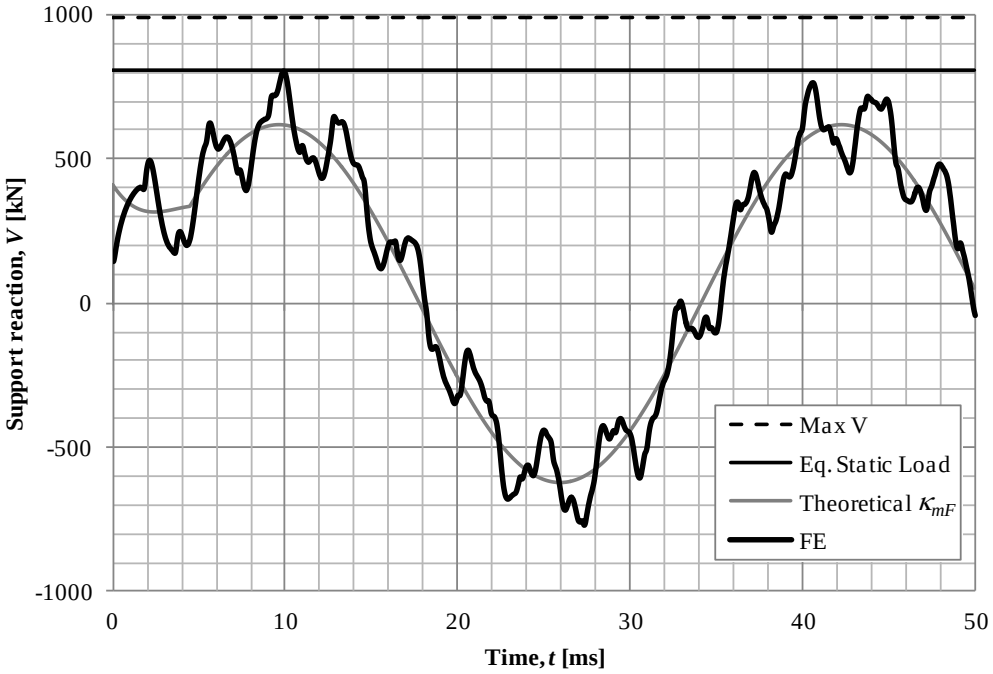

Figure 6.6. The support reactions over time for load case 3 with peak pressure 1250 kPa and 4.48 ms duration.

Figure 6.7, shows the support reaction during the initial five milliseconds. It can be seen that using varying transformation factors will again underestimate the support reaction, see. The solution with a varying stiffness still provides a very good agreement, but does not occur at the correct time. It can also be seen that the theoretical transformation factors do not overestimate the support reaction as was the case for load case 1.

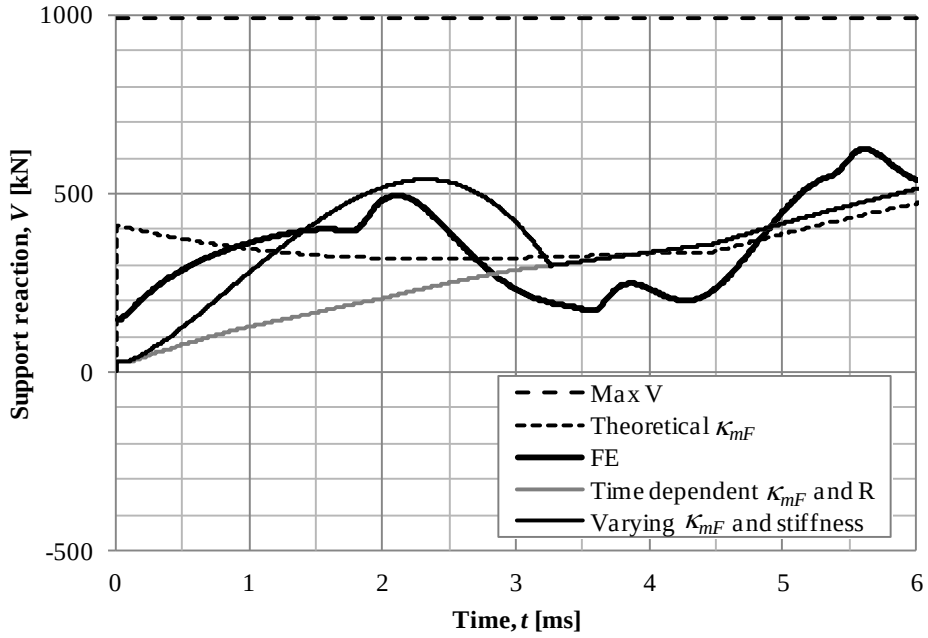

Figure 6.7. FortV with varying transformation factor and equivalent static load overrates the reaction for load case 3.

The above analyses have used an equivalent state II model. The concrete may be uncracked initially, which mean that a state I model should be used. More detailed analyses must be carried out in order to determine which Young's modulus that should be used. This must take concrete cracking and reinforcement yielding into account. An attempt was made and is presented in Appendix I. However, a good convergence was never found for that model.

A higher Young's modulus will increase the magnitude of the support reaction and shear forces, see Figure 6.8. It can also be seen that the small local peaks occur more frequently in state I because of the faster wave propagation. The time between the local peaks in both states is approximately the time it takes for the load to travel three metres, i.e. the beam length. The initial peak support reaction is considered to be true, but the magnitude of the later peaks is probably lower because of damping as seen in Section 5.2.2.

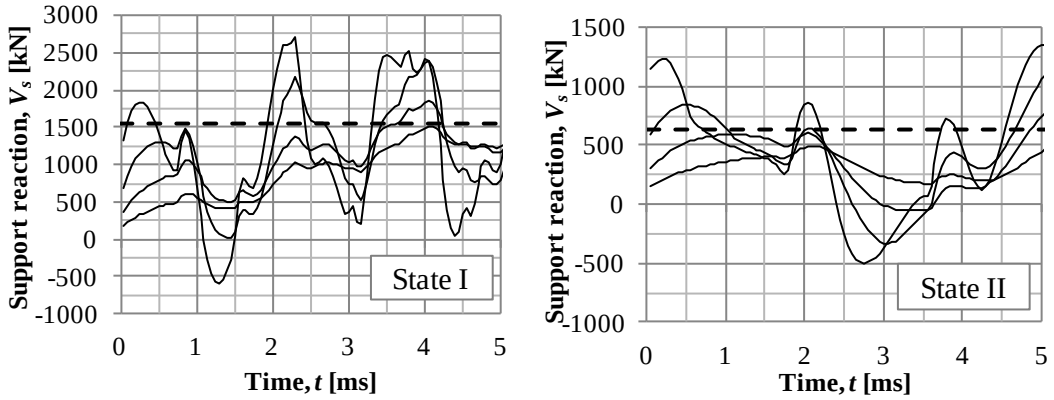

Figure 6.8. The support reaction for a state I and II model respectively subjected to different load cases 0, 1, 2 and 3. The dotted line is the support reaction with the equivalent static load.

The magnitude increase happens because the support reaction depends on the internal resistance. When the internal resistance increases, the static equivalent load also increases. This is represented in Figure 6.8 with a black dotted line. In state II, the peak initial support reaction for both load case 0 and 1 cannot be described by the equivalent load. In contrast, the initial support reaction for load case 1 is taken into account in state I. It seems like the equivalent load can be used to estimate the initial peak conservatively if the ratio between the peak pressure and static equivalent load is small. A maximum value of the ratio between peak pressure and equivalent static load, for which the peak support reaction is lower than the equivalent static load, was obtained as 19. This was found by using other load cases until the equivalent static load did not describe the initial peak conservatively. The equivalent static load is consequently on the safe side if

$$F_{peak} \leq 19 R_m \tag{6-9}$$

However, only some load situations have been considered and more investigations must be performed in order to determine this constant accurately.

If the time dependent transformation factors are used together with a varying stiffness according to equation (6-7) it can be seen that the magnitude of the initial support reaction is reasonably well described for both the state I, Figure 6.9, and state II, Figure 6.10, models for the different load cases. It is only for load case 0 in the state II model that it gives an unsafe peak value. The time when it occurs is however not correct. The method describes the second peak. The agreement would probably be improved if the stiffness is calculated for every deformation shape and not just taken from the calibrated relationship in equation (6-7).

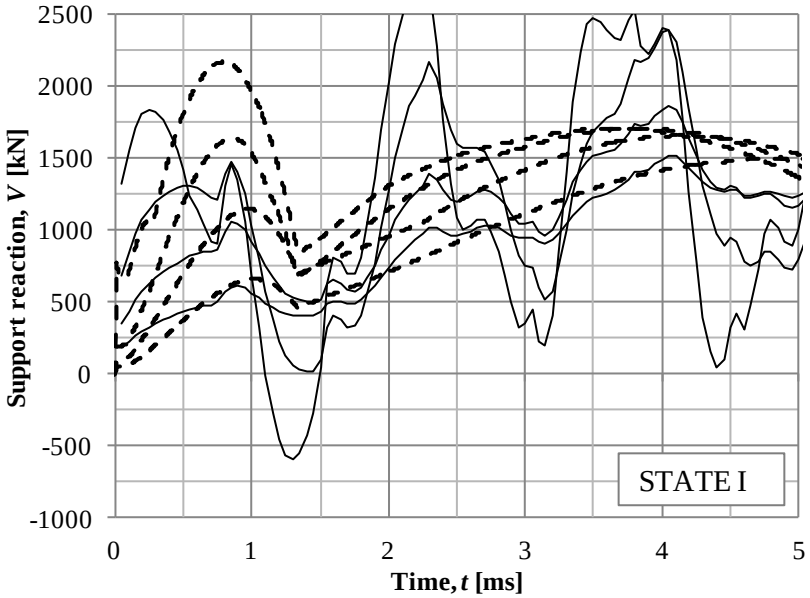

Figure 6.9. The support reaction in state I for different load cases obtained from FE analysis (solid line) and SDOF model with time dependent transformation factors and stiffness (dotted line).

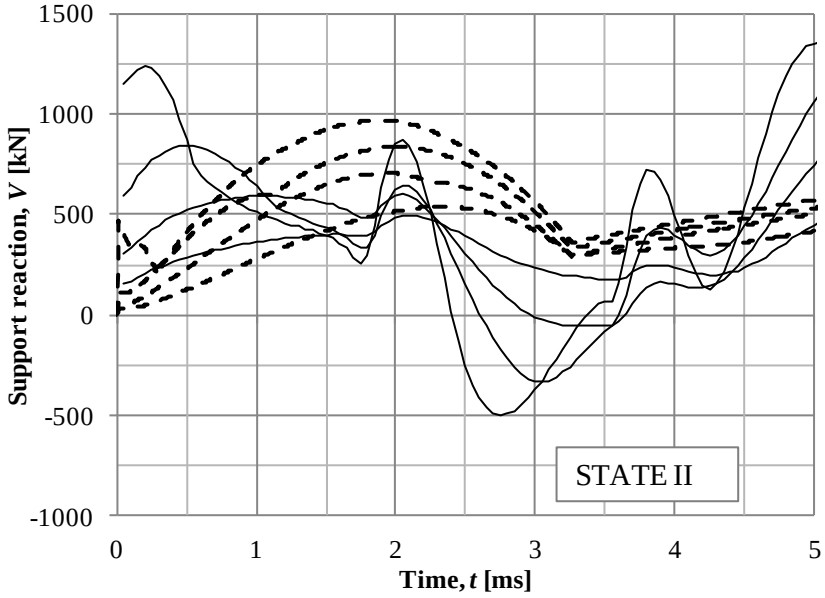

Figure 6.10. The support reaction in state II for different load cases obtained from FE analysis (solid line) and SDOF model with time dependent transformation factors and stiffness (dotted line).

6.3 Ideal plastic analysis

The same analyses as in section 6.2 are carried out for the ideal plastic case. As can be seen in Figure 6.11, the support reaction has a high peak in the first milliseconds and later oscillates between maximum and minimum plastic reaction force. The later oscillations start when the maximum deflection of the midpoint is reached and are believed to occur since the FE-analysis actually has not an ideal plastic response, just a very high Young's Modulus. The response will consequently be similar to an elasto-plastic response with very high Young's modulus but with much smaller displacements than in the case of elasto-plastic analysis.

Similarly to the elastic case, the maximum value of the support reaction is overestimated with Fortifikationsverket's approach. However, the mean value of the FE-analysis' reaction force over time can be well estimated when the actual internal resistance is used in the method. It takes the initial peak into consideration before it corresponds to the peak values of the plastic support reactions. For higher peak pressures, load case 1, it gets slightly overestimated, as seen in Figure 6.11, while there is a better agreement for less intense loads, load case 3, see Figure 6.12. This could be because actual deformation shape is not the expected.

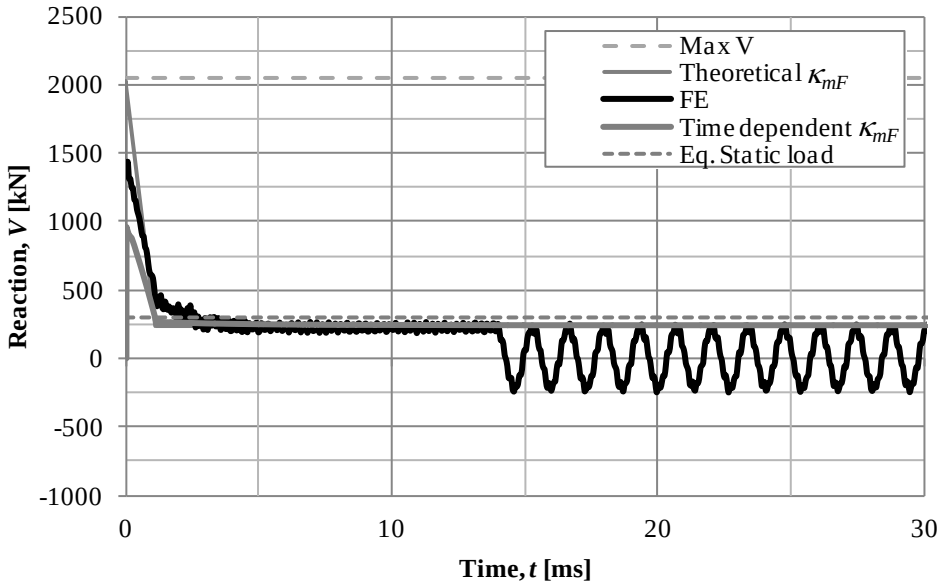

Figure 6.11. Reactions for the ideal plastic model calculated for load case 1.

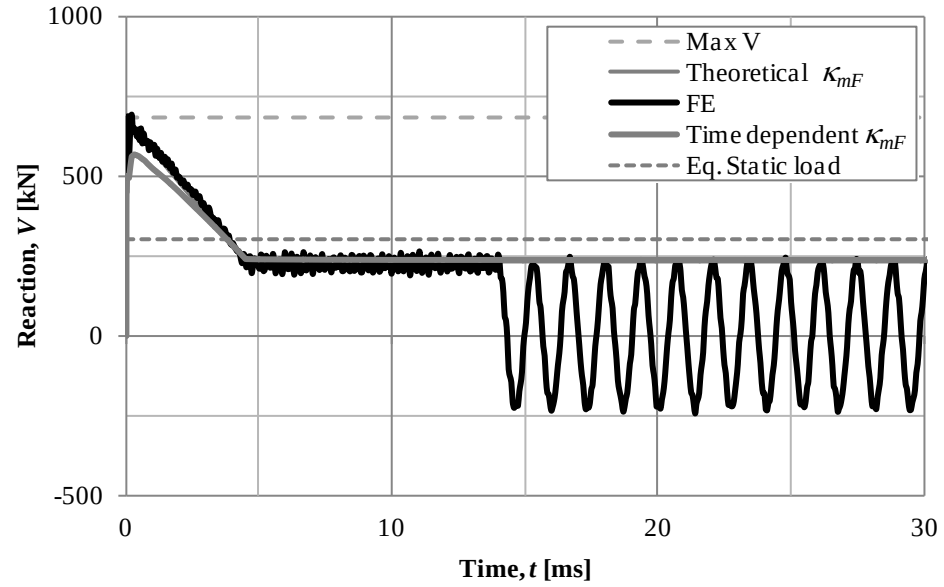

Figure 6.12. The reaction over time for a less intense load, load case 3.

The equivalent static load slightly overestimates the peaks in the late oscillations of the FE-model well but misses the first peak. This is because it does only consider contribution from half the internal resistance as discussed. The difference between the peak obtained in the FE analysis and the reaction due to the equivalent static load is relatively large, for a load with peak pressure P = 5000 kPa the difference is four times as large, as can be seen in Figure 6.13. The time dependent transformation factors are also introduced here, but they give a slightly lower reaction force.

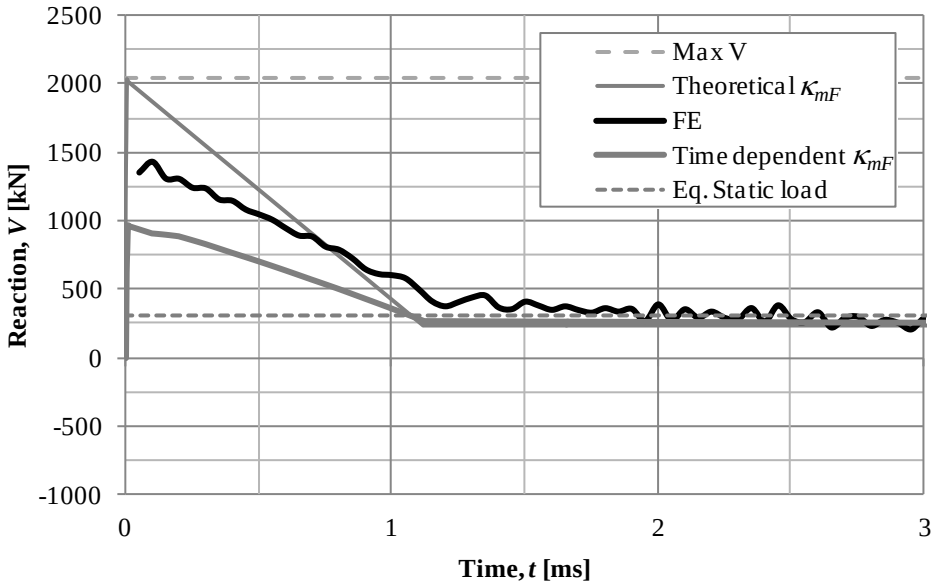

Figure 6.13. Early reactions according to the different methods for load case 1.

If the plastic analysis is performed with load case 3, it can be seen that the theoretical values of the transformation factors give a good agreement with the average of the FE analysis and will not overestimate the peak value in the early stage, see Figure 6.12 and Figure 6.14. Also, the peak is very well approximated with the maximum value. This is a consequence of that the internal resistance is close to the maximum internal resistance at the same time as the peak load is present.

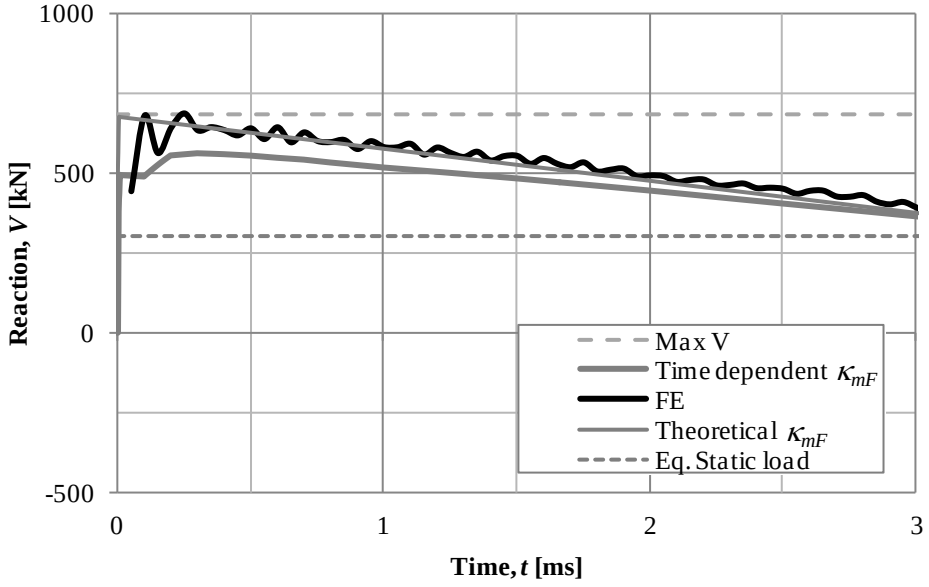

Figure 6.14. Reactions in early stage of the analysis for load case 3.

6.4 Elasto-plastic

The dynamic support reaction has been calculated similarly to the linear elastic and ideal plastic cases by using the proposed methods. The initial support reaction becomes high compared to the later support reaction in the oscillations, see Figure 6.15. This reaction will be overlooked or overestimated by the different approaches, as seen in Figure 6.16.

The hand calculation of maximum support reaction overestimates the reaction force considerably. This is discussed for the other material idealisations and depends on that the maximum internal resistance does not occur at the same time as the peak load.

The equivalent load gives a slightly conservative value of the late oscillations but does not capture the early peak. It agrees well with the peak values in the late phase.

The theoretical transformation factor used for the elasto-plastic model is the plastic transformation factor $\kappa_{mF} = 0.667$. This gives a good estimation of the reaction force when the structure oscillates but a phase shift occurs similarly to the displacement described in Section 4.1.3. In addition, it will give a conservative large support reaction initially.

If the varying transformation factors are used in Fortifikationsverket's approach with an internal resistance from the modified SDOF approach, this phase shift will not occur and the reaction force will be in good agreement in the late oscillations. However, the initial support reaction will be underestimated, i.e. the same response as to what has been observed for the linear elastic and the ideal plastic material models in Sections 6.2 and 6.3, respectively.

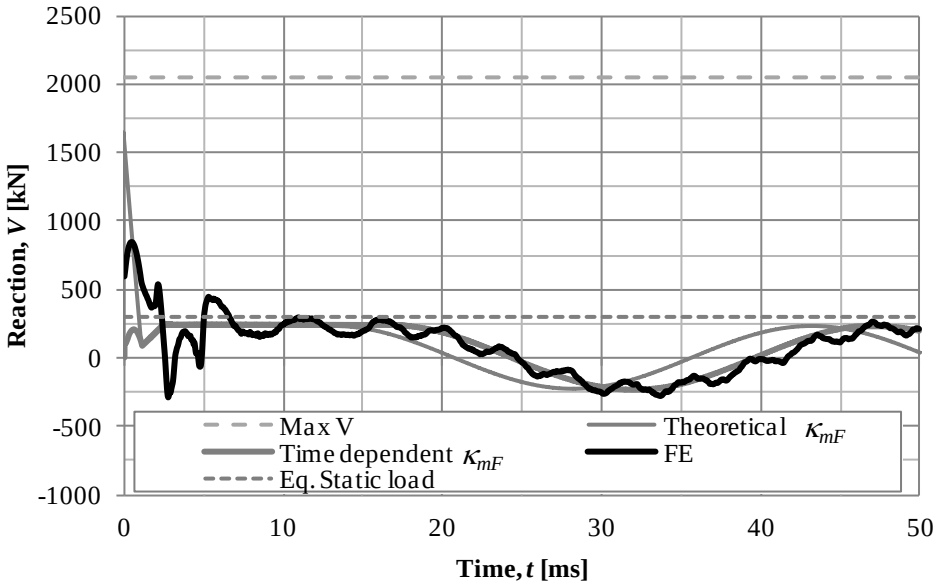

Figure 6.15. Reactions for the elasto-plastic model calculated for load case 1.

If a varying stiffness is also introduced, according to equation (6-7) a good estimation of the initial peak is obtained, see Figure 6.16. The peak support reaction will however not occur at the same time, which has also been observed in the linear elastic case.

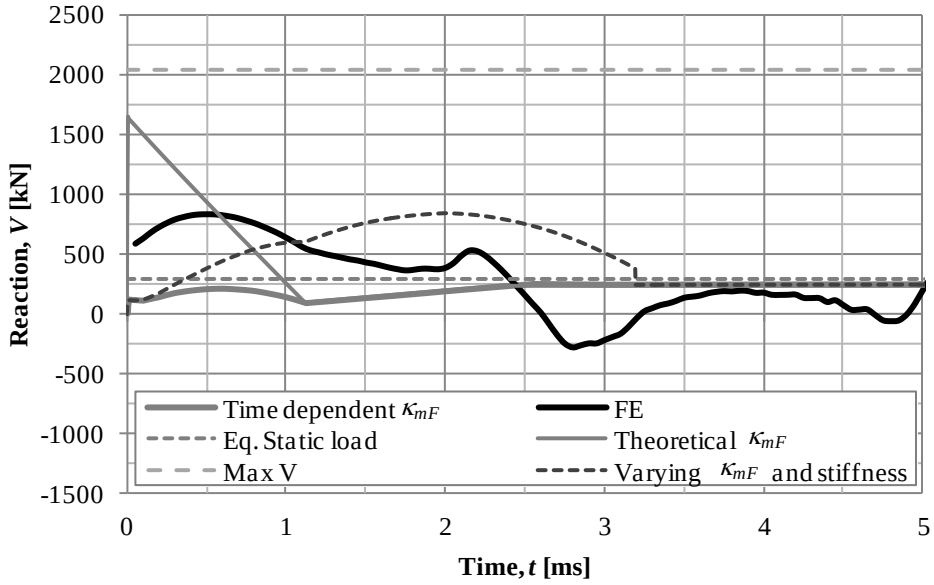

Figure 6.16. The early reaction force with different methods for load case 1.

The same observations are made for a less intense load, load case 3, see Figure 6.17. The maximum values overestimate the reaction. However, neither of the proposed methods captures the early peak. It is only if a varying stiffness according to equation (6-7) is introduced that the initial peak is covered as seen in Figure 6.18.

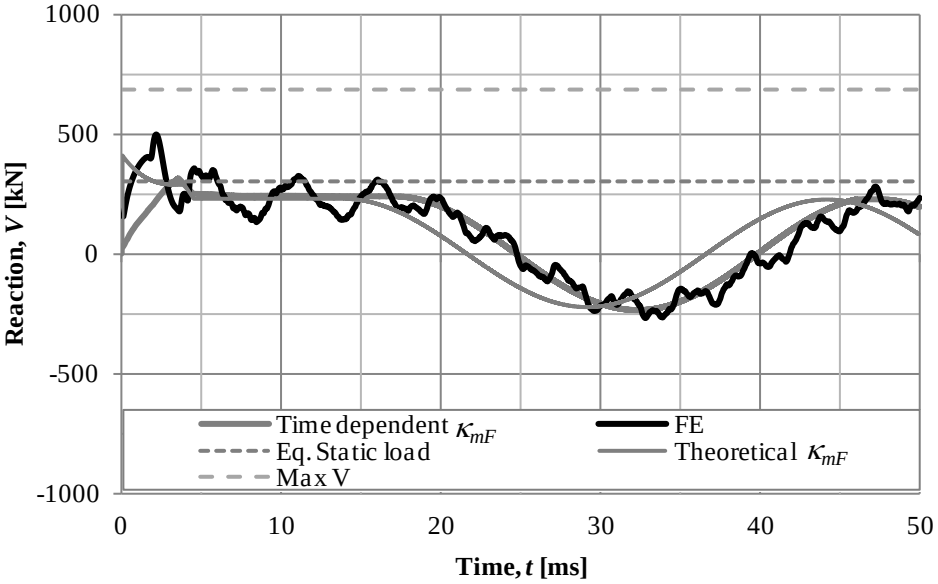

Figure 6.17. Reactions for the elasto-plastic model calculated for load case 3.

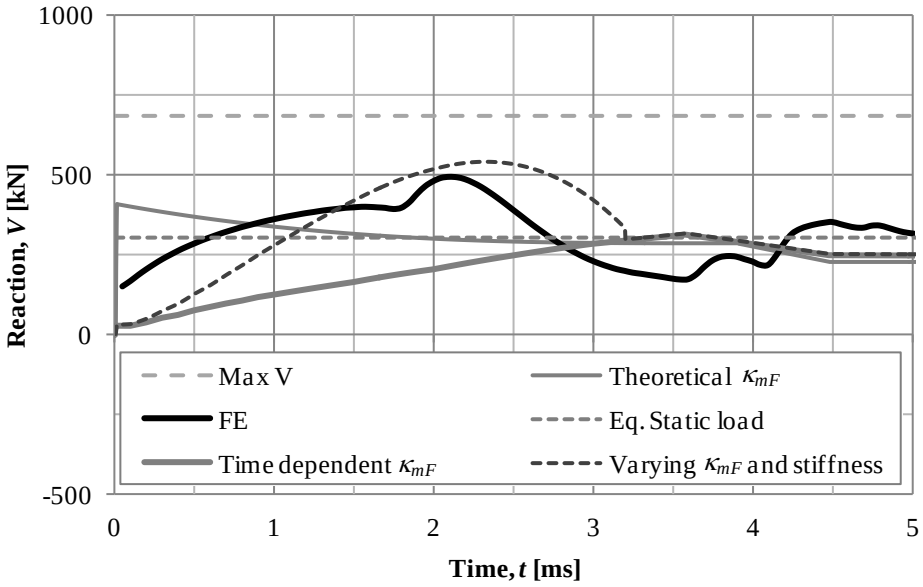

Figure 6.18. Reactions in early stage of the analysis for the elasto-plastic model for load case 3.

6.5 Discussion of results

A large support reaction occurs initially in a structure subjected to a highly intensive impulse load. Since this reaction force occurs very early, the behaviour of the structure is elastic. The initial peak is higher than the later support reaction when the structure has a plastic behaviour.

Several methods have been compared and the result suggests that the following could be concluded about the design approaches:

The maximum support reaction is greatly overestimated with the method that does not vary with time since the maximum external force does not occur at the same time as the maximum internal resistance.

The initial support reaction cannot be adequately predicted using by the static equivalent load only. The static equivalent load is only based on the maximum internal resistance, which leads to an underestimation of the initial peak. In addition, the support reaction for the later oscillations is overestimated with 25%. However, it can be used for conservative estimations for the later phase if knowledge about the early peak support reaction exists.

The support reaction for the late phase is dependent on the transformation factors according to Fortifikationsverket's approach. However, the initial support reaction is overestimated when using theoretical transformation factors. This could also be used conservatively in design.

Implementation of varying transformation factors provides initial support reactions on the unsafe side. The stiffness is higher initially, because of the different displacement shape and the internal resistance could be increased according to Ardila-Geraldo (2010) soon after load arrival. This estimates the peak very well but not the time when it happens. A more general stiffness could be taken out for every time step to get a better agreement. However, the maximum value is of main importance and not the

time of occurrence. This approach is the most accurate approach to determine the early peak support reaction, but also the most complex. The theoretical transformation factors could be used in a conservative design. This would be preferable since the method is less time consuming.

In a real reinforced concrete beam, the section could be uncracked and a state I model should be used. This would introduce larger initial forces in the structure. However, the suggested design approach with using a varying stiffness and time-dependent transformation factors can capture this response as well. More research needs to be done to see which state model that describes the initial peak the best.

7 Direct shear

7.1 SDOF model

The simplified SDOF-approach for direct shear, described in Section 2.5.3, has been used for the beam described in Chapter 3 in order to examine the risk of failure in direct shear.

$$m \cdot \ddot{\Delta} + R(\Delta) = V_s(t) \tag{7-1}$$

where m is the beam's mass, Δ is the shear slip, $R(\Delta)$ is the direct shear resistance and $V_s(t)$ is the support reaction. Here, m represents the full mass since the initial transformation factors are almost 1.0 due to the initial near rigid body motion.

The direct shear resistance function was calculated according to Table 2.6 and is shown in Figure 7.1. The ultimate slip, Δ_{max}, becomes very large, due to much bending reinforcement and large diameter bars. Since the resistance function is purely empirical, this value should probably be handled with great care. The steel used when the method was proposed did in general have more plastic deformation than today, Johansson (2012). The large ultimate slip gives a high direct shear capacity since it consumes much energy.

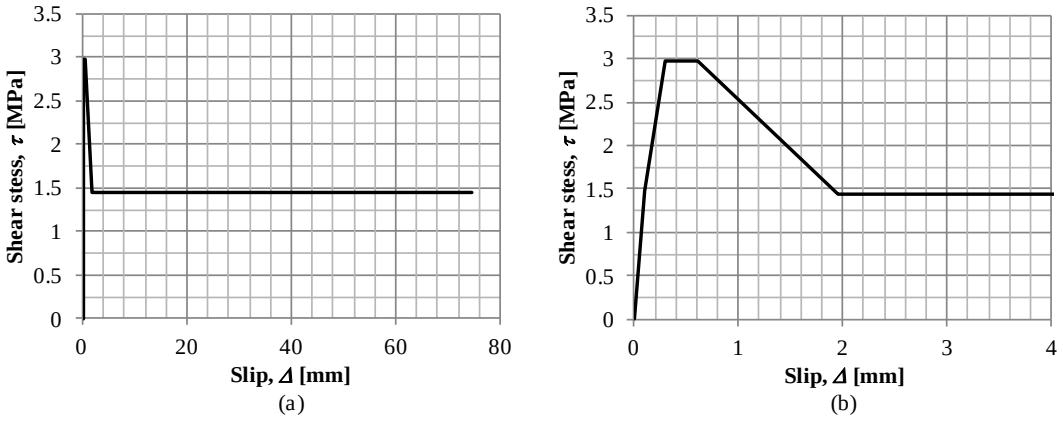

Figure 7.1. Direct shear resistance function. a) The entire resistance curve, b) magnification of the initial resistance.

7.2 Failure criteria

When examining the risk of dynamic direct shear failure, Δ_3 = 0.6 mm is used as a failure criterion with a tri-linear resistance function. This is the same criterion that Krauthammer *et al*. (1993) has used in previous work. Another alternative has been used by Low and How (2002), who have simplified it further to just a bilinear relationship with the same area under the graph in order to investigate the failure mode, see Figure 7.2. This makes the potential incorrectness with Δ_{max} unimportant. Using Δ_{max} as failure criterion makes the direct shear capacity unreasonably high.

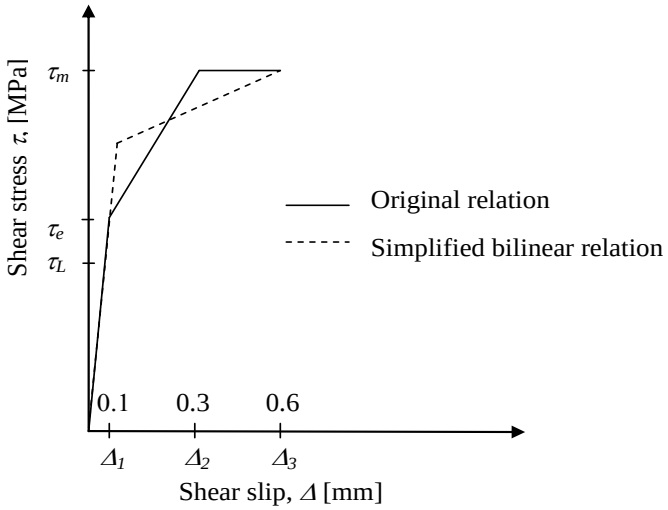

Figure 7.2. Simplified bilinear relation used by Low and How (2002) compared with the original relation used by Krauthammer et al. (1993). The areas under the graphs are equal.

Since the flexural and direct shear response occurs at different times, they are uncoupled and the support reaction could be calculated with the SDOF model for flexure using FortV's method. As seen in Chapter 6 this provides a conservative estimate of the reaction force but is here used as an estimate. The general appearance of the support reaction is shown in Figure 7.3. The first peak is dependent on how impulsive the load is.

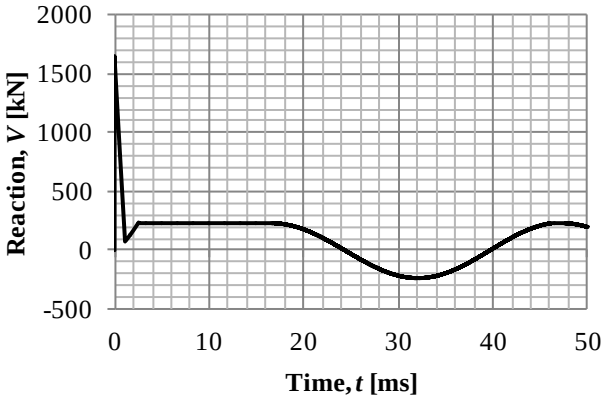

Figure 7.3. General appearance of the support reaction for elasto-plastic response.

The criterion of failure in bending is taken from the plastic rotational capacity. The maximum plastic deformation is in Section 3.4.1 calculated to

$$u_{pl} = 22.6\,\text{mm} \tag{7-2}$$

The elastic deformation will dissipate some energy and the total allowed deformation can in line with definition of elasto-plastic deformation in Section 2.4.1.4 be expressed as

$$u_{ep,d} = u_{pl} + \frac{u_{el}}{2} = u_{pl.d} + \frac{R}{2k} = 22.6 + \frac{606}{2 \cdot 8.42 \cdot 10^{7}} = 26.2\,\text{mm}. \tag{7-3}$$

7.3 Iso-damage curves

Iso-damage curves were constructed for flexure and direct shear failures by investigating at which pressure and impulse intensity the failure criteria were reached. The direct shear failure was assumed to happen early before any significant bending effect happens.

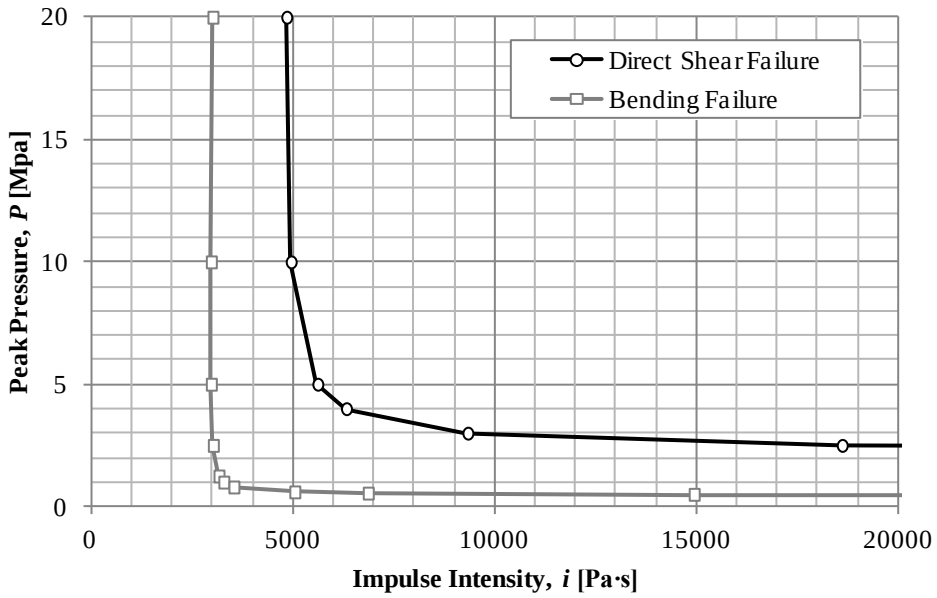

Figure 7.4. Iso-damage curves for bending and direct shear.

In Figure 7.4, it can be seen that for any combination of peak pressure and impulse intensity, the beam will fail in bending and hence the direct shear failure would not need to be considered for this beam. If direct shear would occur, the beam would have failed in bending anyway a couple of milliseconds later.

In previous experiments and comparisons by Chee (2008), it is shown that direct shear failure occurs if the load is very impulsive and of high magnitude and that flexural failure happens when the load has lower magnitude with longer duration, see Figure 7.5. The experiment indicated with a triangle would fail in both modes but failed firstly in direct shear.

The requirement for bending failure used by Chee (2008) is much greater than what is used in this thesis. The slab element used is 1.2 x 4.8 x 0.15 m and has an ultimate displacement of 14 inch, i.e. 355 mm. This had a reinforcement percentage of 0.5 %. It was not possible to find which steel class that was used. The concrete had cylinder compression strength 52 MPa i.e. higher than in this example. The authors of this thesis did not succeed to recreate the iso-damage curves in Figure 7.5. This was due to that a slab flexural resistance curve has been used, which is not treated in this thesis. Also, some parameters may have been misinterpreted.

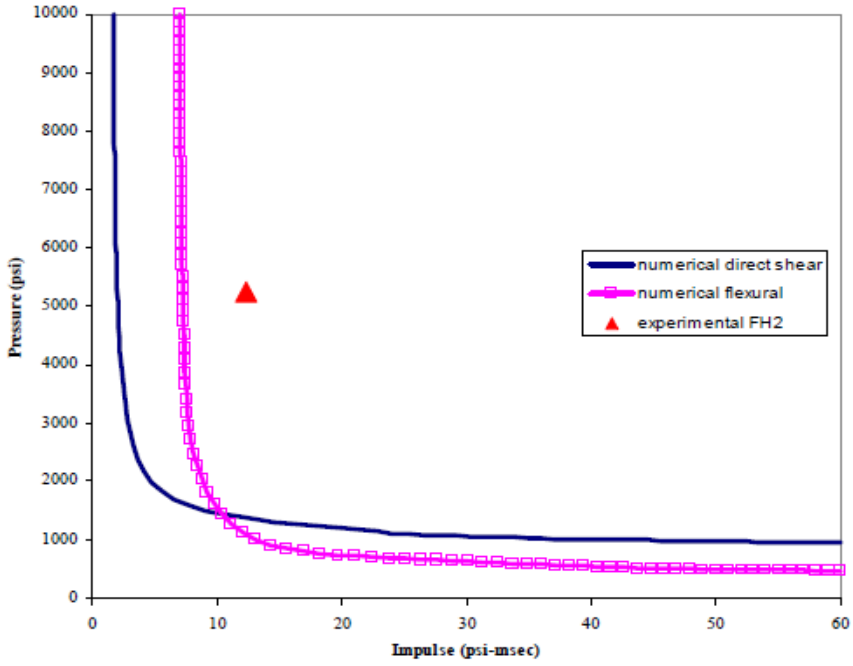

Figure 7.5. Iso-damage curves for one of the experiments carried out by Kieger and Getchell (1982), from Chee (2008)

The failure criterion used in Eurocode 2, CEN (2004), can be an underestimation of the allowed bending deformation therefore the beam was given a higher plastic rotational capacity in order to examine the effect of this.

$$u_{pl} = 2 \cdot u_{pl,d} = 45\,\text{mm} \tag{7-4}$$

and the total deformation

$$u_{ep} = u_{pl} + \frac{u_{ep,el}}{2} \approx 50\,\text{mm} \tag{7-5}$$

Using this modified failure criterion, the moment failure is still the governing parameter for all loads but the failure curves are closer to each other. It could be seen that a three times as high rotational capacity would give a risk of direct shear failure and iso-damage curves more similar to Figure 7.5.

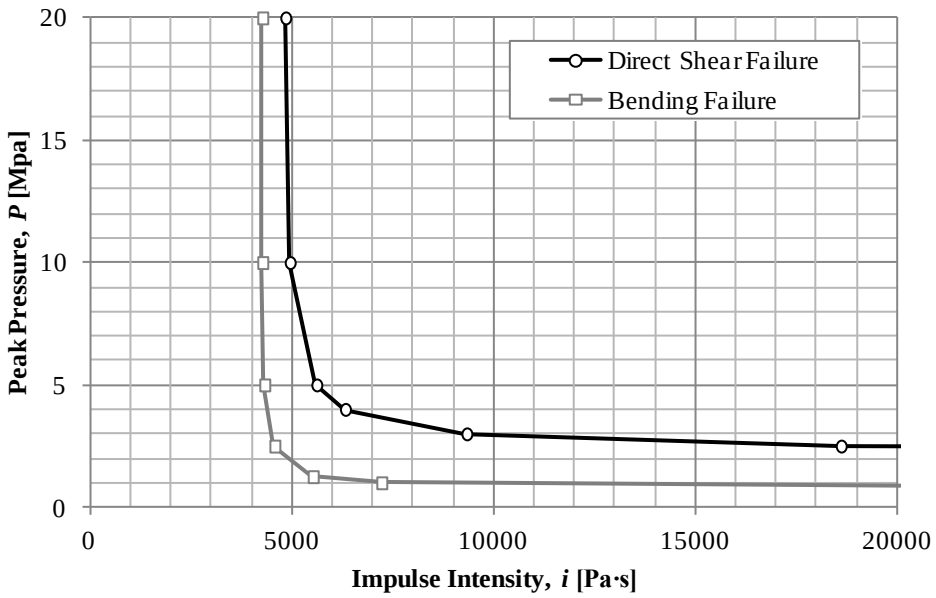

Figure 7.6. Iso-damage curves when using a larger rotational capacity for bending failure.

In the reliability analyses performed by Low and How (2002), it was found that a stiffer and shorter beam would be more susceptible to fail in direct shear. Therefore, the simplified SDOF system for direct shear were also implemented for shorter and deeper beams, but the flexible mode of failure still turned out to be the most dangerous, i.e. the iso-damage curves were schematically the same as in Figure 7.4.

The influence of the concrete strength was also analysed. This study was made with the same beam but with a lower concrete strength. The results show that the difference between bending and direct shear capacity decreased with decreased concrete strength, but that the beam would still fail in bending for all load cases. The influence of using the state I stiffness when calculating the reaction force was also investigated. A direct shear failure would still only occur if the beam would fail in bending.

7.4 Discussion of results

In this chapter iso-damage curves for direct shear and bending failure were created. Direct shear failure will not be the governing failure criterion in these analyses. If it would occur, the structure would have failed in bending later anyway.

The calculations carried out in this thesis show that it is not necessary to consider the direct shear failure phenomenon the simply supported beam studied here. This can depend on that the design rotational capacity of the structure used in Eurocode is too conservative, which leads to a lower capacity in bending. For instance, the allowed deformation in bending used by Chee (2008) is 350 mm for a 4.8 m slab compared to Eurocode, which gives a value of 22 mm for a 3 m slab. These two sections have approximately the same reinforcement ratio but the steel class used by Chee (2008) could not be found. Evidently, more parameters govern the plastic rotation capacity but the principle difference can be seen.

The constructed iso-damage curves for direct shear failure may therefore be correctly described with the used approach. However, more investigations are needed to determine whether this is true. The direct shear resistance function is empirical and it

is important to investigate if it is up to date. In Europe, new types of reinforcement steel are used today compared to those used in for example the 1980's, which may not have the same properties. This is probably the reason why the ultimate failure slip is very high. This is however no problem if the shear slip corresponding to 0.6 mm is seen as the failure criterion. Since the definitions of the different regions are fixed values, these should be further investigated for smaller or larger cross sections. Intuitionally, empirical models should be handled with care and this is also what is recommended here.

More studies of how the boundary conditions affect the reaction force needs to be carried out. It is possible that a clamped beam may have another response than for a simply supported beam. Most of the reported direct shear failures have occurred in slabs. This may also be a subject for further studies.

Regarding the actual design, it is important to realise that the shear reinforcement should not be arranged vertically when strengthening a structure against direct shear failure. This would not contribute to the resistance of direct shear since the direct shear crack propagates almost vertically. The reinforcement should therefore be placed with an angle to the shear plane. In Section 5.5 the arrangement of the bending reinforcement is discussed. It is there recommended that no curtailment is performed. Since the moment close to the edges is very small when the direct shear takes place, this reinforcement can contribute to the direct shear resistance. If the shear reinforcement is placed with an angle to the longitudinal axis it could contribute to the normal shear capacity as well as the direct shear capacity of the beam.

8 Final conclusions and recommendations

8.1 Conclusions

The initial deformation shape for a beam subjected to a uniformly distributed impulse load differs considerably to the expected shape when statically loaded. This means that the current theoretical values of transformation factors for the plastic and elasto-plastic material response poorly describe the early deformation. However, later on there is a rather good agreement with the theoretical transformation factors.

Time dependent transformation factors can be obtained from FE analyses and implemented in the SDOF system. This will cause an energy loss in the system and consequently too small displacements. Therefore, a method for preserving energy in the system, while varying the transformation factors, is introduced. This makes the displacement agreeing well with the FE analyses for all material models studied.

Even a simplified relationship for the time dependent transformation factors can be used if the preserve energy scheme is used in the SDOF model with elasto-plastic material model. This relationship uses the transformation factors for elastic and plastic theoretical deformation shape when the response is elastic and plastic, respectively.

The moment for a beam with elastic material response will be underestimated when using the equivalent static load. The more intense the load is the larger deviation. However, damping decreases the deviation considerably. Similarly, the shear force is not described adequately with the equivalent static load. Both the support reaction and the shear force close to the centre are underestimated.

Distribution of moment and shear force will not be as expected for a static load. This means that care should be taken when the reinforcement is arranged in a concrete member. A recommendation is to not make any curtailment and that shear reinforcement, if needed, should be extended towards the centre.

The initial reaction force is governed by elastic behaviour and will be of great magnitude. Several methods for determining the support reaction have been investigated:

- Using the maximum value of Biggs' and FortV's approach will result in a considerable overestimation of the reaction.
- Determining the reaction with the static equivalent load leads to an underestimation for the initial reaction. For the later phase, though, the reaction is overestimated with 25 %.
- Using time dependent pressure and internal resistance together with the theoretical transformation factors in FortV's approach will cause an overestimation of the initial reaction. This approach will represent the later phase rather well.
- Implementation of varying transformation factors provides initial support reactions on the unsafe side. The internal resistance could be increased according to Ardila-Geraldo soon after load arrival. This estimates the peak very well but not the time when it occurs.

The evaluated simplified SDOF model for direct shear failure shows that this failure criterion will not be governing for the case presented in this thesis. The examined examples in this report will always also fail in bending later if it fails in direct shear. This may be a consequence of that the model is empirical or that input data have been misinterpreted. This should be handled with great care. This can also be due to a very strict value for the plastic rotation capacity used for bending, which has been seen to be less strict in other studies.

Using an equivalent Young's modulus in ADINA will have a significant impact on the results, but as long as the corresponding change in velocity is less than 3 times the initial value it is seen as a good approximation. For higher changes the user should be cautious.

8.2 Further studies

The method using energy preservation in the SDOF analysis works well. Some further work investigating how high accuracy that is needed for the transformations factors can be done. It is interesting to investigate if the relationship can be further simplified or if values for more time increments should be used. It would be preferable to determine a simplified relationship that can be used to calculate both the displacement and reaction for different load cases and boundary conditions.

It is not clear how the initial peak value of the support reaction is supposed to be treated and it can differ a lot between different design codes. This is a subject that needs further study, although some investigations are covered in this report. A suggestion is to find a reaction force as a function of the properties of the impulse load and the transformation factors, which represent a good estimate of the peak value and time of occurrence.

Investigations of to what extent the equivalent static load can be used for design is needed. In this report it is shown that it is not always on the safe side to base the design on an equivalent static load. It would be of interest to study the influence of varying stiffness i.e. how the moment and shear distribution would be affected by curtailment of the reinforcement. Moreover, the response when using other material properties such as steel and timber should be explored. Some suggestions of how to treat this in design is preferable. If an elastic material is going to be used in design, an up-scaling factor could be introduced for moments and shear forces. This factor could take damping into account. More investigations should be carried out in this subject.

This thesis presents how the direct shear problem is treated in different design codes today and also tried to implement this into a simplified SDOF model. However, the knowledge of the direct shear failure phenomenon is still vague, and there is need of further study. A suggestion is to study the importance of direct shear design and how this should be treated. Also study when the risk of direct shear failure occurs and how a so called direct shear crack propagates through the member. This is not treated well in design today and further study of this crack propagation and how it should be designed for should be investigated.

The Young's modulus affects the wave propagation through the beam. It is necessary to investigate which Young's modulus that should be used in a FE analysis with a simplified bi-linear material behaviour in order to describe cracking and reinforcement yielding and how this will affect the deformation shape.

9 References

ADINA, 2010. *Theory and Modelling Guide*. Vol 1: ADINA Solids & Structures Report ARD 10-7, ADINA R & D, Inc., Watertown, MA. USA.

ADINA (2012), E-mail contact with Zhang X., Ph.D., Wang R., Walczak J., Ph.D. ADINA R&D, Inc. Watertown, MA. USA.

Al-Emrani, M. Engstöm, B. Johansson, M. Johansson. P., 2008. *Bärande konstruktioner*. Report 2008:12, Chalmers University of Technology, Division of Structural Engineering, Göteborg, Sweden.

Ardila-Giraldo, O. A., 2010. Investigation on the Initial Response of Beams to Blast and Fluid Impact. Ph. D. Purdue University.

Augustsson R. och Härenstam M., 2010. *Design of reinforced concrete slab with regard to explosions*. Division of Structural Engineering, Concrete Structures, Chalmers University of Technology, Master Thesis 2010:38, Göteborg, Sweden.

Biggs J.M., 1964. *Introduction to Structural Dynamics*. McGraw-Hill Inc., New York, USA.

Boverket, 2004. *Boverkets handbok om betongkonstruktioner, BBK 04*. Boverket. Karlskrona

CEB, 1993. *CEB-FIP model code.* Comité Euro-international du béton. EPF Laussanne. T Telford, London, Great Britain, p. 437.

CEN, 2004. Eurocode 2: Design of concrete Structures – Part 1-1: General rules and rules for buildings. European Comittee for Standardization, Brussels, Belgium.

Chee K. H., 2008. *Analysis of shallow buried box structures subjected to airblast loads*. Master's thesis. University of Florida.

Craig Jr., R. R. and Kurdila, A. J., 2006. *Fundamentals of Structural Dynamics.* 2nd ed. Holboken, New Jersey. John Wiley & Sons, Inc.

Crawford, J. E., Krauthammer, T., Karagozian, J. and Hinman, E. (1999). "Structural components – Analysis and design examples." *Structural design for physical security: state of the practice*. Chapter 4, ASCE, SEI, Reston, Va.

Department of Defense (DoD), 2008. *Unified Facilities Criteria: Structures to Resist the Effects of Accidental Explosions*. UFC 3-340-02.

Ek K.J. och Mattsson P., 2009. *Design with Regard to Blast- and Fragment Loading*. Division of Structural Engineering, Concrete Structures, Chalmers University of Technology, Master Thesis 2009:81, Göteborg, Sweden.

Engström B., 2011a. *Design and analysis of continuous beams and columns*, Report 2007:3, Edition 2011. Division of Structural Engineering, Concrete Structures, Chalmers University of Technology, Göteborg, Sweden.

Engström B., 2011b. *Design and analysis of slabs and flat slabs*. Division of Structural Engineering, Concrete Structures, Chalmers University of Technology, Göteborg, Sweden.

Fortifikationsverket, (2011). *FortSkydd. Bilaga till Fortifikationsverkets Konstruktionsregler FKR 2011.* Dnr 4535/2011, Försvarsmakten

Low, Y. L., Hao, H., 2002. Reliability analysis of direct shear and flexural failure modes of RC slabs under explosive loading. *Engineering Structures.* 24. pp.189-198.

Johansson, M. 1997. *Armeringsseghetens inverkan på deformationsförmågan hos betongkonstruktioner*. Avdelningen för Betongbyggnad, Chalmers Tekniska Högskola, Rapport 97:1, Göteborg.

Johansson, M. 2000. *Structural Behaviour in Concrete Frame Corners of Civil Defence Shelters, Non-linear Finite Element Analyses and Experiments*. Department of Structural Engineering, Division of Concrete Structures, Chalmers University of Technology, Göteborg, Sweden.

Johansson, M. och Laine, L., 2007. *Bebyggelsens motståndsförmåga mot extrem dynamisk belastning*, Delrapport 1: *Last av luftstötvåg*. Räddningsverket, Rapport B54-232/07, Karlstad.

Johansson, M. och Laine L., 2009. *Bebyggelsens motståndsförmåga mot extrem dynamisk belastning*, Delrapport 3: *Kapacitet hos byggnader*. MSB, Rapport MSB 0142-10, Sverige.

Johansson, P. and Lantz, H., 2009. *Crack Control of Reinforced Concrete with Continuous Edge Restraint.* Master's thesis 2009:43. Division of Structural Engineering, Concrete structures, Chalmers University of Technology.

Johansson, M. (2012), Ph. D., Reinertsen Sverige AB, Sweden.

Kieger S. A., Getchell J. V., Slawson T. R. and Hyde D. W. 1980-1984, *Vulnerability of shallow-buried flat-roof structures*. Technical Report SL-80-7, Parts 1-6. U.S. Army Waterways Experiment Station, Vicksburg, MA.

Krauthammer, T., Bazeos, N., and Holmquist, T.J., 1986. "Modified SDOF analysis of RC box type structures." *J. Struct. Eng.*, ASCE 112 (4), 726–744.

Krauthammer, T., Assadi-Lamouki, A. and Shanaa, H. M., 1993. Analysis of impulsively loaded reinforced structural elements. *Computers & Structures*. 48 (5). pp. 851-871.

Krauthammer, T., 2008. *Modern Protective Structures.* CRC Press, Chapters 5&6, pp 195-290.

Laine, L., 2012. *Markstötvåg.* MSB. Publikationsnummer: MSB344. Sverige

Mattock, A. H., and Hawkins, N. M., 1972. Shear Transfer in Reinforced Concrete-Recent Research. *PCI Journal*, pp. 55-75.

MSB, 2011. *Skyddsrum SR 09.* Med tillägg 2011. Beställningsnummer: B54-141/11. Sverige

Nyström, U., 2006. *Design with regard to explosions*. Division of Structural Engineering, Concrete Structures, Chalmers University of Technology, Master Thesis 2006:14, Göteborg, Sweden.

Ross, T.J., 1983. *Direct Shear Failure in Reinforced Concrete Beams under Impulsive Loading,* Technical Report AFWL-TR-83-84, Air Force Weapons Laboratory, Kirtland AFB, NM.

Slawson, T. R., 1984. *Dynamic shear failure of shallow-buried flat-roofed reinforced concrete structures subjected to blast loading*. Technical Report SL-84-7, Structures Laboratory, U.S. Army Waterways Experiment Station, Vicksburg, MS

Svedbjörk, G., 2010. *Tvärkraft i FKR*. Presentation på möte för verkansgruppen, 2010-05-27, Drammen, Norge.

APPENDIX A The central difference method

The central difference method is an explicit method for approximating the solution for a second order differential equation such as the equation of motion. The deformation at time *t+Δt* is approximated by considering the equation of motion at time *t*.

$$m\ddot{u}_t + c\dot{u}_t + ku_t = F(t) \tag{A-1}$$

where m is the mass, c is the damping, k is the stiffness, F(t) is the external force acting on the structure at time t and u_t, $\dot{u}_t$ and $\ddot{u}_t$ is the displacement, velocity and acceleration respectively.

By using the central difference approximations as shown in Figure A.1, the acceleration at time t can be written as:

$$\ddot{u}_t = \frac{1}{2\Delta t}\left(u_{t+\Delta t} - 2u_t + u_{t-\Delta t}\right) \tag{A-2}$$

The velocity at time t can correspondingly be approximated as:

$$\dot{u}_t = \frac{1}{2\Delta t}\left(u_{t+\Delta t} - u_{t-\Delta t}\right) \tag{A-3}$$

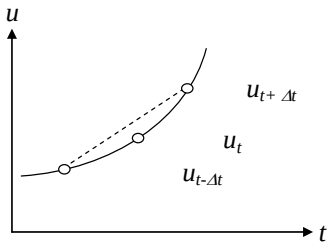

Figure A.1. The central difference scheme. The method uses $u_{t-\Delta t}$ and u_t in order to solve $u_{t+\Delta t}$

Following expression is obtained if equation (A-2) and (A-3) are inserted into the equation of motion (A-1):

$$u_{t+\Delta t} = \left(\frac{m_t}{\Delta t^2} + \frac{c_t}{2\Delta t}\right)^{-1}\left(F_t - R_t + \frac{2m_t u_t}{\Delta t^2} - \left(\frac{m_t}{\Delta t^2} - \frac{c_t}{2\Delta t}\right)u_{t-\Delta t}\right) \tag{A-4}$$

where

$$R_t = k_t \cdot u_t \tag{A-5}$$

The above equation can be solved if the deformation at time *t* and for the previous time *t-Δt* is known. This method needs a start value of the displacement which corresponds to the time -Δt. This start value can be calculated as

$$u_{-\Delta t} = u_0 - \Delta t \cdot \dot{u}_0 + \frac{\Delta t^2}{2}\ddot{u}_0 \tag{A-6}$$

Hence, the deformation at time $t+\Delta t$ can be found if the deformation at time t is known. This can be a problem when dealing with a non-linear response while unloading and reloading, because the equation (A-4) is derived with the assumption of linear elastic response. It is relatively easy to apply this function with a non-linear response by calculating a corresponding internal resistance force for the actual time t as a function of the displacement at time t, the stiffness k and the residual deformation u_{res}. In Figure A.2 below this is illustrated how this is solved for an elasto-plastic material model.

where

$$u_{res} = u_{\max}(t) - \frac{R_m}{k} \tag{A-7}$$

$$R(i) = k \cdot \left(u(i) - u_{res}\right) \tag{A-8}$$

Note that u_{max}(t) can change with time because at the time step i the absolute maximum value may not have occurred yet, it is the maximum value so far.

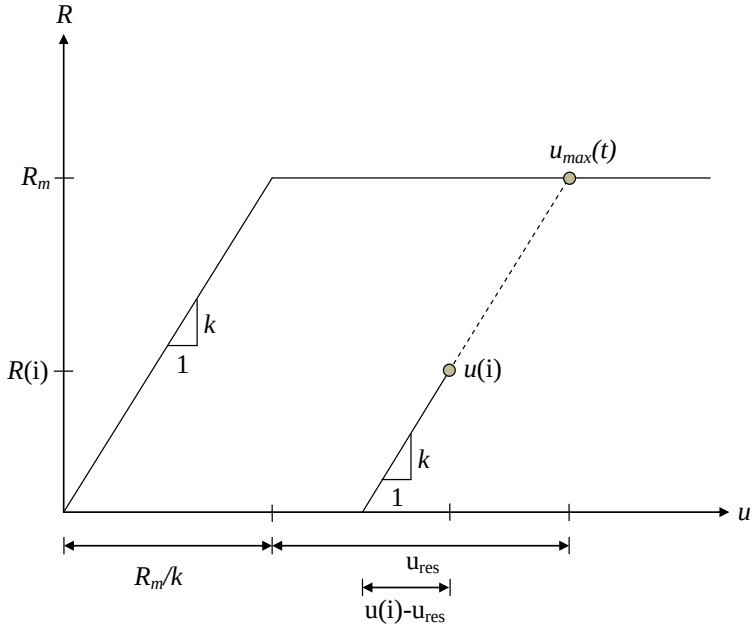

Figure A.2. Illustration of how the resistance is calculated for an elasto-plastic material model when using the Central Difference Method.

It can be seen that if u(i) is the actual maximum u_{max}(t) then the resistance R_m is obtained, which is the expected case.

APPENDIX B Derivation of expressions for maximum shear

B.1 Fortifikationsverket

In this appendix the expressions used in the Swedish design approach, FortV (2011), is presented. These expressions have been derived by Svedbjörk (2010).

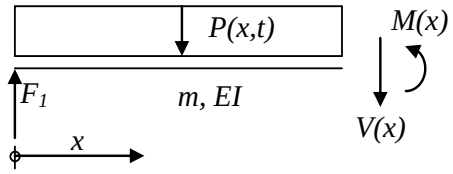

Figure B.1. A cut of a simply supported beam showing load, reaction force and section forces.

Vertical force equilibrium

$$\downarrow: \quad \int_0^x m(x)\ddot{u}\,dx = \int_0^x P(x,t)\,dx + V(x) - F_1 \tag{B-1}$$

where

$m(x) = m = \text{constant}$

$P(x) = P = \text{constant}$

Establish equilibrium when $x = L/2 \rightarrow V(L/2) = 0,\ u(L/2) = u_s$

The integral in the left hand expression in equation (B-1) can be rewritten as:

$$\int_0^{L/2} m\ddot{u}\,dx = m \cdot \frac{2}{L} \int_0^{L/2} \frac{\ddot{u}(x)}{\ddot{u}_s}\,dx \cdot \frac{L}{2}\ddot{u}_s \tag{B-2}$$

Because the acceleration has the same shape as the deformations the definition of the transformation factor in equation (B-4) can be used. By considering this equation (B-2) can be rewritten with help of equation (B-4) as

$$\int_0^{L/2} m\ddot{u}\,dx = \kappa_F \frac{m\ddot{u}_s L}{2} \tag{B-3}$$

where

$$\kappa_F = \frac{1}{L}\int_0^L \frac{u(x)}{u_s}\,dx \tag{B-4}$$

The right hand side expression in equation (B-1) is reduced to

$$\int_0^{L/2} p(x,t)\,dx + V(L/2) - F_1 = p(t)\cdot\frac{L}{2} - F_1 \tag{B-5}$$

which combined with equation (B-3) results in

$$\kappa_F \frac{m\ddot{u}_s L}{2} = p(t)\cdot\frac{L}{2} - F_1 \tag{B-6}$$

Next, the free body of a single degree of freedom system in the centre point of the beam is considered

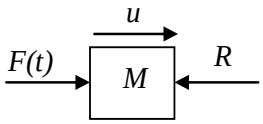

Figure B.2. A free body diagram of a single degree of freedom system.

$$\begin{aligned} R &= qL \\ F(t) &= p(t)L \end{aligned} \tag{B-7}$$

Horizontal force equilibrium gives

$$\rightarrow:\ \kappa_m M\cdot\ddot{u}_s + \kappa_k qL = \kappa_F\, p(t)L \tag{B-8}$$

where

$$\kappa_k = \kappa_F$$

$$M = mL$$

Combining equation (B-6) and (B-8) yields

$$\frac{\kappa_m}{\kappa_F}\left(p(t)L - 2F_1\right) + \kappa_F\cdot qL = \kappa_F\cdot p(t)L \tag{B-9}$$

which can be rewritten as

$$F_1(t) = \left[\left(1-\frac{\kappa_F^2}{\kappa_m}\right)p(t) + \frac{\kappa_F^2}{\kappa_m}q\right]\frac{L}{2} \tag{B-10}$$

B.2 Position of resultant in Biggs' max reaction calculation expression

When calculating the dynamic reaction the expressions derived by Biggs (1964) are commonly used. In this appendix it is shown how the expression for the lever arm of the inertia force is derived for a simply supported beam.

Make cut and take moment equilibrium to get an expression for the moment along the beam.

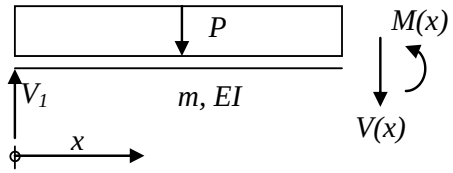

Figure B.3. A cut of a simply supported beam showing load, reaction force and section forces.

$$\text{Moment around x}: M(x) = -\frac{Px^2}{2} + V_1 x \tag{B-11}$$

Bernoulli beam equation gives us the definition of the moment as:

$$-EI\frac{d^2w}{dx^2} = M(x) \tag{B-12}$$

Integrating over time results in:

$$-EI\frac{dw}{dx} = \int M(x)dx = \left\{V_1 = \frac{PL}{2}\right\} = \int -\frac{Px^2}{2} + \frac{PL}{2}x\,dx = -\frac{Px^3}{6} + \frac{PLx^2}{4} + C \tag{B-13}$$

A second integration is performed in order to obtain an expression for the displacement:

$$w(x) = \frac{\int -\frac{Px^3}{6} + \frac{PLx^2}{4} + Cx\,dx}{-EI} = \frac{\frac{Px^4}{24} - \frac{PLx^3}{12} - Cx + D}{EI} \tag{B-14}$$

It is known that the displacement at the supports is zero i.e.

$$\begin{aligned} w(0) &= 0 \\ w(L) &= 0 \end{aligned} \tag{B-15}$$

The integration constants can then be determined as:

$$D = 0$$

$$\frac{PL^4}{24} - \frac{PL^4}{12} - CL = 0 \Rightarrow CL = \frac{PL^4}{24} - \frac{PL^4}{12} \Rightarrow C = -\frac{PL^3}{24} \tag{B-16}$$

By inserting (B-11) into (B-9), the expression for the deflection can be written as:

$$w(x) = \frac{\frac{Px^4}{24} - \frac{PLx^3}{12} - \left(-\frac{PL^3}{24}\right)x}{EI} = \frac{P}{24EI}\left(x^4 - 2Lx^3 + L^3x\right) \tag{B-17}$$

In order to obtain an expression for the deflection shape the expression for the deflection is divided with the maximum deflection at the midpoint which is:

$$w_{\max} = \frac{5PL^4}{384EI} \tag{B-18}$$

and this result in the expression for the deflections shape:

$$\phi(x) = \frac{w(x)}{w_{\max}} = \frac{\frac{P}{24EI}\left(x^4 - 2Lx^3 + L^3x\right)}{\frac{5PL^4}{384EI}} = \frac{16}{5L^4}\left(x^4 - 2Lx^3 + L^3x\right) \tag{B-19}$$

The lever arm used in Biggs (1964) is calculated as the area times the lever arm for each small element divided with total area which can be stated as

$$L_i = \frac{\int_0^{L/2} \phi(x)x\,dx}{\int_0^{L/2} \phi(x)\,dx} = \frac{\int_0^{L/2} \frac{16}{5L^4}\left(x^5 - 2Lx^4 + L^3x^2\right)dx}{\int_0^{L/2} \frac{16}{5L^4}\left(x^4 - 2Lx^3 + L^3x\right)dx} = \frac{\left[\frac{L^3x^3}{3} - \frac{2Lx^5}{5} + \frac{x^6}{6}\right]_0^{L/2}}{\left[\frac{L^3x^2}{2} - \frac{2Lx^4}{4} + \frac{x^5}{5}\right]_0^{L/2}} =$$

$$= \frac{\frac{L^2}{4}\left[\frac{L^4}{6} - \frac{2L^4}{40} + \frac{L^4}{96}\right]}{\frac{L^2}{4}\left[\frac{L^3}{2} - \frac{2L^3}{16} + \frac{L^3}{40}\right]} = L\frac{\frac{1}{6} - \frac{1}{20} + \frac{1}{96}}{\frac{1}{2} - \frac{1}{8} + \frac{1}{40}} = \frac{61}{192}L \tag{B-20}$$

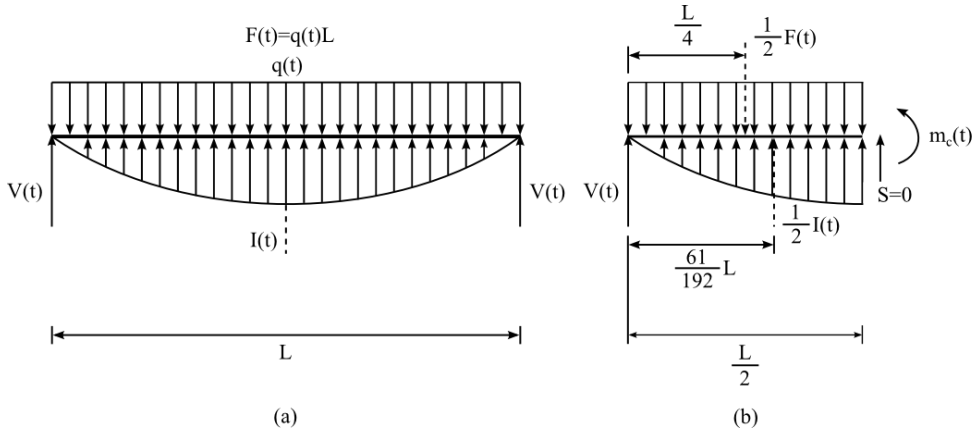

Figure B.4. The assumed distribution of the inertia force I and the corresponding lever arm for a simply supported beam.

Figure B.4 can later on be used to set up equilibrium and obtain the expression for the dynamic reaction. This is shown in section 2.4.2.5.

APPENDIX C Derivation of shear span

In this appendix the expressions used in the Swedish design approach, FortV (2011), is presented. The derivation of the shear span is for the early response where a direct shear failure can occur. A cut is made in the midpoint of the beam, see Figure C.1. Because of the initial rigid body response the moment is assumed to be zero in the midpoint and maximum close to the supports, see Figure C.2. Therefore the shear force distribution is obtained as illustrated in Figure C.3.

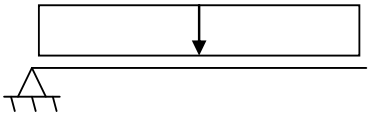

Figure C.1. A simply supported beam with a cut in the midpoint.

Moment, due to rigid body motion in the early stage there will be zero moment in the middle of the beam. The moment will occur close to the supports where a concentrated curvature is obtained.

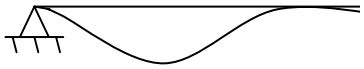

Figure C.2. Moment distribution in the early stage of a beam subjected to an impulse load. Due to the rigid body response the moment is zero in the midpoint.

Shear force

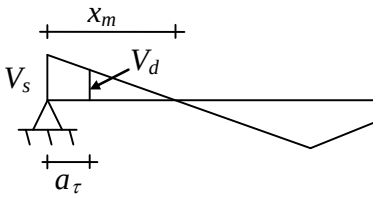

Figure C.3. The shear force distribution in the early stage of a beam subjected to an impulse load. This shear force distribution corresponds to the moment distribution in Figure C.2.

V_d is the design shear force and should be determined at a distance a_τ from the support.

The resistance function for shear force g(x), the ratio between the design shear force V_d and the shear force capacity V_{Rd}, can be written as

$$g(x) = \frac{V_d}{V_{Rd}} \tag{C-1}$$

The shear force at the distance x from the support can be approximated as

$$V_d = V_s\left(1 - \frac{x}{x_m}\right) \tag{C-2}$$

The expression in equation (C-2) assumes a linear variation of the shear force. This is not the case when the beam is subjected to an intense impulse load. So this approximation is not valid in this case.

The shear resistance can be assumed as

$$V_{Rd}(x) = \frac{k}{x/d} \tag{C-3}$$

where k is just a constant not of importance and is not shown in the derivation.

Inserting (C-2) and (C-3) into (C-1) gives

$$g(x) = \frac{V_s}{kd}\left(1 - \frac{x}{x_m}\right)x \tag{C-4}$$

The maximum value of the resistance function is obtained when

$$x = \frac{x_m}{2} \tag{C-5}$$

Therefore, the shear force capacity should be controlled at a distance of half the distance between zero-shear force points.

$$a_\tau = \frac{x_m}{2} \tag{C-6}$$

In order to find where the shear force is zero, x_m, inertia forces close to the supports must be considered. This is done by assuming acceleration in the zero-shear force point equal to the rigid body motion acceleration and let it decrease linearly until zero at the supports, as shown in Figure C.4.

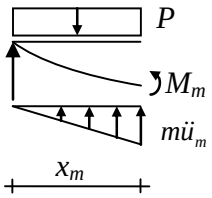

Figure C.4. A cut of the beam at the distance x_m from the support.

For a rigid body motion no resistance will impede the acceleration and the max value of the inertia force is

$$m\ddot{u} = P \tag{C-7}$$

Moment equilibrium around the support is established

$$\frac{Px_m^2}{2} - \frac{Px_m}{2}\cdot\frac{2x_m}{3} - M_m = 0 \tag{C-8}$$

The maximum moment M_m can be expressed as the ultimate moment resistance

$$M_m = \frac{q_{eq} L^2}{8} \tag{C-9}$$

By using equation (D-9) and (D-8)

$$\frac{x_m}{L} = \sqrt{\frac{3 \cdot q_{eq}}{4 \cdot P}} \tag{C-10}$$

If the inertia forces close to the support are neglected the length x_m will increase and the beam must be examined at a greater distance from the support. This corresponds to setting the term $\frac{P x_m}{2} \cdot \frac{2 x_m}{3}$ in equation (C-8) to zero and equation (C-11) will be obtained. This is used in FortV (2010) as design value. There is also an additional term that provides safety because a_τ is not zero for very high pressures. The safe side estimation of x_m can be obtained from

$$\frac{P x_m^2}{2} - \frac{q_{eq} L^2}{8} = 0 \tag{C-11}$$

And is

$$\frac{x_m}{L} = \sqrt{\frac{1 \cdot q_{eq}}{4 \cdot P}} \tag{C-12}$$

A term 0.05 is added to this distance to provide safe side solutions

$$\frac{x_m}{L} = 0.05 + 0.5\sqrt{\frac{q_{eq}}{P}} \tag{C-13}$$

Finally, the shear span can be calculated from equation (D-6) as

$$a_\tau = 0.025 + 0.25\sqrt{\frac{q_{eq}}{P}} \tag{C-14}$$

The same method can be used to show how the shear span is calculated for a beam with fixed supports.

$$a_\tau = 0.02 + 0.7\sqrt{\frac{q_{eq}}{P}} \tag{C-15}$$

APPENDIX D Energy preservation while varying transformation factors

A consequence of varying the transformation factors, and thereby the mass, is that the kinetic energy will drop. Since energy cannot disappear the kinetic energy is preserved in the SDOF-model by using the following calculation scheme.

The procedure follows the central difference method described in Appendix A until the mass changes. When it does, the previous mass is used to obtain the deformation that should have been if the mass had been constant i.e. if mass changes at time *t*:

$$u_{t+\Delta t} = \left(\frac{m_{t-1}}{\Delta t^2} + \frac{c_t}{2\Delta t} \right)^{-1} \left(F_t - R_t + \frac{2m_{t-1}u_t}{\Delta t^2} - \left(\frac{m_{t-1}}{\Delta t^2} - \frac{c_t}{2\Delta t} \right) u_{t-\Delta t} \right) \tag{D-1}$$

The mean velocity between time *t* and $t+\Delta t$ can be found as

$$\dot{u}_t = \frac{u_{t+\Delta t} - u_t}{\Delta t} \tag{D-2}$$

The kinetic energy is now

$$W_{k,t} = \frac{m_t \dot{u}_t^{\,2}}{2} \tag{D-3}$$

This is a slightly larger or smaller value than what it should be because of the change of mass in the system. Therefore the velocity is altered so that the same kinetic energy is maintained:

$$\dot{u}'_t = \dot{u}_t \sqrt{\frac{m_{t-1}}{m_t}} = \dot{u}_t \sqrt{\frac{\kappa_{m,t-1}}{\kappa_{m,t}}} \tag{D-4}$$

This velocity can be used to calculate the displacement at time $t+\Delta t$ *as*

$$u'_{t+\Delta t} = u_t + \Delta t \cdot \dot{u}'_t \tag{D-5}$$

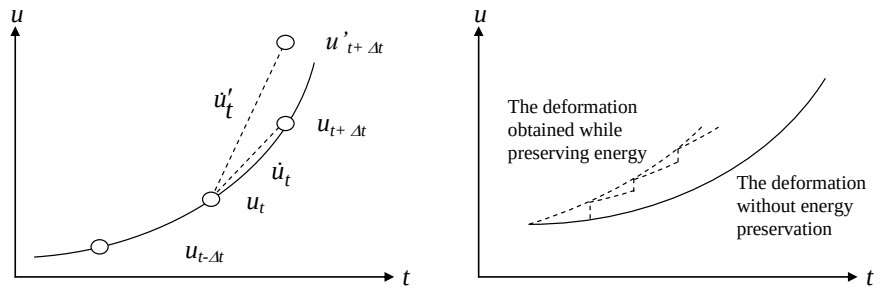

Figure D.1. Calculation scheme for preserving the energy. A new velocity $\dot{u}'_t$ *at time t is calculated to preserve the kinetic energy and is then used to find the deformation* $u'_{t+\Delta t}$ *at time* $t+\Delta t$.

APPENDIX E Energy balance for other load cases

E.1 Introduction

While varying transformation factors in the SDOF system a sudden loss of energy occurs which is due to the change in mass, i.e. change in kinetic energy. Due to this problem a method to preserve the energy is introduced. The difference between energy levels when not preserving energy, when preserving energy and the energy obtained in the FE analysis is presented in the graphs below for different load cases and beams. Where load case 0 have a peak pressure P_{peak} = 10 Mpa and load duration t_{Δ} = 0.56 ms, load case 1 have a peak pressure P_{peak} = 5 Mpa and load duration t_{Δ} = 1.12 ms and load case 3 have a peak pressure P_{peak} = 1.25 Mpa and load duration t_{Δ} = 4.48 ms.

They are presented for two different beams; a beam with the length L = 3 m with the width b = 1 m and the depth h = 0.4 m and a beam with the length L = 5 m and with the same cross-section.

E.2 Beam L=3 m

E.2.1 Elastic load case 0

SDOF without energy preservation

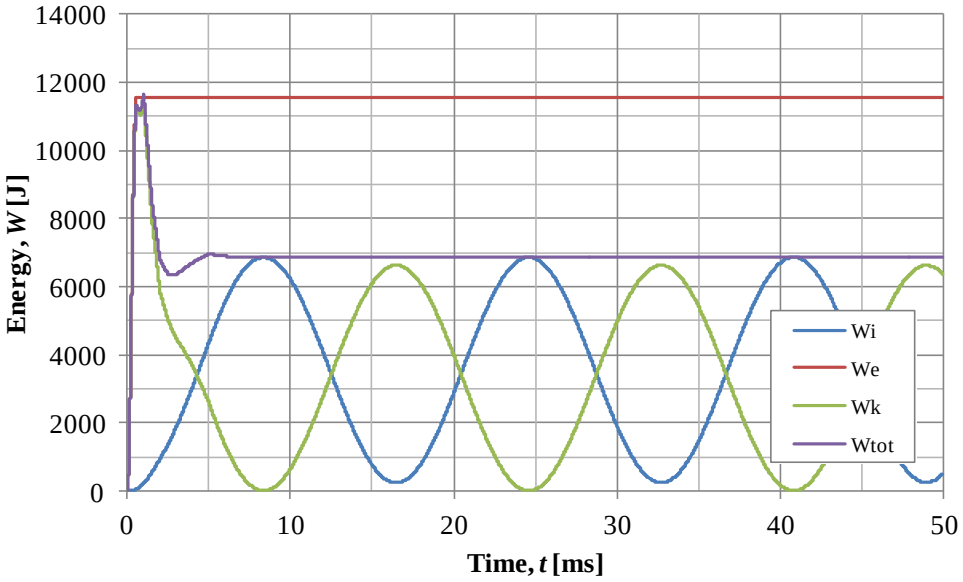

SDOF with energy preservation

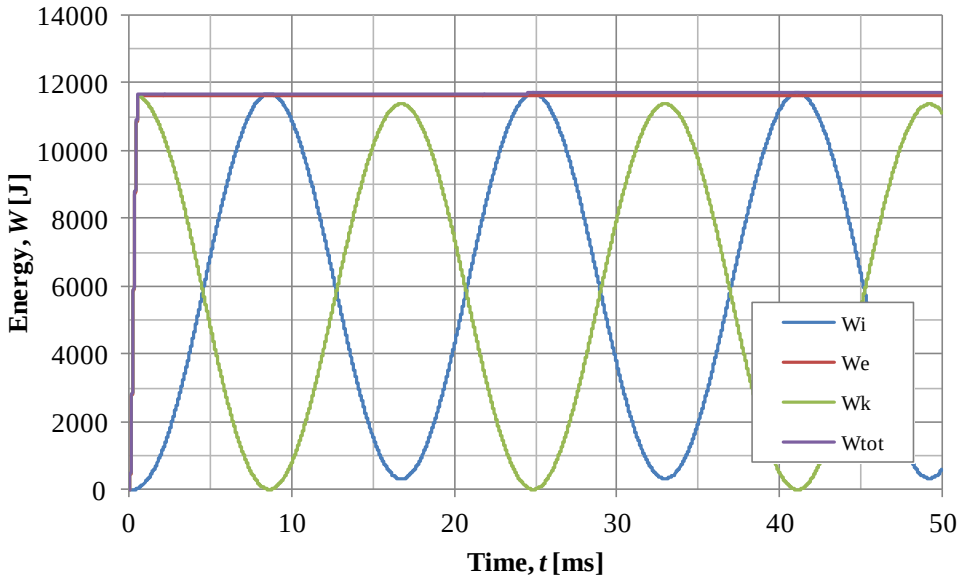

FE analysis

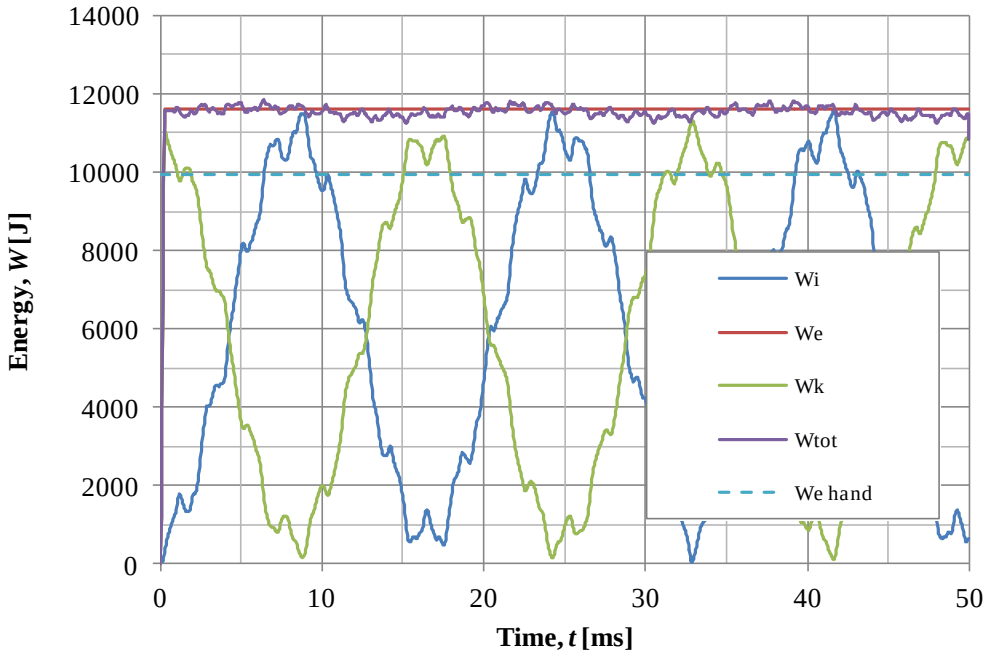

E.2.2 Elastic load case 3

SDOF without energy preservation

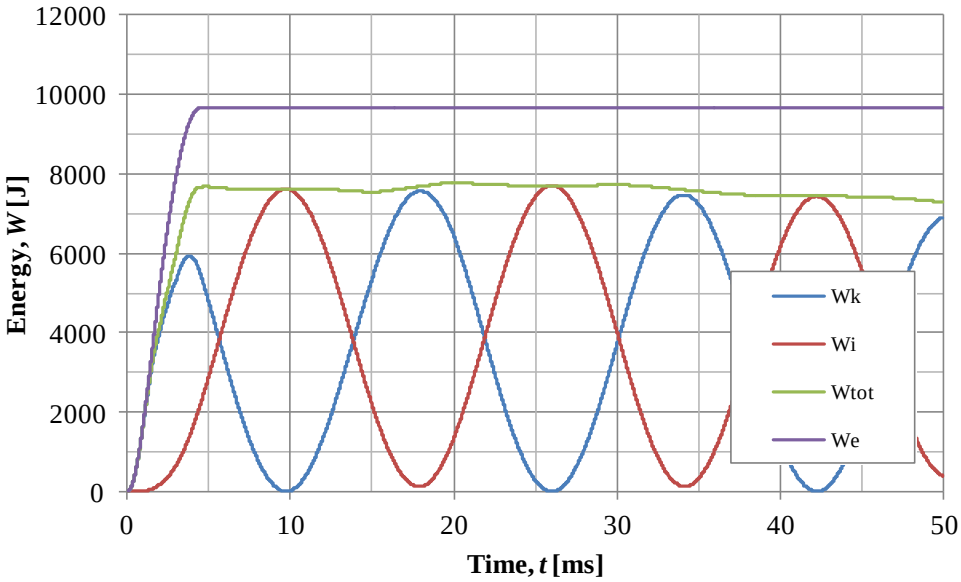

SDOF with energy preservation

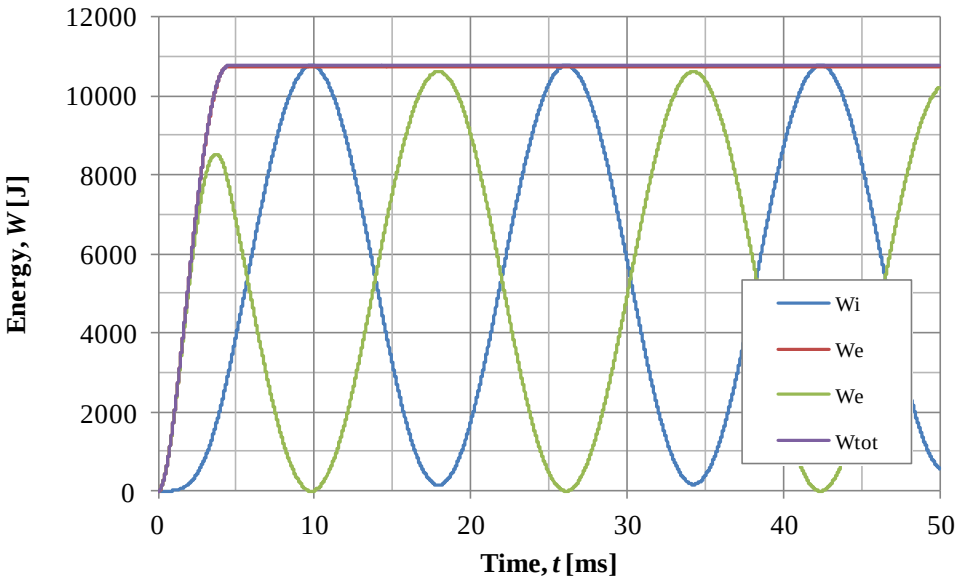

FE analysis

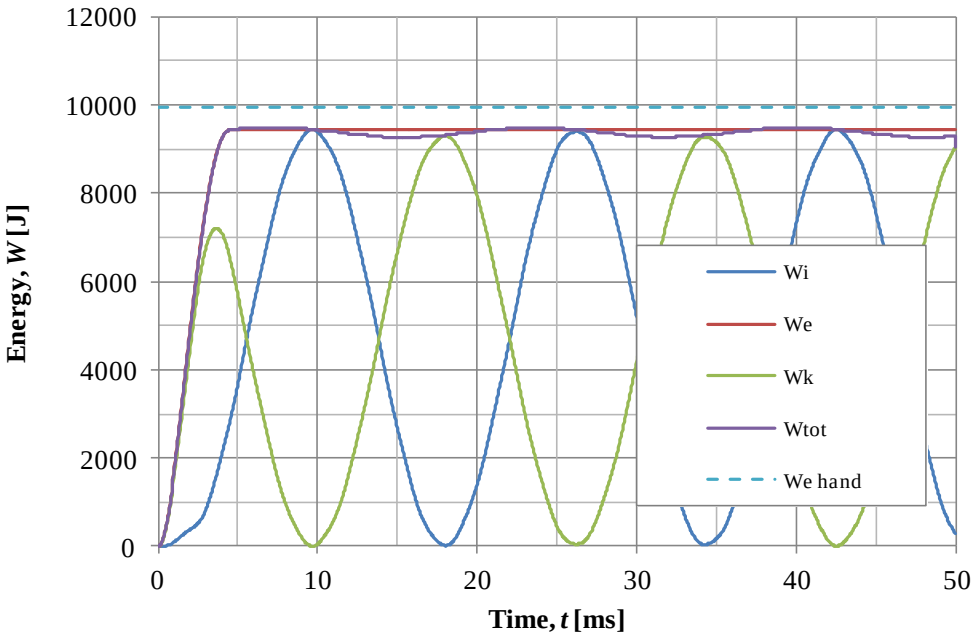

E.2.3 Plastic load case 3

SDOF without energy preservation

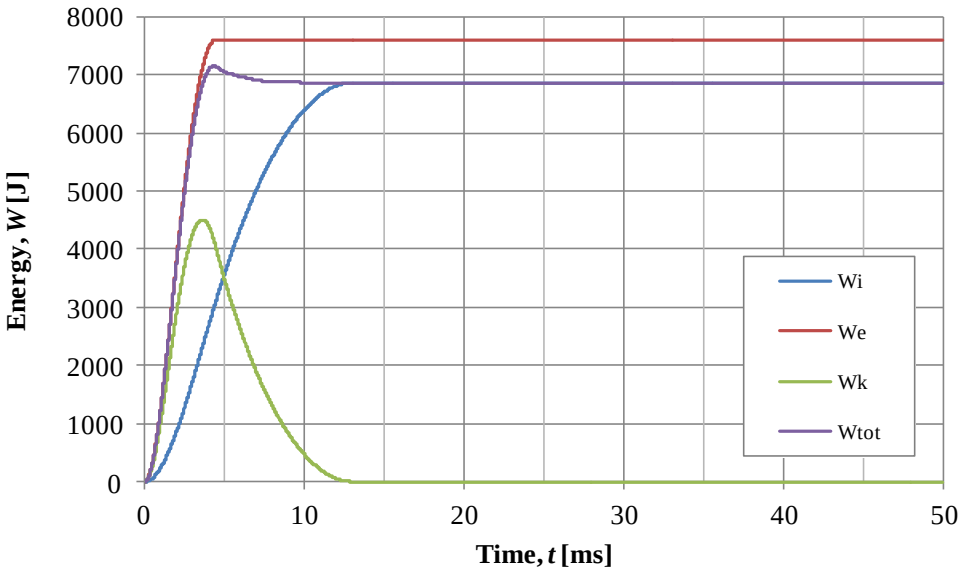

SDOF with energy preservation

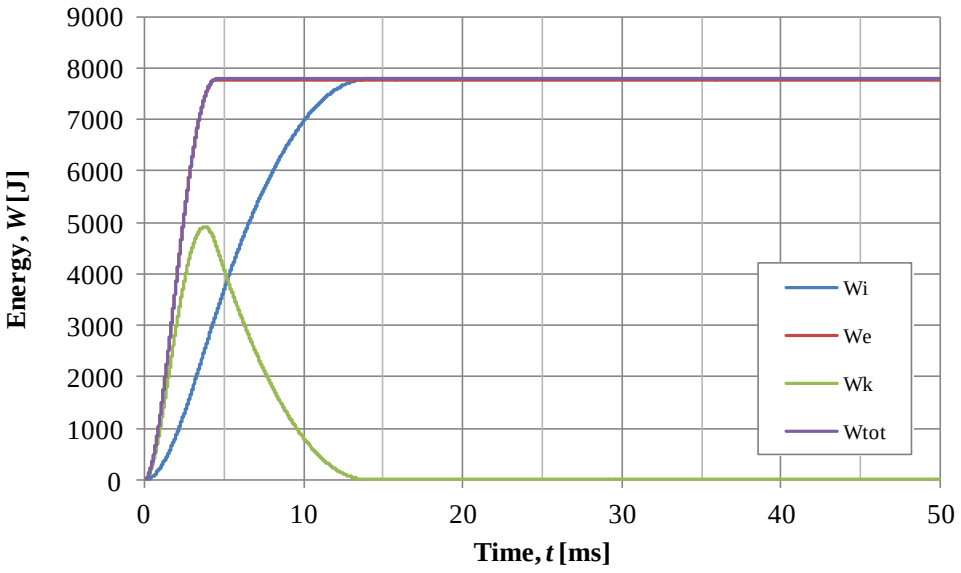

FE analysis

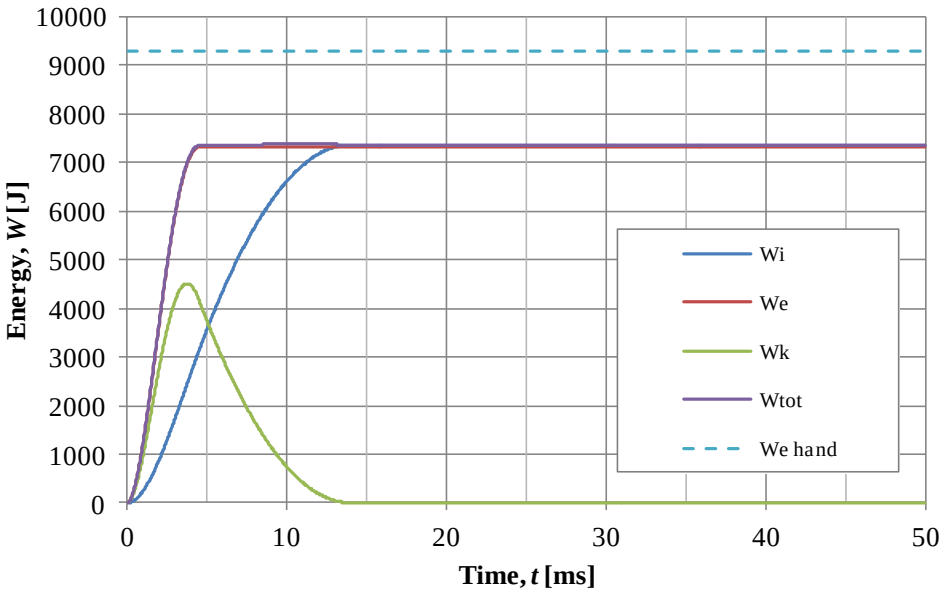

E.2.4 Elasto-plastic load case 3

SDOF without energy preservation

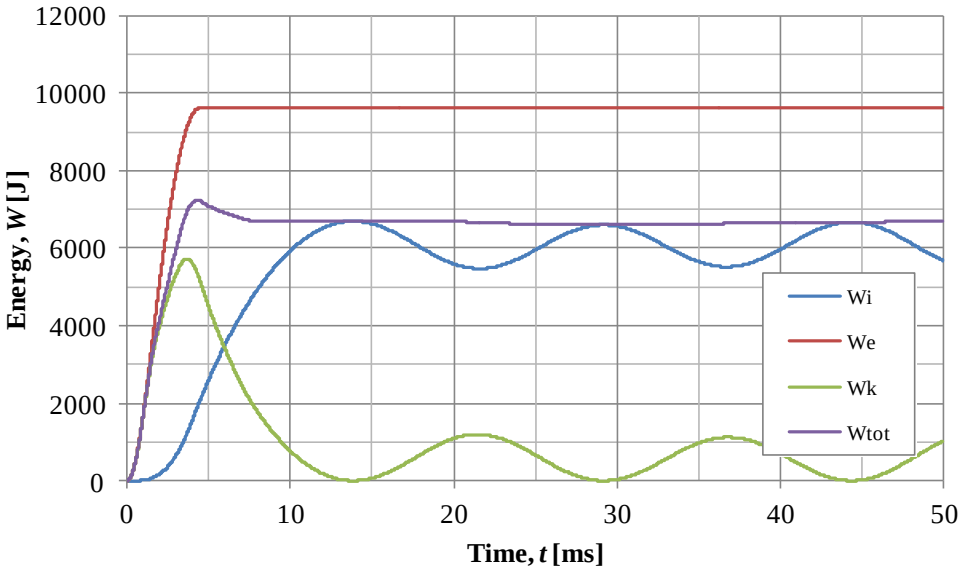

SDOF with energy preservation

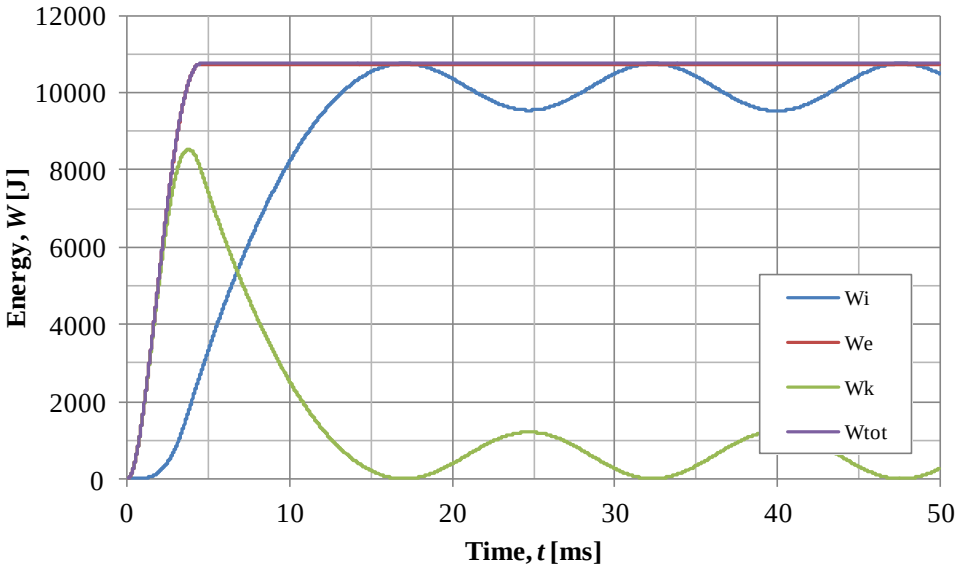

FE analysis

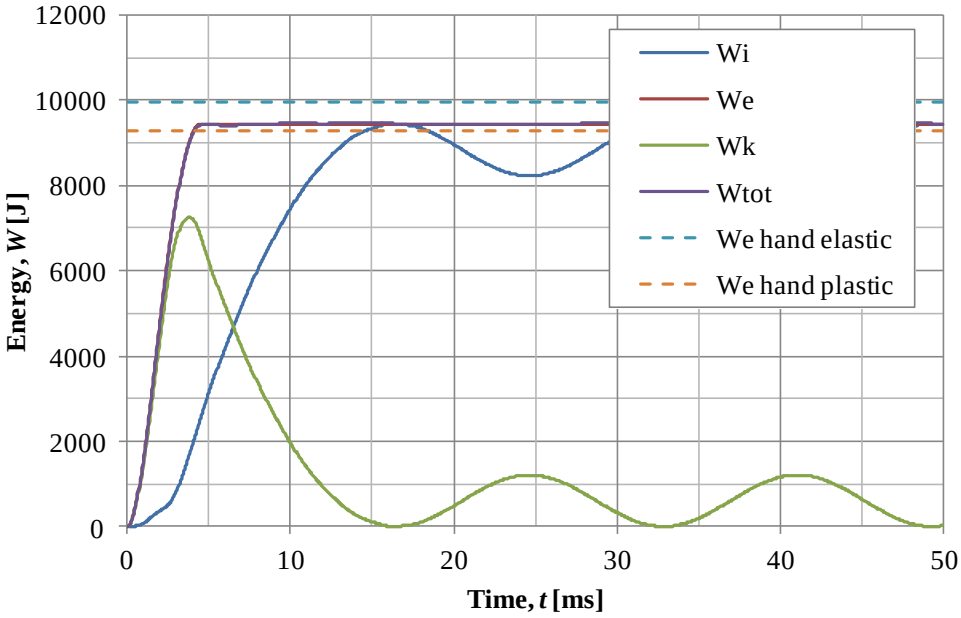
12000
10000
8000
6000
4000
2000
0
Energy, W [J]
0
10
20
30
40
50
Time, t [ms]
Wi
We
Wk
Wtot
We hand elastic
We hand plastic

E.3 Beam *L*=5 m

E.3.1 Elastic load case 1

SDOF without energy preservation

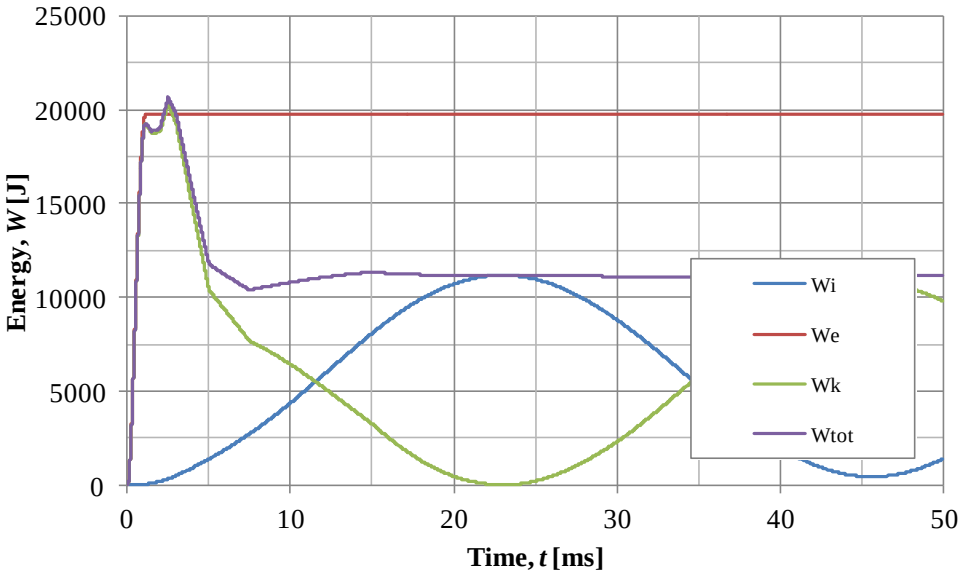

SDOF with energy preservation

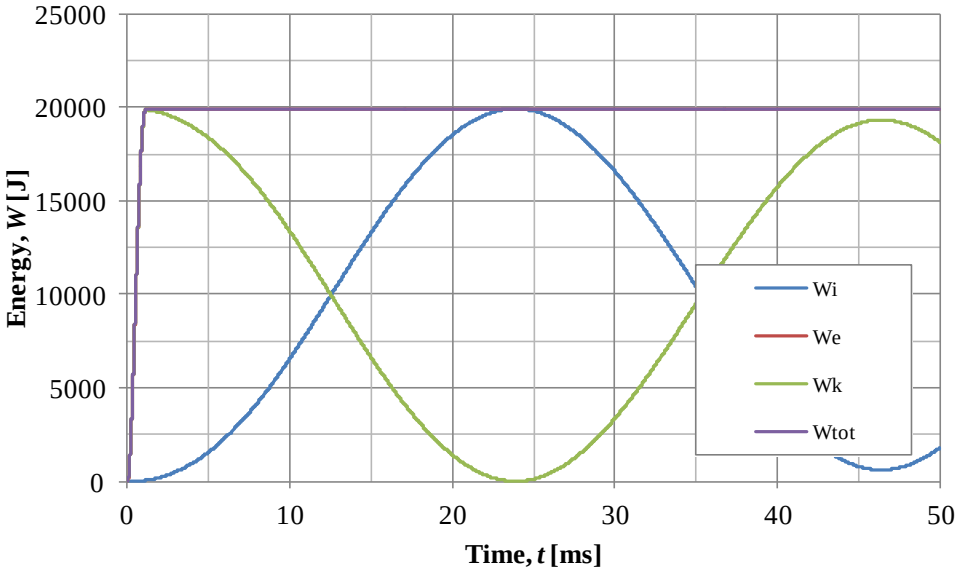

FE analysis

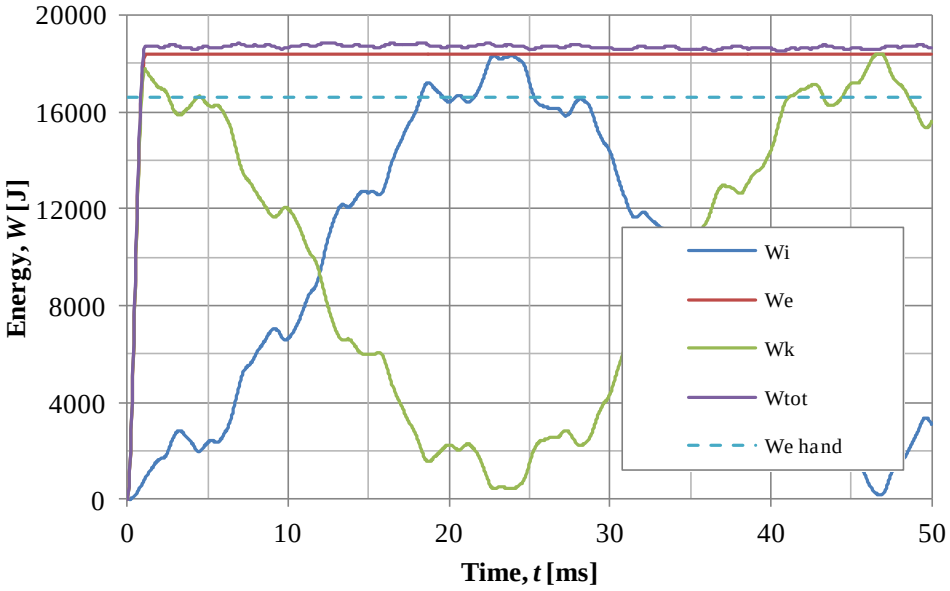

E.3.2 Plastic load case 1

SDOF without energy preservation

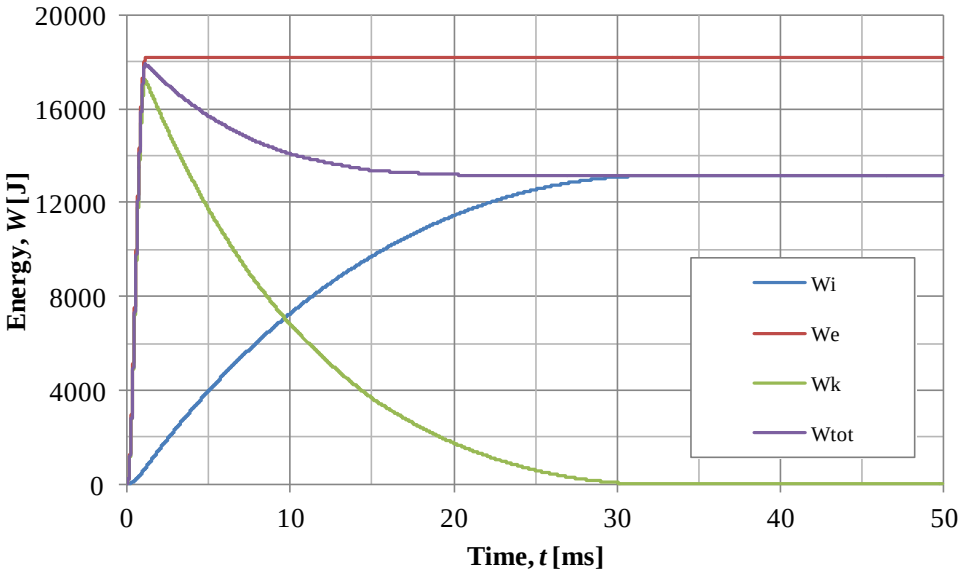

SDOF with energy preservation

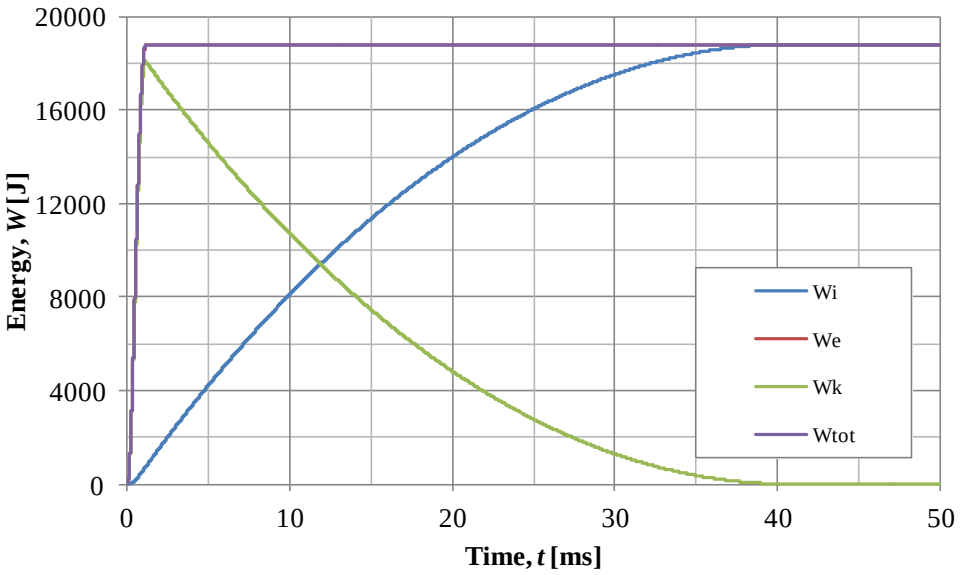

FE analysis

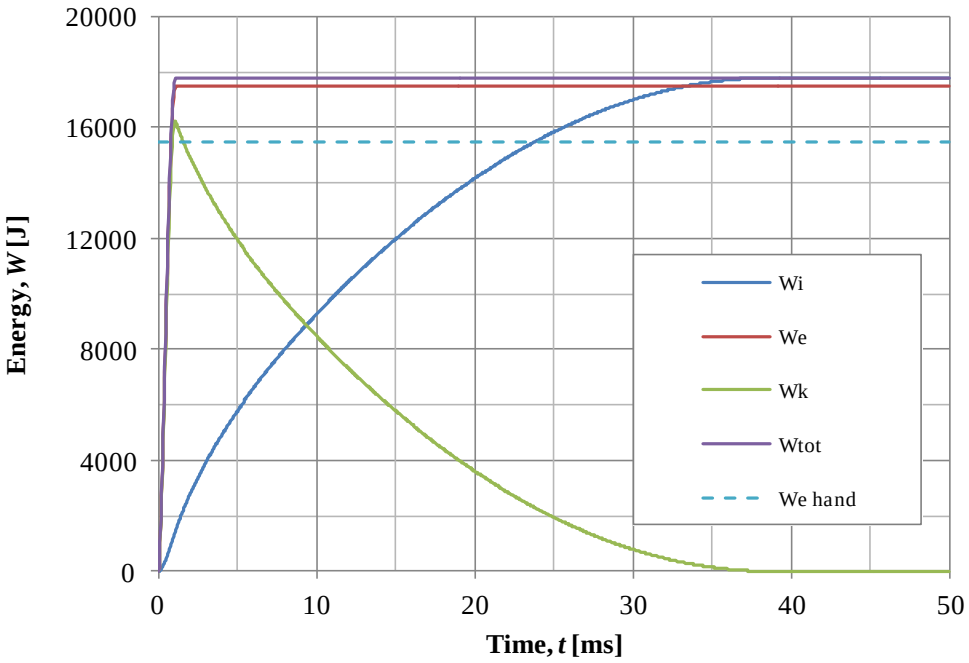

E.3.3 Elasto-plastic load case 1

SDOF without energy preservation

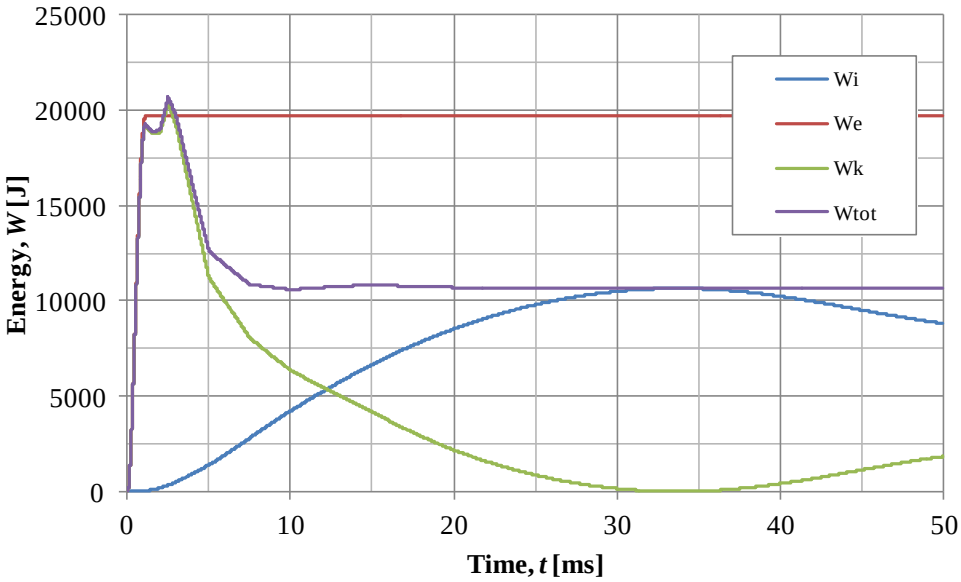

SDOF with energy preservation

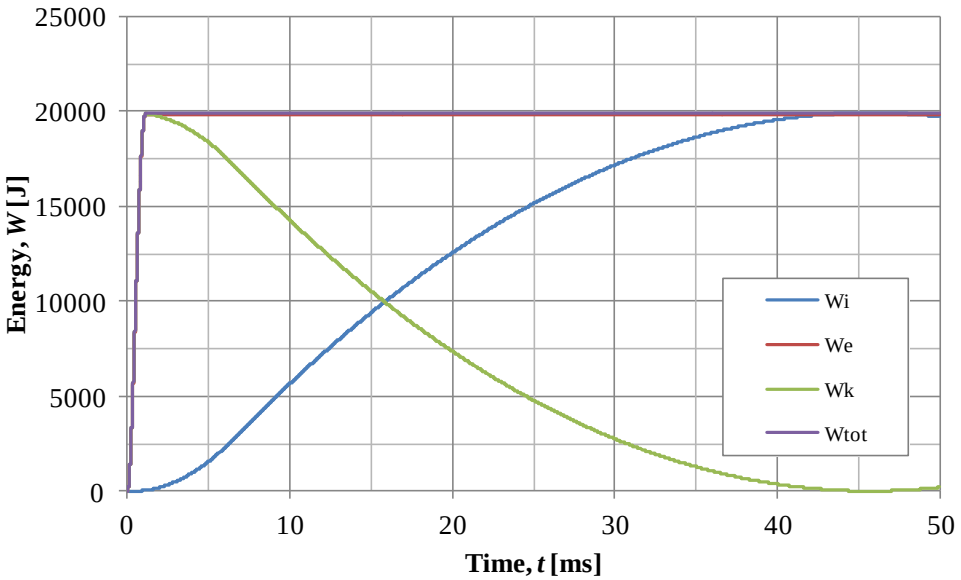

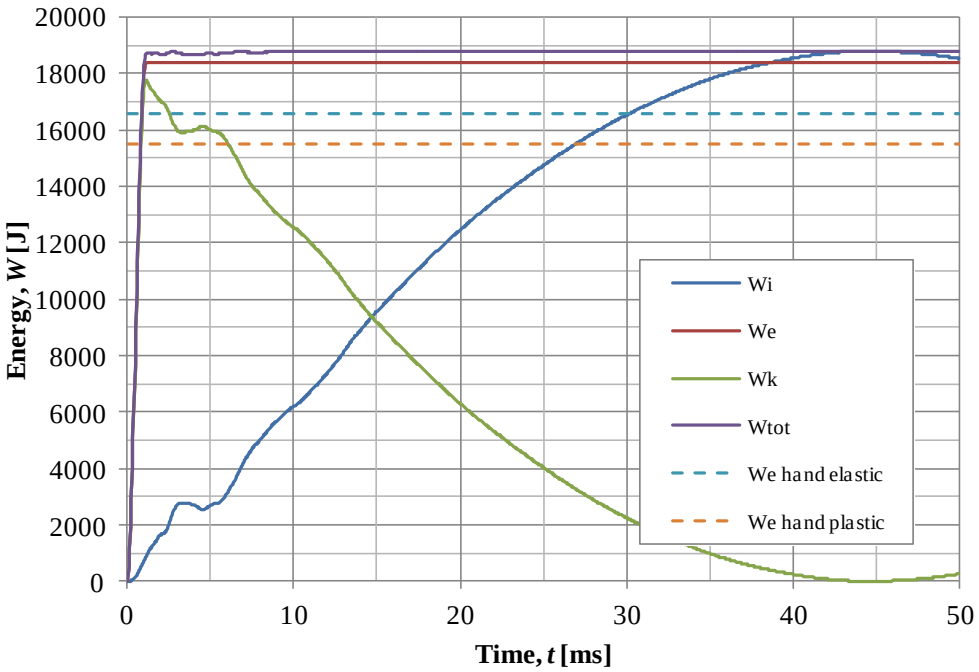
20000
18000
16000
14000
12000
10000
8000
6000
4000
2000
0
Energy, W [J]
0
10
20
30
40
50
Time, t [ms]
Wi
We
Wk
Wtot
We hand elastic
We hand plastic

APPENDIX F Transformation factors for different load cases and dimensions

F.1 Introduction

Here values of the transformations factors κ_m, κ_f and κ_{mf} for load case 1, 2 and 3 are presented. Where load case 1 have a peak pressure $P_{peak} = 5$ Mpa and load duration $t_\Delta = 1.12$ ms, load case 2 have a peak pressure $P_{peak} = 2.5$ Mpa and load duration $t_\Delta = 2.24$ ms and load case 3 have a peak pressure $P_{peak} = 1.25$ Mpa and load duration $t_\Delta = 4.48$ ms.

They are presented for two different beams; a beam with the length $L = 3$ m with the width $b = 1$ m and the depth $h = 0.4$ m and a beam with the length $L = 5$ m and with the same cross-section.

F.2 Beam L=3 m

F.2.1 Load case 1

Elastic

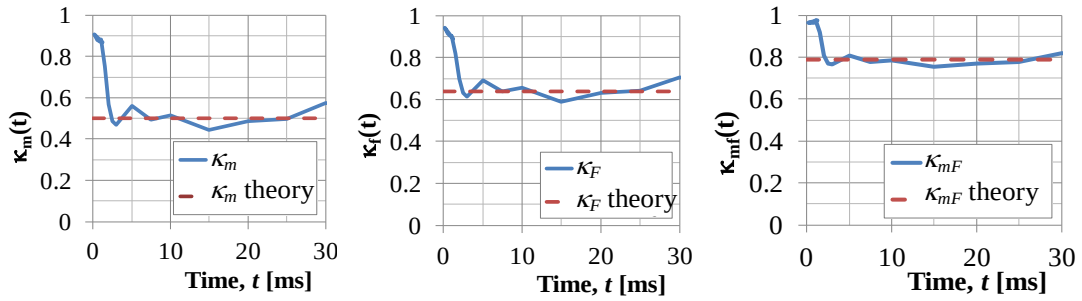

Plastic

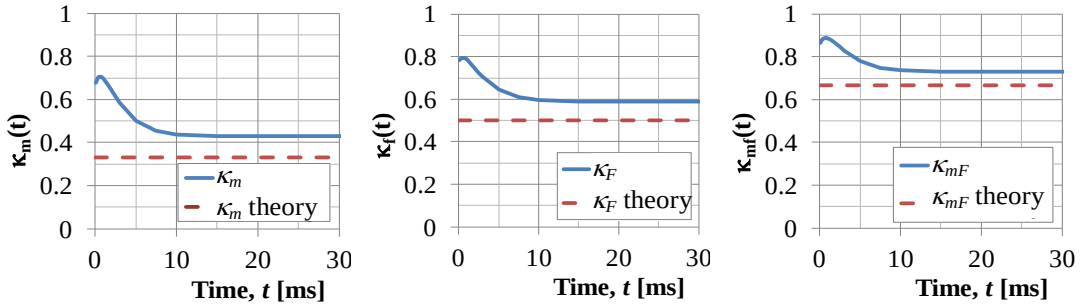

Elasto-plastic

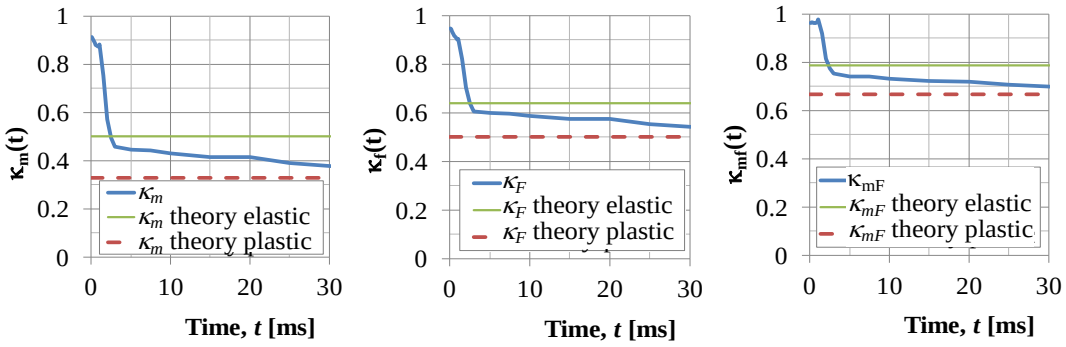

F.2.2 Load case 2

Elastic

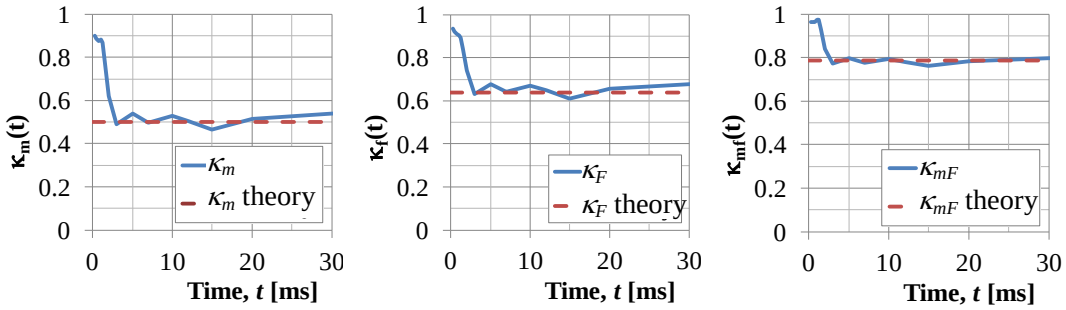

Plastic

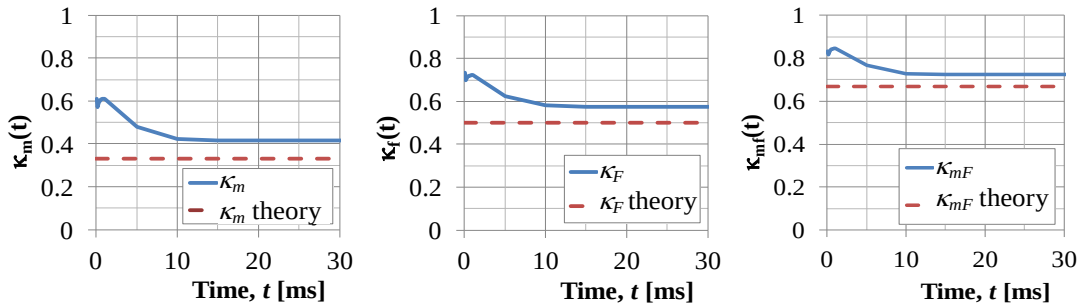

Elasto-plastic

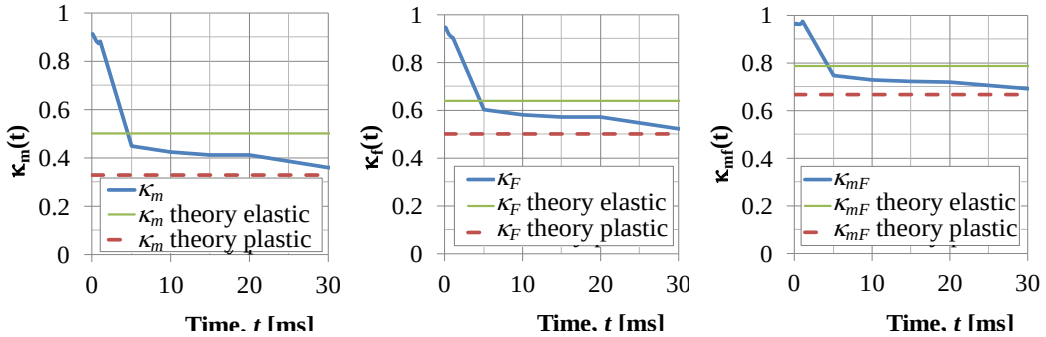

F.2.3 Load case 3

Elastic

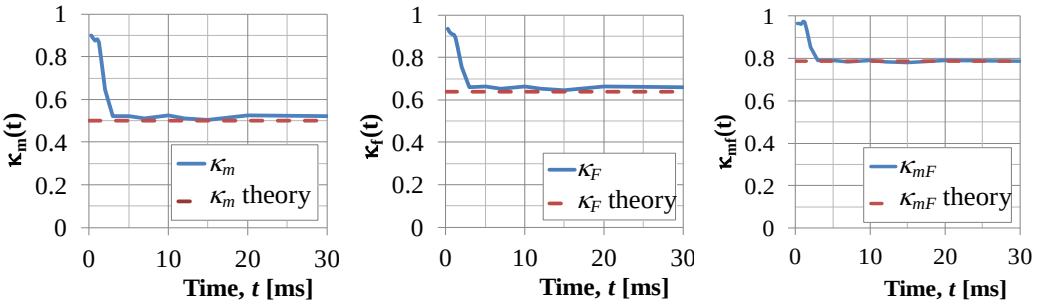

Plastic

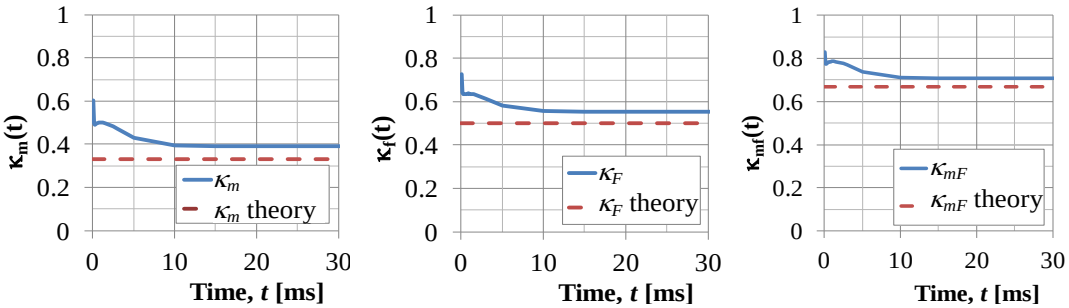

Elasto-plastic

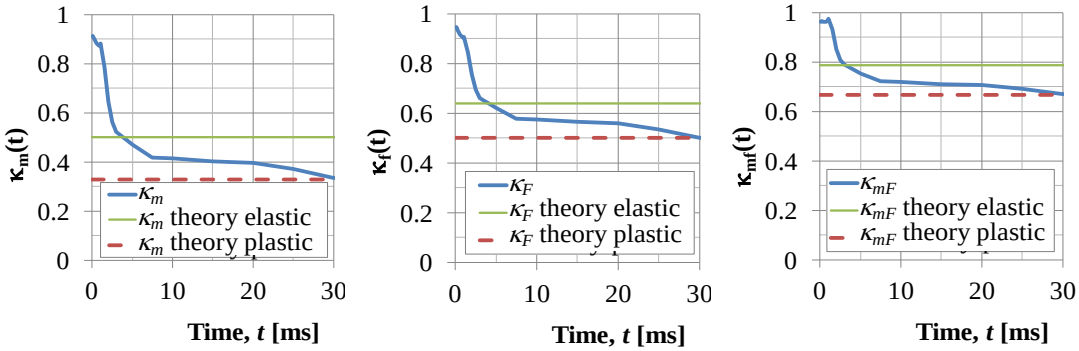

F.3 Beam *L*=5 m

F.3.1 Load case 1

Elastic

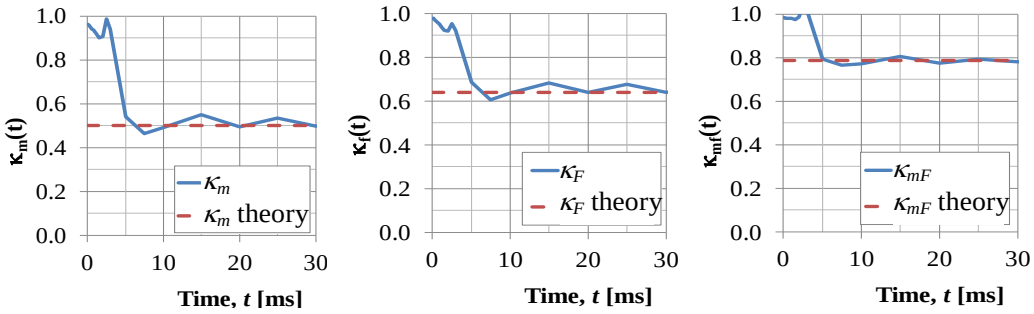

Plastic

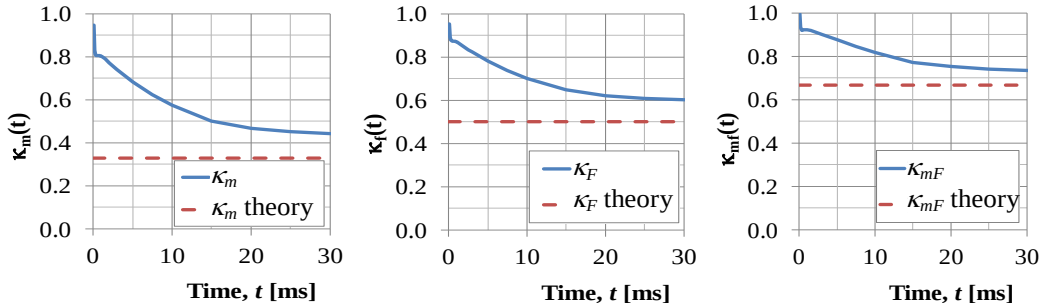

Elasto-plastic

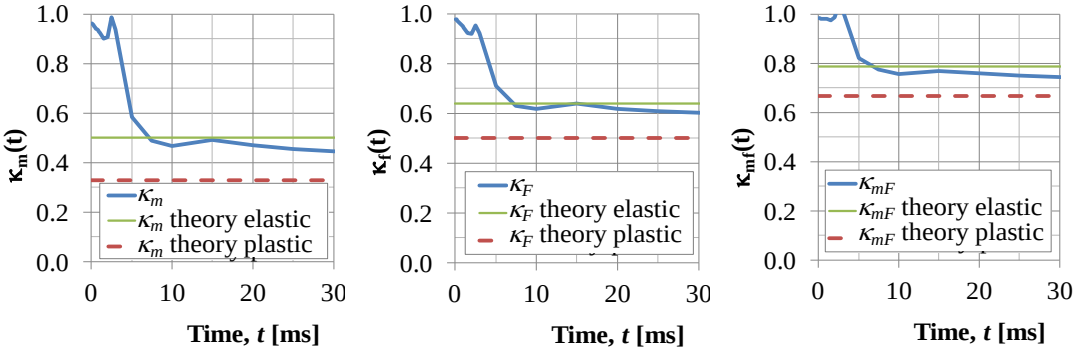

APPENDIX G Deformations and moment and shear distributions over time

The deformation shape and the moment and shear distributions are described in Chapter 4, 5 and 6. This appendix gives a more comprehensive picture of how the deformation changes with time. The corresponding moment and shear distributions are shown together with the deformation shape for simply supported beams assuming linear elastic, ideal plastic and elasto-plastic response. The load case that has been used here is load case 1, which has a peak pressure of 5000 kPa with a time duration of 1.12 ms. The intention here is to show the variation and this is the same for all the load cases although it is more extreme for highly intense loads.

Firstly the variation in time of displacement and moment in midpoint and the support reaction is shown. Further, the normalised deformation shape and the moment and shear distribution are shown for different times. The time interval is concentrated in the early phase since this deviates most from the expected deformations. The results are only shown for the first oscillation.

G.1 Elastic

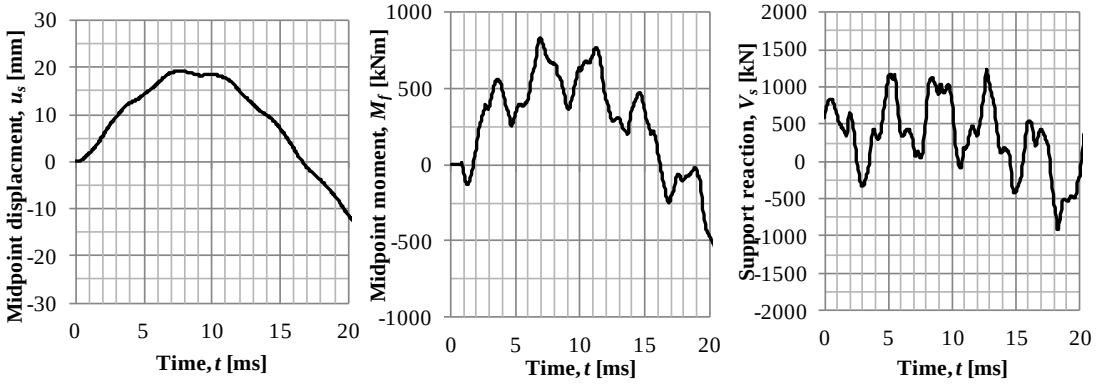

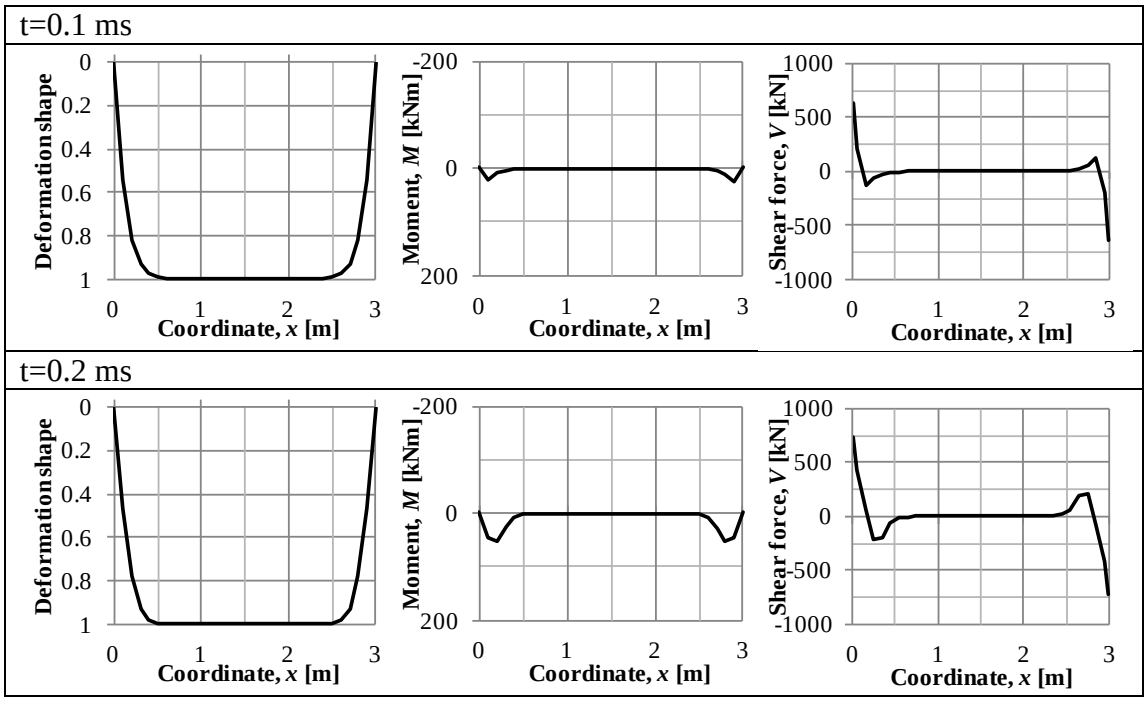

t=0.3 ms

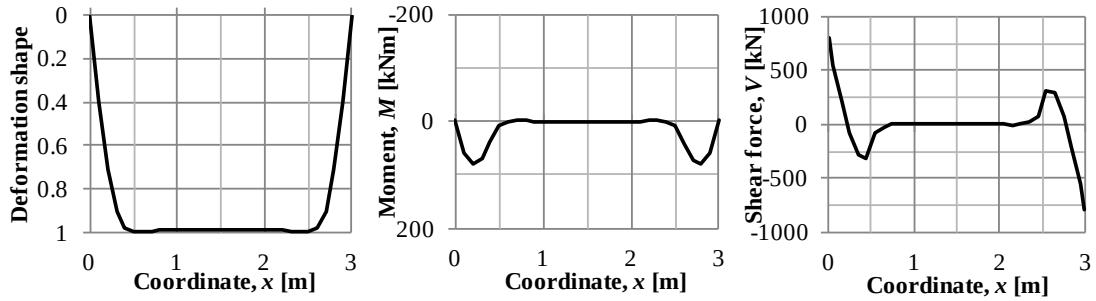

t=0.4 ms

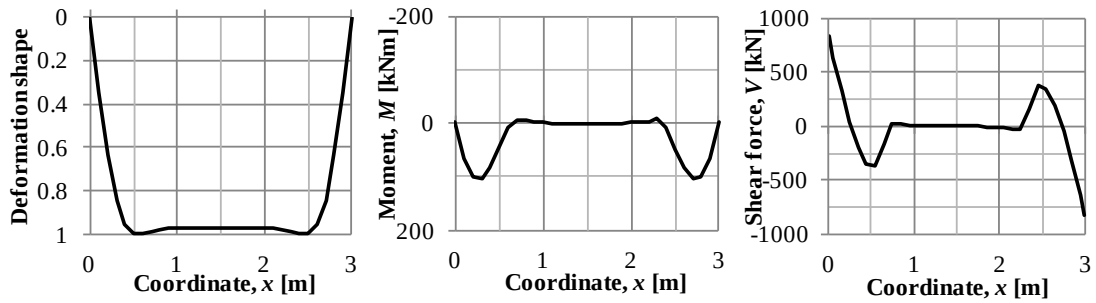

t=0.5 ms

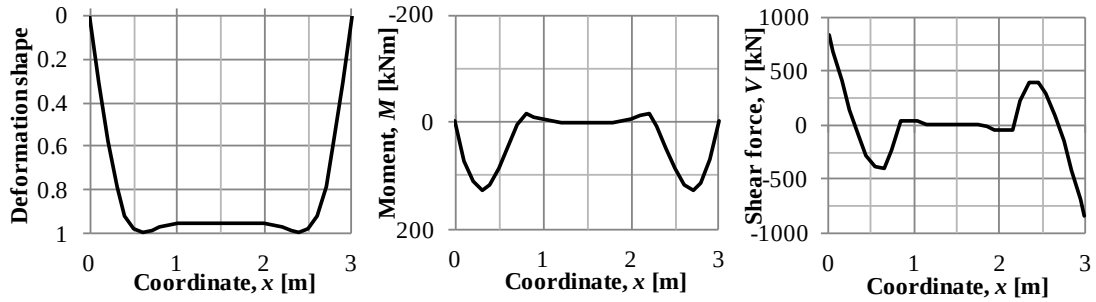

t=0.6 ms

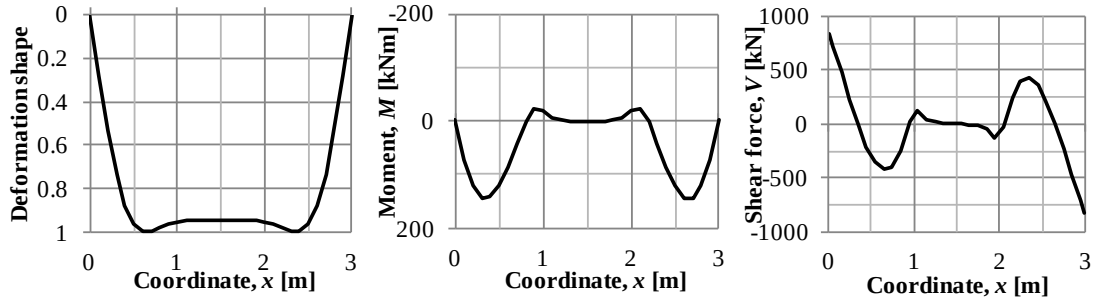

t=0.7 ms

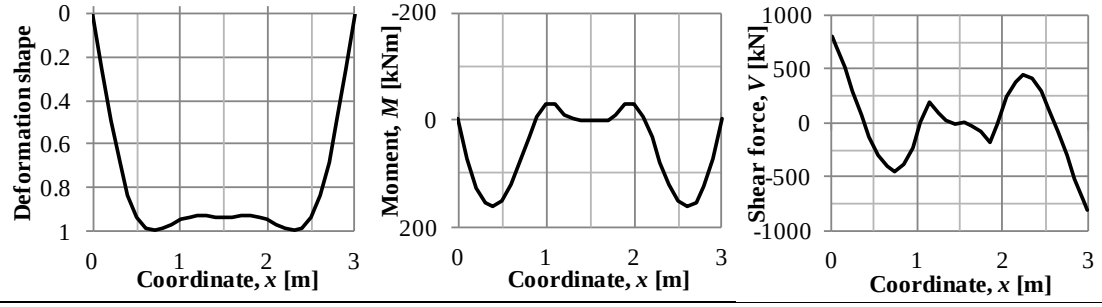

t=0.8 ms

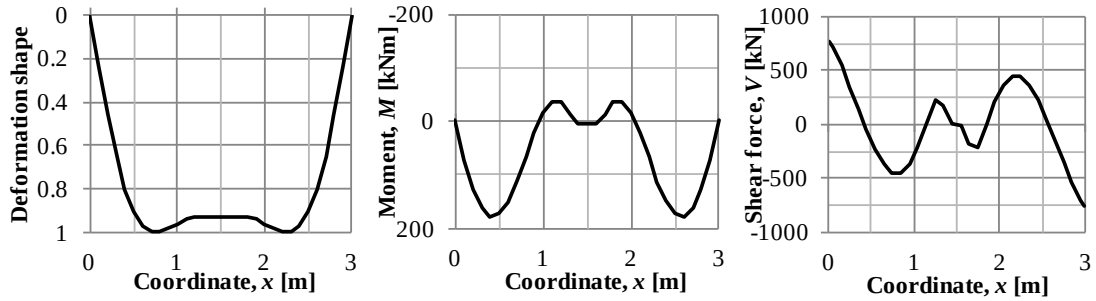

t=0.9 ms

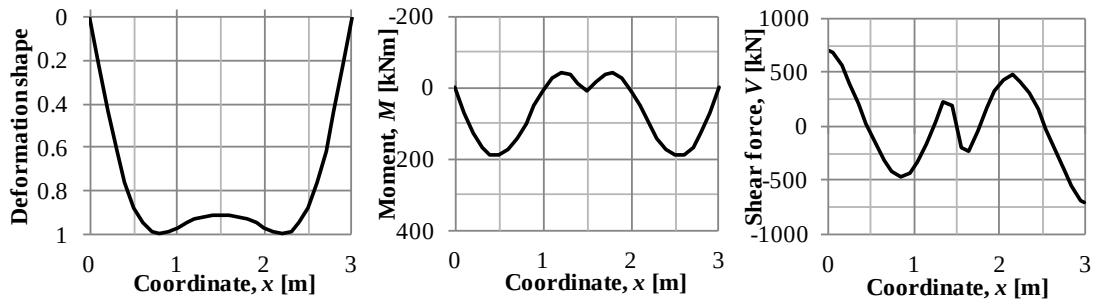

t=1 ms

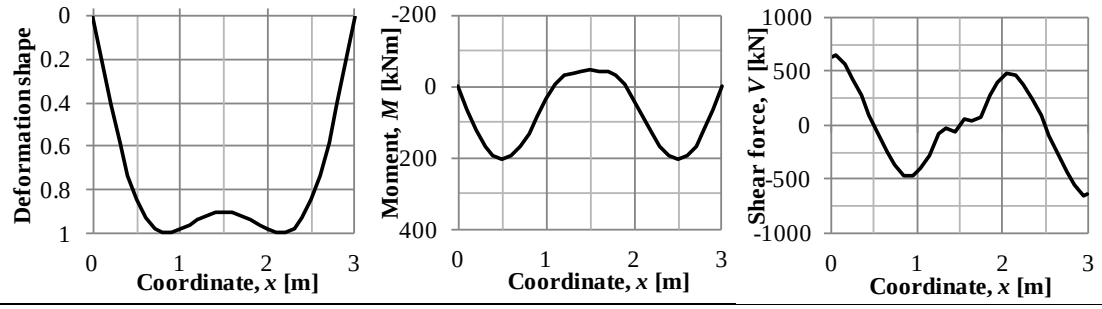

t=1.5 ms

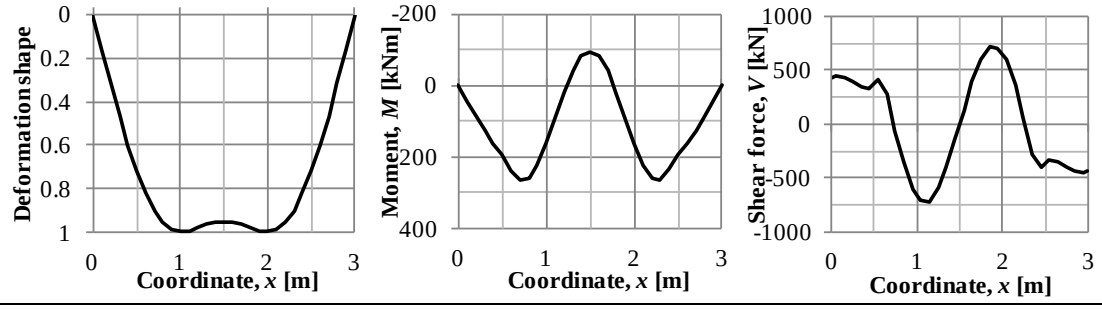

t=2 ms

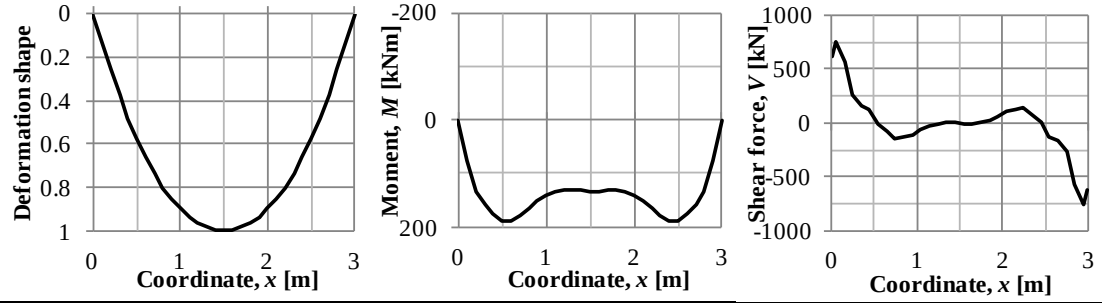

t=2.5 ms

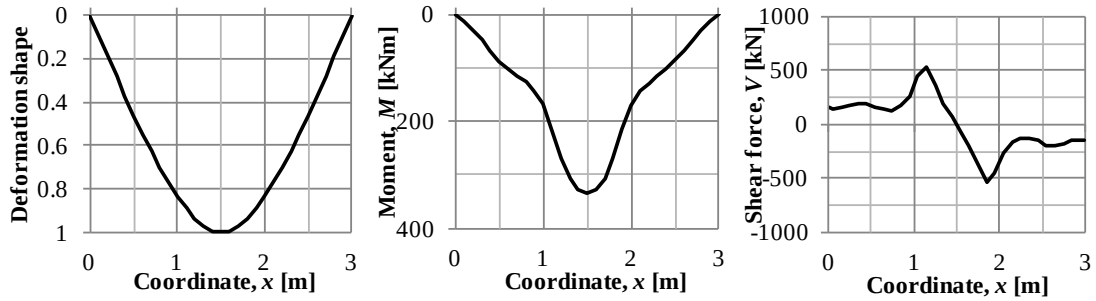

t=3 ms

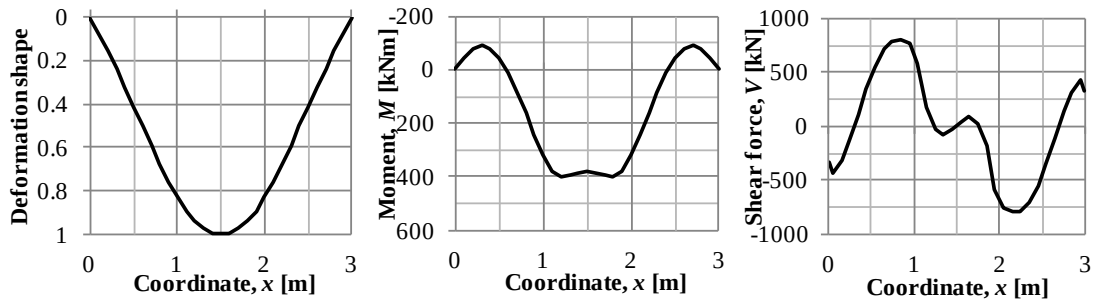

t=3.5 ms

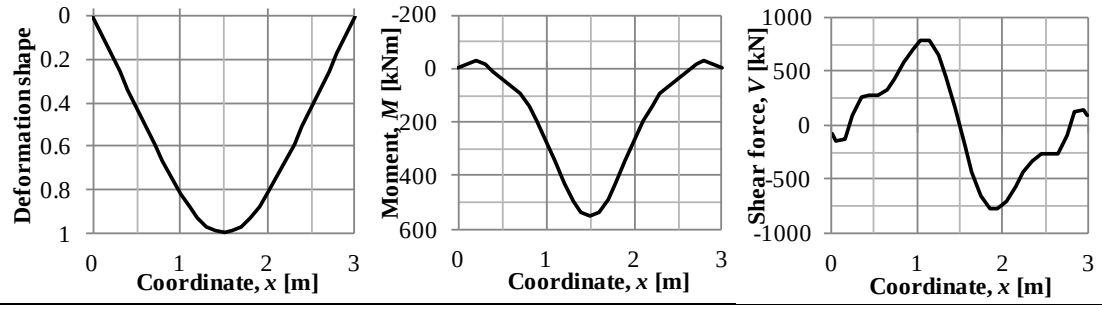

t=4 ms

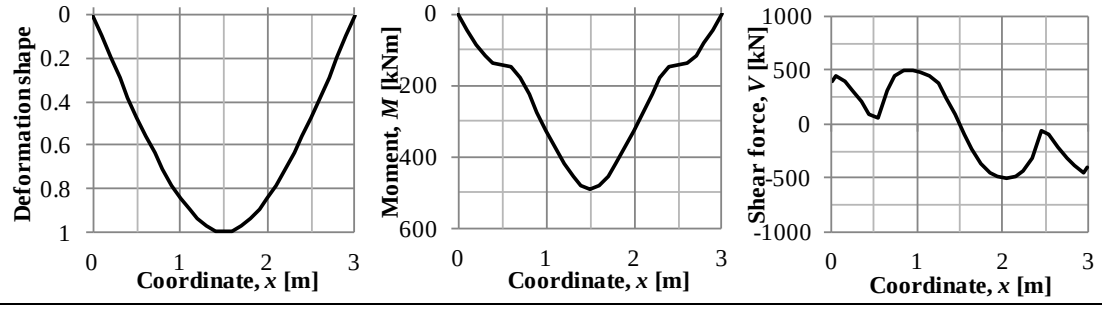

t=4.5 ms

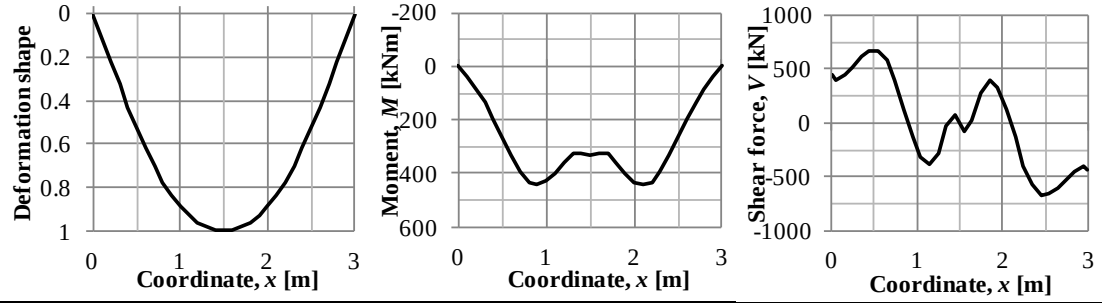

t=5 ms

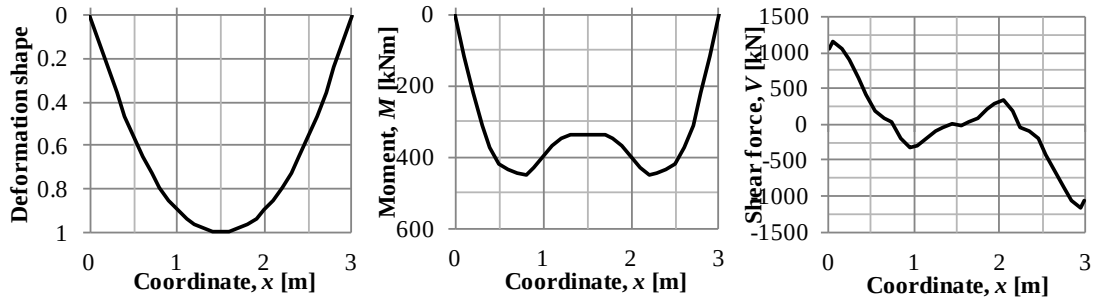

t=6 ms

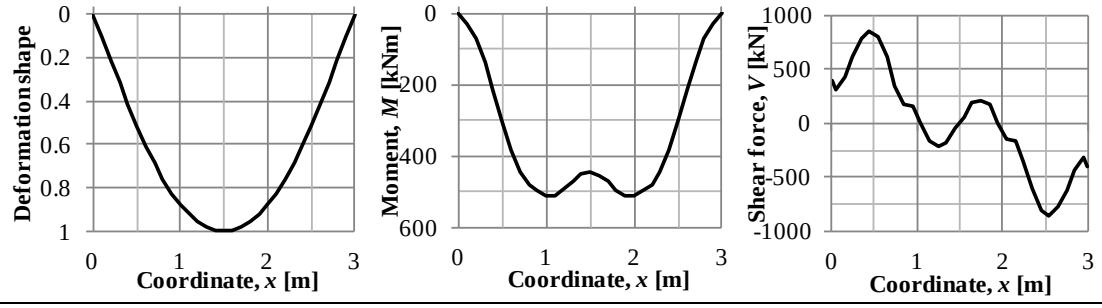

t=7 ms

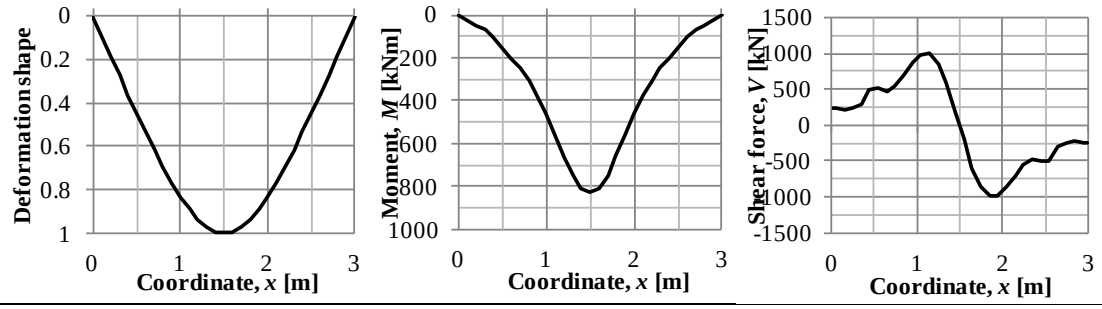

t=8 ms

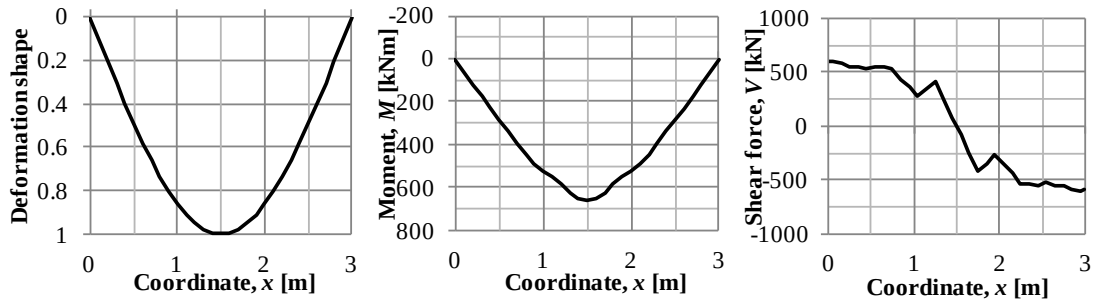

t=9 ms

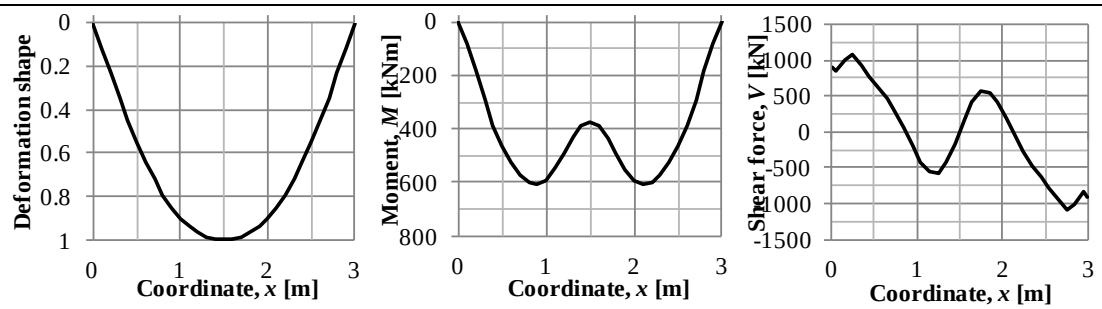

t=10 ms

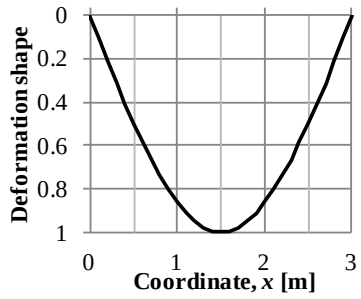

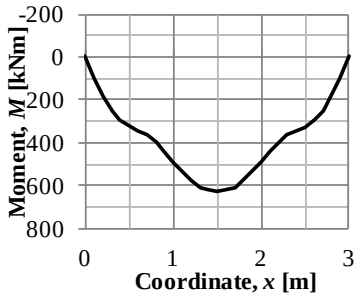

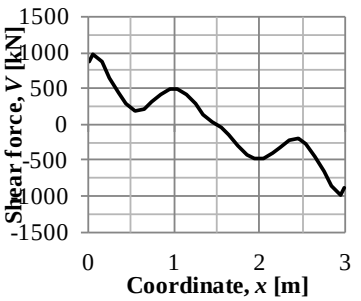

t=11 ms

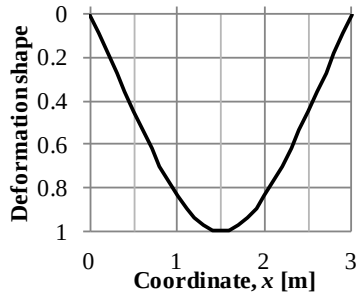

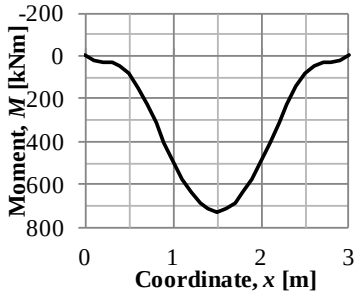

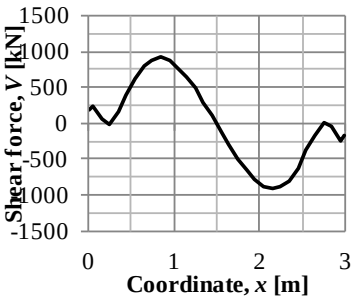

t=12 ms

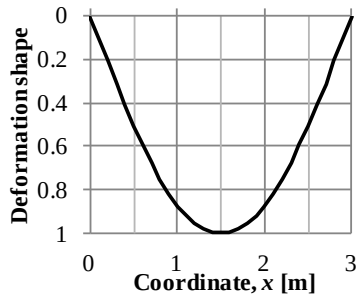

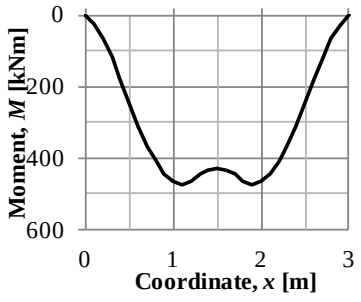

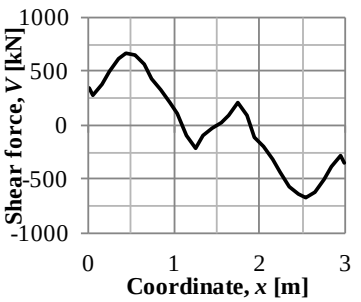

t=13 ms

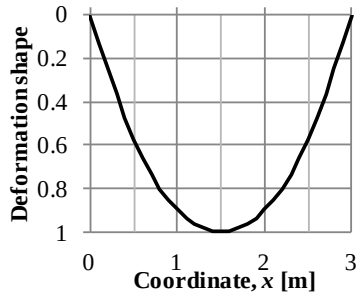

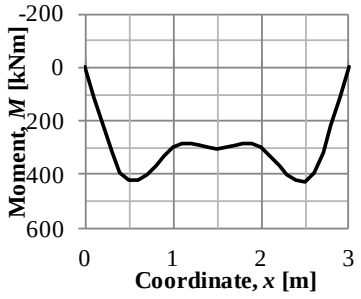

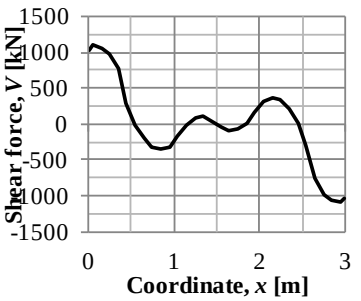

G.2 Ideal plastic

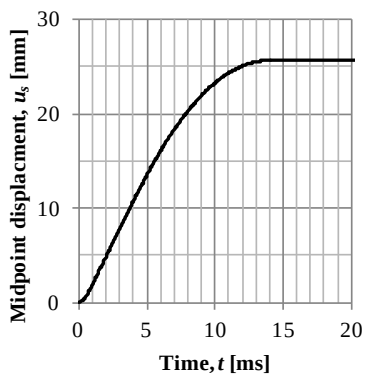

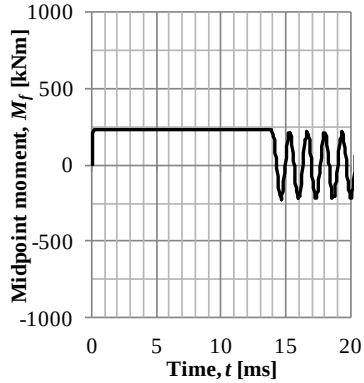

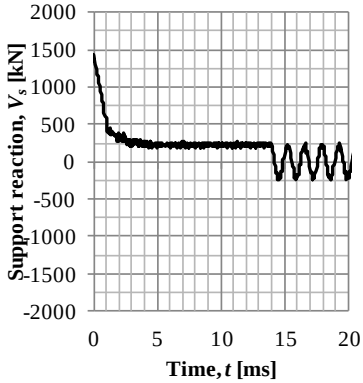

t=0.1 ms

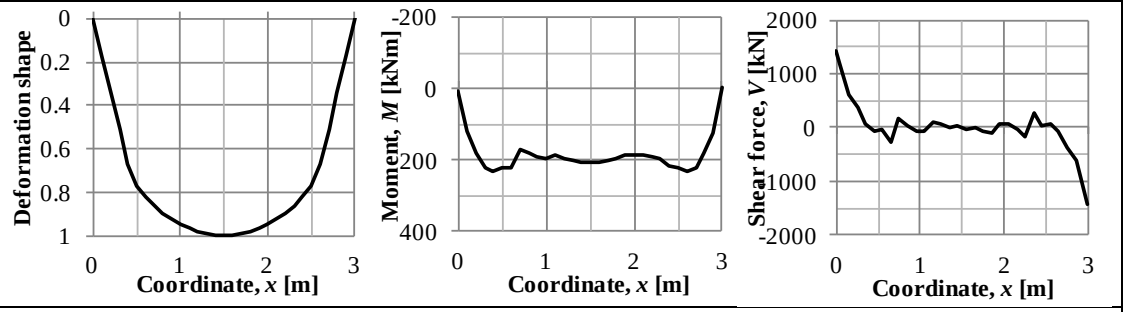

t=0.2 ms

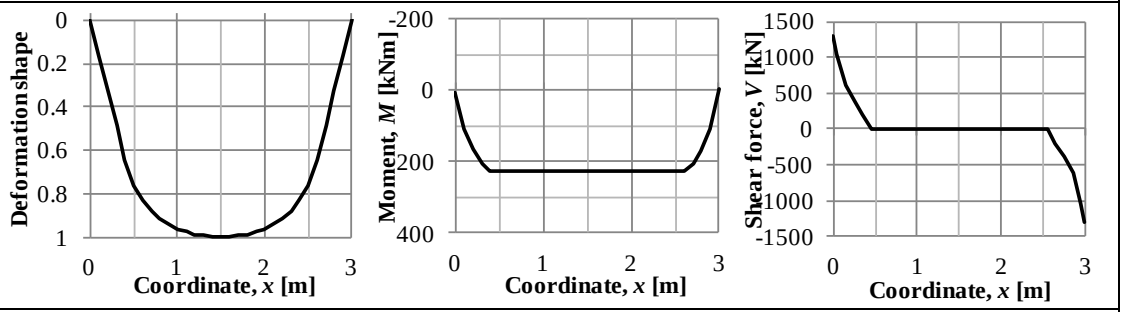

t=0.3 ms

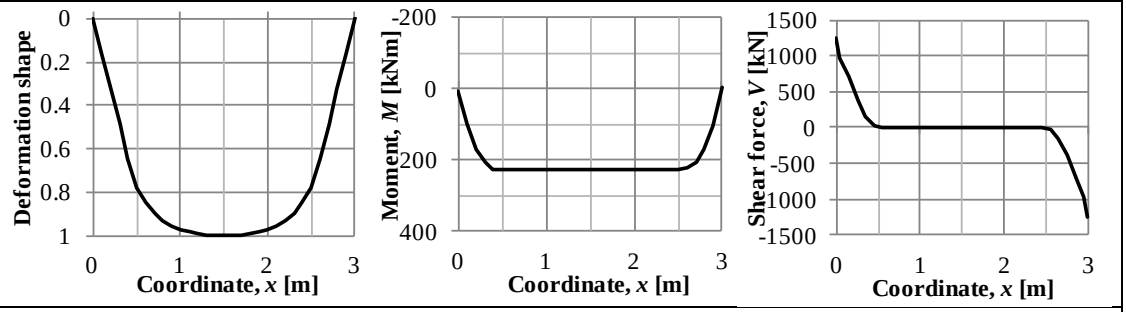

t=0.4 ms

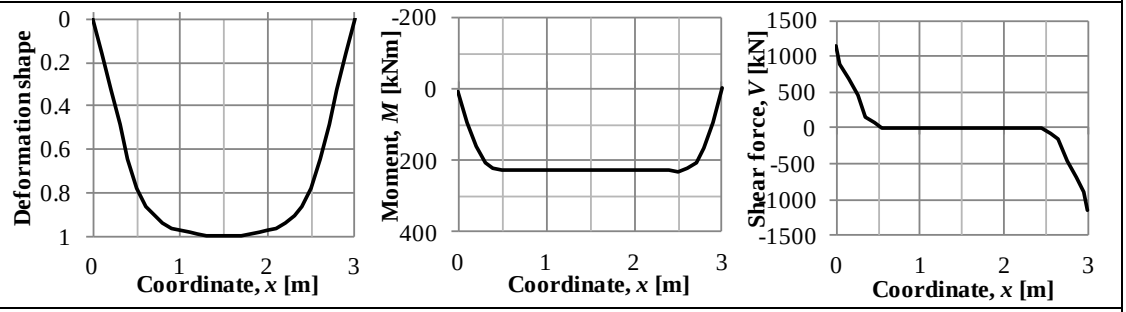

t=0.5 ms

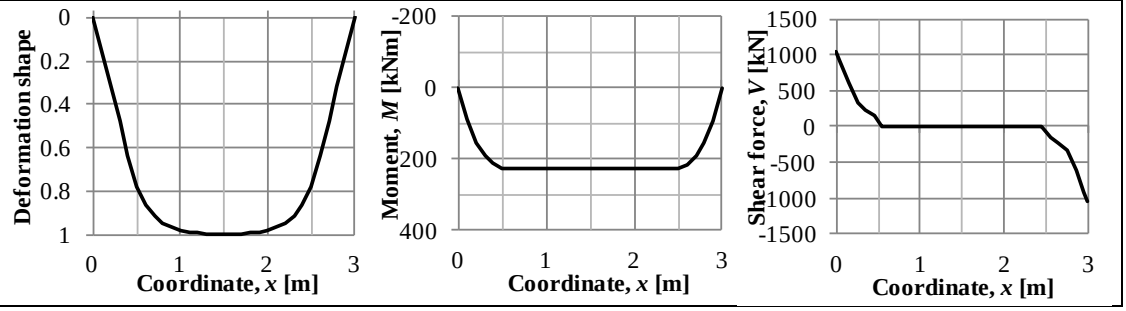

t=0.6 ms

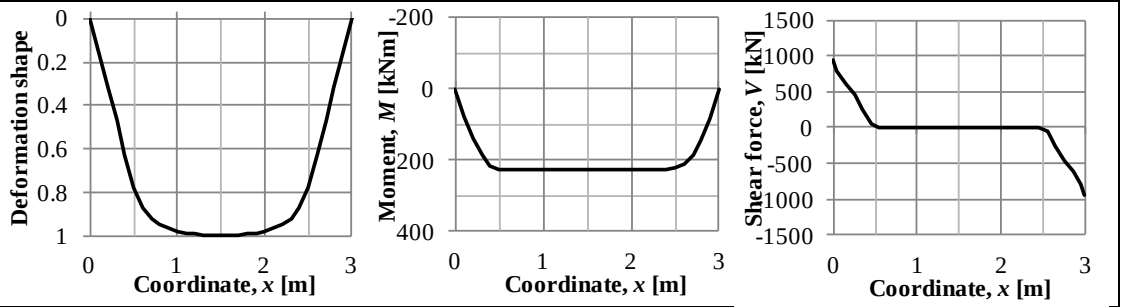

t=0.7 ms

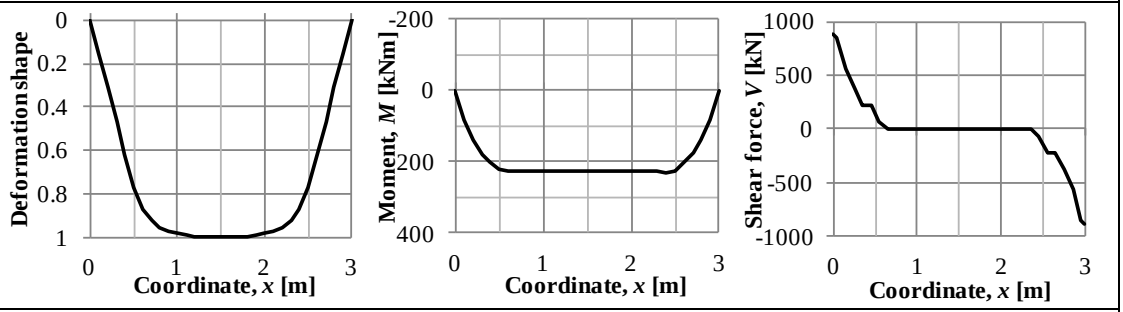

t=0.8 ms

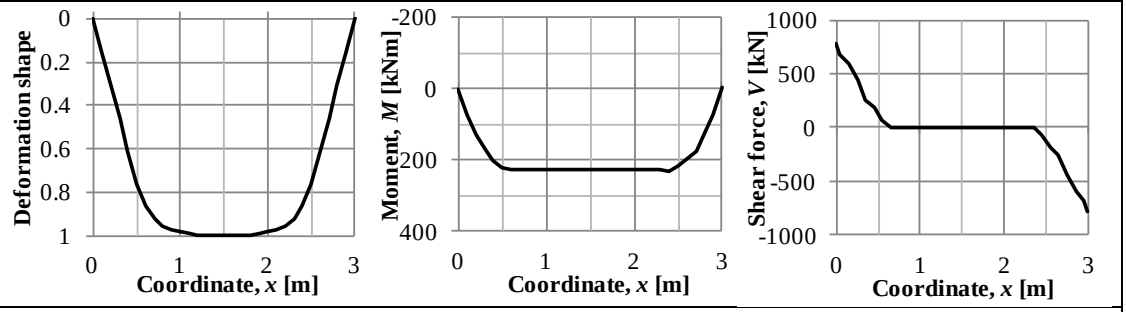

t=0.9 ms

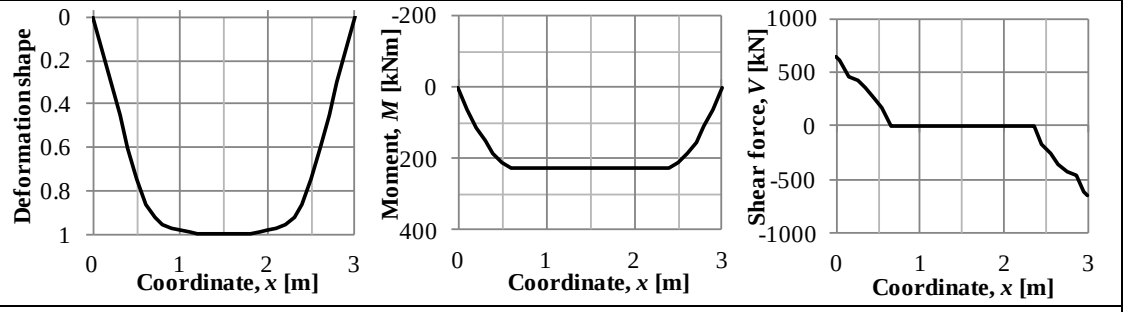

t=1 ms

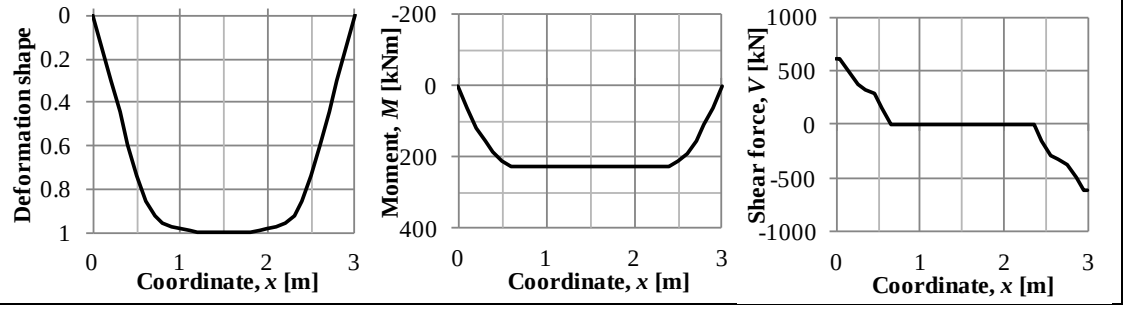

t=1.5 ms

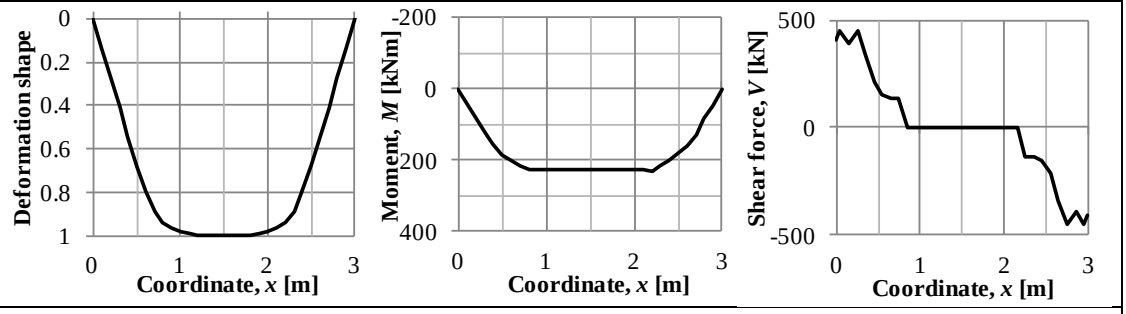

t=2 ms

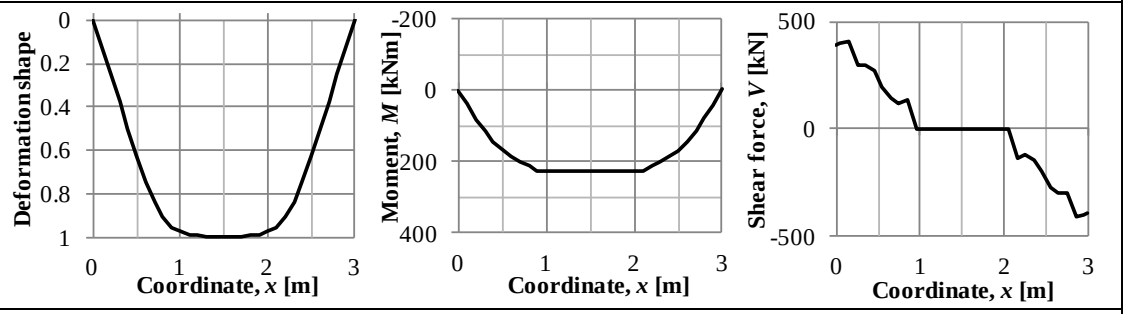

t=2.5 ms

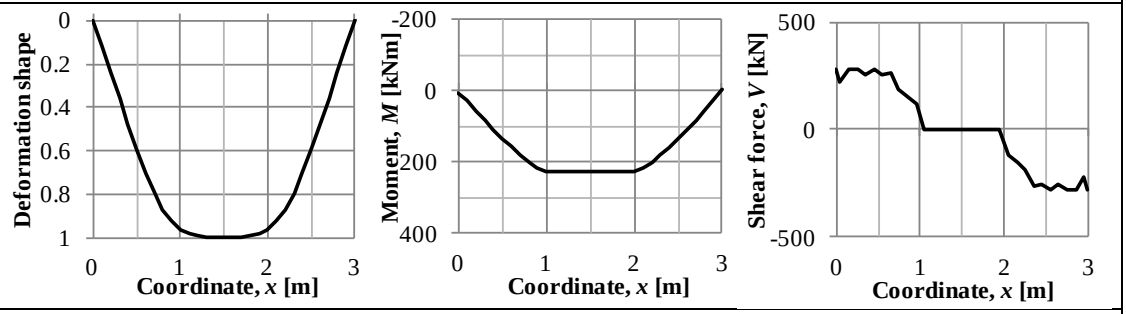

t=3 ms

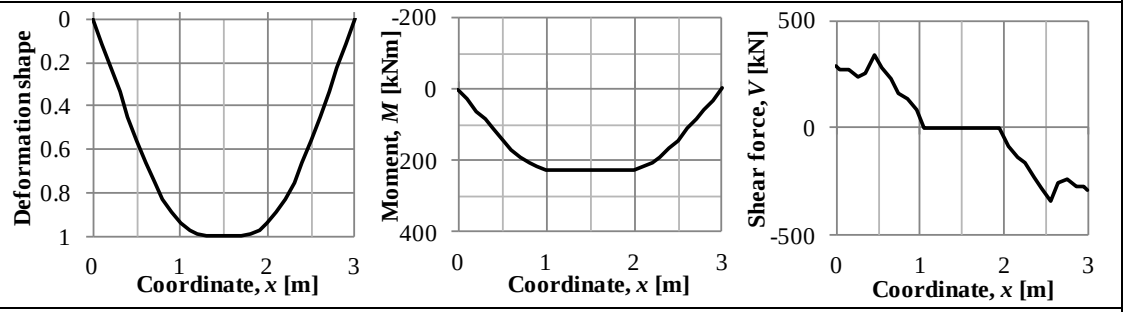

t=3.5 ms

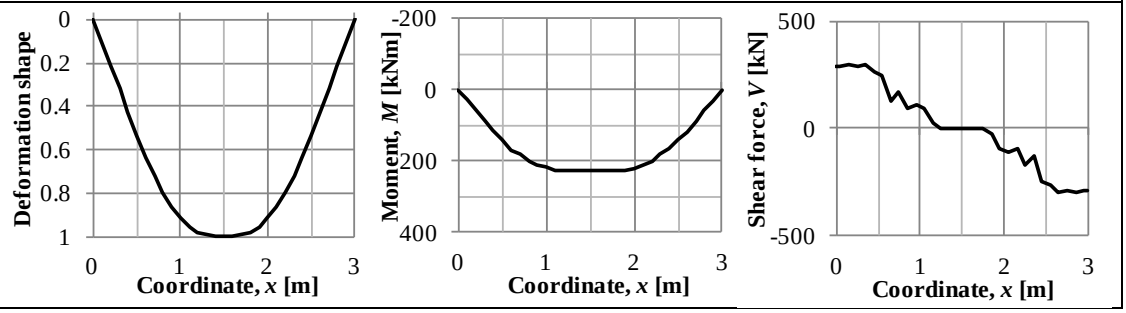

t=4 ms

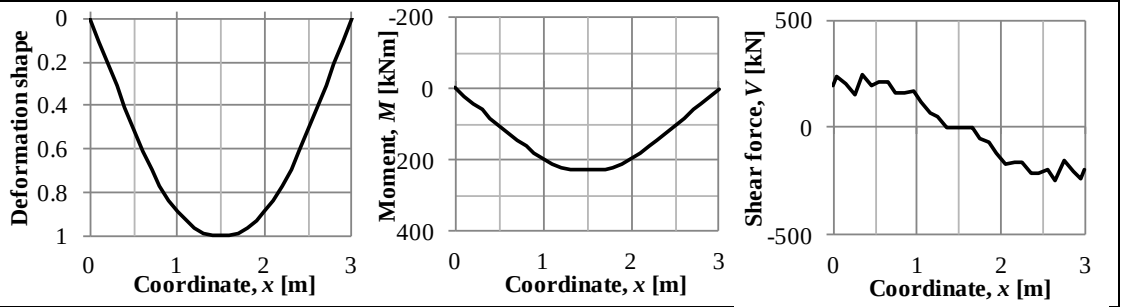

t=4.5 ms

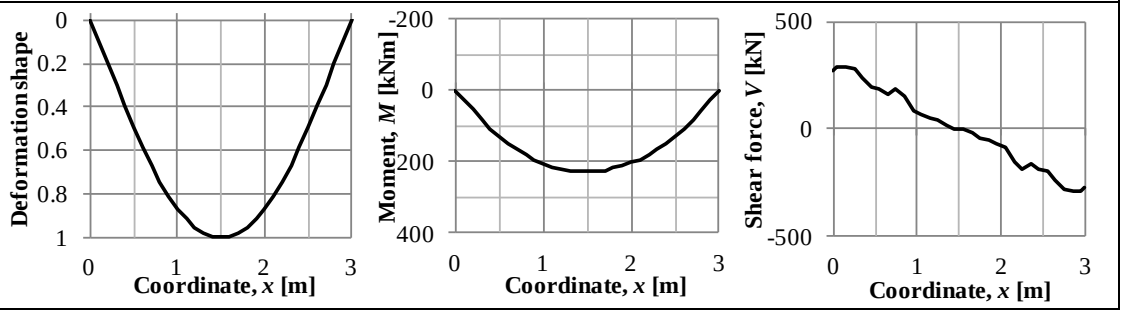

t=5 ms

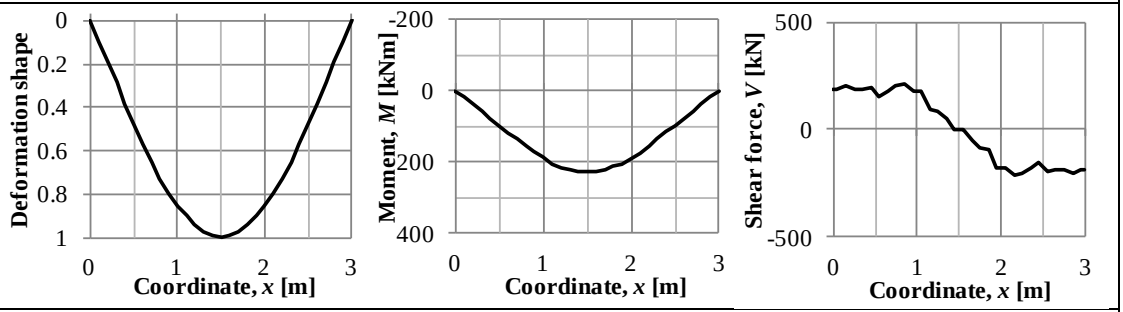

t=6 ms

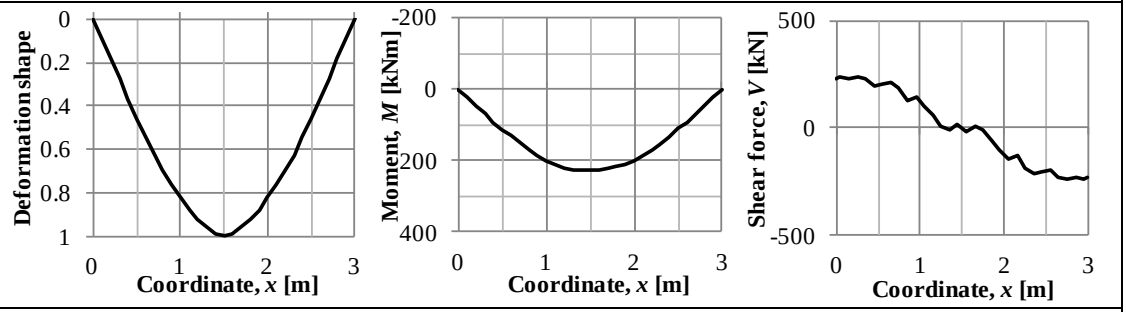

t=7 ms

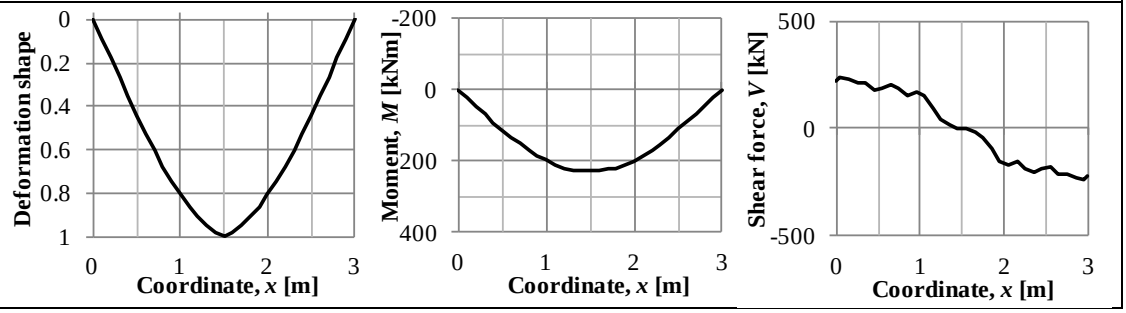

t=8 ms

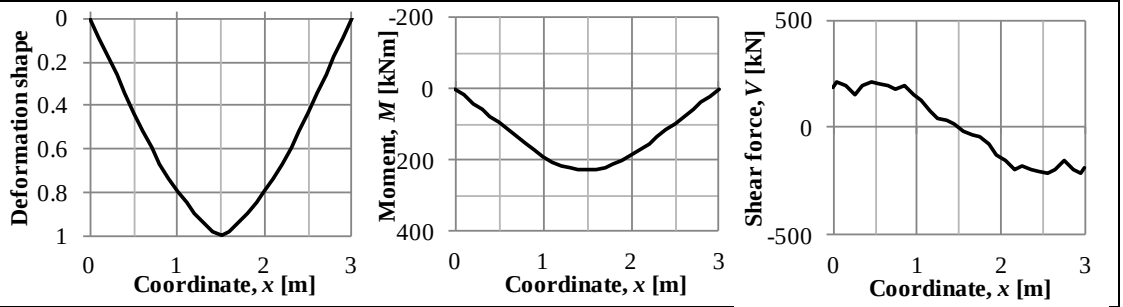

t=9 ms

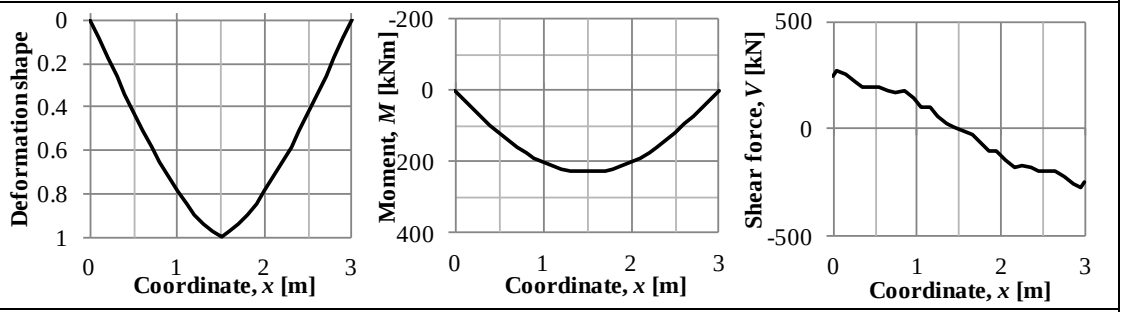

t=10 ms

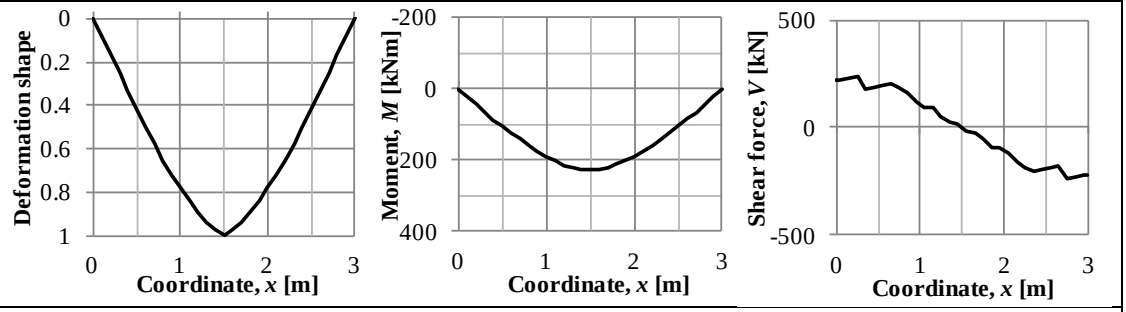

t=11 ms

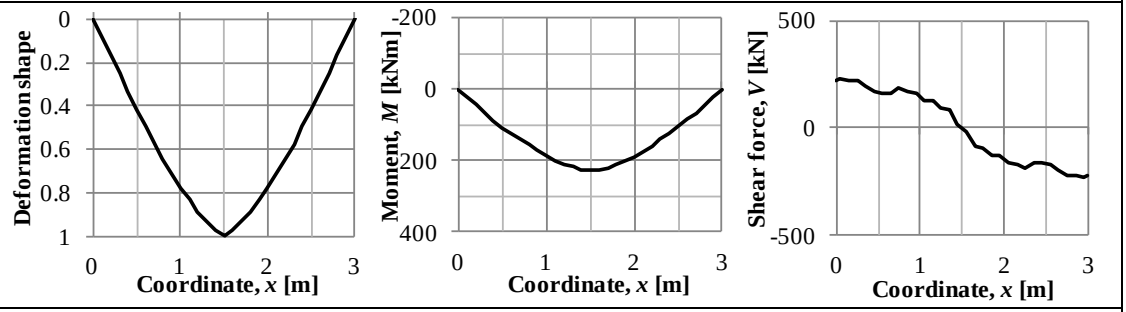

t=12 ms

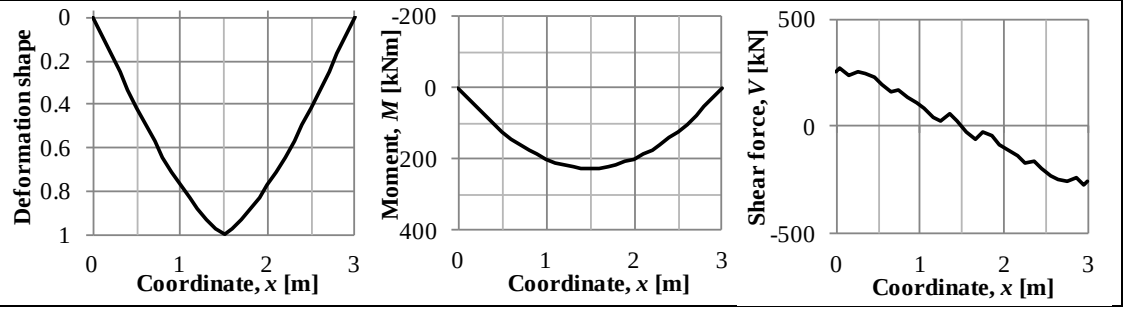

t=13 ms

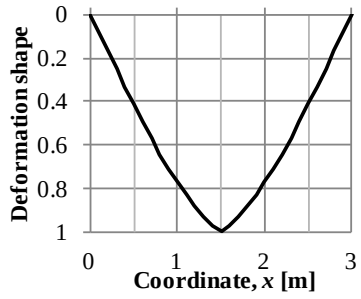

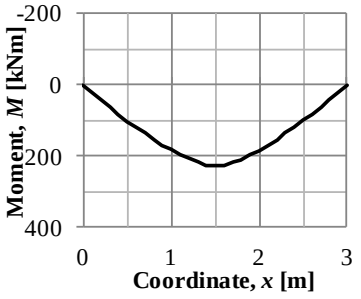

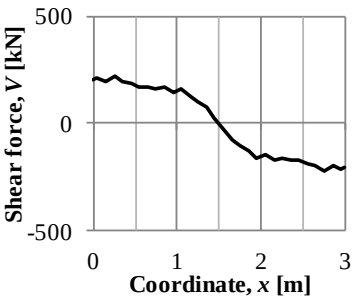

t=14 ms

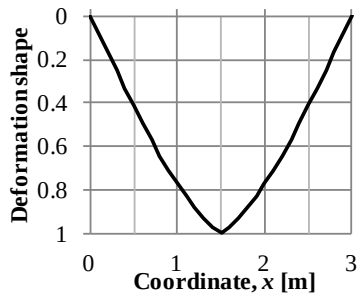

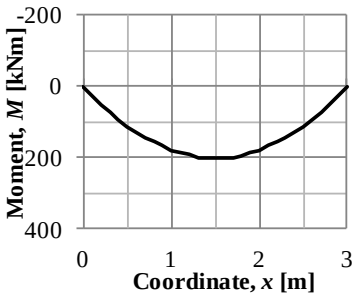

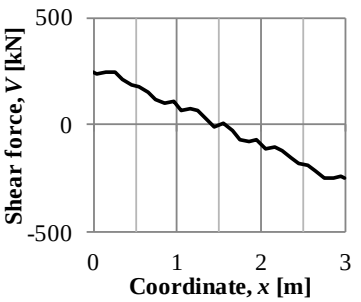

G.3 Elasto-plastic

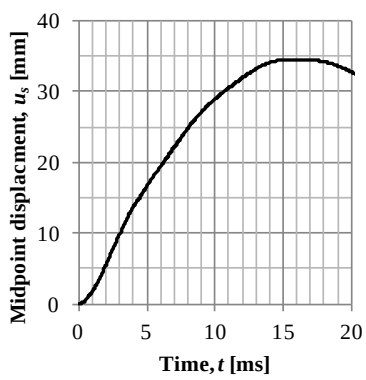

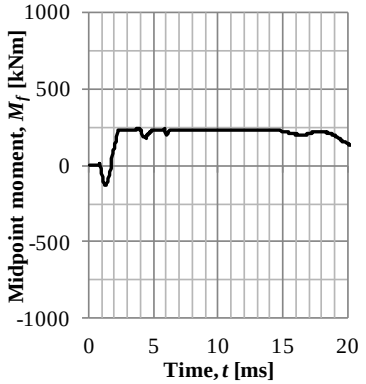

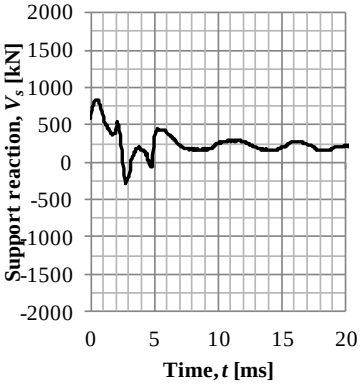

t=0.1 ms

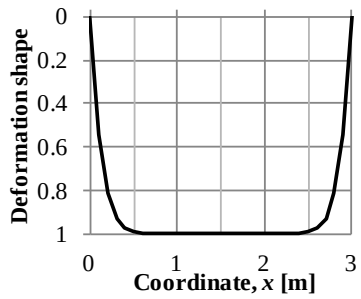

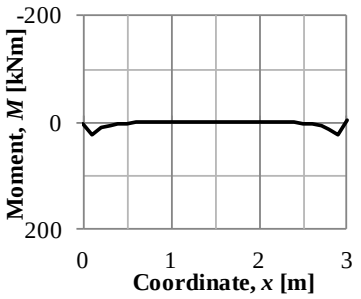

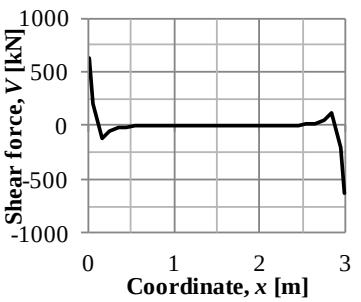

t=0.2 ms

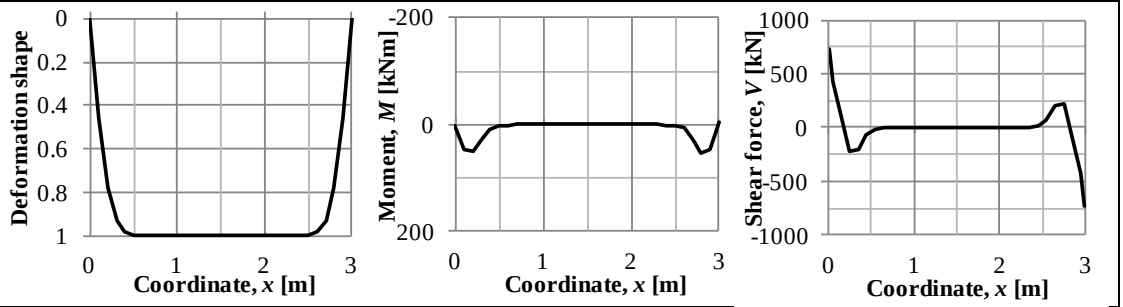

t=0.3 ms

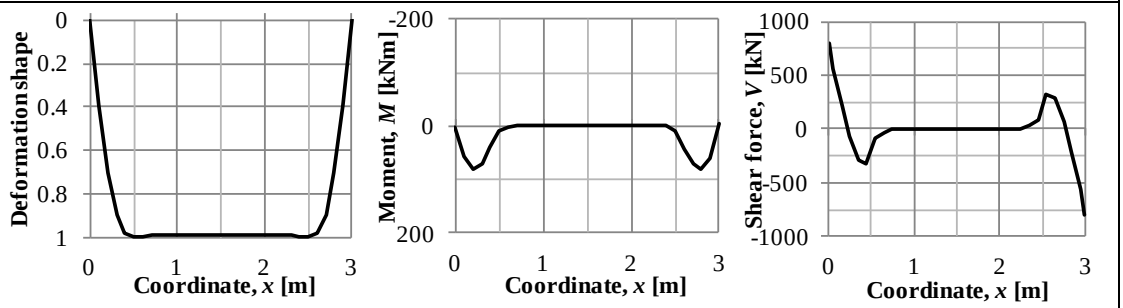

t=0.4 ms

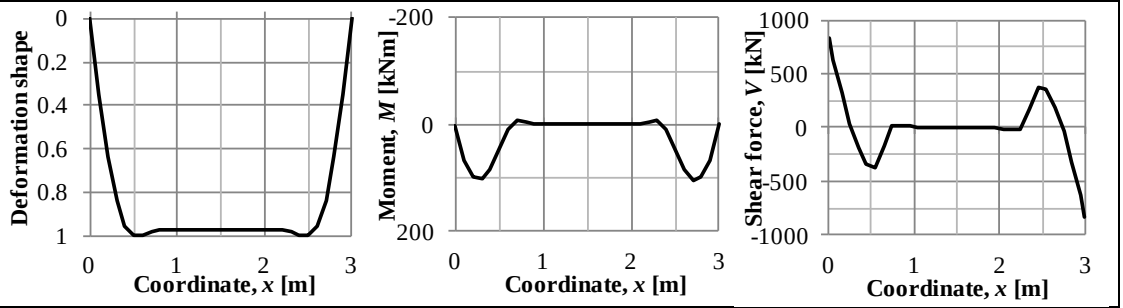

t=0.5 ms

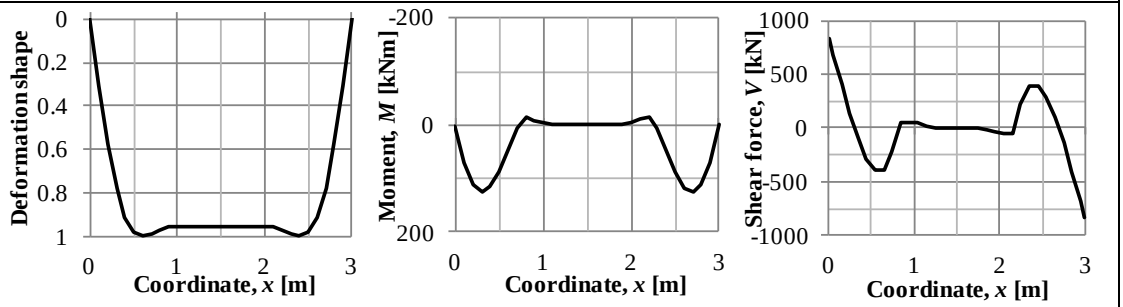

t=0.6 ms

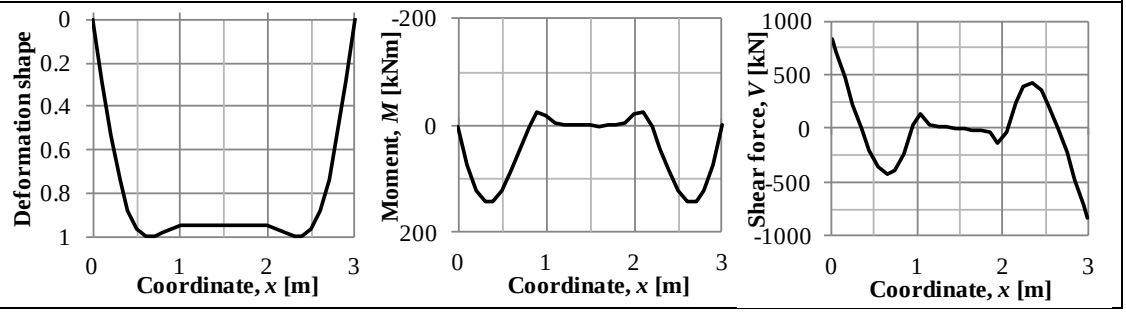

t=0.7 ms

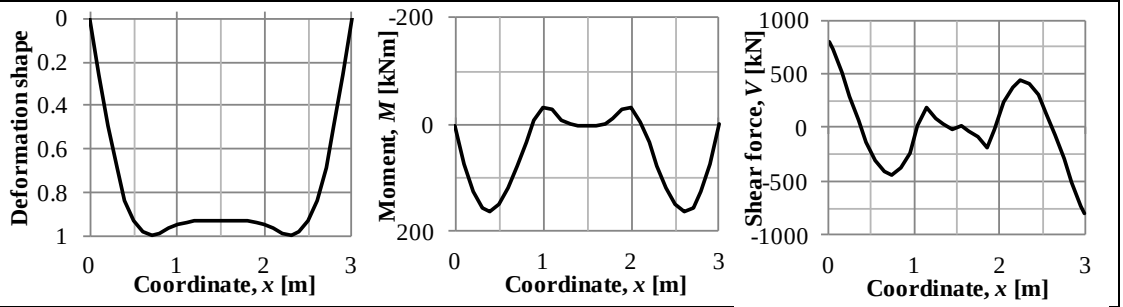

t=0.8 ms

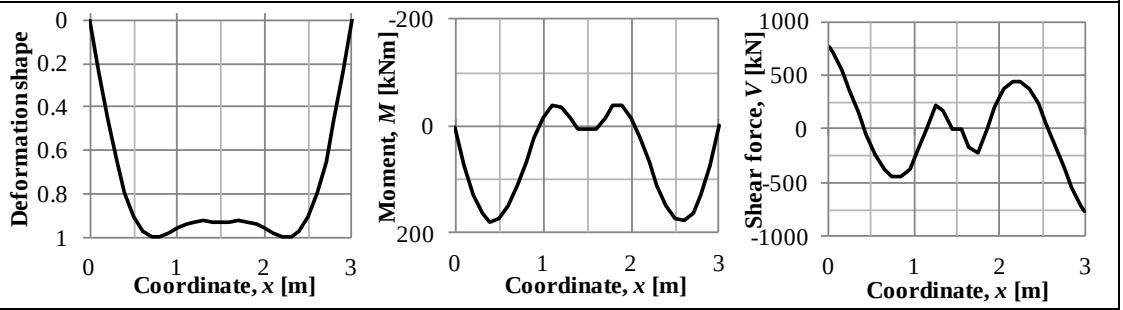

t=0.9 ms

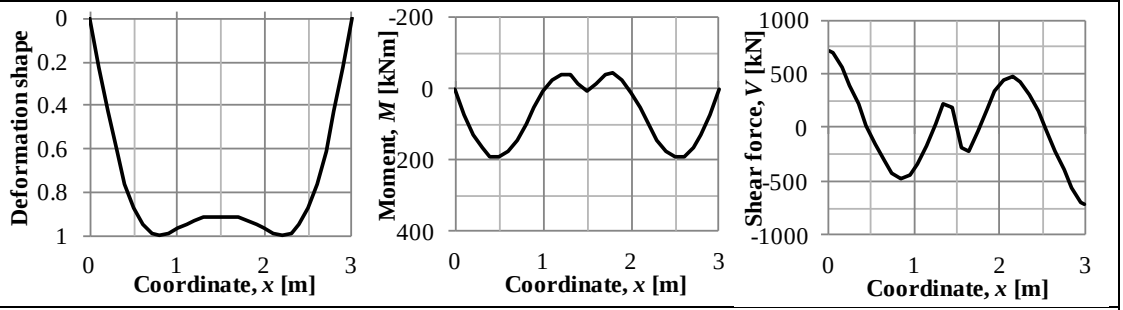

t=1 ms

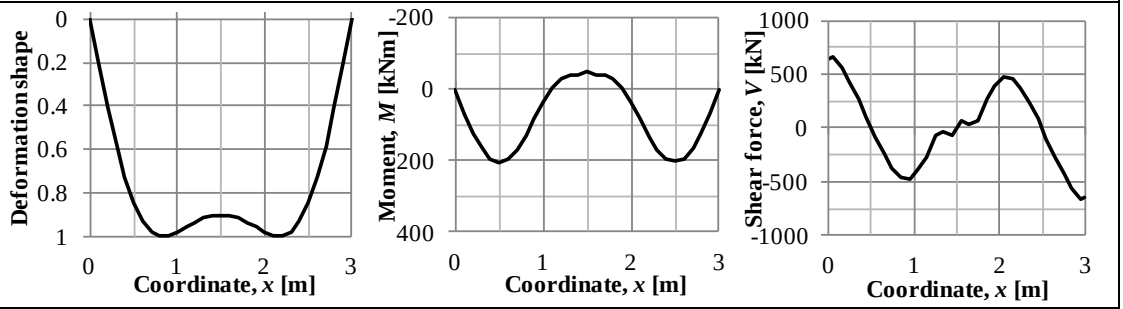

t=1.5 ms

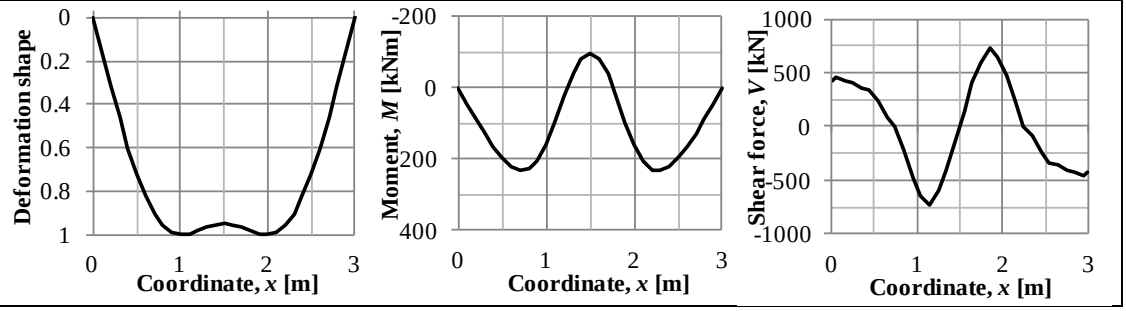

t=2 ms

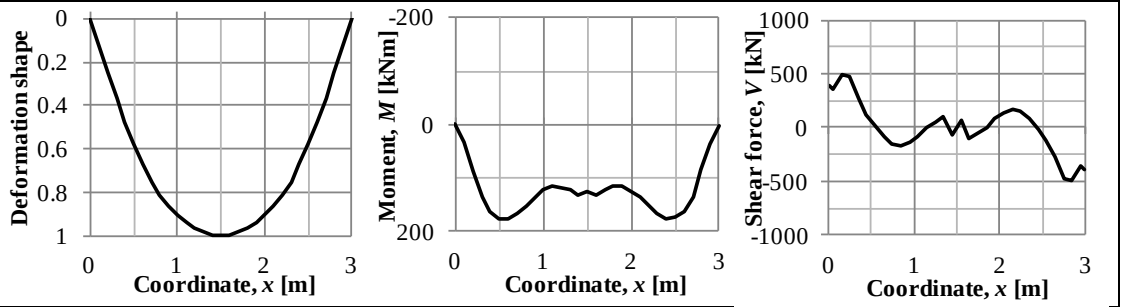

t=2.5 ms

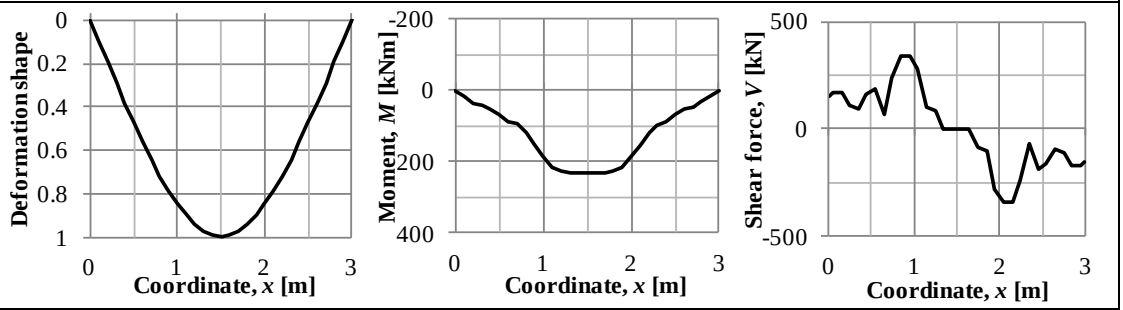

t=3 ms

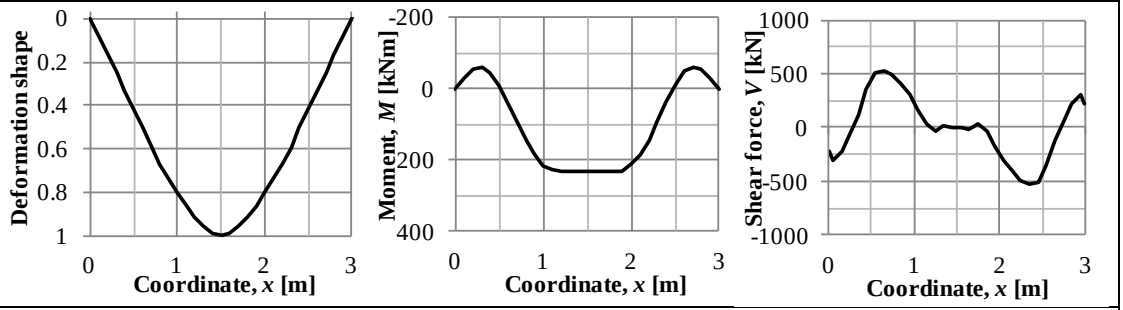

t=3.5 ms

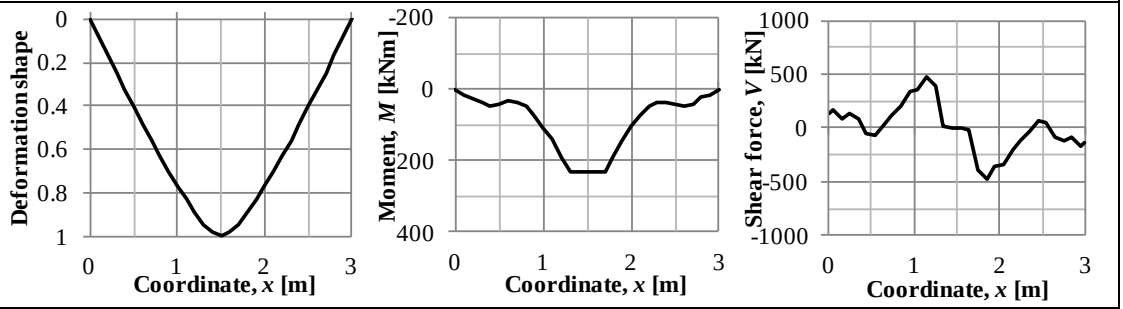

t=4 ms

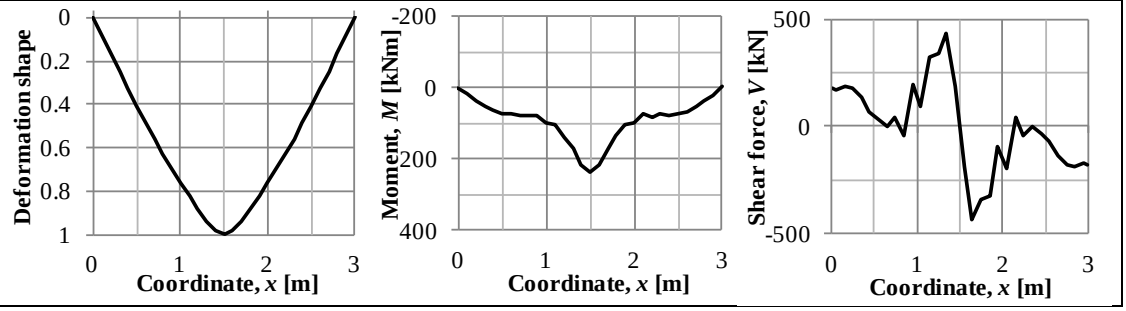

t=4.5 ms

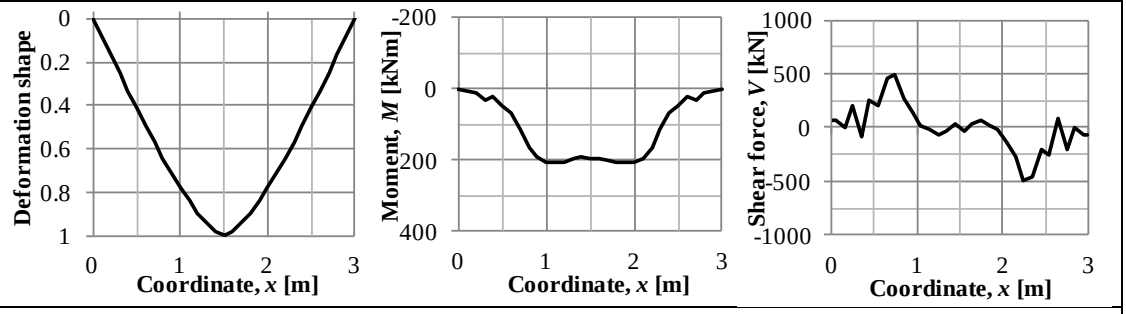

t=5 ms

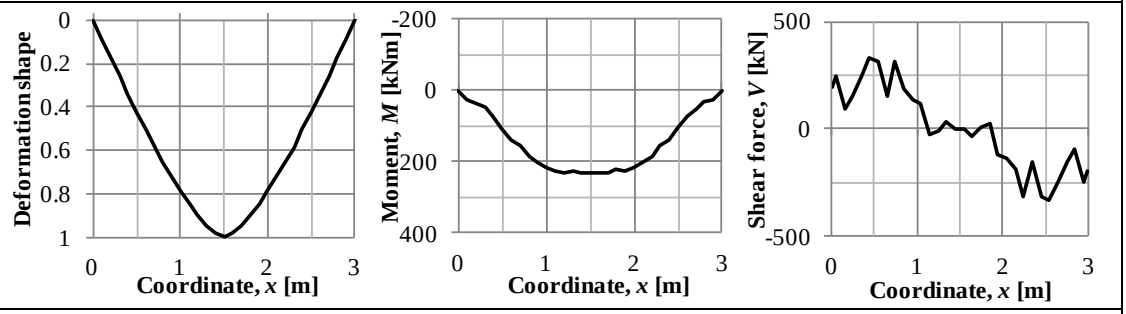

t=6 ms

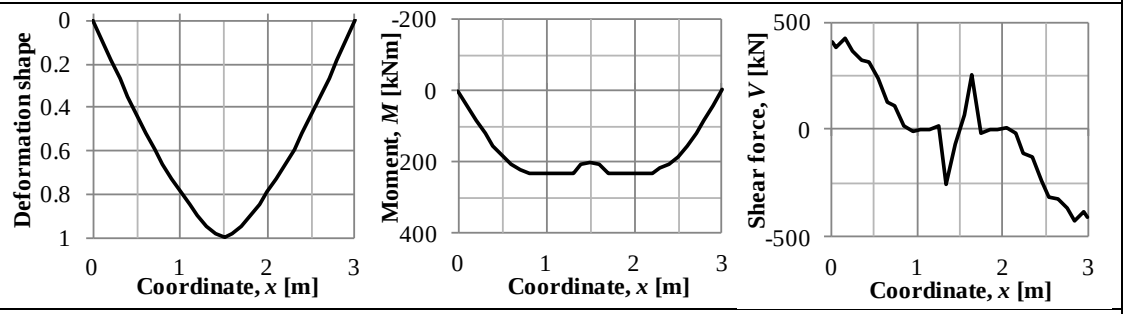

t=7 ms

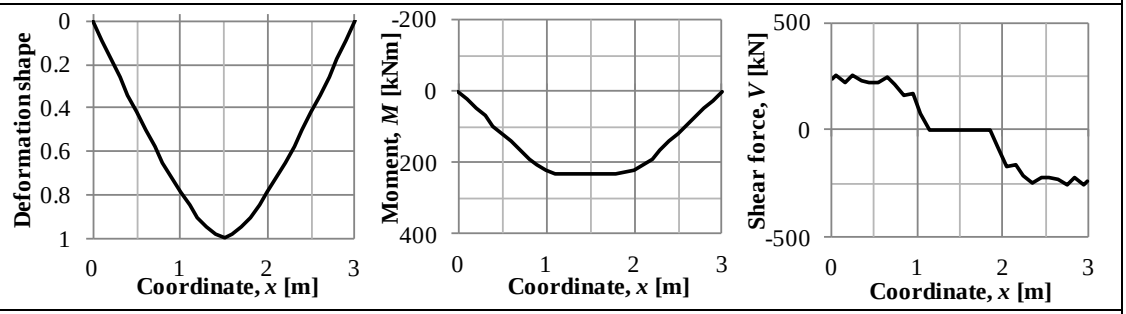

t=8 ms

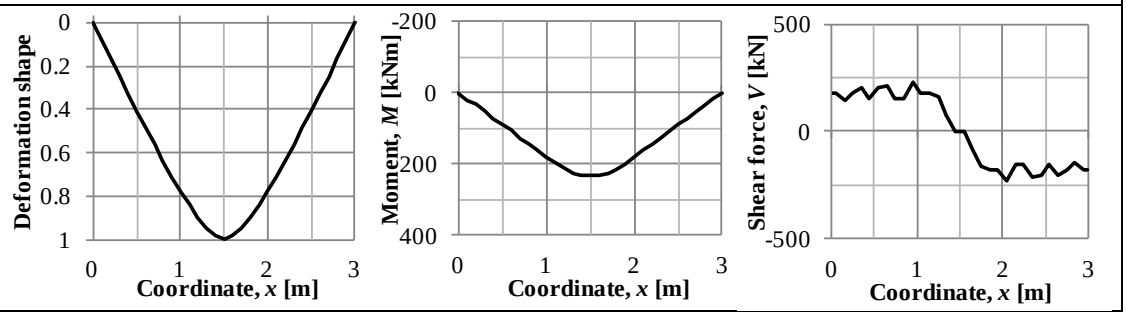

t=9 ms

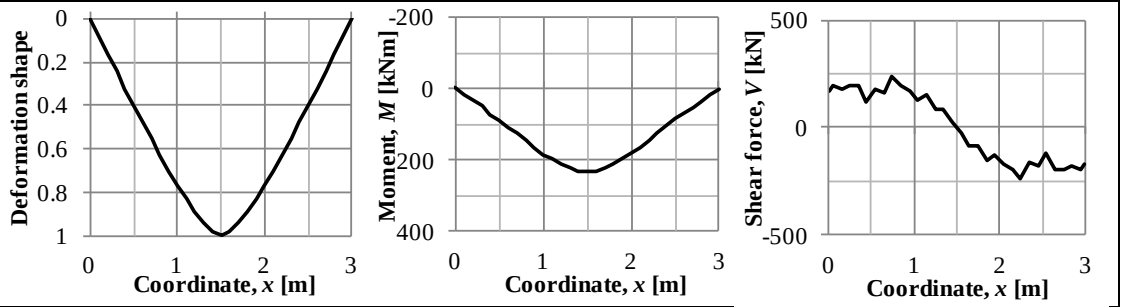

t=10 ms

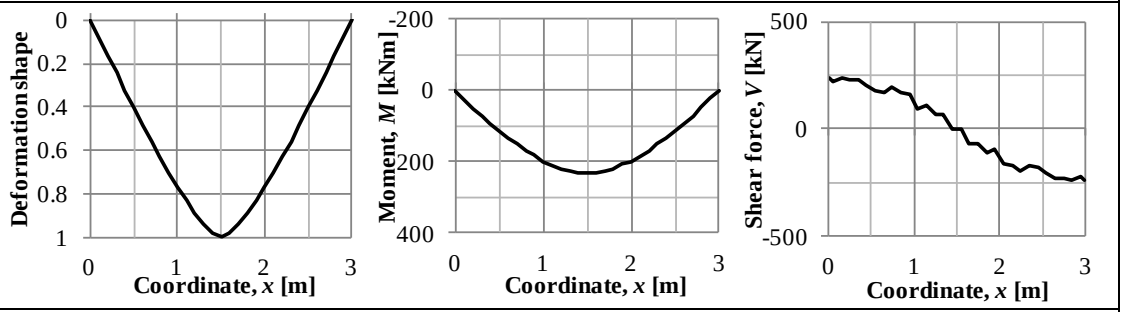

t=11 ms

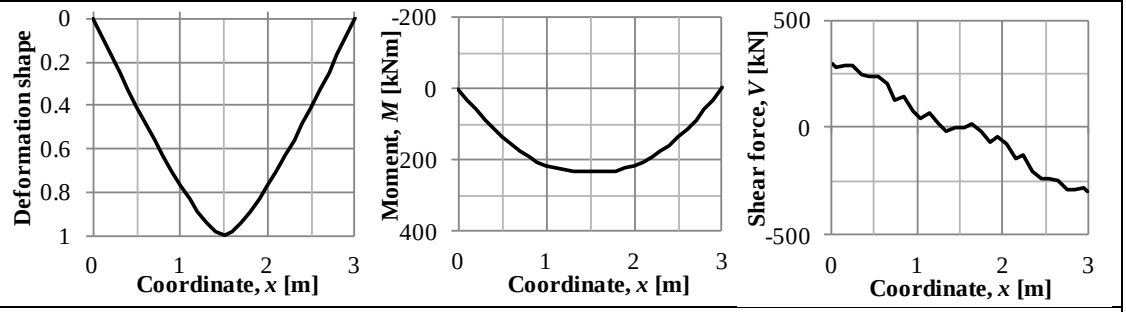

t=12 ms

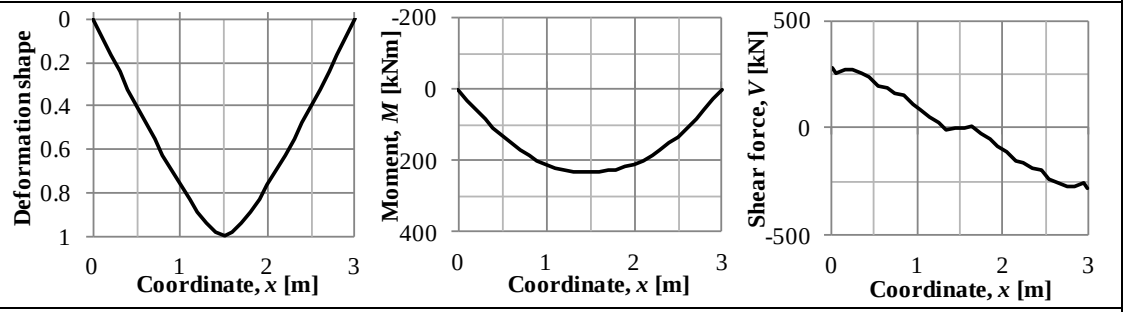

t=13 ms

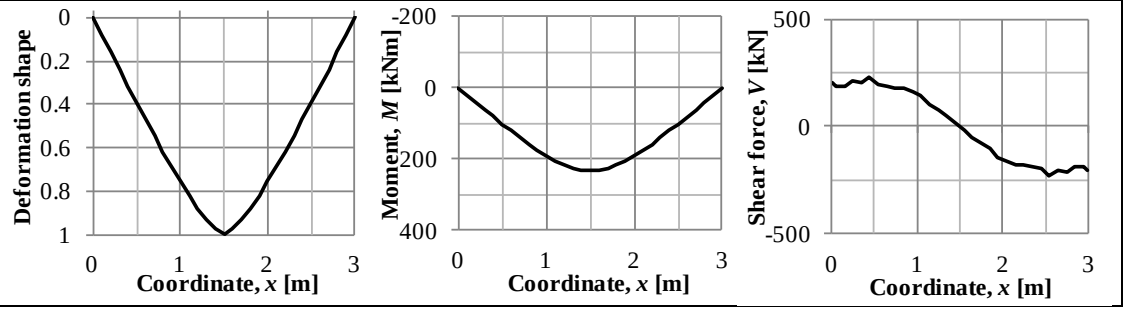

t=14 ms

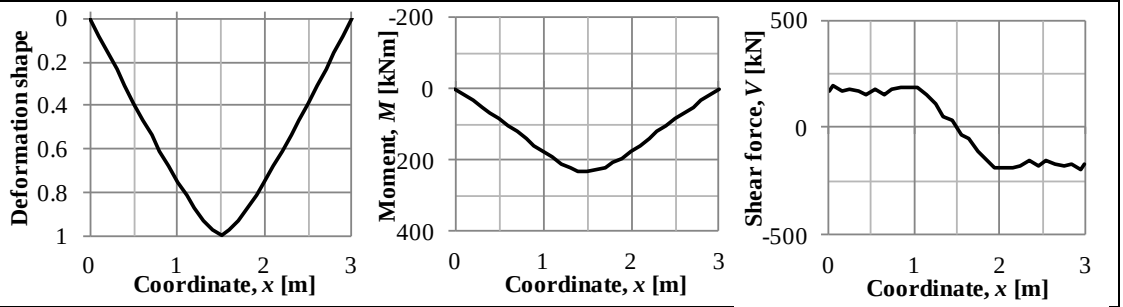

t=15 ms

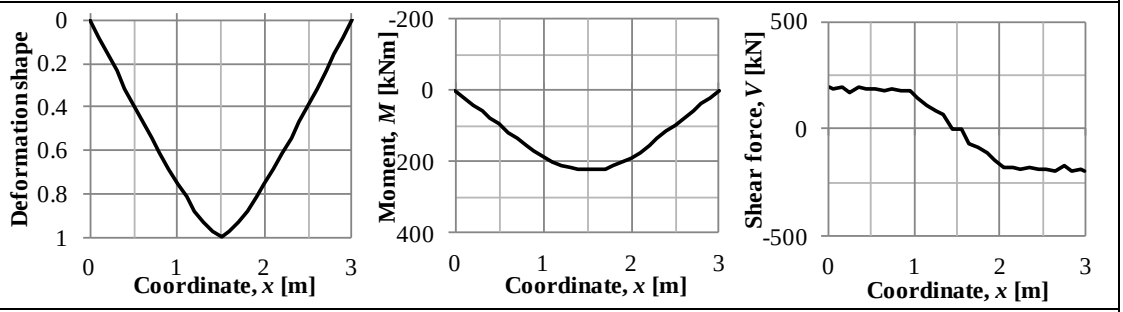

t=16 ms

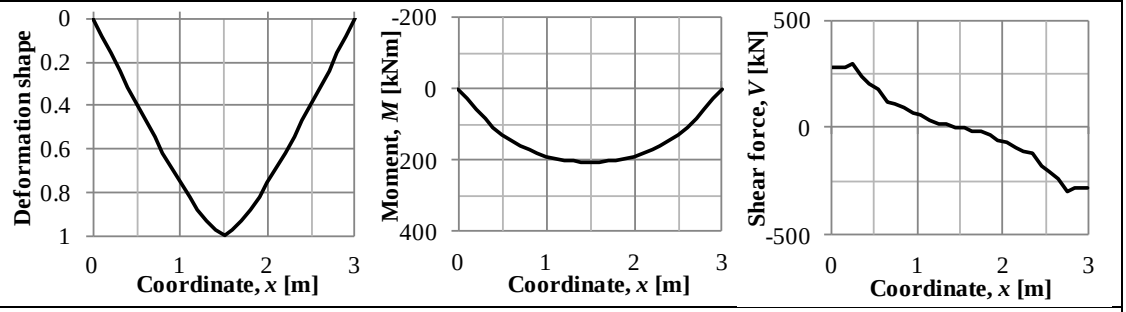

t=17 ms

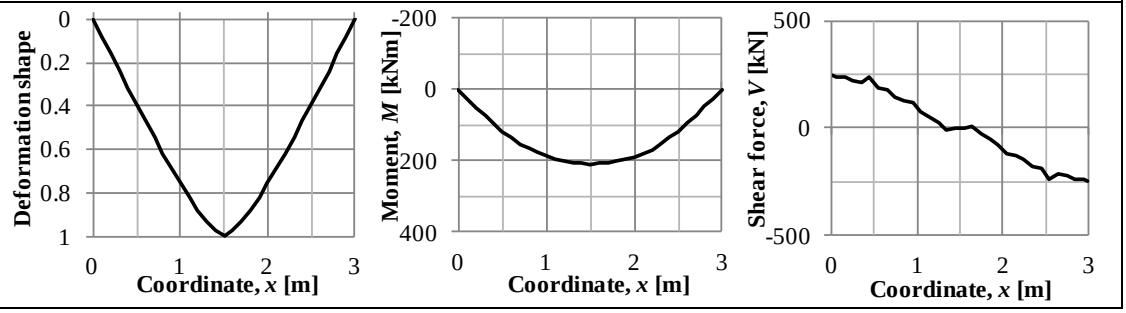

APPENDIX H INFLUENCE OF DAMPING

In the elastic case, it is seen that the moment and shear demand is underestimated when using an equivalent static load. However, the analyses in Section 5.2 do not consider damping and it is shown that this has a significant impact on the result. This Appendix will firstly show the moment and shear envelops for the undamped case Section H.1, and then for damped case, Section H.2. Some basic theory of how the damping is introduced is also presented in Section H.2.

Three different cross-sections with elastic response have been used. The height is varied while the amount of reinforcement is kept constant. The level of reinforcement is also kept constant, see Figure H.1. The investigation is performed with the load case 1 and 3, described in Section 3.2**Error! Reference source not found.**.

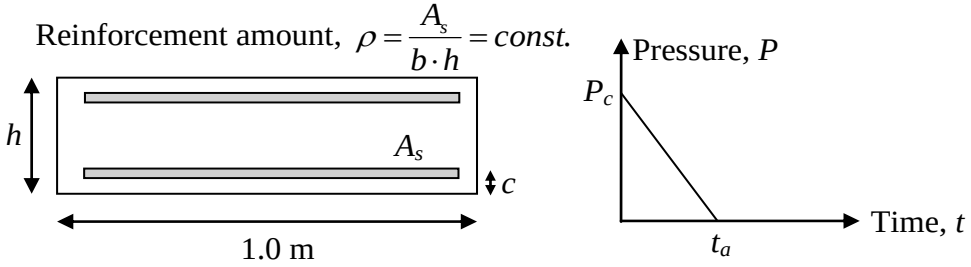

Figure H.1. Description of the used cross sections and the load

The results have been compared and shown as the ratio between peak pressure and equivalent static load for the section. Input data is shown in Table H.1.

Table H.1. Investigated cross sections and loads.

h [mm]	A_s [mm^2]	q_{eq} [kN/m^2]	P_c [kPa]	P_c/q_{eq}
400	1571	539	1250	2.32
300	1178	384	1250	3.26
200	785	228	1250	5.48
400	1571	539	5000	9.27
300	1178	384	5000	13.02
200	785	228	5000	21.93

Firstly, the envelops and their relative error ξ when not considering damping is shown for the different ratios. The envelops are taken for one oscillation. The value of the support reaction obtained by using Fortifikationsverket's approach is also shown next to the diagrams.

H.1. Undamped case

Ratio	Figure	Relative error
$\frac{P_c}{q_{eq}} = 2.32$	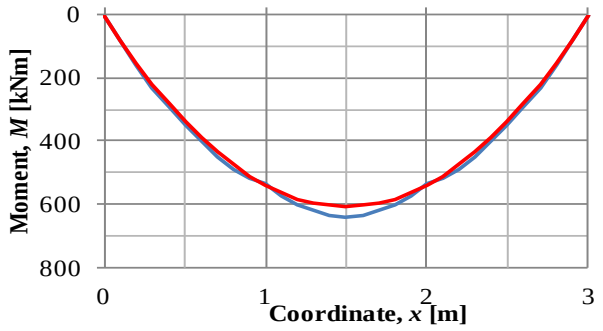	$\xi = \frac{661-607}{607} = 8.9\,\%$
	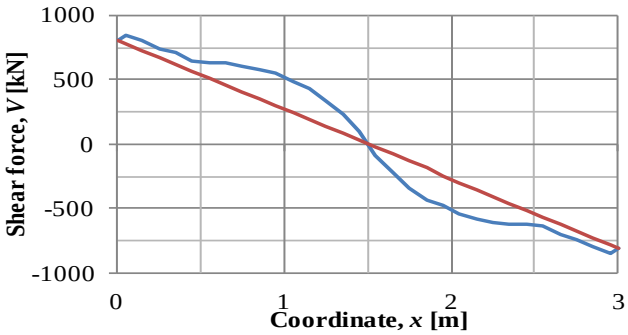	$V_s^{FortV} = 1010\,\text{kN}$ $\xi = \frac{847-809}{809} = 4.6\,\%$
$\frac{P_c}{q_{eq}} = 3.26$	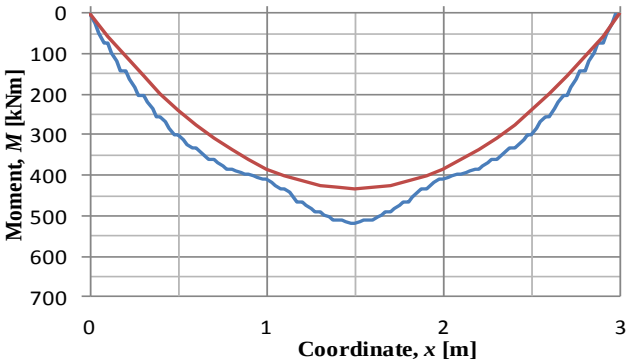	$\xi = \frac{517-432}{432} = 19.7\,\%$
	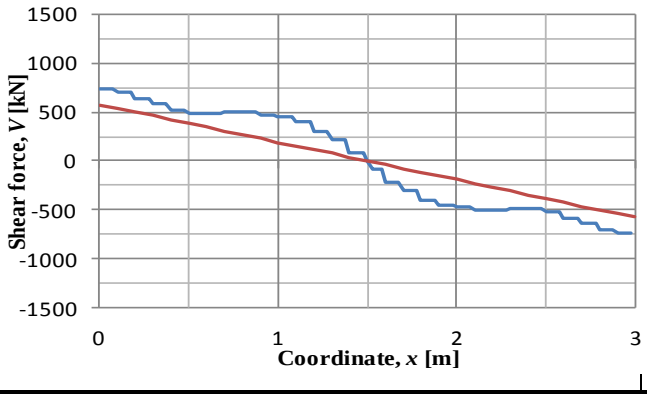	$\xi = \frac{733-576}{576} = 27.2\,\%$ $V_s^{FortV} = 819\,\text{kN}$

Ratio	Figure	
$\frac{P_c}{q_{eq}} = 5.48$	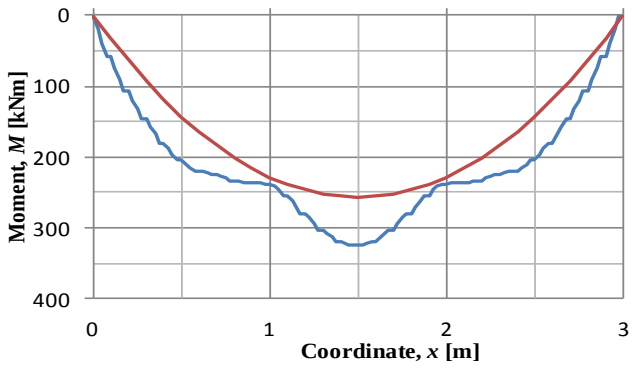	$\xi = \frac{325-257}{257} = 26.4\,\%$
	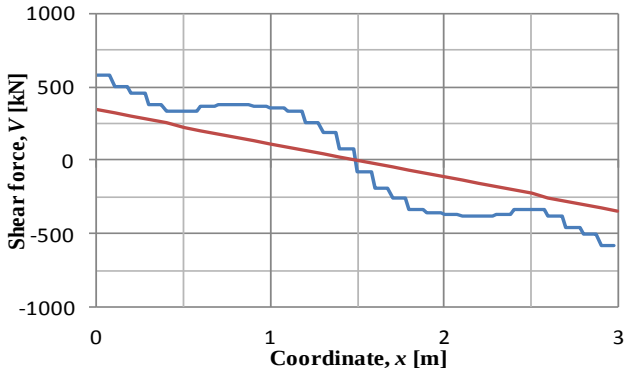	$\xi = \frac{578-342}{342} = 69.0\,\%$ $V_s^{FortV} = 620\,\text{kN}$
$\frac{P_c}{q_{eq}} = 9.27$	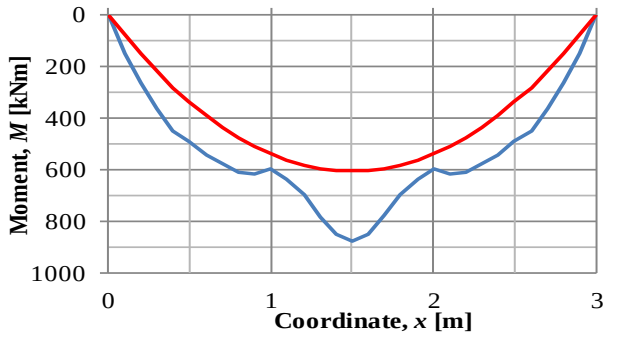	$\xi = \frac{855-607}{607} = 40.9\%$
	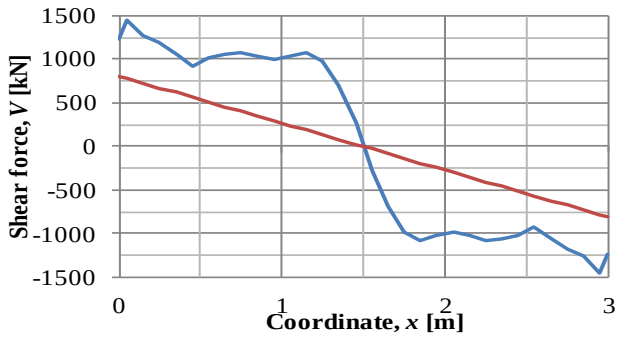	$\xi = \frac{1501-809}{809} = 85.5\,\%$ $V_s^{FortV} = 2060\,\text{kN}$

Cross-section	Load case 1	
$\frac{P_c}{q_{eq}} = 13.02$	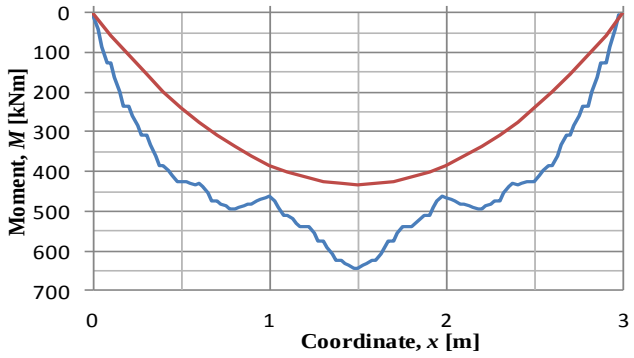	$\xi = \frac{642 - 432}{432} = 48.6\,\%$
	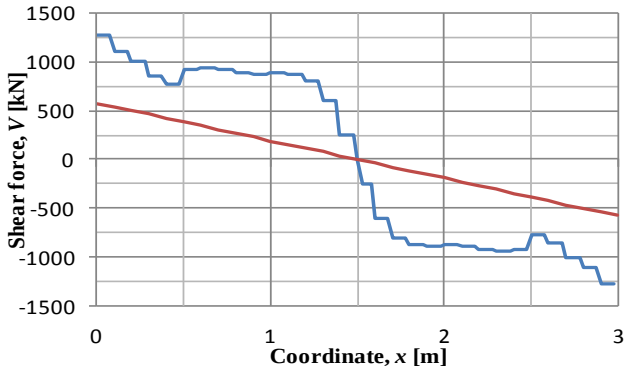	$\xi = \frac{1266 - 576}{576} = 120\,\%$ $V_s^{FortV} = 1870\,\text{kN}$
$\frac{P_c}{q_{eq}} = 21.93$	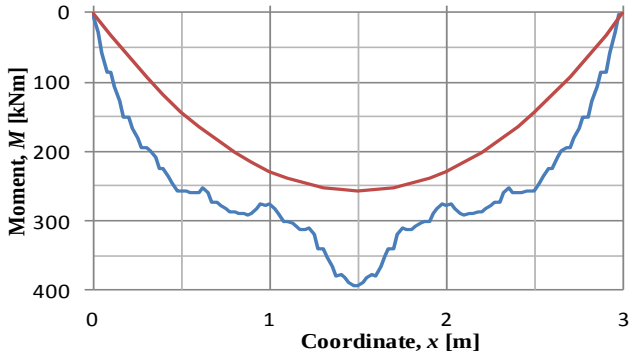	$\xi = \frac{393 - 257}{257} = 52.9\,\%$
	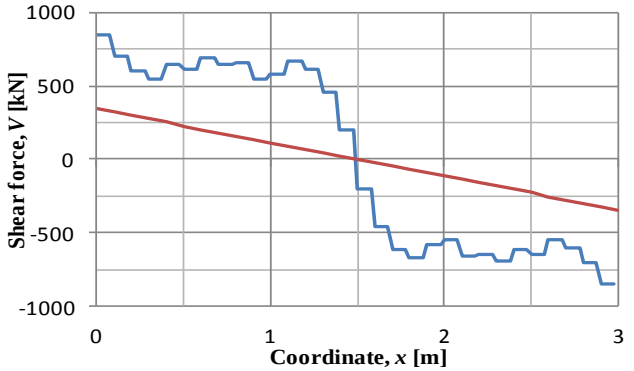	$\xi = \frac{847 - 342}{342} = 148\,\%$ $V_s^{FortV} = 1640\,\text{kN}$

H.2 Damped case

A real structure always has some damping but this is not considered in the thesis since it should not affect the initial result considerably. Since the moment and shear force are much higher than expected in the linear elastic case, a check has been performed to see if the peaks are significantly affected by damping. The damping that has been used is 5 % Rayleigh damping.

Rayleigh damping is defined with two factors α and β. These relate the damping ratio to every mode. α tends to damp lower modes and β tends to damp higher modes. The damping ratio for mode *i* can according to Craig Jr. and Kurdila (2006) be written as

$$\gamma_i = \frac{\alpha}{2\omega_i} + \frac{\beta \cdot \omega_i}{2} \tag{H-1}$$

where γ_i is the damping ratio for mode *i*. Damping is introduced with a damping matrix, which depends on the mass and stiffness matrices

$$\mathbf{C} = \alpha \cdot \mathbf{M} + \beta \cdot \mathbf{K} \tag{H-2}$$

In explosion design many frequency modes are of interest; for instance, the rigid body motion can only be described by using many modes. It is of interest to see how much the peaks in support reactions and moments are influenced by using a damping ratio of 5 %. Rayleigh damping is constructed so that it will have a lower value between the two specified values and higher value for higher or lower modes.

An example of how the α- and β-factors for the normal cross-section with subjected to load case 1 is shown below.

The period of the oscillations is rather regular and hence the mode frequency can be calculated. It is estimated that 5 peaks occur during approximately 20 ms for load case 1. This would give a natural period of

$$T_2 = \frac{20}{5} = 4 \text{ ms} \tag{H-3}$$

And a corresponding natural frequency of

$$\omega_2 = \frac{2\pi}{T_2} = \frac{2\pi}{4 \cdot 10^{-3}} = 1571 \text{ rad/s} \tag{H-4}$$

The damping ratio for this mode can be set to 5% but in order to not overdamp this mode a factor of 1.5 has been applied to the frequency.

$$\omega_2 = 1.5 \cdot 1571 = 2356 \text{ rad/s} \tag{H-5}$$

All modes below this frequency are of interest and the fundamental mode of vibration can be written as

$$\omega_1 = \frac{\pi^2}{l^2}\sqrt{\frac{EI}{m/l}} = \frac{\pi^2}{3^2}\sqrt{\frac{5.547\cdot 10^9 \cdot 5.33\cdot 10^{-3}}{2400\cdot 0.4}} = 192 \text{ rad/s} \tag{H-6}$$

The damping ratio is also set to 5 % for this mode. By using eq. (2-46) with mode frequencies from (H-4) and (H-6) the input parameters for ADINA can be found as.

$$\begin{aligned} \alpha &= 17.79 \\ \beta &= 3.92\cdot 10^{-5} \end{aligned} \tag{H-7}$$

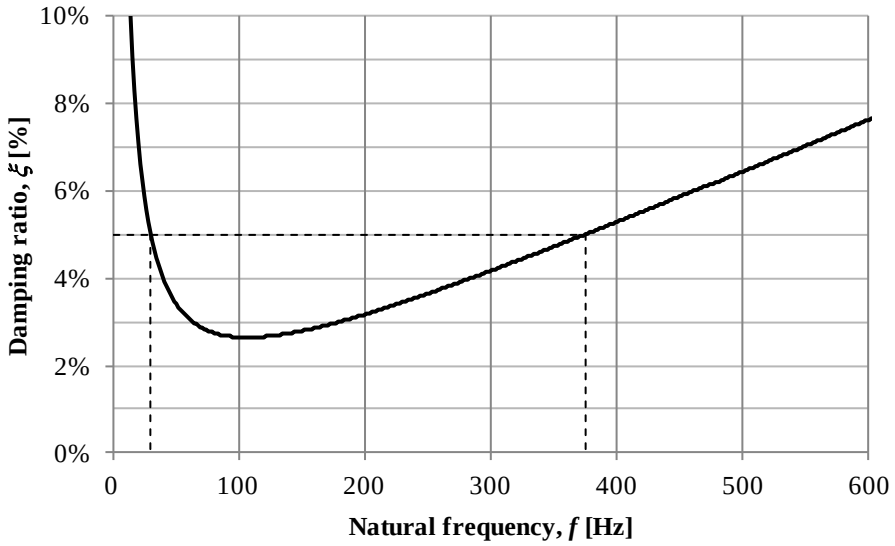

Figure H.2. Typical Rayleigh damping used for the cross-sections.

Ratio	Figure	Relative error
$\frac{P_c}{q_{eq}} = 2.32$	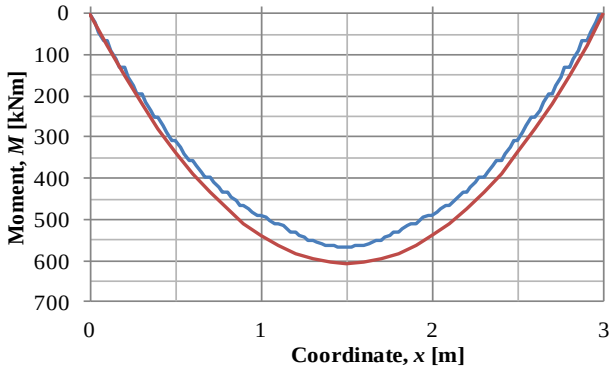	$\xi = \frac{576 - 607}{607} = -5\,\%$
	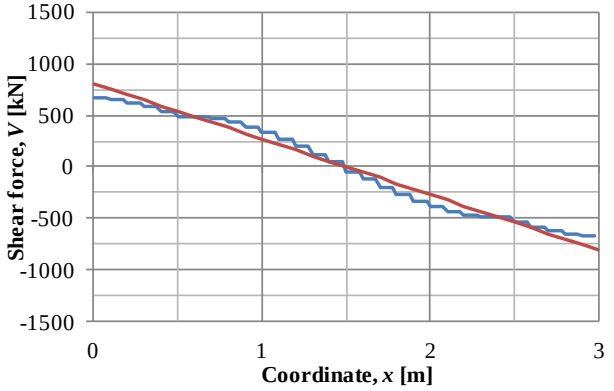	$V_s^{FortV} = 1010\text{kN}$ $\xi = \frac{667 - 809}{809} = -18\,\%$
$\frac{P_c}{q_{eq}} = 3.26$	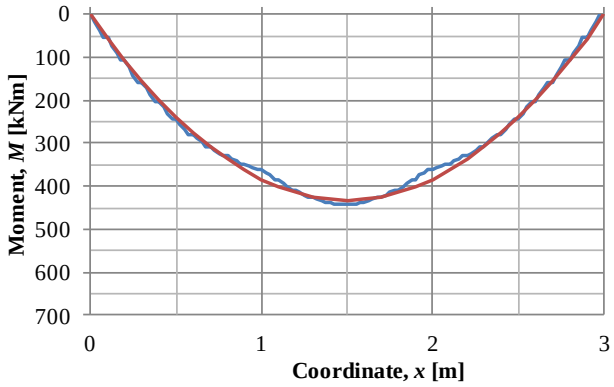	$\xi = \frac{443 - 432}{432} = 3\,\%$
	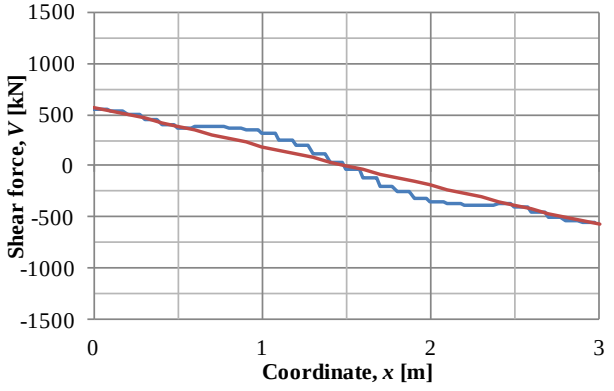	$\xi = \frac{544 - 576}{576} = -6\,\%$ $V_s^{FortV} = 819\text{kN}$

Ratio	Figure	
$\frac{P_c}{q_{eq}} = 5.48$	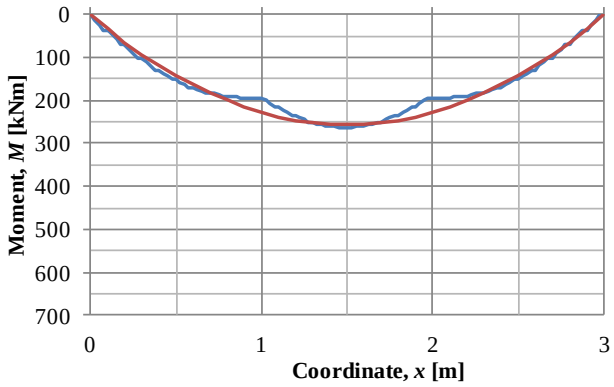	$\xi = \frac{264 - 257}{257} = 3\%$
	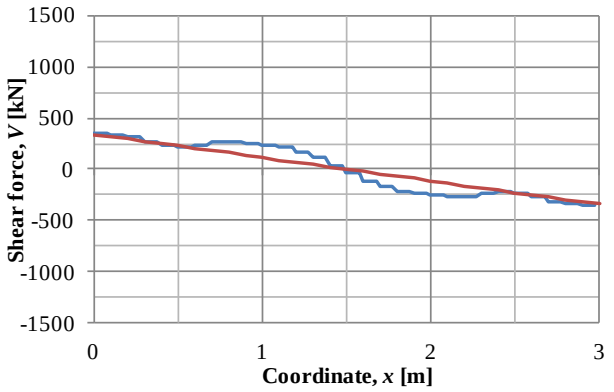	$\xi = \frac{357 - 342}{342} = 4\,\%$ $V_s^{FortV} = 620\,\text{kN}$
$\frac{P_c}{q_{eq}} = 9.27$	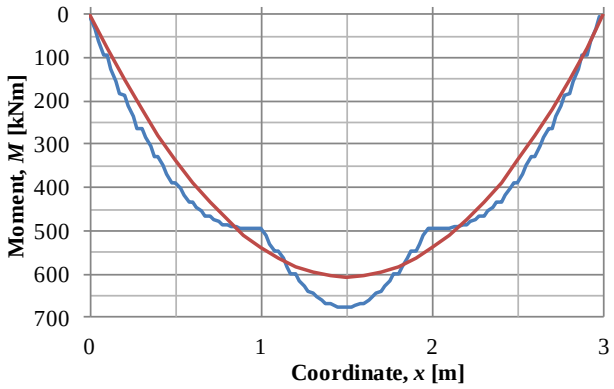	$\xi = \frac{678 - 607}{607} = 12\%$
	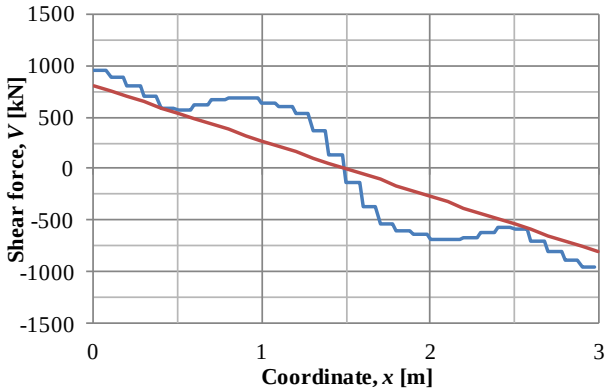	$\xi = \frac{951 - 809}{809} = 18\,\%$ $V_s^{FortV} = 2060\,\text{kN}$

Ratio	Figure	Relative error
$\frac{P_c}{q_{eq}} = 13.02$	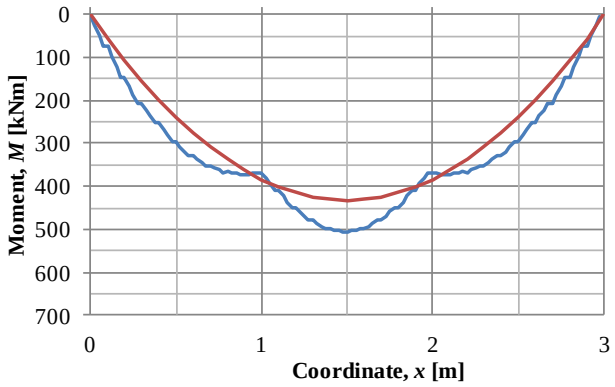	$\xi = \frac{506 - 432}{432} = 17\,\%$
	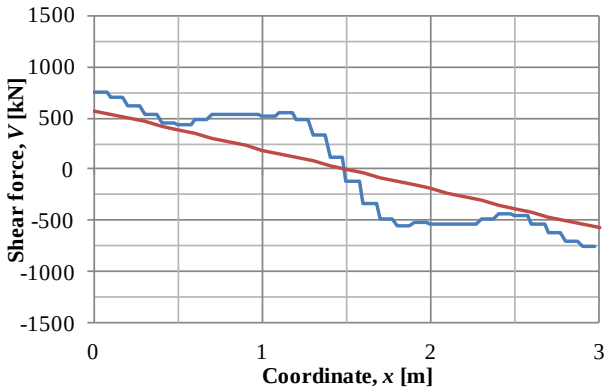	$\xi = \frac{748 - 576}{576} = 30\,\%$ $V_s^{FortV} = 1870\,\text{kN}$
$\frac{P_c}{q_{eq}} = 21.93$	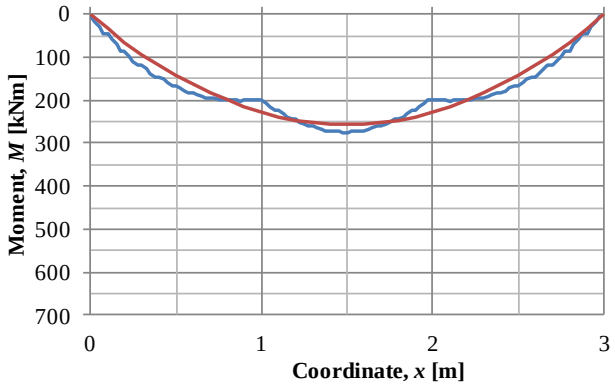	$\xi = \frac{275 - 257}{257} = 30\,\%$
	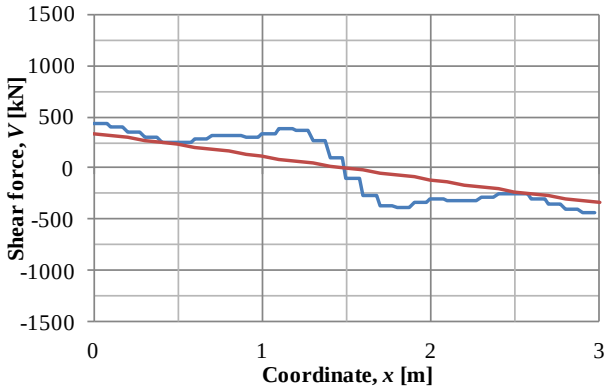	$\xi = \frac{441 - 342}{342} = 29\,\%$ $V_s^{FortV} = 1640\,\text{kN}$

APPENDIX I Detailed Analysis

I.1 Orientation

The choice of material model influences the result considerably as seen in previous Chapters 4 to 6. The choice of Young's modulus affects the wave speed, which in turn changes the deformation shape. It has also been shown that the magnitude of the support reaction depends on the initial stiffness, which may be the uncracked stiffness. The deformation shape then affects the simplified models significantly and thereby the result. The non-linearity of a reinforced concrete beam is above modelled by a simplified plastic bi-linear relationship.

In order to obtain better accuracy of the solutions the model could be refined. For this purpose a 2D-solid finite element model is going to be used, explicitly modelling concrete cracking and reinforcement yielding. Furthermore, the crack pattern will be investigated and perhaps intentions of a direct shear crack can be detected.

The previously used reinforced concrete beam will be further examined and compared to the solution in previous chapter and differences will be discussed.

Due to this thesis time limitation, the detailed analysis was never completed. The model assuming bond slip between concrete and reinforcement bars was created but provided strange results. Therefore, results will only be shown for the full bond model in order to give a brief discussion of encountered problems and results.

I.2 Modelling technique

I.2.1 Introduction

There is a possibility to use a concrete model in ADINA in which non-linearity of the concrete is taken into account. This is of interest because the beam is going to be modelled as detailed as possible. It requires much more information than a linear elastic material model. Therefore, it is not often used unless the problem requires great accuracy. However, it provides the designer with crack patterns, and possibility of reinforcement yielding, making it a more complicated model. The modelling technique follows the procedure in Johansson and Lantz (2009), which considers restraint cracking of concrete edge beams, and will be described below. Their way of modelling can be used with some modifications for this problem.

I.2.2 Geometry

The beam that is going to be analysed has the same dimensions as the example carried out in Chapter 3, see Figure I.1. It will be modelled with a symmetric boundary condition, only allowed to deform in vertical direction without rotations, in the centre since the two sides are symmetric. The support at the edges is difficult to model appropriately to get convergence. Therefore, an elastic material has been used closest to the support, indicated with a shaded area in Figure I.1. The beam is simply supported, which means that only the vertical movement is prevented. This will not influence the result significantly and it avoids concrete crushing locally.

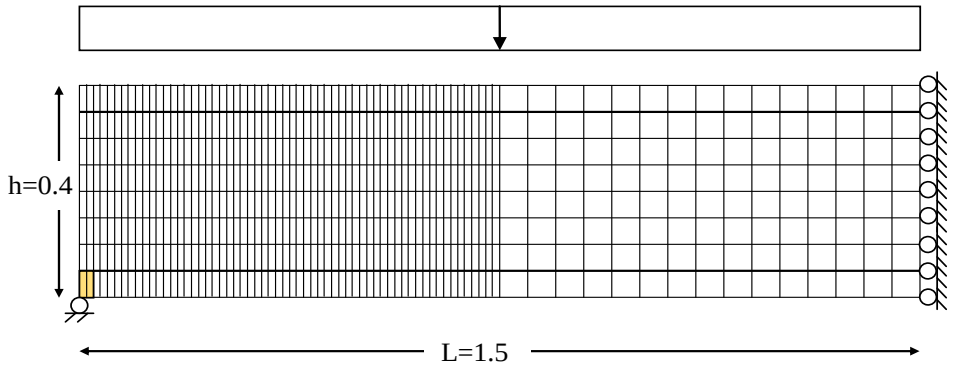

Figure I.1. The model of the simply supported reinforced concrete beam.

The concrete in the beam will be modelled with four node 2D-solid plain stress elements, quadratic with side lengths 50 mm. The numbers of elements cannot be increased in the vertical direction due to node limitations of 900 nodes. Since it is of interest to investigate a direct shear crack close to the support, the mesh has been refined to 10 mm in longitudinal direction while keeping the length in the vertical direction 50 mm.

The steel reinforcement is modelled with two node truss elements with the same length as the concrete elements. They are modelled on the actual level of the reinforcement in the top and bottom with distributed areas. The connection between the steel reinforcement and the concrete is made with either full bond, where the reinforcement bars and concrete share a node or with non-linear springs, described in Section I.2.5.

I.2.2 Loading and solution method

The beam will be subjected to the archive bomb, load case 1, see Section 3.2.

The analysis will be performed with an implicit method since the explicit method has given strange solutions in Chapter 3. The explicit method would otherwise be preferred for this type of problem since it would reduce the calculation effort. The composite bathe method for implicit integration is used since ADINA (2010) recommends it. The time step must be set to a very small value in order to get convergence. Convergence was found for a time step of 1 μs.

I.2.3 Concrete

Concrete is weak in tension and strong in compression. This can be shown with the uniaxial stress-strain relationship in Figure I.2.

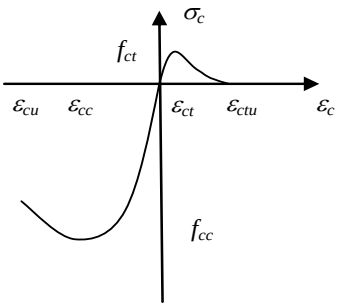

Figure I.2. Uniaxial stress-strain relationship for concrete

Some different parameters must be input in ADINA in order to describe the material response. The values of strengths, ultimate strengths and the corresponding strains can be input as they are but the ultimate tensile strain in concrete is a function of fracture energy G_f, Young's modulus E_c, concrete tensile strength f_{ct}, a length. The relationship can be described as

$$\varepsilon_{ctu} = \xi \cdot \varepsilon_{ct} \tag{9-1}$$

Where ξ is the input variable in ADINA defined as

$$\xi = \frac{2 \cdot G_f \cdot E_c}{l \cdot f_{ct}^2} = \frac{2 \cdot 50 \cdot 33 \cdot 10^9}{0.05 \cdot \left(2.9 \cdot 10^6\right)^2} = 7.98 \tag{9-2}$$

The length for perfectly bonded reinforcement bars is described with the average crack distance, s_m , Johansson (2000). This can be found from Eurocode 2.

$$s_m = \frac{s_{\max}}{1.7} \tag{9-3}$$

$$s_{\max} = k_3 \cdot c + k_1 \cdot k_2 \cdot k_4 \frac{d_b}{\rho_{p.eff}} \tag{9-4}$$

$$\rho_{p.eff} = \frac{A_s + A'_s}{A_{c.eff}} \tag{9-5}$$

$$A_{c.eff} = h_{c.eff} \cdot b - A_s - A'_s \tag{9-6}$$

$$h_{c.eff} = \min \begin{cases} 2.5(h-d) \\ \dfrac{h-x_u}{3} \\ 0.5h \end{cases} \tag{9-7}$$

where, h is the height of the cross-section, d is the effective depth, x_u is the height of the compression zone in the ultimate limit state, b is the width, A_s and A'_s are the area of the top and bottom reinforcement respectively, d_b is the bar diameter and c is the concrete cover. The factors k are

$$\begin{aligned} k_1 &= 0.8 \quad \text{for good bond conditions} \\ k_2 &= 0.5 \quad \text{for bending} \\ k_3 &= 3.4 \quad \text{recommended value} \\ k_4 &= 0.425 \quad \text{recommended value} \end{aligned} \tag{9-8}$$

Inserting values will eventually give the mean crack distance of

$$s_m = 154 \text{ mm} \tag{9-9}$$

This will give the input value for ADINA as

$$\xi = \frac{2 \cdot G_f \cdot E_c}{l_{el,1} \cdot f_{ct}^2} = \frac{2 \cdot 80 \cdot 33 \cdot 10^9}{0.154 \cdot \left(2.9 \cdot 10^6\right)^2} = 4.1 \tag{9-10}$$

If the bond is described with a stress-slip relationship the length should be taken as the element length, Johansson (2000). The element length should be taken as the element length perpendicular to the crack propagation see Figure I.3.

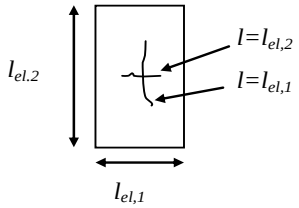

Figure I.3. Definition of the element length for different crack directions through an element.

The cracks will propagate mainly vertically and therefore the element length that should be used is the longitudinal length. This requires different element lengths for the ξ value model since the mesh is refined closer to the supports.

$$\xi_1 = \frac{2 \cdot G_f \cdot E_c}{l_{el,1} \cdot f_{ct}^2} = \frac{2 \cdot 80 \cdot 33 \cdot 10^9}{0.05 \cdot \left(2.9 \cdot 10^6\right)^2} = 7.98 \tag{9-11}$$

$$\xi_2 = \frac{2 \cdot G_f \cdot E_c}{l_{el,2} \cdot f_{ct}^2} = \frac{2 \cdot 80 \cdot 33 \cdot 10^9}{0.01 \cdot \left(2.9 \cdot 10^6\right)^2} = 39.24 \tag{9-12}$$

The compressive ultimate stress σ_{cu} can be described as

$$\sigma_{cu} = \frac{k\eta - \eta^2}{1+(k-2)\eta} f_{cc} \tag{9-13}$$

where

$$k = 1.05 E_c \frac{|\varepsilon_{c1}|}{f_{cc}} \tag{9-14}$$

$$\eta = \frac{\varepsilon_{cu}}{\varepsilon_{c1}} \tag{9-15}$$

ε_{cu} is the ultimate strain and ε_{c1} is the strain at maximum stress Engström (continuous beams). According to Eurocode 2, CEN (2004)

$$\varepsilon_{c1} = 2.0‰ \quad \text{and} \quad \varepsilon_{cu} = 3.5‰ \tag{9-16}$$

which gives

$$\sigma_{cu} = 16.8\,\text{MPa} \tag{9-17}$$

The input variables in ADINA are shown in Table I.1.

Table I.1. Input variables for the concrete material model in ADINA.

f_c	- 20 MPa	ξ_2	39.24
f_{cu}	- 16.8 MPa	G_f	80 Nm/m^2
f_{ct}	2.9 MPa	ε_{c1}	- 2.0 ‰
E_c	33 GPa	ε_{cu}	- 3.5 ‰
ξ	4.1	ρ	2400 kg/m^3
ξ_1	7.98	ν	0.2

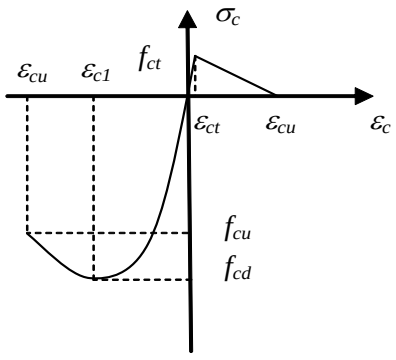

I.2.4 Reinforcement

The steel reinforcement has a simpler stress strain relationship and it can be explained by a bilinear material model similar to the idealised elasto-plastic model used in Chapter 4. It is explained by Table I.2. The steel reinforcement is modelled with a small strain hardening in order to avoid convergence problems in the FE-analysis.

Table I.2. Input variables for the steel reinforcement material model in ADINA.

f_{yd}	435 MPa
E	200 GPa
E'	0.2 GPa
ε_u	10 %
ρ	7800 kg/m^3
ν	0.3

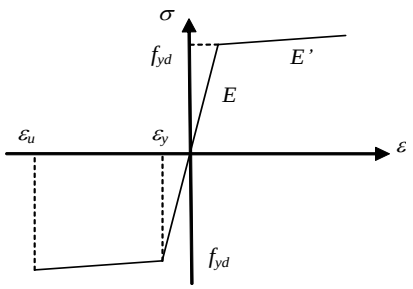

I.2.5 Bond between reinforcement and concrete

Bond between steel reinforcement and concrete depends on mechanical interlocking and friction. It can be explained by bond stress-slip relationship according to Figure I.4. The bond can either fail by pull-out of the reinforcement bars or transverse splitting of the concrete. This relationship does only consider pull out of the reinforcement.

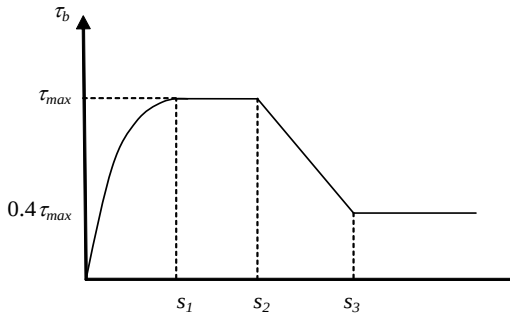

Figure I.4. Bond stress-slip relationship for concrete and steel reinforcement bars.

The initial bond stress before the maximum stress is reached can according to CEB-FIP (1993) be expressed as

$$\tau_b = \tau_{\max} \cdot \left(\frac{s}{s_1} \right)^{0.4} \tag{9-18}$$

The input parameters are described in Table I.3 for good bond conditions, CEB-FIP (1993)

Table I.3. Data for bond stress between reinforcement and concrete

τ_{max}	$2.5\sqrt{f_{ck}} = 13.7$ MPa
s_1	1.0 mm
s_2	3.0 mm
s_3	Clear rib spacing = 7.0 mm

In a simplified model, full bond between the reinforcement and the concrete can be assumed. This is achieved in ADINA by making sure that the nodes of the reinforcement bars and the concrete nodes coincide.

However, in a more detailed model, the bond between steel reinforcement and concrete needs to be modelled in ADINA with non-linear springs. To model this, the reinforcement nodes are placed 2 mm displaced in the horizontal direction from the concrete nodes they are bonded with, see Figure I.5. The reinforcement nodes are then fixed in the vertical direction relative to the concrete nodes and are therefore forced to have the same displacement in this direction. In the horizontal the reinforcement is connected to the concrete nodes with the non-linear springs to simulate the bond-slip relation. The relationship described in Figure I.4. with data from Table I.3. was used for the non-linear springs. The springs require a force and therefore the stress must be multiplied with the total surface area i.e.

$$F_b = \tau_b \cdot A_{surf} = \tau_b \cdot n \cdot \pi \cdot \phi \cdot l_{el} \tag{9-19}$$

In the end nodes only half of the force will be used since the length is only half the length.

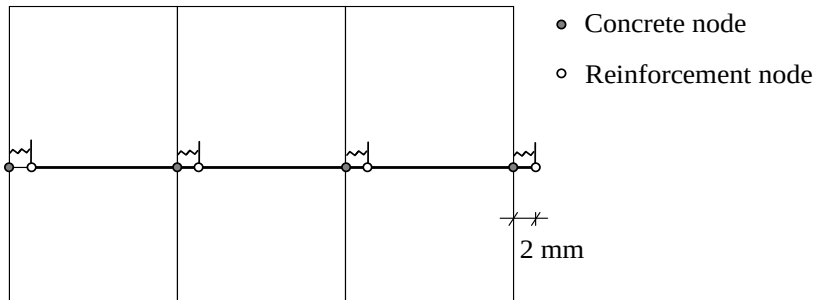

Figure I.5. The non-linear springs connects the reinforcement to the concrete with a bond stress-slip relationship. The springs are actually placed horizontal to the reinforcement node but are shown above for clarity.

I.2.6 Verification

For verification of the 2D-solid element model in ADINA, the displacement results from elastic beam elements have been used. 2D-solids provide a similar initial deformation shape and size for a state II beam modelled with equivalent Young's modulus. The wave is propagating somewhat differently and it is probably due to this fact that the solutions diverge slightly, see Figure I.6. The wave propagation is different for a shear wave, see Section 3.5.4. The correct wave form is hard to determine since ADINA must use the critical time step in order to model the wave propagation correctly. This time step has not been used in the comparisons made here since it is hard to determine for a shear wave. The midpoint displacement is almost the same although a slight divergence in the structures Eigen period is present in Figure I.7.

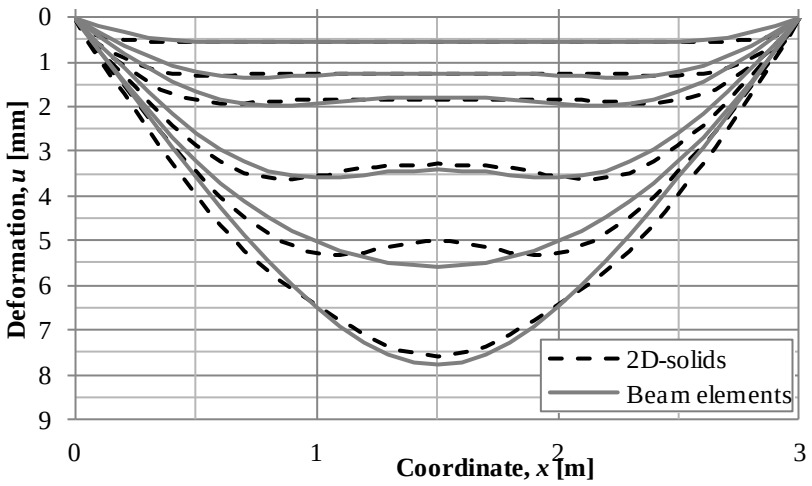

Figure I.6. Initial deformation between 2D-solid elements and beam elements

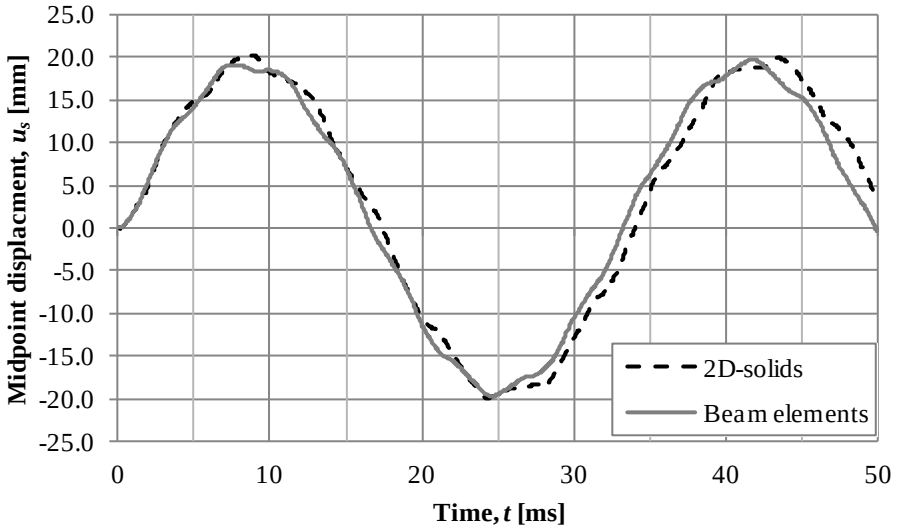

Figure I.7. Midpoint displacement for the two element types.

The material model must also be verified in order to use it for dynamic analyses. Verification is only done for the full bond model, which is the only model that dynamic results are presented for. A study of a single element is performed and gave the input values back. Another verification follows and is performed with an incremented static load until failure. The moment capacity is calculated in Section 3.3 to be

$$M_{Rd} = 227 \text{ kNm} \tag{9-20}$$

Cracks will occur when the stress in the lower fibre is greater than the concrete tensile stress. If the influence of reinforcement is neglected it can be calculated as

$$\begin{aligned} M_{crit} &= f_{ct,b} \cdot W_{el} = f_{ct}\left(1-\frac{h}{1000}\right)\cdot W_{el} = \\ &= 2.9\cdot 10^{6}\left(1-\frac{400}{1000}\right)\cdot\frac{0.4^2}{6} = 93\,\text{kNm} \end{aligned} \tag{9-21}$$

The moment M_y that causes the reinforcement to yield is calculated with a state II model with steel strain equal to the yield strain. The concrete is assumed to remain elastic and the concrete stress can therefore be calculated. From force equilibrium

$$\rightarrow: \quad f_{yd} A_s = \frac{E_c \varepsilon_c b x}{2} \quad \text{with} \qquad \varepsilon_c = \varepsilon_s \frac{x}{d-x} \tag{9-22}$$

assuming no normal force is present, the height of compression zone can be calculated as

$$x = -\frac{f_{yd} A_s}{E_c \varepsilon_y b} + \sqrt{\left(\frac{f_{yd} A_s}{E_c \varepsilon_y b}\right)^2 + 2\frac{f_{yd} A_s d}{E_c \varepsilon_y b}} = 74.2\,\text{mm} \tag{9-23}$$

And the moment M_y can be determined as

$$M_y = \frac{E_c \varepsilon_y b x^2}{2(d-x)} \frac{x}{3} + f_{yd} A_s (d-x) = 205\,\text{kNm} \tag{9-24}$$

The moment in mid span is plotted against the corresponding curvature Figure I.8. The presented theoretical values are also shown here for comparison. The moment has been calculated by using the stress distribution in the concrete and the stress reinforcement. The curvature is taken as the strain, ε, in the outermost fibre divided by the height of the compressed zone, x. This assumes a linear distribution of strain.

$$M = \int_A \sigma \cdot z \, dA \tag{9-25}$$

$$\frac{1}{\mathrm{r}} = \frac{\varepsilon}{x} \tag{9-26}$$

These have reasonable accuracy. The crack initiation is more obvious when investigating the appearance of cracks in the result window and starts at M = 88 kNm. Yield occurs in the reinforcement at M = 217 kNm. This is also reasonable. The ultimate capacity is higher than expected. A small steel hardening has been introduced, and can be one of the reasons. Another reason is that it seems like the beam has too high fracture energy.

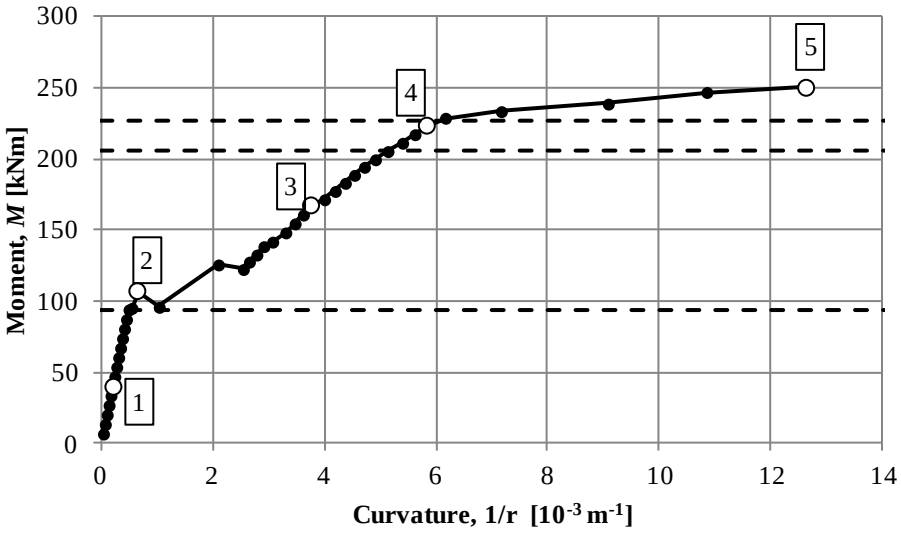

Figure I.8. Moment-curvature relationship for section in mid span of the reinforced concrete model subjected to a static load. The crack patterns for the times denoted with numbers are shown in Figure I.9.

The crack pattern for the beam statically loaded until failure is shown in Figure I.9. The crack patterns are shown for the times shown in Figure I.8 above. It can be seen that cracks form close to the support, which is modelled with an elastic material, for a very low load. This is not expected. Cracking starts in the centre. It can be seen that the cracks have a small distance between them. The distance is larger for fully developed cracks.

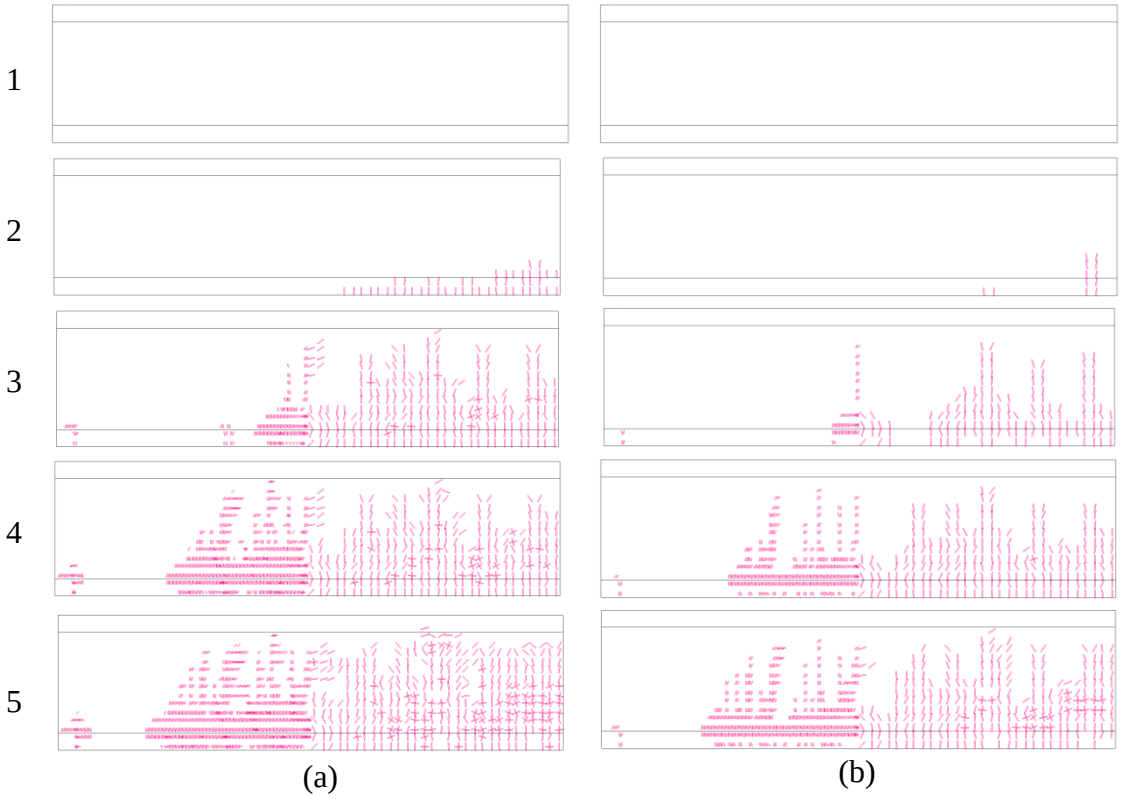

Figure I.9 Crack pattern for a statically loaded reinforced concrete beam. a) open cracks, b) fully developed cracks.

I.3 Results

Due to this project's time limitation the results of the detailed analysis is not complete and needs to be further investigated in future studies. Nevertheless, they are incorporated in this thesis in order to provide some guidelines and observations made using the concrete model available in ADINA. Several problems were encountered when loading the reinforced concrete beam with a very high impulsive load. The load cases used when examining the behaviour of an idealised reinforced concrete beam using beam elements in Chapters 3 and 4 were too impulsive and caused early failure. The failure occurred close to the support and depended on the layout of the elastic area. Convergence was not achieved when the whole structure was modelled with the concrete model.

The failure close to the support is not believed to be a direct shear crack due to problems modelling the support. Several support models were tried out, Figure I.10:

a). Support in mid plane, with and without elastic materials.

b). Modelling of an extended support with boundary condition further away.

c and d). Increasing size of elastic area, both vertically and horizontally.

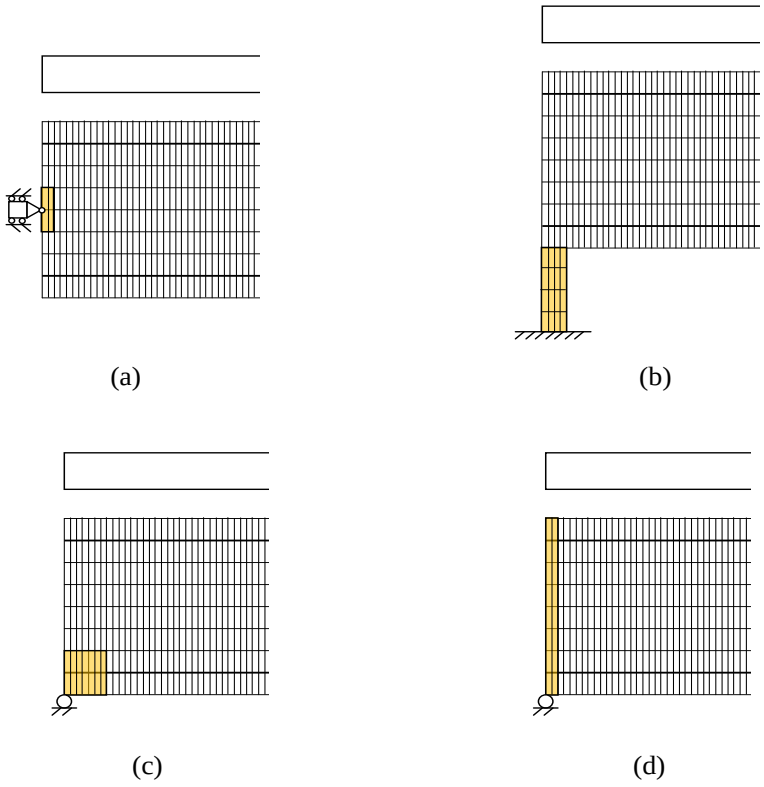

Figure I.10. Different support layouts give different results.

Schematic pictures of the failures at the supports are shown in Figure I.11.

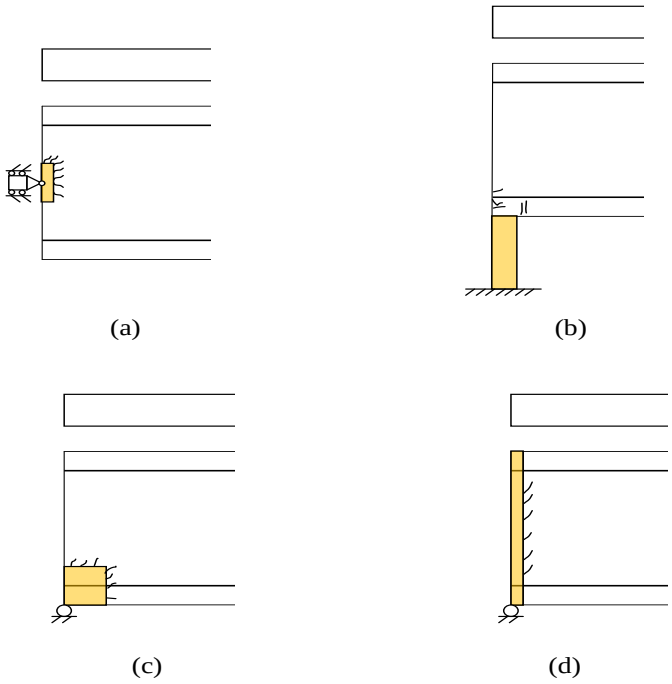

Figure I.11. Schematic picture of how cracks developed close to the support or the elastic zone.

For a smaller impulse intensity, i = 1000 Pa•s, see Figure I.12, failure close to the supports is not initially obtained and the concrete beam get a behaviour closer to the expected. Since no expected behaviour was found for the model with perfect bond or the model assuming a bond slip relationship for highly impulsive loads, results for the less intense load will only be shown for perfectly bonded reinforcement.

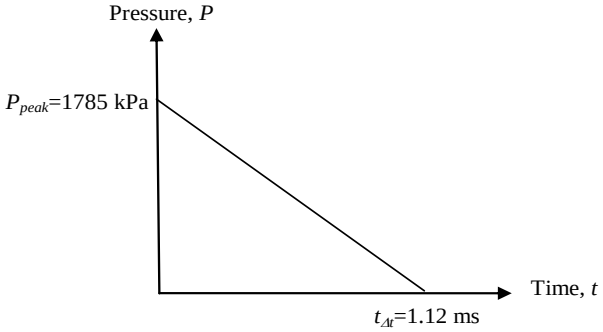

Figure I.12. The load used for the detailed reinforced concrete model.

When the response of the detailed analysis is compared against the corresponding SDOF system and a FE-analysis with elasto-plastic beam elements the real concrete behaviour gives a smaller displacement, see Figure I.13. A slight divergence is expected since the simplified model uses an equivalent stiffness, compare Figure 3.3. The displacement for the SDOF model is solved with load-mass transformation factor 0.667 which gives a slightly different period but a reasonable description of the maximum value as seen in Section 4.1.3.

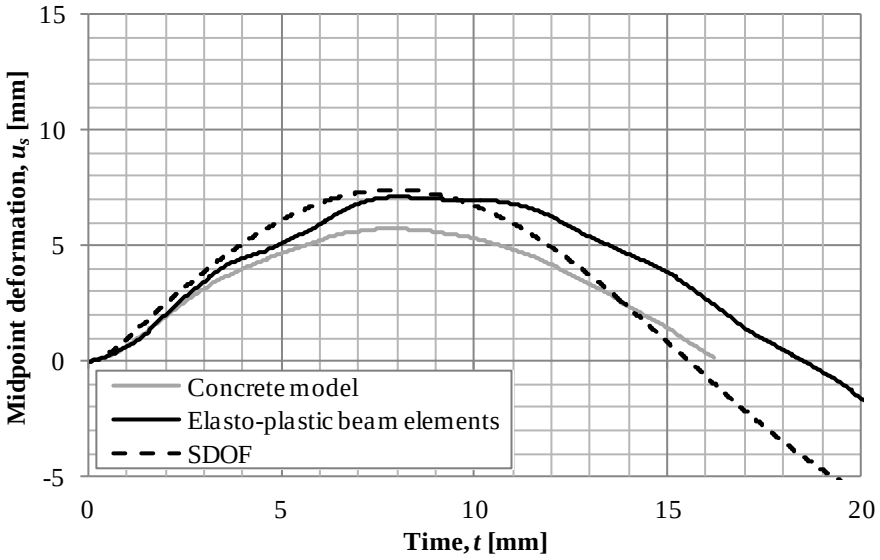

Figure I.13. Midpoint displacement for impulse loading according to Figure I.12.

The initial displacement shape, shown in Figure I.14, is similar to what has been seen for the elasto-plastic case. It is shown with symmetry across mid span. The wave form can be identified after 0.5 ms but disappears and the deformed shape of the beam will be more similar to an elastic bending shape. There is also a tendency to a rigid body motion in the beginning. The displacement at the support is non-zero since the chosen line is the centre line and will consequently be compressed.

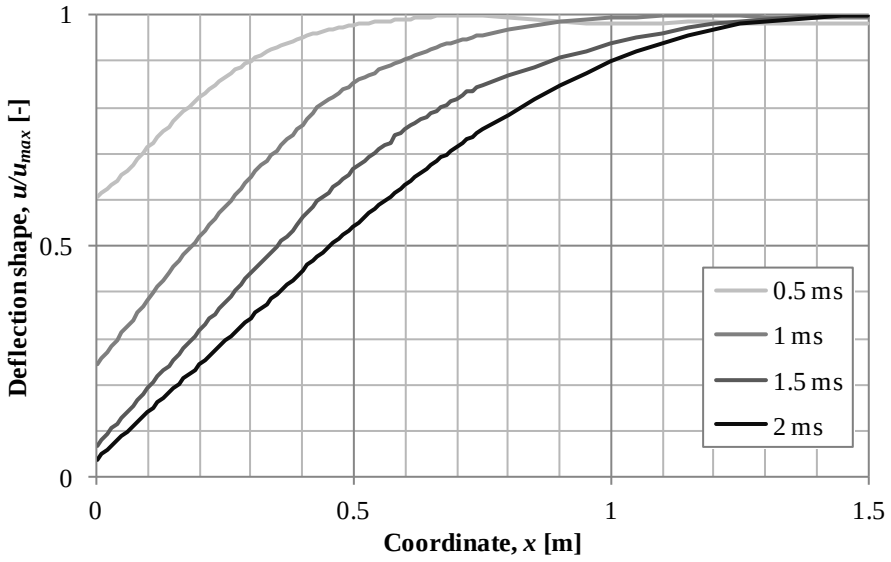

Figure I.14. Displacement shape for the concrete model for impulse loading according to Figure I.12.

The reinforcement will just yield before the structure will oscillate back. It fails close to the support when the structure oscillates back, which supports the hypothesis that there is modelling issues close to the support and that the crack is not a direct shear crack when the structure is subjected to a higher load.

The crack pattern for the statically loaded reinforced concrete beam is shown in Figure I.15 for different times. This figure shows all cracks to the left and fully developed cracks to the right. Cracks occur at the boundary between the elastic area

and concrete area, which is not expected. The only interesting about crack pattern is the order they occur. Bending cracks form closer to the support before in the centre. This is a consequence of the rigid body motion. It can also be seen that reasonable distance between the cracks is obtained although some small cracks occur between the reinforcement and the bottom edge between the main cracks. No fully developed cracks have formed in the centre part until 1 ms. It can also be seen that the cracks close when the beam oscillates back.

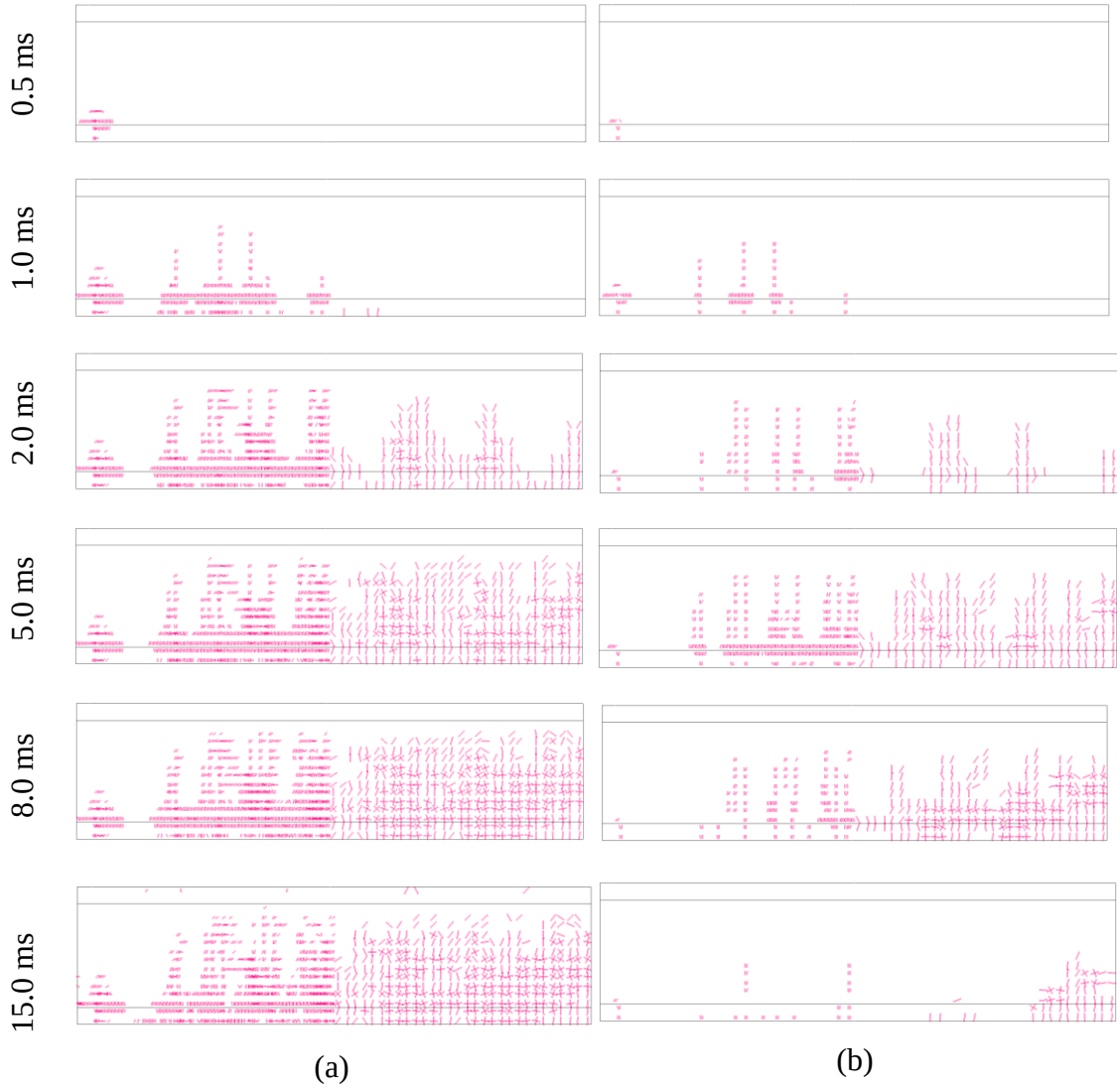

Figure I.15. Crack pattern for a) open cracks and b) fully developed cracks for different times for impulse loading according to Figure I.12.

As mentioned in the introduction of the result section, more studies need to be done in this subject. The result from this investigation can be taken into account and evaluated further. Especially, the problem modelling the support must be solved in order to get a better behaviour of the beam with real reinforced concrete behaviour.